NASA/TM—2006-213863

Comprehensive Report of Fan Performance From Duct Rake Instrumentation on 1.294 Pressure Ratio, 806 ft/sec Tip Speed Turbofan Simulator Models

Robert J. Jeracki
Glenn Research Center, Cleveland, Ohio

February 2006

The NASA STI Program Office . . . in Profile

Since its founding, NASA has been dedicated to the advancement of aeronautics and space science. The NASA Scientific and Technical Information (STI) Program Office plays a key part in helping NASA maintain this important role.

The NASA STI Program Office is operated by Langley Research Center, the Lead Center for NASA's scientific and technical information. The NASA STI Program Office provides access to the NASA STI Database, the largest collection of aeronautical and space science STI in the world. The Program Office is also NASA's institutional mechanism for disseminating the results of its research and development activities. These results are published by NASA in the NASA STI Report Series, which includes the following report types:

- TECHNICAL PUBLICATION. Reports of completed research or a major significant phase of research that present the results of NASA programs and include extensive data or theoretical analysis. Includes compilations of significant scientific and technical data and information deemed to be of continuing reference value. NASA's counterpart of peer-reviewed formal professional papers but has less stringent limitations on manuscript length and extent of graphic presentations.

- TECHNICAL MEMORANDUM. Scientific and technical findings that are preliminary or of specialized interest, e.g., quick release reports, working papers, and bibliographies that contain minimal annotation. Does not contain extensive analysis.

- CONTRACTOR REPORT. Scientific and technical findings by NASA-sponsored contractors and grantees.

- CONFERENCE PUBLICATION. Collected papers from scientific and technical conferences, symposia, seminars, or other meetings sponsored or cosponsored by NASA.

- SPECIAL PUBLICATION. Scientific, technical, or historical information from NASA programs, projects, and missions, often concerned with subjects having substantial public interest.

- TECHNICAL TRANSLATION. English-language translations of foreign scientific and technical material pertinent to NASA's mission.

Specialized services that complement the STI Program Office's diverse offerings include creating custom thesauri, building customized databases, organizing and publishing research results . . . even providing videos.

For more information about the NASA STI Program Office, see the following:

- Access the NASA STI Program Home Page at ***http://www.sti.nasa.gov***

- E-mail your question via the Internet to help@sti.nasa.gov

- Fax your question to the NASA Access Help Desk at 301–621–0134

- Telephone the NASA Access Help Desk at 301–621–0390

- Write to:
  NASA Access Help Desk
  NASA Center for AeroSpace Information
  7121 Standard Drive
  Hanover, MD 21076

NASA/TM—2006-213863

Comprehensive Report of Fan Performance From Duct Rake Instrumentation on 1.294 Pressure Ratio, 806 ft/sec Tip Speed Turbofan Simulator Models

Robert J. Jeracki
Glenn Research Center, Cleveland, Ohio

National Aeronautics and
Space Administration

Glenn Research Center

February 2006

Available from

NASA Center for Aerospace Information
7121 Standard Drive
Hanover, MD 21076

National Technical Information Service
5285 Port Royal Road
Springfield, VA 22100

Available electronically at http://gltrs.grc.nasa.gov

Contents

Comprehensive Report of Fan Performance from Duct Rake Instrumentation on 1.294 Pressure Ratio, 806 ft/sec Tip Speed Turbofan Simulator Models

Robert J. Jeracki
National Aeronautics and Space Administration
Glenn Research Center
Cleveland, Ohio 44135

Abstract

A large scale model representative of an advanced ducted propulsor-type, low-noise, very high bypass ratio turbofan engine was tested for acoustics, aerodynamic performance, and off-design operability in the NASA Glenn 9- by 15-Foot Low-Speed Wind Tunnel. This test was part of NASA's Advanced Subsonic Technology Noise Reduction Program. The low tip speed fan, nacelle, and an un-powered core passage (with core inlet guide vanes) were simulated. To measure fan aerodynamic performance, four rakes with total pressure and temperature probes were installed in the bypass duct, upstream of the stators. Core inlet guide vanes were instrumented with total pressure or total temperature probes, measuring performance in the fan hub region. Several wind tunnel runs with nearly the same hardware installed are compared, to identify the repeatability of the fan performance measurements. In other wind tunnel runs, fan performance was measured with two different fan blades made from different material and intended for the same design operation (graphite composite material over a titanium spar and solid titanium), three fan blade angles (cruise design, –9 degrees lower for takeoff, and even lower at –15 degrees), and two fan rubstrip designs (smooth and a casing treatment for stall management).

As might be expected, the effect of the stall management casing treatment was a performance penalty. The amount of recirculating flow at the fan tip was larger than required for the desired stall margin improvement, however. Reducing that flow would also reduce the resulting performance penalty. There was a somewhat surprising performance difference between the titanium and graphite composite blades, mostly away from the fan operating speed lines. Though both blades showed some indication of a flow transition (near the blades tip) as the fan flow was reduced, the transition occurred near the takeoff operating lines with the titanium blades and resulted in high blade stress instabilities.

Though the pressure and temperature ratios were low for this fan design, the techniques used to improve thermocouple measurement accuracy gave repeated data runs with the adiabatic efficiency agreeing within one percent. The measured fan adiabatic efficiency at takeoff was 93.7 percent which matched the design intent well.

Nomenclature

AARPT12.5	Area average of all 10 total pressure averages in the bypass duct, psi
AARTT12.5	Area average of all 10 total temperature averages in the bypass duct, °R
AARPTCI	Area average of all 5 total pressure averages in the core inlet, psi
AARTTCI	Area average of all 5 total temperature averages in the core inlet, °R
ADP	Advanced Ducted Propulsor
ARPT12.5	STA 12.5 total pressure averaged at each of 10 bypass duct radii, psi

ARTT12.5	STA 12.5 total temperature averaged at each of 10 bypass duct radii, °R
ARPTCI	Core inlet total pressure averaged at each core inlet radius, psi
ARTTCI	Core inlet total temperature averaged at each core inlet radius, °R
CFD	Computational Fluid Dynamic (computer flow calculations)
EADAAR12	Bypass adiabatic efficiency, $(RAARPT12^{(2/7)}-1)/(RAARTT12-1)$
FCT	Fan Casing Treatment, rubstrip design for stall margin improvement
GC	Graphite Composite blade material
IGV	Inlet Guide Vanes of the core passage
Mo	Freestream Mach number
M_{local}	Mach number based on specific local pressure measurements
MS	Axial model station referenced to the fan stacking axis as 170.000, in
P_{STD}	Standard day pressure, 14.696 psi
PS	Static pressure, psi
PT	Total pressure, psi
PTo	Freestream total pressure, psi
RAARPT12	Bypass pressure ratio, AARPT12.5/PTo
RAARTT12	Bypass temperature ratio, AARTT12.5/TTo
RPMc	Rotor rpm corrected to standard day conditions, rpm
RPMck	RPMc/1000, rpm/1000
STA	Station, in standard engine nomenclature (i.e., 0 is far upstream, 2.0 is just upstream of the fan, 12.5 is between the fan and bypass duct stator, ∞ is far downstream)
T_{STD}	Standard day temperature, 518.67 °R
TI	Titanium blade material
TPS	Turbine Powered Simulator
TTo	Freestream total temperature, °R
WBc	Bypass weight flow corrected to standard day conditions, lbm/sec
WCc	Core weight flow corrected to standard day conditions, lbm/sec
WCc,loc	Core weight flow corrected to local core conditions, lbm/sec
WFc	Fan total weight flow corrected to standard day conditions, lbm/sec

Introduction

Fan engine performance test methods have been developed, refined, and standardized through years of experience (refs. 1 and 2). Methods include component tests (inlet, fan, stage, and nozzle), ground test, and altitude test facilities. Flow-through nacelles and small Turbine Powered Simulator (TPS) models have normally been used to evaluate installation effects. Larger TPS models with strain gaged force balances may be used to measure fan engine thrust-minus-drag performance in wind tunnels (ref. 3). Total pressure and total temperature rakes can be installed to measure fan and/or stage performance. NASA Glenn is continuing to test 22-inch diameter fan models of existing and advanced engines to evaluate low noise improvement possibilities and operability or performance improvements (refs. 4 to 8). This is part of NASA's Aeronautics and Space Transportation Technology Enterprise. This report presents fan performance results of an ADP-type, low tip speed, low pressure ratio fan, using fan duct rake total pressure and temperature measurements.

A 22-inch fan diameter model simulating a low tip speed, Advanced Ducted Propulsor (ADP)-type engine is shown in the NASA Glenn 9- by 15-Foot Low-Speed Wind Tunnel (fig. 1(a)), (ref. 9). The tunnel can be run from near zero to 0.2 Mach number, at near ambient barometric pressure, and temperatures from 70 to 75 °F. The simulator is mounted to the front of a strut-

supported high-pressure air turbine. The strut carries heated air to the turbine, lubrication lines to and from the model, and instrumentation leads off of the model to the high-speed data system. A cross section of the simulator is shown in figure 1(b). The engine core simulation consists of an inlet, inlet guide vanes, a flow-through duct with support struts, and a nozzle. The core nozzle exit area was expanded to pass the correct core flow at takeoff conditions, so it does not represent the exact geometry of the engine being simulated. If the core were modeled with a first compressor stage, the core nozzle simulation could match the engine core nozzle geometry more closely.

Fan Performance Test Hardware

The fan engine simulator included a flight-type inlet and nozzle. Some fan performance testing with the duct pressure and temperature probes was done with the flight hardware installed. The results are along a specific operating line of pressure ratio versus fan flow for each freestream Mach number tested. To obtain fan performance maps, a bellmouth inlet and a Variable Fan Exit Nozzle (VFEN) were installed. The bellmouth allowed the fan to be run at low freestream Mach number without inlet flow separations or ingested vortices. The VFEN allowed the nozzle exit area to be reduced, with remotely actuated radial blades acting like butterfly valves. Reducing the nozzle area made the fan run at lower mass flow, through a range of engine operating conditions from high-flow simulating cruise, to lower flow for takeoff, and finally to fan stall. This report is organized to present flight nozzle operating line performance comparisons first, followed by fan performance maps

Instrumentation for Fan Performance

Freestream total pressure and temperature were measured using a cruciform-shaped rake assembly located about 86.5 inches in front of the fan blade stacking axis. There were a total of four pressure probes and five temperature probes located along the arms of the cruciform and centered on the fan centerline axis, accurately measuring the flow conditions coming into the fan. The thermocouple probes were shielded with aspirated stagnation tubes. For acoustic data runs, the freestream cruciform rake and the bypass duct rakes were removed.

Axial locations of instrumentation in the engine simulator are shown in figure 2(a). (Note: MS stands for Model Station in inches, referenced to the fan blade stacking axis as 170.000.) Fan total weight flow was calculated upstream of the fan (standard engine nomenclature Station 2.0, ref. 10) using a ring of nine static pressures in the inlet at MS 164.440 (figs. 2(a) and 3(a)). Core weight flow was calculated using two rakes of five total pressures each, and two rings of four static pressures each, located at MS 195.850, upstream of the core nozzle exit (figs. 2(a) and 3(b)).

Fan performance was measured using four radial rakes midway through the stage bypass duct (engine STA 12.5) at MS 175.000 (figs. 2(a) and 4(a)), and probes in the core inlet (MS 173.844–173.946) attached to the core Inlet Guide Vanes (IGVs) (figs. 2(a) and 4(b)). The four bypass duct rakes had pressure and temperature probe paired together at 10 radial locations, at the centers of equal annular area (a total of 40 pressures and 40 temperatures). The core inlet pressures and temperature probes were located at the centers of 5 equal area annuli, with two measurements at each radius (a total of 10 pressures and 10 temperatures). The bypass duct pressure tubes and thermocouples were shielded with aspirated stagnation tubes, giving high flow angle capability. The thermocouple shields had very high recovery ratio and, therefore, small temperature correction due to flow velocity. The core pressure tubes and thermocouples needed to be smaller, so the shields were smaller and the temperature recovery corrections were larger than the bypass duct probes.

For some of the later runs, the core inlet pressure and temperature probes were missing. They

had been removed to eliminate any possible acoustic contamination during the far-field acoustic testing. For those later test runs, only bypass duct performance is available.

Figure 2(b) is a photograph that shows the fan with the inlet and some of the fan blades removed. Three of the four bypass duct rakes can be seen in front of the stators. Some core probes are also somewhat visible on the core IGVs.

Fan Performance Parameter Calculations

For the bypass duct total pressures, the four total pressures from each duct rake were averaged at each of the ten annular radii in the bypass (ARPT12.5 (1 to 10)). At each rake radius, a linear interpolation was done from the averaged inner-wall static pressure to the averaged outer-wall static pressure. Each static pressure and the corresponding averaged total pressure were used to calculate a local Mach number. A total temperature recovery ratio had been measured in a calibration facility and correlated with Mach number. For the wind tunnel data, the indicated temperature of each thermocouple was corrected by the temperature recovery ratio corresponding to the calculated local Mach number at each radius. The four total temperatures from each duct rake were averaged at each of the ten annular radii in the bypass (ARTT12.5 (1 to 10)). Then, the ten annular averages of total pressure and temperature were averaged (based on equal areas) to yield a single value of averaged radial total pressure and temperature (AARPT12.5 and AARTT12.5). The bypass total pressure and total temperature ratios are the ratios of the averaged total values to the fan inlet reference values,

$$\text{RAARPT12} = \text{AARPT12.5}/\text{PTo},$$

and,

$$\text{RAARTT12} = \text{AARTT12.5}/\text{TTo}.$$

The bypass duct adiabatic efficiency is then calculated from these ratios as,

$$\text{EADAAR12} = (\text{RAARPT12}^{2/7}-1)/(\text{RAARTT12}-1).$$

For the core inlet total pressure, the pairs of total pressures were averaged at each of the five annular radii in the core inlet (ARPTCI (1 to 5)). Each of the five averaged total pressures was then used with the averaged core inlet static pressure to calculate a local Mach number. The total temperature recovery ratio for the core probes had not been calibrated. Instead, the recovery ratio was predicted based on the aspirated thermocouple geometry (ref. 11). The geometry (aspiration area) was then adjusted slightly to make the corrected temperature level consistent with the bypass duct temperatures. The indicated temperature of each thermocouple was then corrected by the temperature recovery ratio corresponding to the calculated local Mach number at each radius. The pairs of total temperatures were also averaged at each of the five annular radii in the core inlet (ARTTCI (1 to 5)). Then, the five annular averages of total pressure and temperature were averaged (based on equal areas) to calculate the annular averaged radial core inlet total pressure and total temperature (AARPTCI and AARTTCI). The core inlet total pressure and temperature ratios are the ratios of the core inlet averaged total values to the fan inlet reference values (AARPTCI/PTo and AARTTCI/TTo).

The total fan pressure and temperature ratios (combining the bypass and core values) were calculated as the weight-flow averages of the bypass and core values. With the bypass and core flows, the weighted averages were,

$$\text{Fan Ratio} = ((\text{Bypass Duct Ratio} * \text{WBc})+(\text{Core Inlet Ratio} * \text{WCc}))/(\text{WFc}),$$

where WBc, WCc, and WFc are the bypass, core, and total fan weight flows, respectively, corrected to standard day conditions.

The fan inlet total weight flow calculation used a Computational Fluid Dynamic (CFD) analysis of the inlet to predict the actual flow, including viscous effects. The freestream total pressure and local surface static pressure at the weight flow static pressure location (from the CFD solution) were used to calculate an "ideal" local Mach number and a correlating weight flow parameter (WFP). The WFP was chosen to be the Mach number part of the weight flow equation,

$$WFc_{ideal} = Constant * P_{STD}/(T_{STD})^{0.5} * Area * (M_{local}/(1.0+0.2*M_{local}^{2})^{3}),$$

and,

$$WFP = M_{local}/(1.0+0.2*M_{local}^{2})^{3}.$$

So, for totally uniform flow, the corrected flow would be a constant slope times the WFP value. Correlating the predicted actual flow (with boundary layer and static pressure gradient effects) with WFP made the correlation nearly a straight line,

$$WFc_{CFD} = f_{correlation}(WFP_{CFD}).$$

The averaged cruciform rake measurements of freestream PTo and TTo and the averaged static pressure at the inlet weight flow static pressure location were used to calculate the actual corrected fan weight flow for each wind tunnel data point. The freestream total pressure and the local static pressure were used to calculate the "ideal" local Mach number and WFP. Then, the actual total fan weight flow corrected to standard day conditions (WFc) was calculated from the WFP and the CFD-predicted flow correlation.

The core weight flow was calculated using a method similar to the fan inlet total weight flow. The flowfield was predicted along the core duct, back to the fully developed flow at the weight flow rake near the core nozzle. The total pressures from the CFD solution at the radii of the actual rake were averaged to get the averaged core flow total pressure. Similarly, the total temperatures from the CFD solution were also averaged. The total pressure and the averaged inner and outer duct static pressures were used to determine the "ideal" core flow rake Mach number and the core WFP, which were then used to correlate the predicted actual flow, corrected to the local core total pressure and total temperature as,

$$WCc_{local} = WC_{CFD} * (TTCW/T_{STD})^{0.5} / (PTCW/P_{STD}).$$

Each wind tunnel data point used the core flow rake averaged total pressure, core inlet averaged total temperature, and averaged static pressure at the core weight flow location. The total pressure and the local static were used to calculate the "ideal" local Mach number and the WFP. The actual core weight flow corrected to local conditions (WCc_{local}) was calculated from the "ideal" local WFP and the predicted flow correlation as,

$$WCc_{local} = f_{correlation}(WFP).$$

Then, the actual flow corrected to standard day was calculated using $PTCW/P_{STD}$ and $TTCI/T_{STD}$ as,

$$WCc = WCc_{local} * (PTCW/P_{STD})/(TTCI/T_{STD})^{0.5}.$$

The bypass weight flow corrected to standard day conditions was calculated as the difference between the fan total corrected flow and the core corrected flow,

$$WBc = WFc - WCc.$$

Fan Blade Configurations

The fan blade design intent was to simulate a low tip speed, variable pitch (stagger) ADP-type fan. The takeoff tip speed and rpm, corrected to standard day conditions, were 840 ft/sec and 8,750 rpm, respectively. The design is described in reference 12. Table 1 is a summary of fan blade design parameters and operating point parameters at the three noise measurement points: takeoff, approach, and cutback. The blade was designed as a graphite composite (GC) blade on a Titanium spar and a base button. The spar base was attached to the shank within the hub with a pin that allowed the blade to pivot in the flatwise direction (pin-root). At the base of the shank was a gear segment that allowed the fan blades to be locked and tested at different pitch angles. The cruise design angle was defined as 0 (zero) degrees. The takeoff angle was closed (farther away from axial) by 9 degrees from the cruise design angle, and identified as –9 degrees. A third, lower angle of –15 degrees was also tested.

A solid Titanium (TI) blade set was designed and fabricated to be an aerodynamically similar replacement for the composite pin-root fan. A circular dovetail attachment allowed the same split hub to be used. The hub was designed with a split across the fan rotation axis at the fan stacking axis (MS 170.000). Gear segments were attached to the base of the dovetail to allow the same blade angle change capability as the pin-root, GC blades. For structural tuning, the inboard blade thickness was increased starting at about 60 percent span. The thickness matched the GC design at the root. The maximum increase in thickness/chord ratio of 0.015 occurred from 10 to 20 percent span. The total camber in the hub region was decreased by less than 4 percent. These changes were predicted to have negligible effect on the aerodynamic performance of the fan.

Two different rubstrips were tested, installed in the fan casing over the fan blade tips. To minimize possible tip rubs and damage to the blades, the tip clearance was made to be 0.055 inches at fan takeoff operating speed. That would represent a worst-case, worn engine clearance, and would be a worst-case for noise and performance. The baseline rubstrip was completely smooth. The second rubstrip had a Fan Casing Treatment (FCT) installed, designed to increase fan stall margin. Fan tip flow downstream of the fan was recirculated forward and injected upstream of the fan at the tip. It was expected that there would be some acoustic and performance penalty with the FCT rubstrip installed. The fan hardware combinations that were tested (blade material, blade angle, and rubstrip) are summarized in table 2.

Fan Operating Line Results and Repeatability, TI Blade, –9 Degrees, FCT Rubstrip

Two aerodynamic data runs with nearly identical fan/nacelle hardware were performed back-to-back with the flight inlet and flight nozzle installed. The TI blades were installed at the takeoff angle (–9 deg) along with the FCT rubstrip. For the second run, only a single, small inlet boundary layer rake was removed (from the inlet flow static pressure location). For both runs, data were taken at 0.20, 0.15, and 0.10 freestream Mach number. The total fan performance results (combining the bypass and core measurements) are presented in figure 5, with the first run plotted with open symbols and the second with solid symbols. The fan total pressure and temperature ratio operating lines (versus fan corrected flow) are shown in figures 5(a) and (b). The two runs are nearly indistinguishable. The adiabatic efficiency, calculated from the pressure and temperature ratios, is shown in figure 5(c). The results show the efficiency repeats within less than 1.0 percent. The bypass duct rake performance results are presented in figure 6. Since the bypass flow is about 90 percent of the total flow, the bypass duct results look very much like the fan total results. The fan bypass pressure ratio and temperature ratio operating lines (versus fan corrected flow) are shown in figures 6(a) and (b). The two runs are nearly indistinguishable, and just slightly lower than the fan total results. The adiabatic efficiency, shown in

figure 6(c), is slightly higher than the fan total efficiency (fig. 5(c)). At flow rates below about 75 lbm/sec, the efficiency is about 92.0 percent. At higher flow the efficiency drops, and at 84 lbm/sec the efficiency is about 84.0 percent. To complete the documentation of the fan operating line performance, the bypass ratio (WBc/WCc) is shown in figure 6d. The bypass ratio varies from about 9.0 at low flow rates to 10.8 at high flow rates. The two runs are nearly indistinguishable.

For selected, repeated operating conditions at Mo = 0.20 (shown in fig. 7(a)), details of the radial distribution of pressure ratio, temperature ratio, and adiabatic efficiency from the bypass duct rakes are shown in figures 7(b) through (i), respectively. The rake measurements at each radius in the core inlet and bypass duct were averaged (eliminating bad measurements), and the results plotted versus the radius. The pressure ratio and temperature ratio plots show only slight differences. These differences are magnified in the adiabatic efficiency plots (figs. 7(d) to (i)), however. Figures 7(e) to (i) show the efficiency more clearly by separating the five different fan speeds. The efficiency differences were about 1.0 percent, and up to 2.5 percent at 5,000 RPMc near the fan tip. (Note: The temperature rise at 5,000 RPMc is only about 16 °F, so 2.5 percent efficiency corresponds to only a 0.6 °F temperature difference). At higher fan speeds the efficiencies were almost identical. Though the core instrumentation was not as good or as reliable as the bypass rakes, for these runs even the core repeatability is quite good. As noted above for figure 5(c), the process of averaging these 10 radial measurements results in bypass duct fan efficiency averages that differ by less than 1.0 percent. The peak efficiency at mid-span radii ranges from about 98.5 percent at high fan speed (takeoff) to about 97.5 at lower fan speed (approach). These results agree very well with the fan design predictions at takeoff, cutback and approach conditions.

TI Versus GC Fan Operating Line Results at –9 Degree Angle, Smooth Rubstrip

Fan operating line performance data were recorded for both the TI and GC blades, at the –9 degree blade angle with the smooth fan rubstrip installed. A comparison of the performance is shown in figure 8 (Note: there were no data recorded at Mach 0.15 for the GC blades). The open symbols are the TI results and the solid symbols are the GC results. In figures 8(a) and (b), the operating line pressure ratio and temperature ratio are quite similar. Noticeable at Mach 0.20, the TI blades operated at a slightly higher corrected flow, pressure ratio, and temperature ratio than the GC blades (comparing points where the same fan speed was run). The adiabatic efficiency (fig. 8(c)) shows little difference between the TI and GC blades at lower fan speeds and flow at Mach 0.20. The efficiency of the GC blades falls off faster at high fan flow, resulting in the TI blades being about 3.0 percent higher at the highest flow (85 lbm/sec). The TI blades appear up to 2.0 percent lower in adiabatic efficiency at 0.10 Mach number, however. Though designed to be aerodynamically the same, the difference in stiffness and weight may cause differences in shape and performance as speed and loading changes. The bypass ratio (fig. 8(d)) shows little difference at 0.20 Mach number, but a much lower bypass ratio for the TI blades at 0.10 Mach number. This is unexpected, since the TI blades are thicker in the hub region and might be expected to perform worse there and result in lower core flow (therefore higher bypass ratio). The TI blades seem to run differently or be more sensitive when running along the lower-flow operating line at Mach 0.10.

For selected, repeated operating fan speeds at Mo = 0.20 (fig. 9(a)), details of the radial distribution of pressure ratio, temperature ratio, and adiabatic efficiency from the bypass duct rakes are shown in figures 9(b) through (i), respectively. The TI blade pressure ratio was higher from the mid span to the tip. The TI blade temperature ratio was higher in the mid-span, but not at the very tip. The resulting efficiency was nearly identical in the hub to mid-span region, about 98.0 to 99.0 percent in the mid-span. The TI blade efficiency was about 1.0 percent better near the tip, for the higher fan speeds. For both blades, the highest fan speed had lower efficiency by 2 to 5 percent near the fan tip.

For the same fan speeds at Mo = 0.10 (fig. 10(a)), details of the radial distributions are shown in figures 10(b) through (i). An instability of the TI blades prevented testing at he higher fan speeds (at the lower fan flow rates of the Mo = 0.10 operating line). The average pressure and radial pressure distributions show the TI blades had a lower pressure rise than the GC from mid-span to the tip as fan speed was increased (TI blades were higher at Mo = 0.20). This significant reduction (with the core region showing no change) explains the unexpected reduction in bypass ratio for the TI blades at Mo = 0.10, noted above. The temperature at mid-span was lower with the TI blades as well. The TI blade efficiency no longer matched the GC blade. At 5,000 RPMc, the TI blade efficiency was higher at mid-span but was lower at the tip. At higher fan speeds, the TI efficiency dropped from mid-span to the tip (which did not happen at Mo = 0.20). This was quite a large difference with only 3 to 4 percent lower fan weight flow reduction on the Mo = 0.10 operating line (below the Mo = 0.20 operating line). Up to 7,740 RPMc, there was very little change in efficiency near the blade tip. The GC blades had reduced efficiency at the highest fan speed by 2 to 3 percent (somewhat less than at Mo = 0.20).

TI Versus GC Fan Operating Line Results at –15 Degree Angle, Smooth Rubstrip

Fan operating line performance data were also recorded for both the TI and GC blades, at a –15 degree blade angle setting with the smooth rubstrip installed. A comparison of the performance is shown in figure 11 (Note: there were no data recorded at Mach 0.15 for the GC blades and no data at Mach 0.20 for the TI blades). The open symbols are the TI results and the solid symbols are the GC results. In figures 11(a) and (b), the operating line pressure ratio and temperature ratio are quite similar. Where the same fan speed was run, the TI blades operated at a higher corrected flow, pressure ratio, and temperature ratio. The adiabatic efficiency (fig. 11(c)) shows little difference between the TI and GC blades at moderate fan speeds and flow. At Mach 0.10 and low flow the GC performance was a percent or so higher, while the TI blades were about 2.0 percent higher in efficiency at the highest speed and flow (75 lbm/sec). However, at 0.20 Mach number the GC blades had a 4.0 percent or greater penalty in efficiency at all speeds (flows). At –15 degrees, the GC blades appear more sensitive to increasing speed and flow that occurred going to 0.20 Mach number. Both the TI and GC blades show a reduction in efficiency as speed and flow were increased, whereas at the –9 degree settings, the efficiency was nearly constant until the higher speeds (flows) were reached. The bypass ratio (fig. 11(d)) shows a higher bypass ratio for the TI blades at 0.10 Mach number. The loading distribution (pressure rise) from the fan hub to tip may explain this.

For selected, repeated operating conditions at Mo = 0.10 (fig. 12(a)), details of the radial distribution of pressure ratio, temperature ratio, and adiabatic efficiency from the bypass duct rakes are shown in figures 12(b) through (i), respectively. The TI pressure ratio was higher, especially near the tip. The TI core pressure ratio was just slightly higher with the –15 degree angle, which may explain the higher bypass ratio with the TI blades. The TI temperature ratio was higher in the mid-span, but not as much at the very tip. The differences are larger than occurred at the –9 degree angle setting (fig. 9). The resulting efficiency was nearly identical in the hub to mid-span region, about 98.0 to 99.0 percent in the mid-span. The TI performance was about 1.0 percent better near the tip, for the higher fan speeds. For both blades, the higher fan speeds had reduced efficiency by 7 to 12 percent near the fan tip (from 73.0 to 66.0 percent and 89.5 to 77.5 percent). This penalty was larger than the 2 to 3 and 2 to 5 percent penalty (at Mo = 0.10 and 0.20, respectively) at the –9 degree angle setting with increased speed. At Mo = 0.10 the penalty at 7,740 RPMc was about 2 to 4 percent with the –15 degree angle, compared to no change at –9 degrees.

–9 and –15 Degree Angle Fan Operating Line Results, TI Blade, Smooth Rubstrip

The change in blade angle from –9 degrees (intended takeoff angle) to –15 degrees reduces the pressure ratio and weight flow obtained for each rotor speed. This is similar to changing the blade design point, except the blade twist is not reoptimized for new operating conditions. A comparison of the performance with the TI blades and smooth rubstrip is shown in figure 13 (there were no data recorded at Mach 0.20 at the –15 degree blade angle). The open symbols are the –9 degree results and the solid symbols are the –15 degree results. In figure 13(a), the pressure ratios follow nearly identical operating lines. But, in figure 13(b), the temperature ratio is higher for the –15 degree setting, at higher fan flows. The adiabatic efficiency (fig. 13(c)) shows the result of the higher temperature ratio. The efficiency at the –15 degree angle is much lower than at –9 degrees for the higher fan flows. At the highest speed and flow, the –15 degree performance was 5 to 10 percent lower. The efficiency is about the same for both angles at low speed and flow. The bypass ratio (fig. 13(d)) shows a higher bypass ratio at –15 degrees. This would be expected, since the –15 degree angle setting closes off the core.

Additional figures 13(e) and (f) show the pressure ratio and corrected fan weight flow versus corrected fan speed. At 8,750 RPMc (Mach 0.15) the pressure ratios are 1.285 and 1.231, for –9 and –15 degree angles, respectively. The corresponding corrected flows are 79.2 and 72.5 lb/sec. The pressure rise (e.g., (pressure ratio-1.0), or 0.285 and 0.231) was reduced about 19 percent, and the flow was reduced by 8 percent, by decreasing the blade angle by 6 degrees.

Another way to look at the adiabatic efficiency figure 13(c) is to identify a lower-loading condition to call its “takeoff” point. At a weight flow of 55 to 60 lbm/sec, the efficiency is about equal to the –9 degree angle efficiency at 80 lbm/sec (its takeoff flow rate). The corresponding fan speed is about 6,750 RPMc, or a 23 percent reduction, and pressure ratio is 1.13 to 1.14, or a pressure rise about ½ that for the –9 degree takeoff point (i.e., 0.14/0.28 = 0.5). The engine noise could be reduced substantially, but at the cost of doubling the number of engines or the engine flow area to get the same thrust.

For selected, repeated operating conditions at Mo = 0.15 (fig. 14(a)), details of the radial distribution of pressure ratio, temperature ratio, and adiabatic efficiency from the bypass duct rakes are shown in figures 14(b) through (i), respectively. The blade angle reduction to –15 degrees reduced the pressure ratio near the fan hub somewhat. The pressure ratio reduction near the fan tip was much larger. Using the RPMc = 8,750 curves, there was about 8 percent reduction in pressure rise (i.e., pressure ratio minus one) near the hub and about 26 percent reduction near the tip. The reduction in temperature rise was similar. The adiabatic efficiency was somewhat higher at the fan hub with the –15 degree angle, and was more dependent on fan speed than with the –9 degree angle. Similarly, the efficiency is much lower at the fan tip and very dependent on fan speed, with about 9.5 percent efficiency loss from 5,000 to 8,750 RPMc, compared to about 1.0 percent loss with the –9 degree blade angle.

–9 and –15 Degree Angle Fan Operating Line Results, GC Blade, Smooth Rubstrip

The GC blades were also tested at –9 and –15 degree angles. A comparison of the –9 and –15 degree angle performance with GC blades is shown in figure 15 (there were no data recorded at Mach 0.15 for either blade angle). The open symbols are the –9 degree results and the solid symbols are the –15 degree results. Overall, the results are the same as with the TI blades shown in figure 13. In figure 15(a), the pressure ratios follow a nearly identical operating line, as occurred with the TI

blades. A slightly higher pressure ratio (at equal weight flows) can be seen for the –15 degree angle at the highest flows. In figure 15(b), the temperature ratio is definitely higher for the –15 degree setting, at higher fan flows. The adiabatic efficiency (fig. 15(c)) shows the result of the higher temperature ratio. At Mach 0.10 the efficiency is high at low weight flow but decreases rapidly at high flow, almost the same as the TI blades at Mach 0.10 and 0.15 (fig. 13(c)). At the highest speed and flow the –15 degree angle performance was 5 to 10 percent lower than with the –9 degree angle. At Mach 0.20, the efficiency is even low at the lower flows, not like the data at the other Mach numbers, where the efficiency remained near 94 percent. The bypass ratio (fig. 15(d)) shows a higher bypass ratio with the –15 degree angle. However, the bypass ratios are closer at low flows for the GC blades and farther apart at low flows for the TI blades.

Additional figures 15(e) and (f) show the pressure ratio and corrected fan weight flow versus corrected fan speed. At 8,750 RPMc (Mach 0.10) the pressure ratios are 1.282 and 1.226, for –9 and –15 degree angles, respectively. The corresponding corrected flows are 78.2 and 71.1 lbm/sec. As was previously seen for the TI blades (at Mach 0.15), the pressure rise was reduced about 20 percent, and the flow was reduced by 9 percent, by decreasing the blade angle by 6 degrees. At Mach 0.20 the pressure rise was reduced about 22 percent and the flow was reduced by 10 percent with the 6 degree blade angle reduction.

For selected, repeated operating conditions at Mo = 0.10 (fig. 16(a)), details of the radial distribution of pressure ratio, temperature ratio, and adiabatic efficiency from the bypass duct rakes are shown in figures 16(b) through (i), respectively. As with the TI blades at 0.15, the blade angle reduction to –15 degrees reduced the pressure ratio near the fan hub somewhat and much larger near the fan tip. Using the 8,750 RPMc curves, there was about 8 percent reduction in pressure rise (i.e., pressure ratio minus one) near the hub and about 25 percent reduction near the tip. The temperature ratio reduction was similar. As with the TI blades, the efficiency is somewhat higher at the fan hub with the –15 degree angle, and more dependent on fan speed than with the –9 degree angle. Similarly, the efficiency is much lower at the fan tip and very dependent on fan speed, with about 9.5 percent efficiency loss from 5,000 to 8,750 RPMc, compared to about 1.0 percent loss with the –9 degree blade angle.

For similar repeated operating conditions at Mo = 0.20 (fig. 17(a)), details of the radial distribution of pressure ratio, temperature ratio, and adiabatic efficiency from the bypass duct rakes are shown in figures 17(b) through (i), respectively. The reductions with the –15 degree blade angle were similar, and just a little larger than at Mo = 0.10. Using the 8,750 RPMc curves, there was about 10 percent reduction in pressure rise near the hub and about 29 percent reduction near the tip. The overall efficiency was lower with the –15 degree angle at Mach 0.20, and the variation with fan speed was less than at Mach 0.10. Similarly, the efficiency was much lower at the fan tip but less dependent on fan speed than at Mach 0.10, with about 6.0 percent efficiency loss from 5,000 to 8,750 RPMc, compared to about 3.5 percent loss with the –9 degree blade angle.

Smooth Versus FCT Rubstrip Operating Line Results, TI Blade, –9 Degree Angle

Fan operating line performance data were recorded with the smooth rubstrip and with the FCT rubstrip installed, with the TI blades at the –9 degree blade angle. A comparison of the performance is shown in figure 18. The open symbols are with the smooth rubstrip and the solid symbols are with the FCT rubstrip. In figure 18(a), the operating line pressure ratios are similar, except the ratios with FCT rubstrip were noticeably lower at higher flow and pressure ratio (comparing points where the same fan speed was run, which are most of the nearby points). The corresponding temperature ratios (fig. 18(b)) appear similar to the pressure ratios. However, the temperature ratios for the smooth and FCT rubstrip were about the same at common fan speeds (or slightly lower with the FCT). The adiabatic efficiency

(fig. 18(c)) is correspondingly lower, by about 3.0 percent, with the FCT installed, even at the lower flow rates. The bypass ratio (fig. 18(d)) is also noticeably lower with the FCT rubstrip installed. The lower pressure ratio in the bypass duct, without a corresponding reduction in the core pressure ratio, would be expected to have this result.

For selected, repeated operating conditions at Mo = 0.20 (fig. 19(a)), details of the radial distribution of pressure ratio, temperature ratio, and adiabatic efficiency from the bypass duct rakes are shown in figures 19(b) through (i), respectively. The pressure ratios with the smooth and FCT rubstrips were equal at the core and out to mid-way in the bypass duct. The FCT rubstrip caused a significantly reduced pressure ratio approaching the tip of the fan. The temperature ratios were equal at the core and out to mid-way in the bypass duct, also. The FCT rubstrip caused a reduced temperature ratio approaching the tip of the fan, except very close to the tip. There, re-circulating flow of the FCT apparently was reheated and showed up as an increase in temperature at the tip, even though pressure ratio was lower at the tip. The resulting efficiency was similar in the hub to mid-span region, about 97.0 to 99.0 percent in the mid-span. The FCT performance penalty was located almost completely in the top 20 percent of the fan annular area, with a loss of about 9 to 11 percent at the tip, and 6 to 8 percent at the next radius inboard. The FCT design intent was to have significantly less re-circulating flow than actually occurred. That would have resulted in much less performance penalty for the FCT. For the smooth rubstrip, the highest fan speed lost about 2.5 to 5.5 percent in efficiency at the last two radii near the fan tip, compared to the lowest speeds. For the FCT rubstrip, that loss was about 2.0 to 7.0 percent in efficiency.

Fan Performance Map Results and Repeatability, GC Blade, –9 Degrees, Smooth Rubstrip

The performance data presented in this report, so far, have been on operating lines with a flight-type inlet and fixed-area flight-type nozzle installed. One of the fan blades (GC blades at –9 degree angle, smooth rubstrip) was tested very early in the test schedule (Run 5) in a full fan mapping configuration and much later in an operating line configuration (Run 40) at the end of the performance phase of the tunnel entry. The mapping configuration was with a bellmouth inlet replacing the flight inlet. A Variable Fan Exit Nozzle (VFEN) replaced the fixed-area flight nozzle, with radial blades operating like a butterfly valve to change the exit area. For the mapping runs, the freestream Mach number was set nominally at 0.05 Mach number to improve the inlet temperature uniformity. Each fan speed was set and data recorded with the VFEN set at a large area. Initially there was no flow through the core (the lowest pressure ratio and highest flow points). Reducing the VFEN area back-pressured the fan, forcing flow into the core, instead of separating off the back side of the fan hub. Further VFEN area reduction allowed performance mapping from cruise conditions, across the takeoff operating line, and toward fan stall.

For the later operating line run (being used for this comparison), data were taken at freestream Mach numbers of 0.10 and 0.20, with the flight inlet and nozzle installed. The bypass rake performance results are presented in figure 20, with the mapping data (Run 5) plotted with open symbols and the Mach 0.10 and 0.20 operating line data (Run 40) with solid symbols. The fan bypass pressure ratio map and temperature ratio map (versus fan corrected flow) are shown in figures 20(a) and (b). The operating line points match the mapping curves almost identically. The bypass adiabatic efficiency is shown in figure 20(c). The results show the efficiency repeats within better than 1.0 percent. At flow rates below about 75 lbm/sec, the efficiency is about 94.0 percent. At higher flow the efficiency drops, and at 83 lbm/sec the efficiency is about 91.0 percent. To complete the documentation of the fan operating line performance, the bypass ratio (W_{bypass}/W_{core}) is shown in figure 20(d). The mapping run bypass ratio varies from about 6 to 15 at low fan speed and 8 to18 at high fan speed. The operating line bypass ratio only varies from 9 at low speed to 12 at high speed.

The bypass ratio changes in different ways for mapping and operating line runs. Decreasing VFEN area in mapping runs increases back-pressure in the bypass duct only (not core), decreasing the bypass flow and the bypass ratio. Decreasing freestream Mach number in operating line runs changes the exit pressure of both the bypass and the core. For the operating line data, the result was increased bypass ratio with reduced flow (from lower freestream Mach number).

TI Versus GC Fan Map Results at –9 Degree Angle, Smooth Rubstrip

Fan map performance data were recorded for both the TI and GC blades, at the –9 degree blade angle with the smooth fan rubstrip installed. A comparison of the performance is shown in figure 21. The open symbols are the TI results and the solid symbols are the GC results. In figures 21(a) and (b), the mapped bypass pressure ratio and temperature ratio are almost the same for the two blade designs near the 0.10 Mach number operating line (shown), but everywhere else the TI and GC curves are different. At high flow, the TI blade pressure ratio and temperature ratio were higher than that of the GC blades. At lower flow, the TI blade pressure ratio and temperature ratio dipped down lower than the GC blades. At flows just above the Mach 0.10 operating line, the TI and GC performance curves cross and, where Mach 0.20 sea level operating line would be, the TI blades operated at a slightly higher corrected flow, pressure ratio, and temperature ratio. This is the same result seen in the operating line comparison (figs. 8(a) and (b)). As noted for those figures, though designed to be aerodynamically the same, the difference in stiffness and weight may cause differences in shape (twist) and performance as speed and loading changes for the TI and GC blades. At flows higher than the operating line, the reduced aerodynamic loading may allow the GC blades to untwist to a lower incidence, further reducing the GC pressure ratio relative to the TI blades. At flows just below the operating line, the increased aerodynamic loading may force the GC blades to twist to a higher incidence, increasing the GC pressure ratio. At much lower flows the two blades approach the same performance.

The bypass adiabatic efficiency (fig. 21(c)) and bypass ratio (fig. 21(d)) show differences between the TI and GC blades, also. For clarity, the efficiency curves were re-plotted separately for each fan speed in figure 22. For a given fan speed, the bypass ratio for the TI blade is higher than for the GC blades at low weight flow, but crosses over and becomes lower than the GC blades at higher flow. A check of the bypass and core flow values showed that the core flow was lower for the TI blades at lower fan flow and higher at high fan flow, which caused the bypass ratio differences.

As noted above, the efficiency for each TI and GC blade speed has been plotted on a separate plot (figs. 22(a) through (e)). At 5,000 RPMc, the few data points with lower efficiency (near 50 lbm/sec) are those where the core was not flowing. For those points, the efficiency is slightly better for the TI blades. The TI blades have nearly the same efficiency as the GC blades near where the core started flowing. At lower flow the TI blade performance fell off to about 1.0 percent below the GC blade. At 6,500 RPMc, the TI blades have nearly the same efficiency as the GC blades. Those points were near where the core started flowing (conditions without core flow were not set with the TI blades). Data were not taken to lower flow for the TI blades because high blade stresses were seen. At 7,740 RPMc, the two points with the highest flow were higher in efficiency than the GC blades by about 1.0 percent. The points near the 0.10 sea level operating line have the same efficiency. The other points at lower flow were lower than the GC blades by about 2.0 percent. At 8,290 (8,300 for GC) and 8,750 RPMc, similar TI efficiency benefit can be seen at flow higher than the 0.10 operating line (up to 2.0 percent higher), and efficiency penalties at flow below the 0.10 operating line (up to 2.0 percent lower). The operating line results (fig. 8(c)) gave the TI blades up to 2.0 percent lower efficiency at 0.10 Mach number, but show little difference above that, and about 3.0 percent higher efficiency than the GC blades at the highest speed (85 lbm/sec).

The peak efficiencies for the TI and GC blades were, respectively, 94.5 and 95.5 at 5,000 RPMc, 94.0+ and 95.0+ at 6,500 RPMc, 94.0 and 95.0 at 7,740 RPMc, 94.0- and 95.0- at 8,290 RPMc, and, 92.5 and 94.5- at 8,750 RPMc.

TI Versus GC Fan Map Results at –9 Degree Angle, FCT Rubstrip

Fan map performance data were recorded for both the TI and GC blades, at the –9 degree blade angle with the FCT fan rubstrip installed. A comparison of the performance is shown in figure 23. The open symbols are the TI results and the solid symbols are the GC results. In figures 23(a) and (b), the mapped fan pressure ratio and temperature ratio are only slightly different at flows below and including the Mach 0.10 operating line (shown). However, at high flow, the TI pressure ratio and temperature ratio were higher than the GC blades (similar to the smooth rubstrip results). The Mach 0.20 operating line would be at slightly higher flow than for the Mach 0.10 line, and the TI blades already show a slightly higher pressure ratio and temperature ratio than the GC blades. This is the same result seen at Mach 0.20 in the smooth rubstrip operating line comparison (fig. 8). However, in this case with the FCT installed, the pressure and temperature ratios at lower flows did not dip to the low levels seen with the smooth rubstrip (fig. 21).

The adiabatic efficiency (fig. 23(c)) and bypass ratio (fig. 23(d)) show differences between the TI and GC blades. For clarity, the efficiency curves were re-plotted separately for each fan speed in figure 24. For a given fan speed, the bypass ratio for the TI blade is slightly higher than for the GC blades at low weight flow, but crosses over and becomes lower than the GC blades at high flow. This is similar to the results with the smooth rubstrip and core weight flow differences are also the reason for the bypass ratio differences.

As noted above, the efficiency for each TI and GC blade speed has been plotted on a separate plot (figs. 24(a) through (c)). At 7,740 RPMc, the two points with the highest flow were higher than the GC blades by less than 1.0 percent (this is 0.5 percent less improvement than with the smooth rubstrip). At the 0.10 sea level operating line, both blades have the same efficiency. The other points at slightly lower flow were only lower than the GC blades by about 0.5 percent (this is about 1.5 percent less penalty than with the smooth rubstrip). At the lowest flow the TI and GC efficiencies are nearly equal again rather than the 2.0 percent reduction with the smooth rubstrip. At 8,290 and 8,750 RPMc, similar benefits can be seen at flow higher than the 0.10 operating line and 1.0 percent to no reduction at flow below the 0.10 operating line.

The peak efficiencies for the TI and GC blades were, respectively, 91.5 and 92.0 at 7,740 RPMc, 91.0+ and 91.0+ at 8,290 RPMc, and, 90.0+ and 91.0 at 8,750 RPMc. The FCT rubstrip minimized the efficiency difference between the blades, but overall both blades had a lower efficiency than either blade with the smooth rubstrip. The penalty with the FCT rubstrip was about 2.0 percent at 7,740 RPMc and about 3.0 percent at the higher fan speeds.

Smooth Versus FCT Rubstrip Fan Map Results, GC Blade, –9 Degree Angle

Fan map performance data were presented in the previous two sections of this report comparing TI and GC blades, firs with the smooth rubstrip and then with the FCT rubstrip. The smooth and FCT rubstrips are compared in this section, at the –9 degree blade angle, with the GC blade installed. A comparison of the performance is shown in figure 25. The open symbols are the smooth rubstrip results and the solid symbols are the FCT results. In figures 25(a) and (b), the mapped fan pressure ratio and temperature ratio are different. The pressure ratio and temperature ratio were lower with the FCT rubstrip than that with the smooth rubstrip. The differences were somewhat greater at higher

flows. At lower flow than the 0.10 Mach number operating line (shown), the pressure ratio and temperature ratio level off as flow is reduced.

The adiabatic efficiency (fig. 25(c)) and bypass ratio (fig. 25(d)) show differences between the smooth and FCT rubstrips. For clarity, the efficiency curves were replotted separately for each fan speed in figure 26. For each fan speed, the bypass ratios matched at lower weight flows, but then the bypass ratio with the FTC rubstrip appears higher at the higher flows. A check of the bypass and core flow values showed that the core flows were nearly the same for both rubstrips at low fan flow, but the core flow was lower for the FCT rubstrip at high fan flow, which caused the bypass ratio differences.

As noted above, the efficiency for each rubstrip and blade speed has been plotted on a separate plot (figs. 26(a) through (c)). The FCT rubstrip performed lower than the smooth rubstrip at all conditions. At 7,740 RPMc, the FCT rubstrip efficiency was lower than with the smooth rubstrip by 2.5 to 4.0 percent, with the penalty at the lowest fan flow rate only 1.0 percent. At 8,300 RPMc (8,290 for FCT), the penalty range was 2.0 to 4.0 percent, with the penalty at the lowest fan flow rate just over 1.0 percent. At 8,750 RPMc the range was 3.0 to 6.0 percent, with the penalty at the lowest fan flow rate again only about 1.0 percent.

The GC blades were used for acoustic testing at Mach 0.10, with the smooth and the FCT rubstrip. The operating speeds for the acoustic points of interest (takeoff, cutback, and approach) were 8,750, 7,525, and 5,425 RPMc, respectively. The Mach 0.10 operating line with the smooth rubstrip was documented directly and is shown in figure 8. The Mach 0.10 operating line conditions with the FCT rubstrip required interpolation from the fan map shown in figure 25. The cutback speed also required a slight extrapolation to the lower fan speed (7,740 RPMc was the lowest speed mapped). The approach speed required using the operating line with the TI blades and the FCT rubstrip (fig. 5) and correcting for the slight change (at that low speed condition) from TI to GC blades. Tables 3 and 4 give the fan weight flow (corrected to standard day), bypass duct pressure ratio, temperature ratio, and adiabatic efficiency, for the GC blades with the smooth and FCT rubstrips, respectively.

Smooth Versus FCT Rubstrip Fan Map Results, TI Blade, –9 Degree Angle

Fan map performance data were recorded for both the smooth and FCT rubstrips, at the –9 degree blade angle, with the TI blade installed. A comparison of the performance is shown in figure 27. The open symbols are the smooth rubstrip results and the solid symbols are the FCT results. In figures 27(a) and (b), the mapped fan pressure ratio and temperature ratio are different. The pressure ratio and temperature ratio were lower with the FCT rubstrip than that with the smooth rubstrip, but the differences are smaller than with the GC blades (fig. 25). The differences between rubstrips were somewhat greater at higher flows. Near the 0.10 Mach number operating line (shown), the pressure ratio and temperature ratio level off as flow is reduced (and actually dip lower with the smooth rubstrip).

The adiabatic efficiency (fig. 27(c)) and bypass ratio (fig. 27(d)) show differences between the smooth and FCT rubstrips. For clarity, the efficiency curves were re-plotted separately for each fan speed in figure 28. For each fan speed, the bypass ratios nearly matched at the lower flows but the bypass ratio curves appear higher for the FTC rubstrip at higher flows, as seen with the GC blades. A check of the bypass and core flow values showed that the core flows were nearly the same for both rubstrips at low fan flow, but the core flow was lower for the FCT rubstrip at high fan flow, which caused the bypass ratio differences.

As noted above, the efficiency for each rubstrip and blade speed has been plotted on a separate plot (figs. 28(a) through (e)). The FCT rubstrip performed lower than the smooth rubstrip at all conditions. At 5,000 RPMc, the FCT rubstrip efficiency was lower than with the smooth rubstrip by 1.0 to 1.5 percent. At 6,250 RPMc, the penalty was about 1.5 to 2.0 percent. At 7,740 RPMc, the penalty ranged from 1.5 to 3.0 percent, with the higher penalty at the higher fan flow rates. At 8,300 and 8,750 RPMc, the penalty range increased to 1.5 to 5.0 percent, with the higher penalty again at the higher fan flows.

Smooth Versus FCT Rubstrip Fan Map Results, TI Blade, –15 Degree Angle

Fan map performance data were recorded for both the smooth and FCT rubstrips, at the –15 degree blade angle, with the TI blade installed. A comparison of the performance is shown in figure 29. The open symbols are the smooth rubstrip results and the solid symbols are the FCT results. In figures 29(a) and (b), the mapped fan pressure ratio and temperature ratio are different. The differences are larger than with the –9 degree angle setting (figs. 27(a) and (b)). The FCT pressure ratio and temperature ratio were lower than with the smooth rubstrip. The differences in pressure and temperature ratio were greater at mid to high fan flows. At flow well below the 0.10 Mach number operating line (shown), the pressure ratio leveled off as flow was reduced with the smooth rubstrip, but not with the FCT, which continued to increase in pressure ratio.

The adiabatic efficiency (fig. 29(c)) and bypass ratio (fig. 29(d)) show differences between the TI and GC blades. For clarity, the efficiency curves were re-plotted separately for each fan speed in figure 30. For each fan speed, the bypass ratios nearly matched at the lower flows but the bypass ratio curves appear higher for the FTC rubstrip at higher flows, as seen with the –9 degree angle. The bypass ratio reduction with the FCT is slightly greater with the –15 degree blade angle than with the –9 degree angle.

As noted above, the efficiency for each fan speed has been plotted on a separate plot (figs. 30(a) through (e)). With the –15 degree blade angle, the data show an increased performance penalty associated with using the FCT rubstrip. At 5,000 RPMc, the FCT rubstrip efficiency was lower than with the smooth rubstrip by 2.0 to 4.0 percent (higher than the 1.0 to 1.5 percent for the –9 degree angle). At 6,250 RPMc, the penalty was also 2.0 to 4.0 percent (higher than the 1.5 to 2.0 percent for –9 degrees). At 7,740 RPMc, the penalty ranged from 3.0 to 5.0 percent (higher than the 1.5 to 3.0 percent with –9 degrees), with the higher penalty at the higher fan flow rates. At 8,290 RPMc, the penalty range increased to 3.5 to 6.0 percent (higher than the 1.5 to 5.0 percent with –9 degrees). And, at 8,750 RPMc the penalty range was 3.5 to 7.0 percent (higher than the 1.5 to 5.0 percent with –9 degrees), with the higher penalty again at the higher fan flows.

Smooth Versus FCT Rubstrip Fan Map Results, TI Blade, 0 Degree Angle

Fan map performance data were recorded for both the smooth and FCT rubstrips, at the 0 degree (design) blade angle, with the TI blade installed. A comparison of the performance is shown in figure 31. The open symbols are the smooth rubstrip results and the solid symbols are the FCT results. In figures 31(a) and (b), the mapped fan pressure ratio and temperature ratio are different, but mostly at the higher fan weight flows. The FCT pressure ratio and, to a lesser degree, temperature ratio were lower than with the smooth rubstrip. Near the 0.10 Mach number operating line (shown), there was not much difference.

The adiabatic efficiency (fig. 31(c)) and bypass ratio (fig. 31(d)) show differences between the smooth and FCT rubstrips. For clarity, the efficiency curves were re-plotted separately for each fan speed in figure 32. For each fan speed, the bypass ratios nearly matched at the lower flows but the bypass ratio curves appear higher for the FTC rubstrip at higher flows, as seen with the other blade angles. The bypass ratio reduction with the FCT is slightly greater with the 0 degree blade angle than with the –9 degree angle. Also, the overall level of the bypass ratio appears higher with the 0 degree blade angle.

As noted above, the efficiency for each fan speed has been plotted on a separate plot (figs. 32(a) through (d)). The FCT performed somewhat lower than the smooth rubstrip at all conditions. At 5,000 RPMc, the penalty was about 0.5 to 1.0 percent. At 6,500 RPMc, the penalty was about

1.0 percent. At 7,740 RPMc, the penalty was about 1.0 to 2.0 percent. And, at the cruise design speed of 8,400 RPMc, the penalty was 1.5 to 2.5 percent. These FCT penalties with the cruise design blade angle are much less than with the –9 and –15 degree angles.

TI Versus GC Single-Radius Map Results at –9 Degree Angle, Smooth Rubstrip

The comparison of TI and GC blade fan maps, at the –9 degree blade angle, with the smooth rubstrip (fig. 21) showed an unusual drop or leveling off of the TI blade pressure ratio as the flow was reduced below the 0.10 Mach number operating line (shown). A further comparison of the performance is shown here in figure 33, where the averaged pressure ratios at individual radii near the blade tip are plotted. The open symbols are the TI results and the solid symbols are the GC results. In figures 33(a) through (c) pressure ratio data from the 10th (outer most), 9th, and 8th radii are shown. At high fan speeds, the TI pressure ratio shows an extreme drop as flow was reduced. The GC blades show a similar but lesser drop, and it occurred at a lower flow. At the 7th radius (fig. 33(d)) the TI pressure ratio drop was reduced, and the GC had very little drop. The plots show that an extensive portion of the TI blade changed its performance as the flow was reduced below the 0.10 Mach number operating line. The GC blade performance change was less and occurred at lower flows (further from the 0.10 Mach number operating line).

As with the averaged pressure ratios, the averaged temperature ratios at individual radii near the blade tip are plotted in figure 34. The open symbols are the TI results and the solid symbols are the GC results. The temperature ratio plots for the 10th (outer most) radius (fig. 34(a)) is very much like the pressure ratio plot of figure 33(a). The TI blades show a temperature drop or leveling-off as the flow was reduced below the 0.10 Mach number operating line. However, the temperature difference between TI and GC blades disappears at the lowest flows (figs. 34(b) through (d)), while the pressure still shows a penalty for the TI blades (figs. 33(b) through (d)).

The effect on the adiabatic efficiency of the different pressure and temperature ratio characteristics are shown in figure 35, where the averaged adiabatic efficiencies at individual radii near the blade tip are plotted. At high fan flow the efficiency of the TI blades is significantly higher than the GC blades near the tip (figs. 35(a) through (c)). At the reduced flows where the pressure and temperature ratio drops were noted, the efficiency of the TI blades drops dramatically below the GC blades. At the 7th radius (fig. 35(d)) the performance differences are similar to but smaller than at the outer three radii.

To clarify TI and GC efficiency differences, the efficiency at each TI blade speed has been plotted on a separate plot (figs. 36(a) through (e)) for the 10th (outer most) measurement. At 5,000 RPMc, the TI efficiency was about 4.0 percent higher than the GC blades at higher flow. At lower flow, near peak efficiency and the 0.10 Mach number operating condition; the TI blades had nearly the same efficiency as the GC blades. At lower flow the TI performance fell off to about 1.0 percent below the GC blade. At 6,500 RPMc, the efficiency was about 4.0 percent higher for the TI blades at higher flow. Data were not taken to lower flow for the TI blades because of the high blade stresses. At 7,740 RPMc, the two points with the highest flow were higher than the GC blades by about 5.5 percent. The points near the peak efficiency and the 0.10 Mach number operating condition have the same efficiency. The other points at lower flow were lower in efficiency than the GC blades by about 3.0 percent. At 8,290 and 8,750 RPMc, the TI efficiency is as much as 8.0 percent higher than the GC efficiency at the highest fan flow. The points near the peak efficiency and the 0.10 Mach number operating condition have the same efficiency. The other points at lower flow were lower in efficiency than the GC blades by about 3.0 percent.

TI Versus GC Single-Radius Map Results at –9 Degree Angle, FCT Rubstrip

The comparison of TI and GC blade fan maps, at the –9 degree blade angle, with the FCT rubstrip (fig. 23) showed very little drop of the TI blade pressure ratio as the flow was reduced below the 0.10 Mach number operating line (shown), much different than the drop with the smooth rubstrip. A further comparison of the performance is shown here in figure 37, where the averaged pressure ratios at individual radii near the blade tip are plotted. The open symbols are the TI results and the solid symbols are the GC results. In figures 37a, b, c, and d, pressure ratio data from the 10th (outer most), 9th, 8th, and 7th radii are shown. At high fan speeds, the TI pressure ratio shows a leveling off as flow was reduced, and some drop at the 8th and 7th radii. The GC blades show a similar leveling, but it occurred at a lower flow. The leveling was less noticeable at 7,740 RPMc than at the higher two fan speeds. Once the GC blade levels off the pressure ratio matches the TI blades almost exactly. The plots show that an extensive portion of the both blades changed performance as the flow was reduced below the 0.10 Mach number operating line. It occurred for the GC blade a lower fan flow.

As with the averaged pressure ratios, the averaged temperature ratios at individual radii near the blade tip are plotted in figure 38. The open symbols are the TI results and the solid symbols are the GC results. These temperature ratio plots are somewhat like the pressure ratio plots of figure 37, but the differences are smaller. The TI blades have a higher temperature ratio at high fan flow, and it dips below the GC blades as the flow was reduced, especially for the 8th and 7th radii. With the FCT rubstrip, both the pressure difference and temperature difference between TI and GC blades disappears at the lowest flows.

The effect on the adiabatic efficiency of the different pressure and temperature ratio characteristics are shown in figure 39, where the averaged adiabatic efficiencies at individual radii near the blade tip are plotted. At high fan flows the efficiency of the TI blades is significantly higher than the GC blades near the tip (figs. 39(a) through (c)). At the lower flows where the pressure and temperature ratio drops were noted, the efficiency of the TI blades drops dramatically below the GC blades. At the 7th radius (fig. 39(d)) the performance differences are similar to but smaller than at the outer three radii.

To clarify TI and GC efficiency differences, the efficiency at each TI blade speed has been plotted on a separate plot (figs. 40(a) through (c)) for the 10th (outer most) measurement. At 7,740 RPMc, at the highest flow the TI blade efficiency was higher than the GC blades by about 3.5 percent. At lower flow, near peak efficiency and the 0.10 Mach number operating condition, the TI blades had nearly the same efficiency as the GC blades. For the next lower point (66 lbm/sec) the TI blade efficiency was about 2.0 percent lower than the GC. Then the lowest flow point for the TI blade is almost exactly equal to the GC efficiency. At 8,290 RPMc, at the highest flow the TI blade efficiency was higher than the GC blades by about 5.5 percent. At lower flow, near peak efficiency and the 0.10 Mach number operating condition, the TI blades had nearly the same efficiency as the GC blades. For the next lower point (69 lbm/sec) the TI blade efficiency was about 3.0 percent lower than the GC. Then the lowest flow point for the TI blade is almost exactly equal to the GC efficiency. At 8,750 RPMc, at the highest flow the TI blade efficiency was higher than the GC blades by about 7.5 percent. At lower flow, near peak efficiency and the 0.10 Mach number operating condition, the TI blades had nearly the same efficiency as the GC blades. For the next lower point (73 lbm/sec) the TI blade efficiency was about 2.5 percent lower than the GC. And, again, the lowest flow point for the TI blade is almost exactly equal to the GC efficiency.

Smooth and FCT Single-Radius Map Results, TI Blades, –9 Degree Angle

The comparison of smooth and FCT rubstrip fan maps, at the –9 degree blade angle, with the GC blades (fig. 25) and TI blades (fig. 27) showed reduced pressure and temperature ratios, and 2.5 to

6.0 percent and 1.0 to 5.0 percent lower efficiency, respectively, with the FCT installed. A further comparison of the performance is shown here in figure 41, where the averaged pressure ratios at individual radii near the blade tip are plotted. The open symbols are the smooth rubstrip results and the solid symbols are the FCT results. In figures 41(a) through (d), pressure ratio data from the 10th (outer most), 9th, 8th, and 7th radii are shown. At low fan speed the smooth and FCT rubstrip pressure ratios look similar, with the FCT somewhat lower than the smooth rubstrip. At high rotor speeds, the pressure ratio is significantly lower for the FCT. The smooth rubstrip results show the unusual drop in the pressure ratio noted in the discussion of figures 21 and 33. There, the pressure ratio drop occurred at lower flow rates for the GC blades than for the TI blades. Here, in figure 41, the effect of the FCT rubstrip on the pressure ratio was to reduce the drop dramatically, at the 10th (outer most) and 9th radii. The reduction was not as large at the 8th radius, and there was not much difference at the 7th radius. Just as with the performance penalty, the FCT tip treatment affected the unusual performance change in the tip region only.

As with the averaged pressure ratios, the averaged temperature ratios at individual radii near the blade tip are plotted in figure 42. The open symbols are the smooth rubstrip results and the solid symbols are the FCT results. The temperature ratio plot for the 10th radius (fig. 42(a)) is different from the pressure ratio plot of figure 41(a), in that the temperature ratios are higher with the FCT rubstrip (the pressure ratio was lower). For the three lower radii (figs. 42(b) through (d)) the temperature ratios were lower with the FCT than with the smooth rubstrip, as were the pressure ratios (figs. 41(b) through (d)). The temperature ratios do not have the sudden drop with reduced fan flow seen for the pressure ratios, but they do level off with the smooth rubstrip installed.

The effect on efficiency of the different pressure and temperature ratio characteristics shown above, are shown in figure 43, where the averaged adiabatic efficiencies at the 10th (outer most) measurement radius near the blade tip is plotted. To clarify smooth and FCT rubstrip efficiency differences, the efficiency of each fan speed has been plotted on a separate plot (figs. 43(a) through (e)). At 5,000 RPMc, the FCT rubstrip efficiency near the fan tip was lower by 5 to 8 percent. At 6,250 RPMc, the FCT rubstrip efficiency near the fan tip was lower by 8 to 11 percent. At 7,740 an 8,300 RPMc, the FCT rubstrip efficiency near the fan tip was lower by 9 to 12 percent. At 8,750 RPMc, the FCT rubstrip efficiency near the fan tip was lower by 10 to 13 percent. This penalty could be reduced if the recirculating flow of the FCT were reduced. The FCT flow rate appeared to be well above that required for stall management.

TI Blade Instability Occurrences

Initial tests with the TI blades installed were fan mapping runs which included strain gages installed on the fan blades. Occasional automatic “VFEN safe” actions occurred due to high fan blade stresses, where the VFEN area would be opened rapidly to a “safe” condition. This was not considered important because the fast acting VFEN easily was able to open and reduce the blade strain. However, when tests on the acoustic operating lines were started with the flight inlet and fixed area nozzle installed, there was no way to quickly move out of high stress conditions except a rig emergency shutdown. There were several high stress instabilities that occurred and began to limit operation to well below the intended takeoff speed of 8,750 RPMc. Between two back-to-back wind tunnel runs, a single inlet boundary layer rake was removed from STA 2.0 directly in front of the fan (removing the slight flow disturbance), and the operating line testing was attempted with a completely clean inlet. The fan instabilities with speed still occurred. At the time there were theories proposed, but no definitive cause of the instability was identified.

The tip radii map performance results shown in this report (e.g., plots at the outer four duct rake radii) show that a dramatic loading change occurred as the flow was driven down in the stall direction by closing the VFEN (along constant RPMc lines). The blades may show an oscillation in performance between high and low loading conditions where this loading change occurs. The data

points where the rapid change in pressure ratio at the 10th (outer most) radius occurred were identified for both blade designs (TI and GC) and both rubstrips (smooth and FCT) from figures 33 and 37.

Figure 44 shows the low flow and high flow (i.e., low performance and high performance) transition points as solid and open circles, for both blade designs with the smooth rubstrip installed. The GC blades are shown in black and the TI blades in red. Fan operating lines for Mach 0.10, 0.15, and 0.20 are also shown. The GC transition points are at lower flow and farther away from the operating lines than the TI blades. Near 70 lbm/sec flow and 1.20 pressure ratio, the lower Mach number operating lines are actually between the transition points for the TI blades (but not for the GC blades). There were two fan instability points identified during testing for the TI blades. One was at Mach 0.10 and the other at Mach 0.125. They are plotted as blue triangles and are located right between to two transition data points for the TI blades.

Figure 45 shows the low flow and high flow transition points as solid and open circles, for both blade designs with the FCT rubstrip installed. As above, the GC blades are shown in black and the TI blades in red. Fan operating lines for Mach 0.10, 0.15, and 0.20 are also shown. The GC transition points are at lower flow and farther away from the operating lines than the TI blades. Again, near 70 lbm/sec flow and 1.20 pressure ratio, the lower Mach number operating lines are actually between the transition points for the TI blades (but not for the GC blades). There were five fan instability points identified during testing for the TI blades. Two were at Mach 0.10, two at Mach 0.15 and one at Mach 0.20. They are plotted as blue triangles, squares, and a diamond, respectively. The Mach 0.10 fan instability points are near high-flow edge of the transition data points for the TI blades. The Mach 0.15 instability points are between the transition data points, near the high-flow edge. And, the Mach 0.20 instability point is located near the high-flow edge of the transition points. The FCT shifted the transition points to somewhat lower fan flows, but since the operating lines were still between the transition points for the TI blades, the FCT did not prevent the occurrence of fan blade instabilities.

Summary of Results

A large scale model representative of a low-noise, high bypass ratio turbofan engine was tested for acoustics and performance in the NASA Glenn 9- by 15-Foot Low-Speed Wind Tunnel. The low tip speed ADP-type fan, nacelle, with an un-powered, flow-through core passage (with core inlet guide vanes) were simulated. The fan duct and core inlet were instrumented with total pressure and total temperature rakes. Fan performance comparisons were made for repeatability, blade material (Titanium and Graphite/Composite), blade angle (–9 degrees, takeoff; –15 degrees, lower loading; 0 degrees, design), and fan rubstrip (smooth and Fan Casing Treatment).

Pairs of operating line runs and fan mapping runs were compared and showed that averaged pressure and temperature ratio (versus fan flow rate) repeated very well, and adiabatic efficiency, from those measurements, repeated within better than 1.0 percent. Similar results were seen in comparisons of the radial distribution of pressure and temperature ratio, and efficiency (still within about 1.0 percent repeatability).

The TI and GC blade operating line performance was documented during fixed area nozzle runs (with the smooth rubstrip installed and a –9 degree blade angle). The TI blades had slightly higher pressure and temperature ratio than the GC blades, at the same fan speeds, and the efficiency was up to 3.0 percent higher at the higher speeds, but up to 2.0 percent lower at lower speeds. This may be the result of slightly different shapes between the TI and GC blades as speed and blade loading were increased. The comparisons of the radial distributions of pressure and temperature ratio showed the TI performance changes (above GC at Mach 0.20 and below GC at Mach 0.20) were mostly from blade mid span to the tip (though the temperature difference disappeared at the tip). The efficiency was nearly the same from the hub through the mid span,

and the TI blade was only 1.0 percent higher near the tip. So, there were moderate performance differences between the TI and GC blades along the Mach 0.10 and 0.20 operating lines.

The TI and GC blade operating line performance was also documented at a –15 degree blade angle (with the smooth rubstrip installed). With the lower –15 degree blade angle setting the trends were similar to the –9 degree data. However, the GC blades showed a 3.0 to 4.0 percent penalty at 0.20 Mach number that was not there at –9 degrees. Also, the efficiency fell increasingly for both blade designs as speed and flow were increased. With the –9 degree angle the efficiencies were nearly constant until the higher speeds and flows were reached, then the efficiency dropped. If the lower flow, high efficiency point were taken as the takeoff condition for a new engine (i.e., reduced fan speed and pressure ratio), the noise would be reduced, but the number of engines or the engine flow area would have to double to get the same thrust.

With the –15 degree angle (both blades), the radial distributions of pressure and temperature ratio were similar to the –9 degree data, with the increase for the TI blades a bit higher from the hub to the tip for –15 degrees. The efficiency distributions showed a penalty further from the tip for both blades. Also, at higher fan speeds, there was 7 to 12 percent lower efficiency near the tip (compared to mid span), a lot larger than the 2 to 5 percent at the –9 degree settings. Similarly, the efficiency was much lower near the fan tip and very dependent on fan speed, with about 9.5 percent efficiency loss from 5,000 to 8,750 RPMc, compared to about 1.0 percent loss with the –9 degree blade angle, at Mach 0.10. However, the loss with increased fan speed at Mach 0.20 was only about 6.0 percent, compared to about 3.5 percent loss with the –9 degree blade angle.

Differences between the smooth and FCT rubstrips were documented along fan operating lines with the TI blades at the –9 degree angle. The pressure ratios were lower with the FCT rubstrip (at equal fan speed) and the temperature ratios were only a little lower. The corresponding efficiency was about 3.0 percent lower at all flow rates. The radial distributions showed the FCT pressure loss occurred from mid span to the tip. There was a temperature loss starting at mid span, also, but recirculating flow caused an increased temperature at the tip, even though the pressure ratio was lower at the tip. The efficiency distribution showed the loss (of 6 to 11 percent) was almost completely in the top 20 percent of the fan annular area.

The TI and GC blade fan mapping performance was documented during VFEN nozzle runs with both the smooth and FCT rubstrips installed (at –9 degree blade angle). Near the 0.10 Mach number operating line, the TI and GC blade pressure and temperature ratios and efficiencies were similar (but lower with FCT). At higher fan flow than the operating line, the TI blades had higher pressure and temperature ratios, and higher efficiencies than the GC blades. At lower flow than the operating line, the TI pressure and temperature ratios and efficiencies dropped lower than the GC. The difference was much less with the FCT rubstrip. The TI blade efficiency benefit at higher flow was 1.0 to 2.0 percent, and 2.0 percent penalty at lower flow. The difference in performance away from the Mach 0.10 operating line may be caused by differing blade twist changes. The TI blade shape would be dominated by centrifugal loads, basically changing with fan speed. The light GC blades may respond to air loads and change twist differently, thereby changing the airfoil angle and loading.

The smooth and FCT rubstrip mapping performance was compared at the –9 degree blade angle, with both the GC blades, and then the TI blades. With both blades the pressure ratio was lower with the FCT rubstrip than with the smooth rubstrip, and the same was true of the temperature ratio except at lower flow rates. The difference was greater with the GC blades than with the TI blades. The efficiency with the FCT rubstrip was lower than with the smooth rubstrip at all conditions. With the GC blades the penalty ranged from 2.5 to 4.0 percent at 7,740 RPMc, 2.0 to 4.0 percent at 8,300 RPMc, and 3.0 to 6.0 percent at 8,750 RPMc. The corresponding penalty with the TI blades ranged from 1.0 to 1.5 percent at 5,000 RPMc, 1.5 to 3.0 percent at 7,740 RPMc, and 1.5 to 5.0 percent at 8,300 and 8,750 RPMc (somewhat less penalty than with the GC blades). The higher penalties occurred at the higher flow rates for each fan speed. The smooth and FCT rubstrip mapping performance was also compared at the –15 degree and zero degree blade

angles, with the TI blade installed. The performance differences were similar to the –9 degree angle data, but the differences were larger with the –15 degree and significantly smaller with the zero degree blade angle.

An unusual drop or leveling off of the TI blade pressure ratio occurred with the smooth rubstrip as the flow was reduced, and was investigated by plotting results at individual radii near the blade tip. The TI pressure ratio showed an extreme drop as flow was reduced, especially at high fan speeds. The GC blades show a similar but lesser drop, and it occurred at a lower flow. The temperature ratio results were similar, but the difference between the TI and GC blades disappeared at lower flows. At high fan flow and speed, the efficiency of the TI blades was significantly higher than the GC blades near the tip (up to 8.0 percent). At the reduced flow where the pressure and temperature drop was noted, the efficiency of the TI blades dropped dramatically below the GC blades (about 3.0 percent).

The performance results of the GC and TI blades at individual radii near the blade tips were also investigated with the FCT rubstrip installed. There was very little drop of the TI blade pressure ratio as the flow was reduced below the Mach 0.10 operating line (quite different from the drop-off with the smooth rubstrip). The temperature ratio changes were similar to the pressure ratio, but smaller. The efficiency differences between the TI and GC blades were similar to the results with the smooth rubstrip (up to 7.5 percent high at high flow and 2.5 percent low at low flow).

A comparison of the performance results at individual radii with the smooth and FCT rubstrips was made with the TI blades, at –9 degree blade angle. As noted above, the FCT rubstrip smoothed out the large drop in pressure ratio as flow was reduced. But, that was accompanied by a lower pressure ratio and higher temperature ratio overall. That resulted in much lower efficiency. (5.0 to 13.0 percent for the outermost radius). This penalty could be reduced if the recirculating flow of the FCT were reduced. The FCT flow rate appeared to be well above that required for stall management.

The unusual changes in loading that were identified near the blade tip were related to several high blades stress instabilities that occurred while testing the TI blades. The operating conditions for the instabilities were shown to occur between two distinct fan flow boundaries where dramatic changes in the blade tip performance occurred. The high and low boundaries for the TI blades occurred near the fixed nozzle operating lines, while the GC blade boundaries were at lower fan flows and away from the fixed nozzle operating lines. This seems to be why the GC blades did not have the instabilities that occurred with the TI blades.

As expected, the effect of the FCT rubstrip was a performance penalty. The amount of recirculating flow at the fan tip was larger than required for the desired stall margin improvement, however. Reducing the FCT flow would also reduce the resulting performance penalty. There was a somewhat surprising performance difference between the TI and GC blades, mostly away from the fixed-nozzle operating lines. Though both blades showed some indication of a flow transition near the blade tips as fan flow was reduced, the transition occurred near the fixed flight-type nozzle takeoff operating lines with the TI blades and resulted in high blade stress instabilities.

Though the pressure and temperature ratios were low for this fan design, the techniques used to improve thermocouple measurement accuracy gave repeated data runs with the adiabatic efficiency agreeing within one percent. The measured fan adiabatic efficiency at takeoff was 93.7 percent which matched the design intent well.

References

1. Society of Automotive Engineers, “In-Flight Thrust Determination,” SAE AIR 1703, Nov. 1985, Reaffirmed Dec. 1992.
2. MIDAP Study Group, “Guide to In-Flight Thrust Measurements of Turbojets and Fan Engines,” AGARDOGRAPH AG-237, 1979.

3. Robert J. Jeracki, “Model Engine Performance Measurement from Force Balance Instrumentation,” NASA/TM—1998-208486, 1998.
4. James Dittmar and David Elliot, “Some Acoustic Results from the Pratt and Whitney Advanced Ducted Propulsor–Fan 1” NASA/TM—1999-209049, 1999.
5. E. Brian Fite, “Report of Fan Performance from Duct Rake Instrumentation on a 1.294 Pressure Ratio, 725 ft/sec Tip Speed Turbofan Simulator Using Vaned Passage Casing Treatment,” NASA/TM—2006-214241, 2006.
6. Richard Woodward, David Elliot, Christopher Hughes, and J.J. Berton, “Benefits of Swept and Leaned Stators for Fan Noise Reduction,” NASA/TM—1998-208661, AIAA–99–0479, 2001.
7. Christopher Hughes, “Aerodynamic Performance of Scale-Model Turbofan Outlet Guide Vanes Designed for Low Noise,” NASA/TM—2001-211352, AIAA–2002–0374, January 2002.
8. John Gazzaniga, “Performance of Advanced Fan Exit Guide Vane Concepts for High Speed Fans,” AIAA–2002–0377, January 2002.
9. Ronald H. Soeder, “NASA Lewis 9- by 15-Foot Low Speed Wind Tunnel Users Manual,” NASA TM–106247, 1993.
10. Society of Automotive Engineers, “Gas Turbine Engine Performance Station Identification and Nomenclature,” ARP 755A, 1974.
11. AGAARD, “Recommended Practices for Measurement of Gas Path Pressures and Temperatures for performance Assessment of Aircraft Turbine Engines and Components,” AGARD-AR no. 245, 1990.
12. David E Hobbs, Robert J. Neubert, et. al., “Low noise Research Fan Stage Design,” NASA CR-195382, 1995.

TABLE 1.—FAN DESIGN PARAMETERS

Pressure Ratio (Bypass, Stage)	
SLTO	1.284
Cruise	1.294
Approach	1.077
Cutback	1.209
Corrected Fan Speed, RPMc	
SLTO	8,750 (104.2%)
Cruise	8,400 (100.0%)
Approach	5,000 (59.5%)
Cutback	7,740 (92.1%)
Corrected Fan Tip Speed, Uc_{TIP} (ft/sec)	
SLTO	840
Cruise	806
Approach	480
Cutback	743
Corrected Specific Weight Flow, WFc/A ($lbm/sec/ft^2$)	
SLTO	36.9
Cruise	42.5
Approach	22.7
Cutback	33.3
Bypass Ratio-Cruise	13.3
Blade Number	0.18
Vane Number	0.45
Hub/tip Ratio	0.426
Diameter-Leading Edge	22.0

TABLE 2.—FAN MODEL CONFIGURATIONS

Blade Design	Blade Angle	Rubstrip
GC	–9 degrees	Smooth
GC	–9 degrees	FCT
GC	–15 degrees	Smooth
TI	–9 degrees	Smooth
TI	–9 degrees	FCT
TI	–15 degrees	Smooth
TI	–15 degrees	FCT
TI	0 degrees	Smooth
TI	0 degrees	FCT

TABLE 3.—ACOUSTIC OPERATING CONDITIONS-GC BLADE WITH SMOOTH RUBSTRIP

Condition	RPMc	WFc (lbm/s)	RAARPT12	RAARTT12	EADAR12
Takeoff	8,750	78.11	1.2816	1.07842	0.9368
Cutback	7,525	68.17	1.2052	1.05782	0.9475
Approach	5,425	49.43	1.0994	1.02915	0.9412

TABLE 4.—ACOUSTIC OPERATING CONDITIONS-GC BLADE WITH FCT RUBSTRIP

Condition	RPMc	WFc (1bm/s)	RAARPT12	RAARTT12	EADAR12
Takeoff	8,750	76.53	1.2685	1.07789	0.9026
Cutback	7,525	66.74	1.1953	1.05712	0.9152
Approach	5,425	49.08	1.0972	1.02904	0.9249

Figure 1(a).—ADP type engine model in the NASA Glenn 9- by 15-Foot Low-Speed Wind Tunnel.

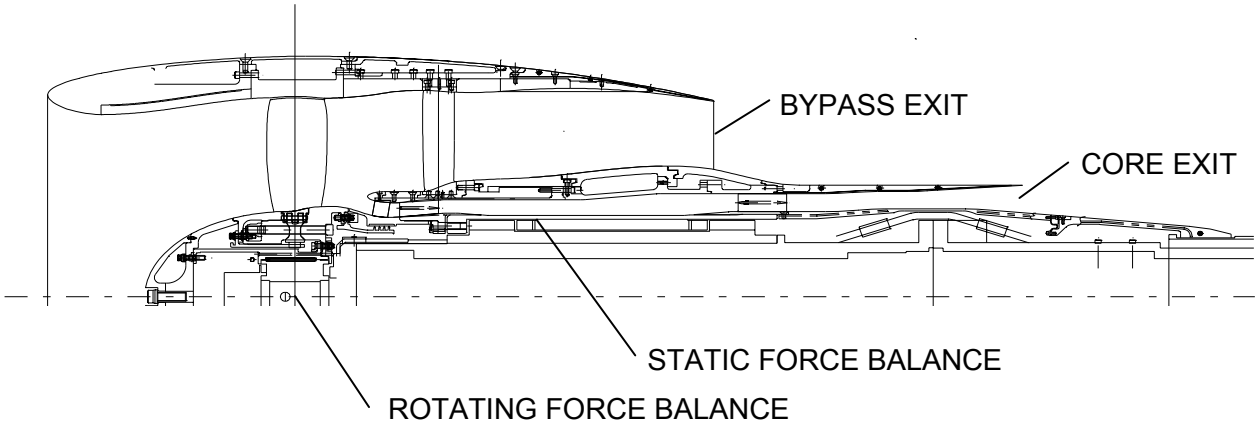

Figure 1(b).—The 22-inch diameter fan engine model cross section.

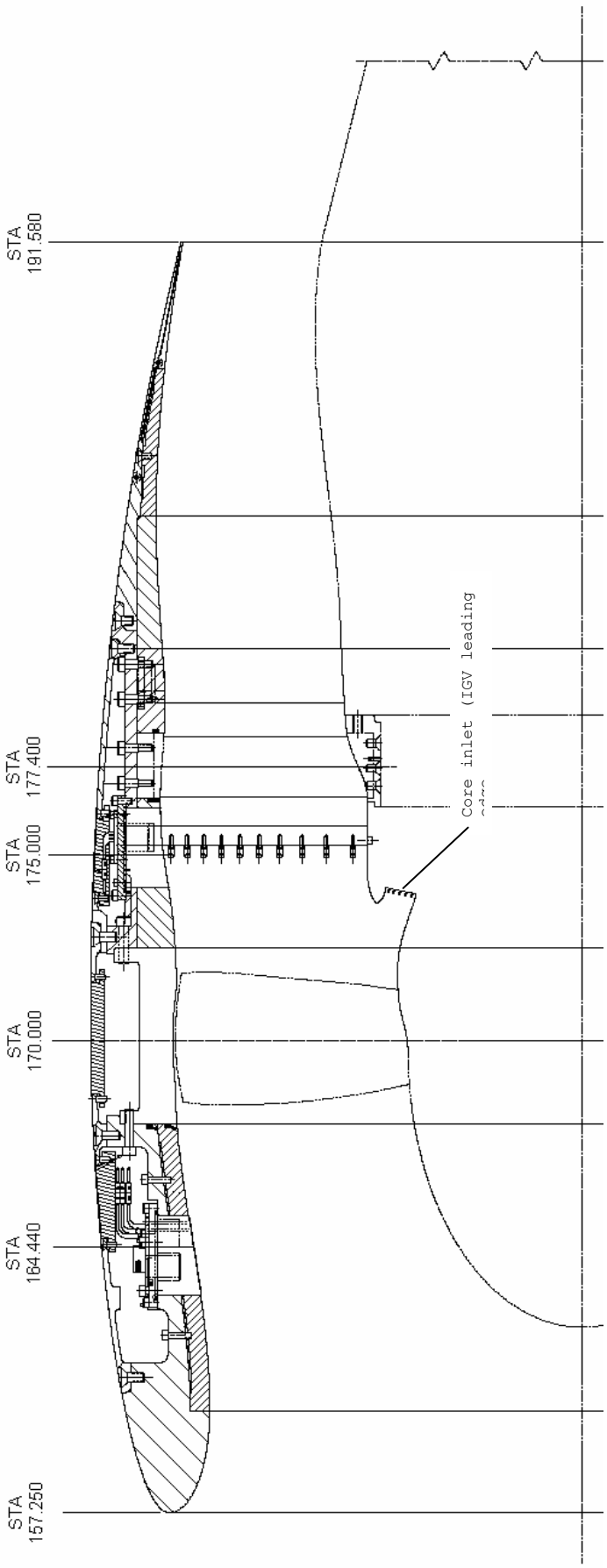

Figure 2(a).—ADP model cross section showing key instrumentation locations.

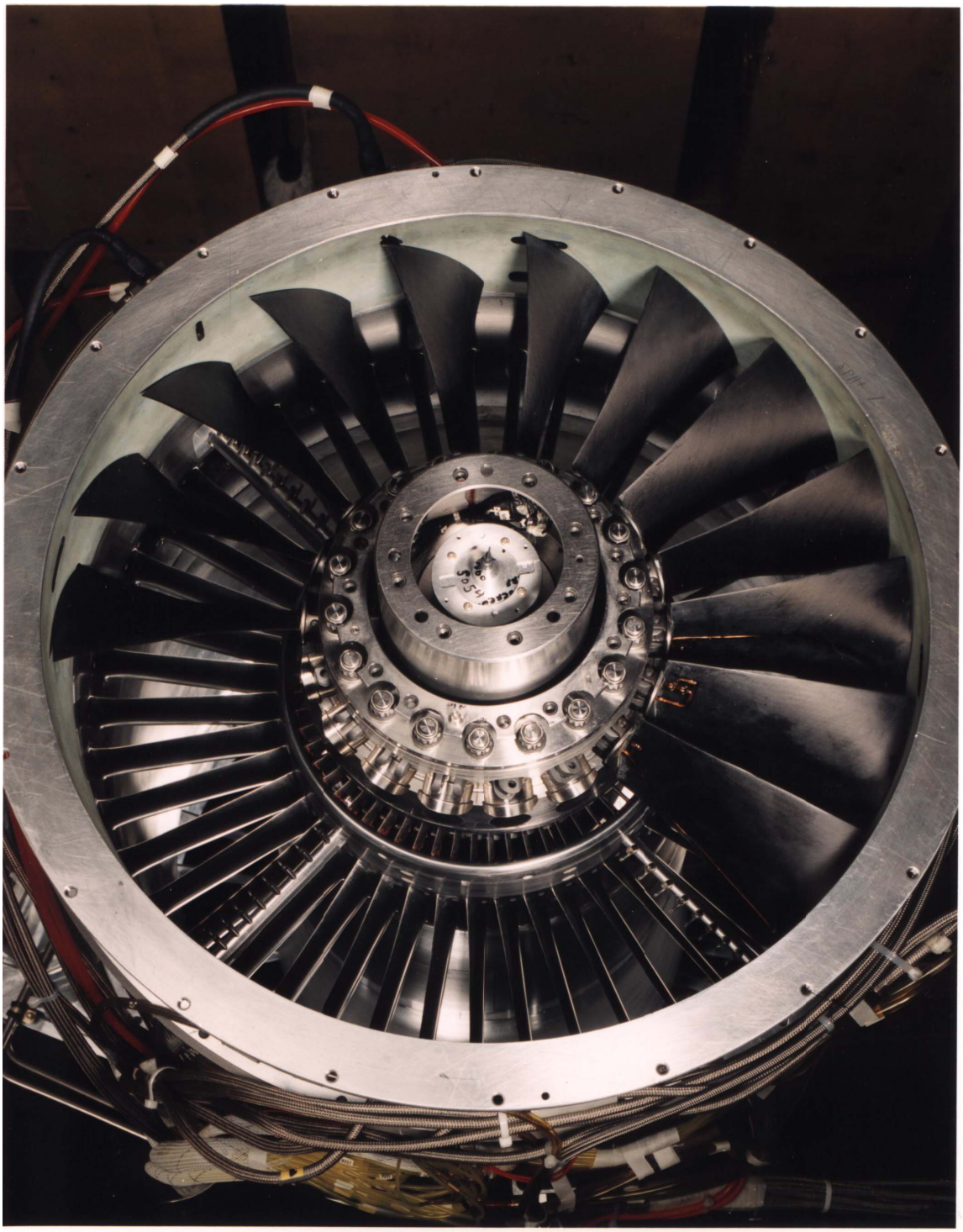

Figure 2(b).—ADP fan model with the inlet and some fan blades removed.

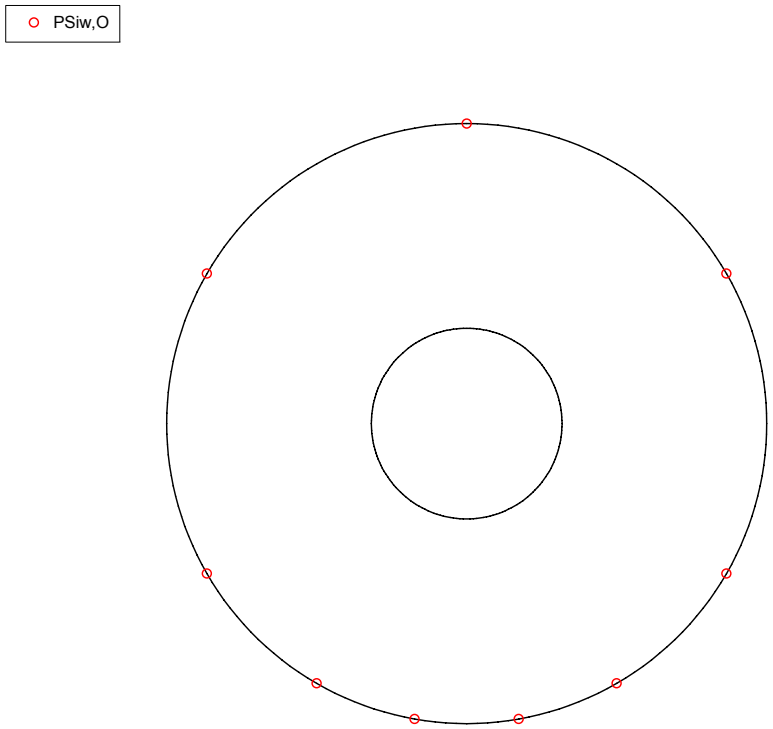

Figure 3(a).—Inlet weight flow instrumentation.

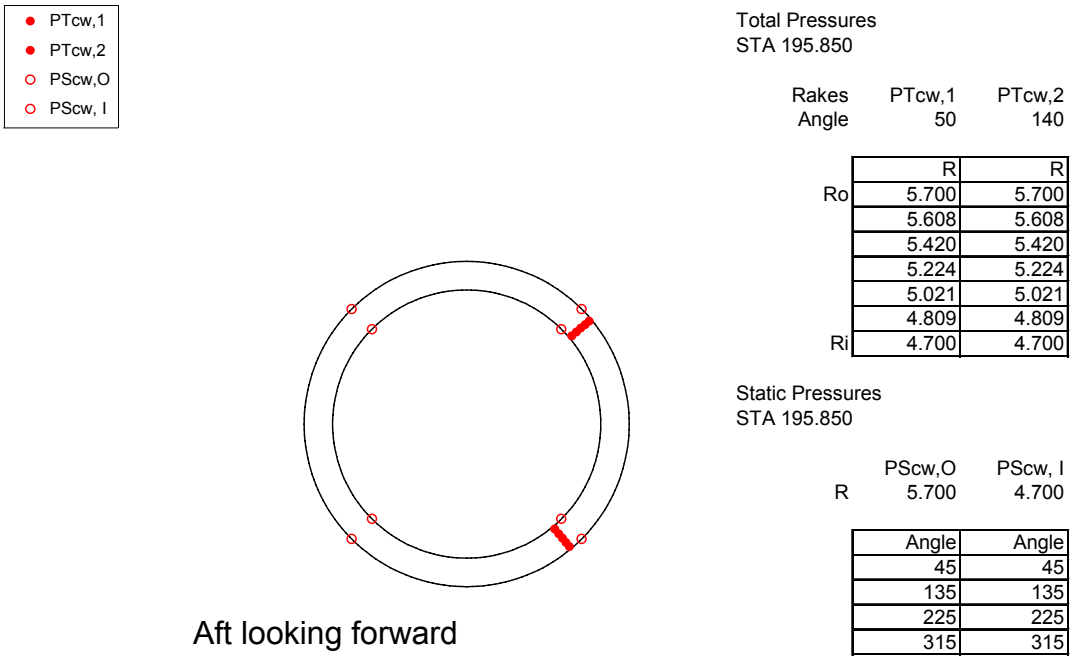

Figure 3(b).—Core weight flow instrumentation.

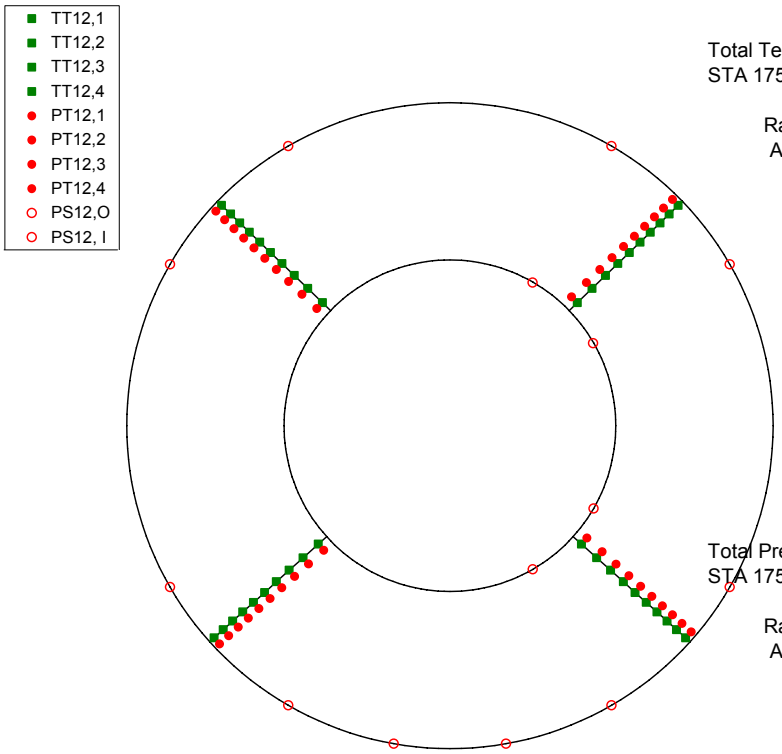

Aft looking forward

Total Temperatures
STA 175.000

Rakes	TT12,1	TT12,2	TT12,3	TT12,4
Angle	46	132	228	314
	R	R	R	R
Ro	11.320	11.320	11.320	11.320
	11.119	11.119	11.119	11.119
	10.685	10.685	10.685	10.685
	10.233	10.233	10.233	10.233
	9.760	9.760	9.760	9.760
	9.263	9.263	9.263	9.263
	8.737	8.737	8.737	8.737
	8.177	8.177	8.177	8.177
	7.577	7.577	7.577	7.577
	6.924	6.924	6.924	6.924
	6.204	6.204	6.204	6.204
Ri	5.810	5.810	5.810	5.810

Total Pressures
STA 175.209

		Offset at Angle	0.355 36.0	
Rakes	PT12,1	PT12,2	PT12,3	PT12,4
Angle	46	132	228	314
	R	R	R	R
Ro	11.320	11.320	11.320	11.320
	11.119	11.119	11.119	11.119
	10.685	10.685	10.685	10.685
	10.233	10.233	10.233	10.233
	9.760	9.760	9.760	9.760
	9.263	9.263	9.263	9.263
	8.737	8.737	8.737	8.737
	8.177	8.177	8.177	8.177
	7.577	7.577	7.577	7.577
	6.924	6.924	6.924	6.924
	6.204	6.204	6.204	6.204
Ri	5.810	5.810	5.810	5.810

Static Pressures

	PS12,O	PS12, I
STA	175.000	
Radius	11.320	

Angle	STA	R	Angle
30	174.300	5.791	0
60	174.300	5.791	270
120	176.000	5.810	0
150	176.000	5.810	270
170			
190			
210			
240			
300			
330			

Figure 4(a).—Fan bypass duct instrumentation.

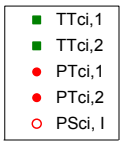

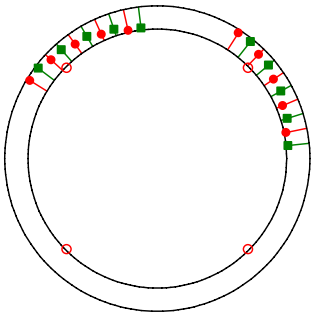

Aft looking forward

Total Temperatures
STA 173.844-173.946

Rakes		TTci,1	TTci,2
	R	Angle	Angle
Ro	5.345		
	5.236	38.574	307.148
	5.085	50.002	318.576
	4.929	61.430	330.004
	4.767	72.858	341.432
	4.601	84.286	352.860
Ri	4.531		

Total Pressures
STA 173.844-3.946

Rakes		PTci,1	PTci,2
	R	Angle	Angle
Ro	5.345		
	5.236	32.860	301.434
	5.085	44.288	312.862
	4.929	55.716	324.290
	4.767	67.144	335.718
	4.601	78.572	347.146
Ri	4.531		

Static Pressures
STA 173.966

	PSci,O	PSci, I
R	None	4.494
		Angle
		45
		135
		225
		315

Figure 4(b).—Core inlet instrumentation.

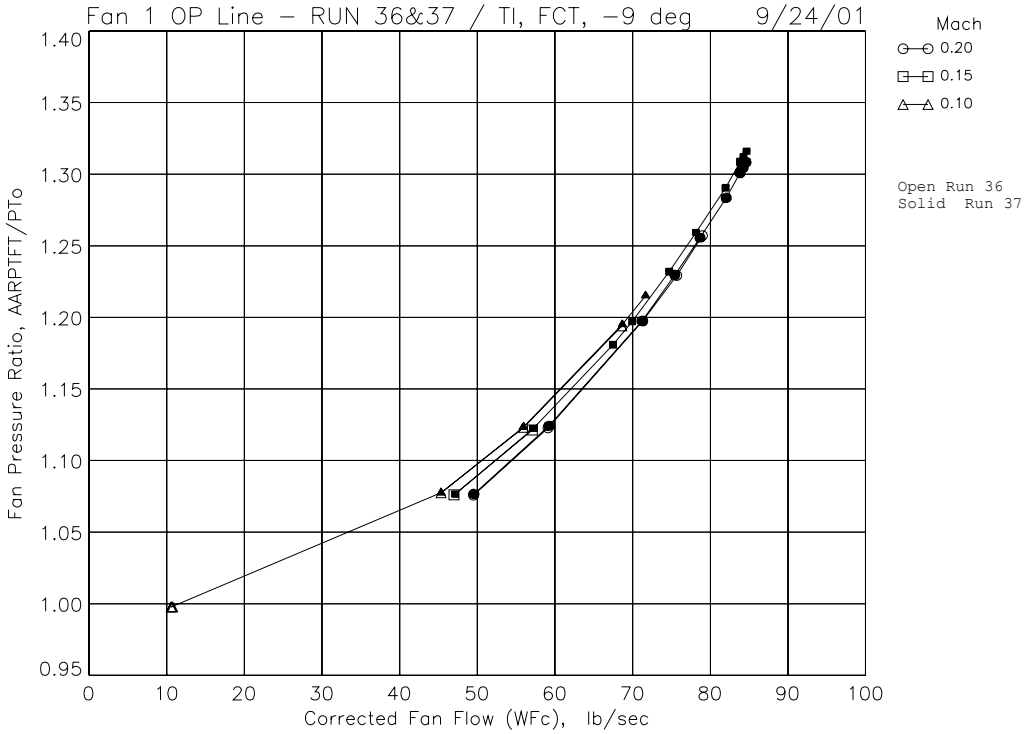

(a) Fan averaged total pressure ratio versus total fan corrected flow.

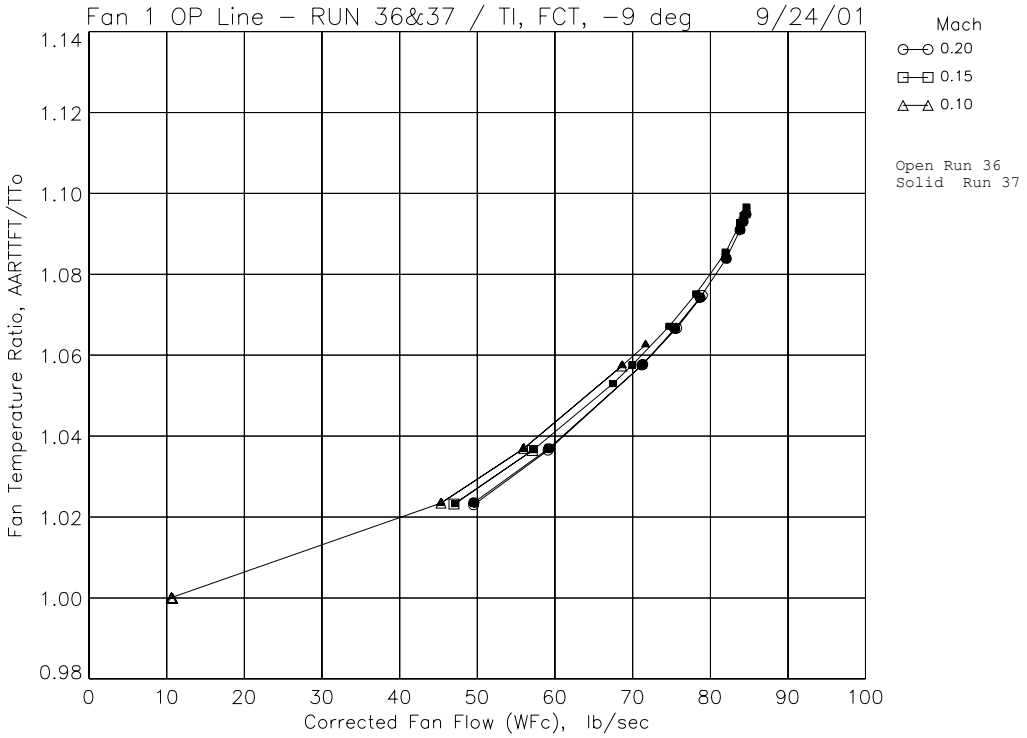

(b) Fan averaged total temperature ratio versus total fan corrected flow.

Figure 5.—Fan operating line results and repeatability with –9 deg blade angle, FCT rubstrip.

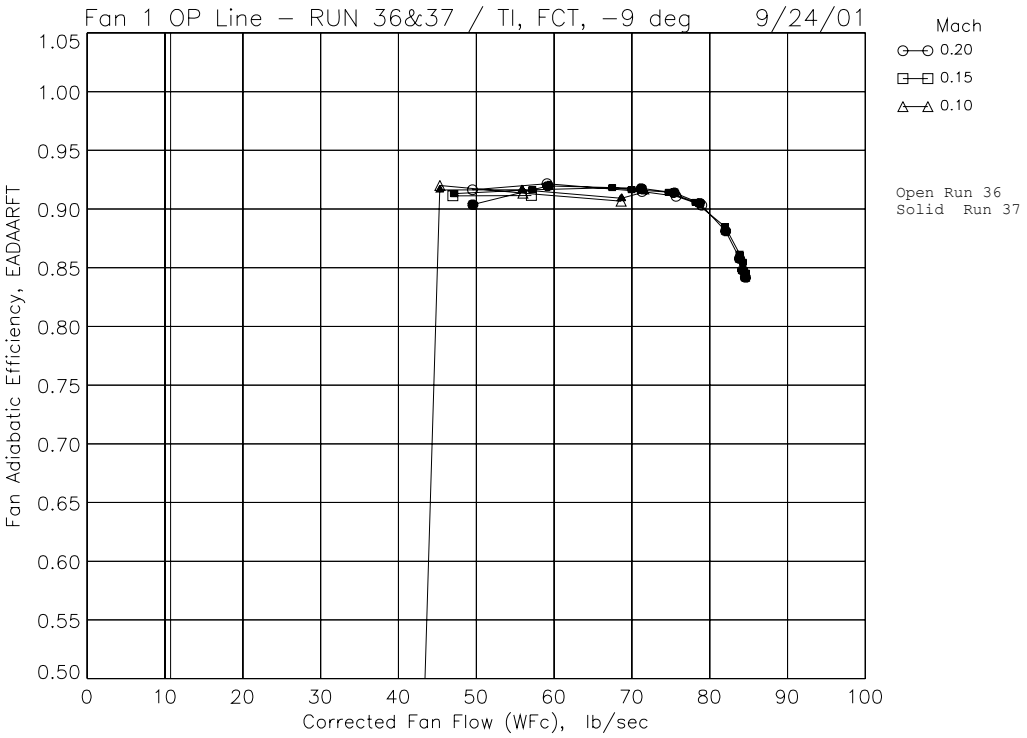

(c) Fan averaged adiabatic efficiency versus total fan corrected flow.

Figure 5.—An operating line results and repeatability with –9 deg blade angle, FCT rubstrip.

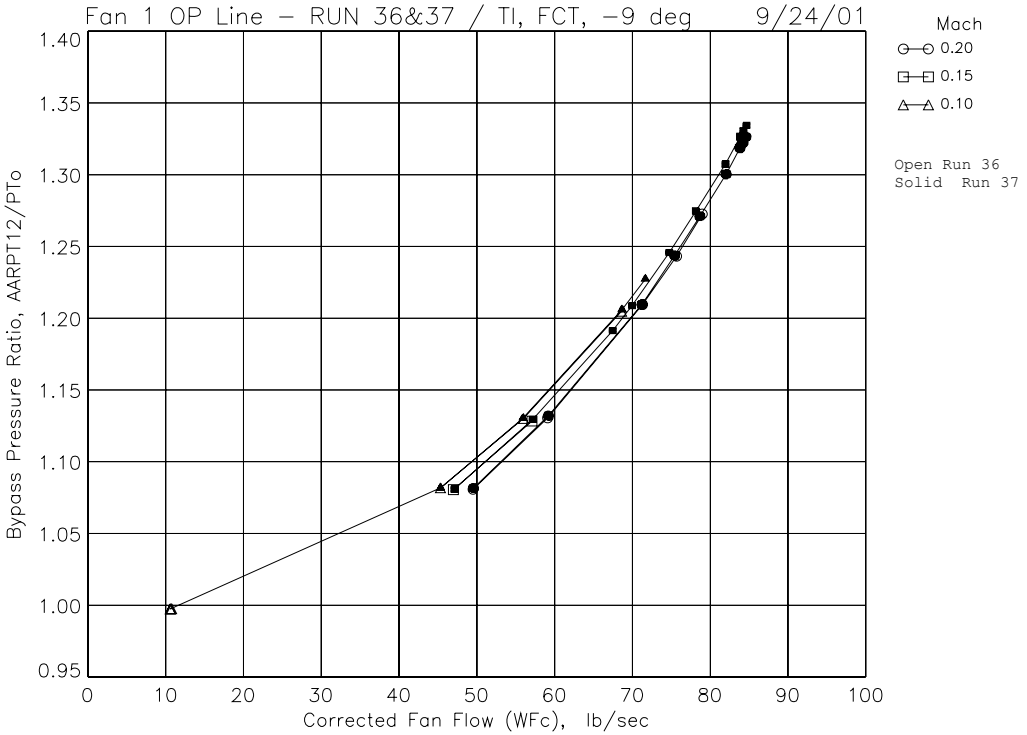

(a) Bypass total pressure ratio versus total fan corrected flow.

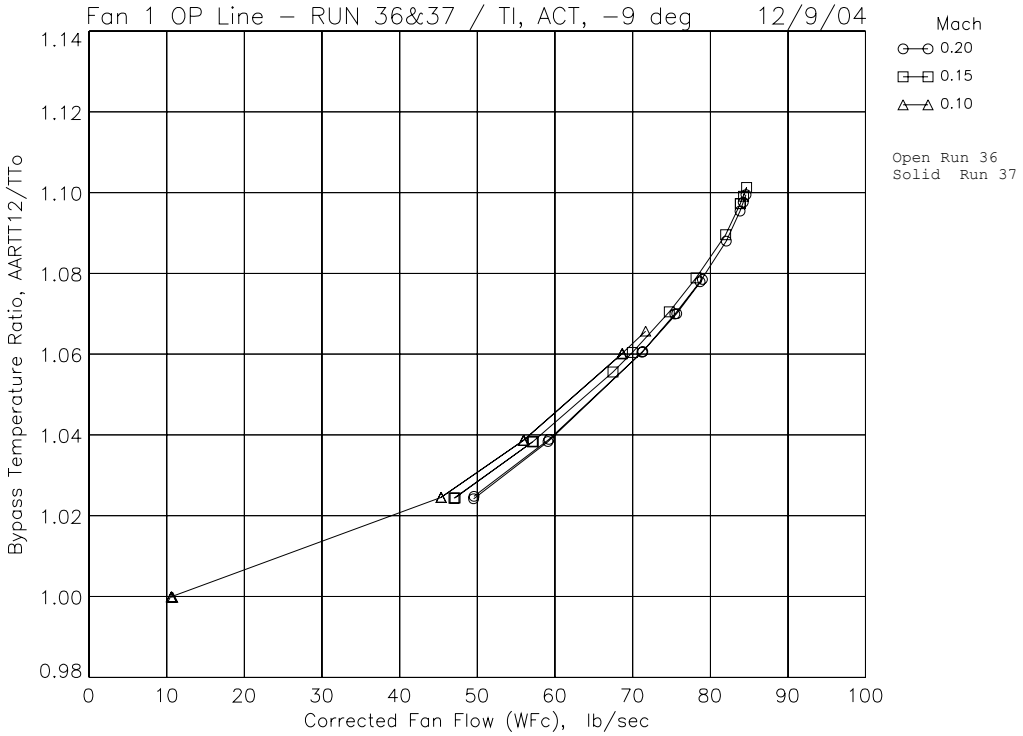

(b) Bypass total temperature ratio versus total fan corrected flow.

Figure 6.—Bypass operating line results and repeatability with –9 deg blade angle, FCT rubstrip.

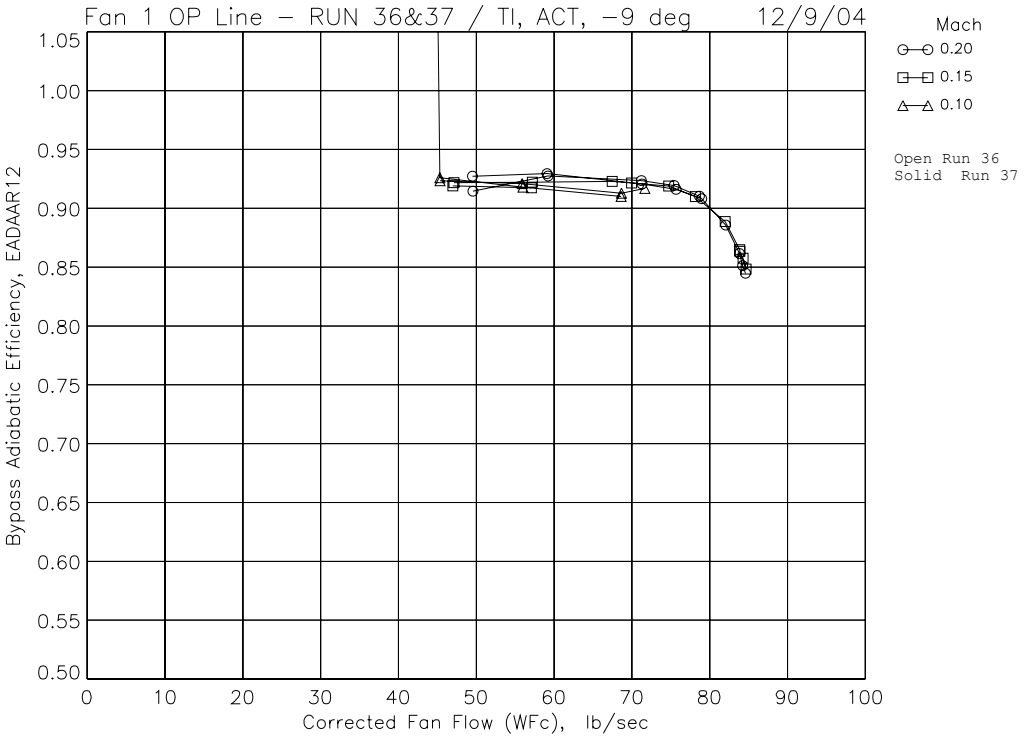

(c) Bypass adiabatic efficiency versus total fan corrected flow.

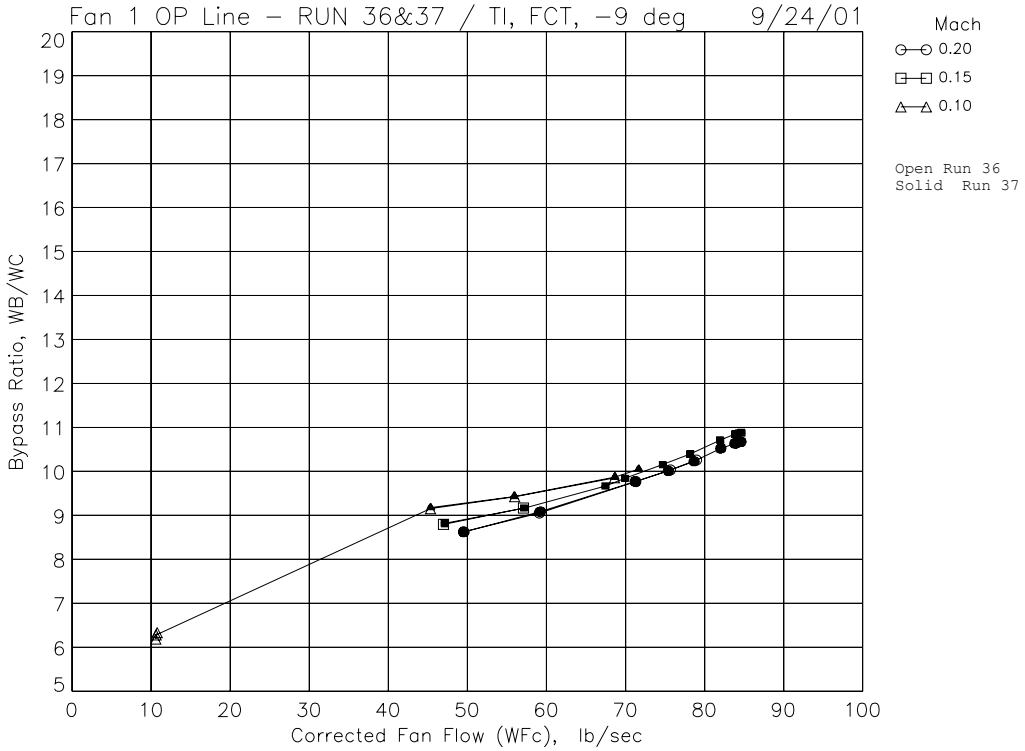

(d) Bypass ratio versus total fan flow.

Figure 6.—Bypass operating line results and repeatability with –9 deg blade angle, FCT rubstrip.

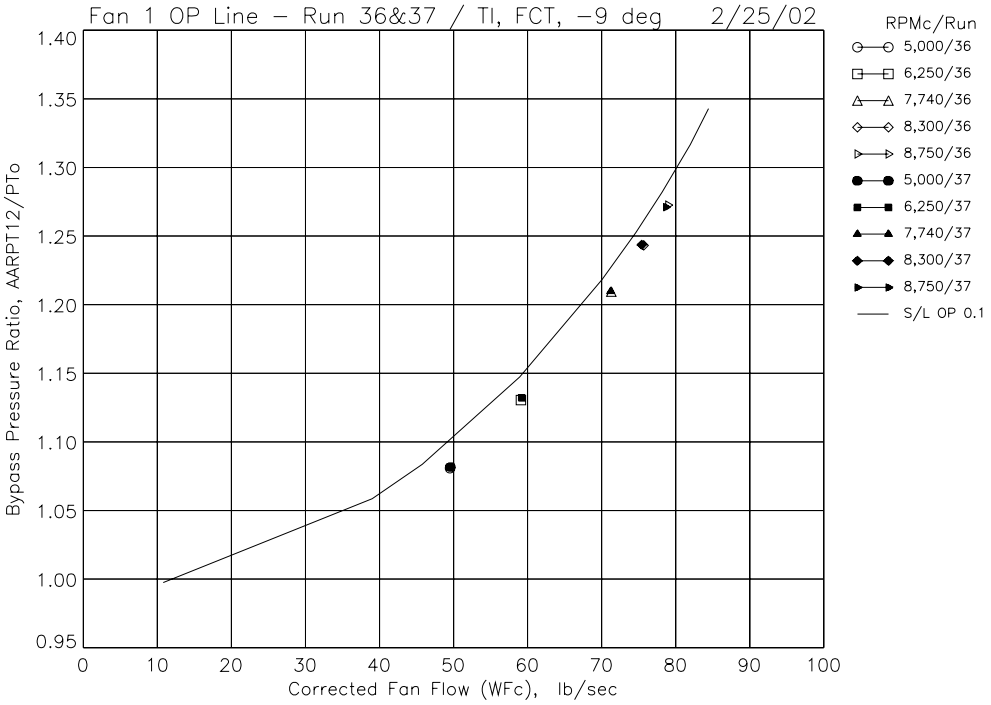

(a) Bypass pressure ratio versus total fan corrected weight flow.

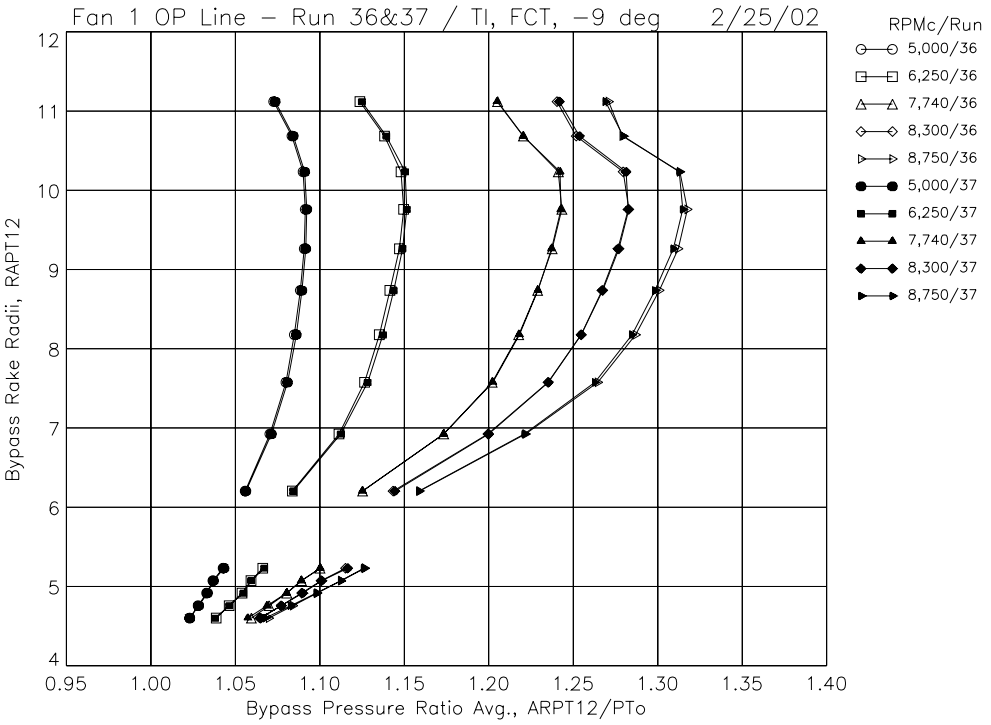

(b) Fan total pressure ratio radial profiles.

Figure 7.—Radial profiles on fan operating line showing results and repeatability with –9 deg blade angle, FCT rubstrip, Mo = 0.20.

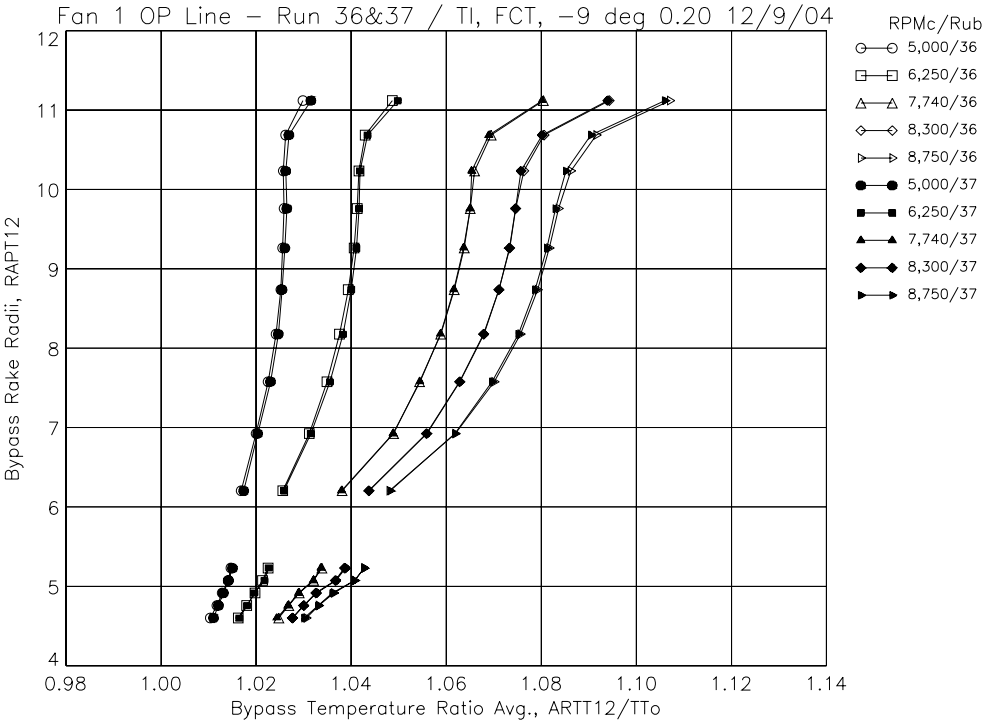

(c) Fan total temperature ratio radial profiles.

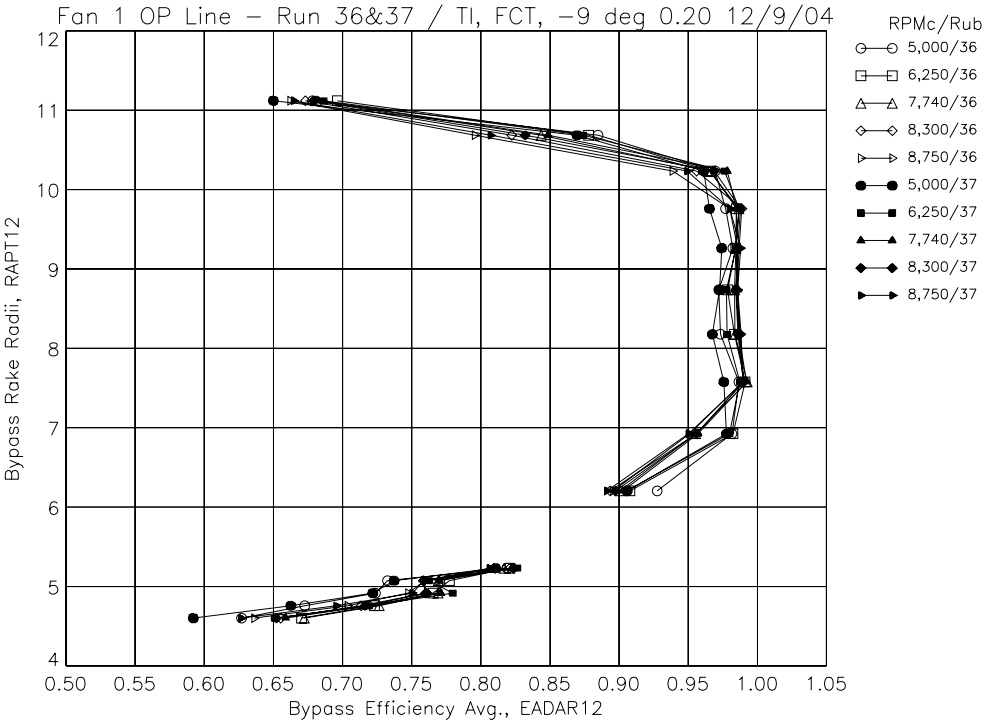

(d) Fan adiabatic efficiency radial profiles.

Figure 7.—Radial profiles on fan operating line showing results and repeatability with –9 deg blade angle, FCT rubstrip, Mo = 0.20.

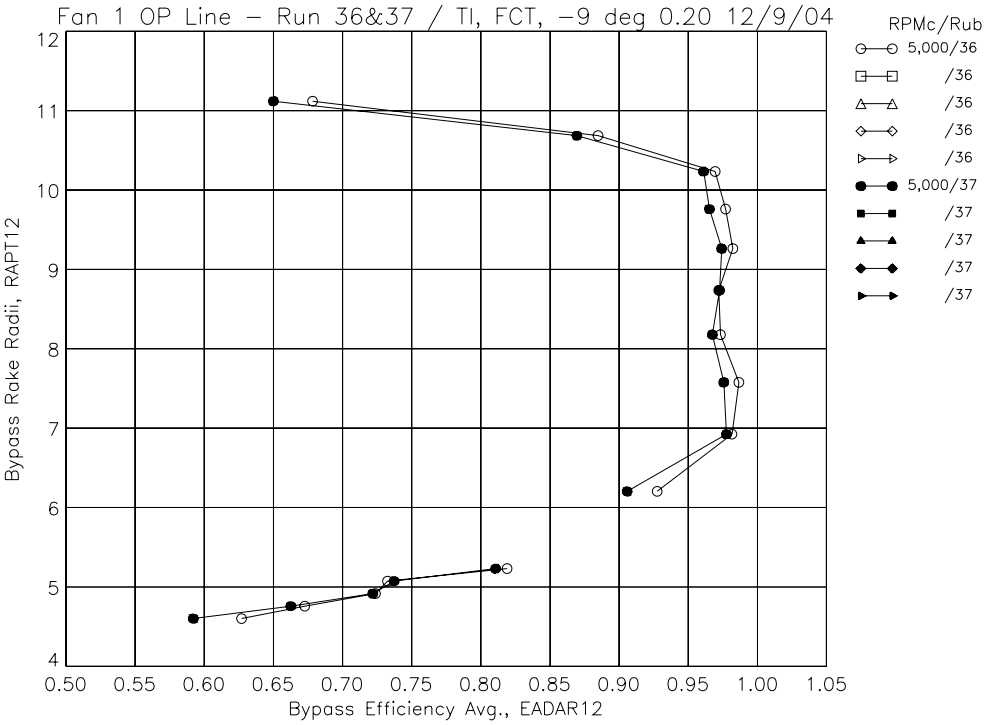

(e) Fan adiabatic efficiency radial profiles, 5,000 RPMc.

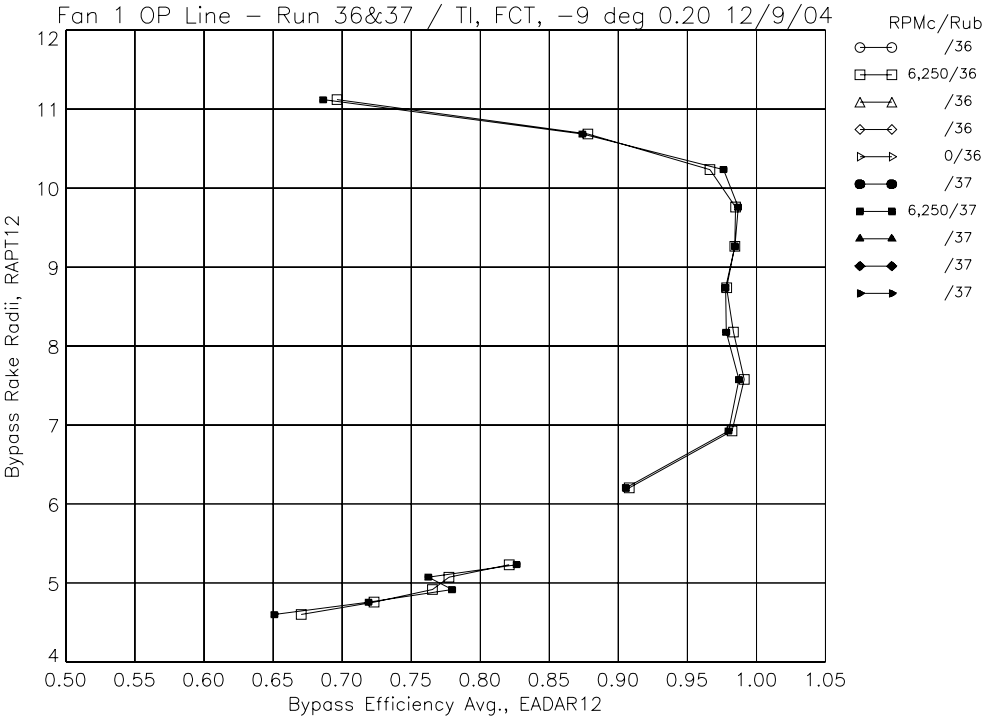

(f) Fan adiabatic efficiency radial profiles, 6,250 RPMc.

Figure 7.—Radial profiles on fan operating line showing results and repeatability with –9 deg blade angle, FCT rubstrip, Mo = 0.20.

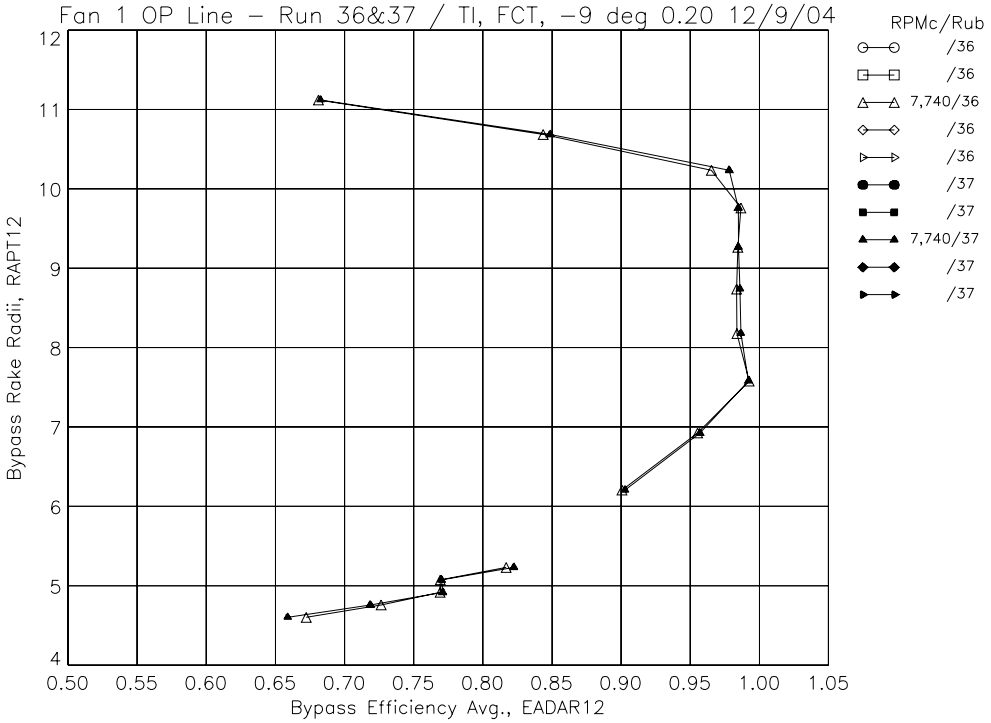

(g) Fan adiabatic efficiency radial profiles, 7,740 RPMc.

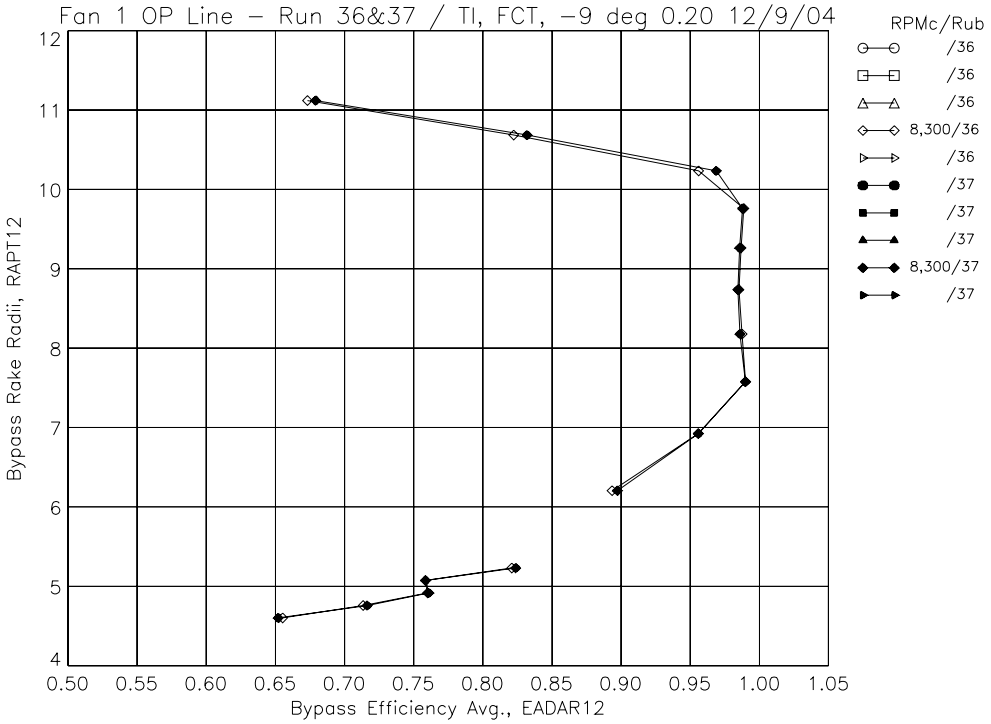

(h) Fan adiabatic efficiency radial profiles, 8,300 RPMc.

Figure 7.—Radial profiles on fan operating line showing results and repeatability with –9 deg blade angle, FCT rubstrip, Mo = 0.20.

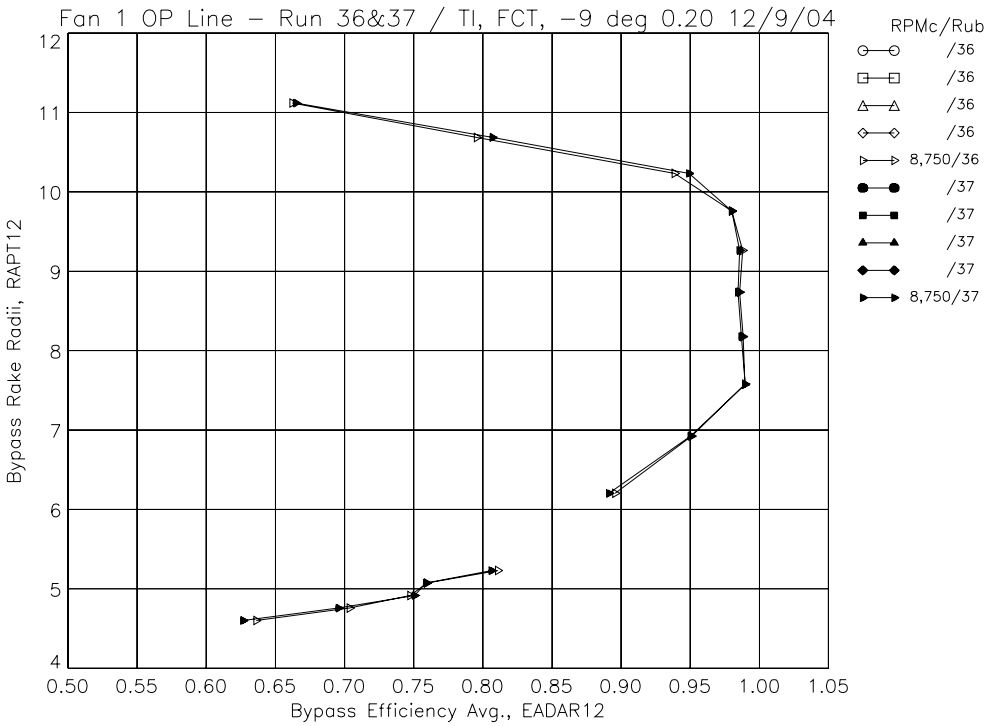

(i) Fan adiabatic efficiency radial profiles, 8,750 RPMc.

Figure 7.—Radial profiles on fan operating line showing results and repeatability with –9 deg blade angle, FCT rubstrip, Mo = 0.20.

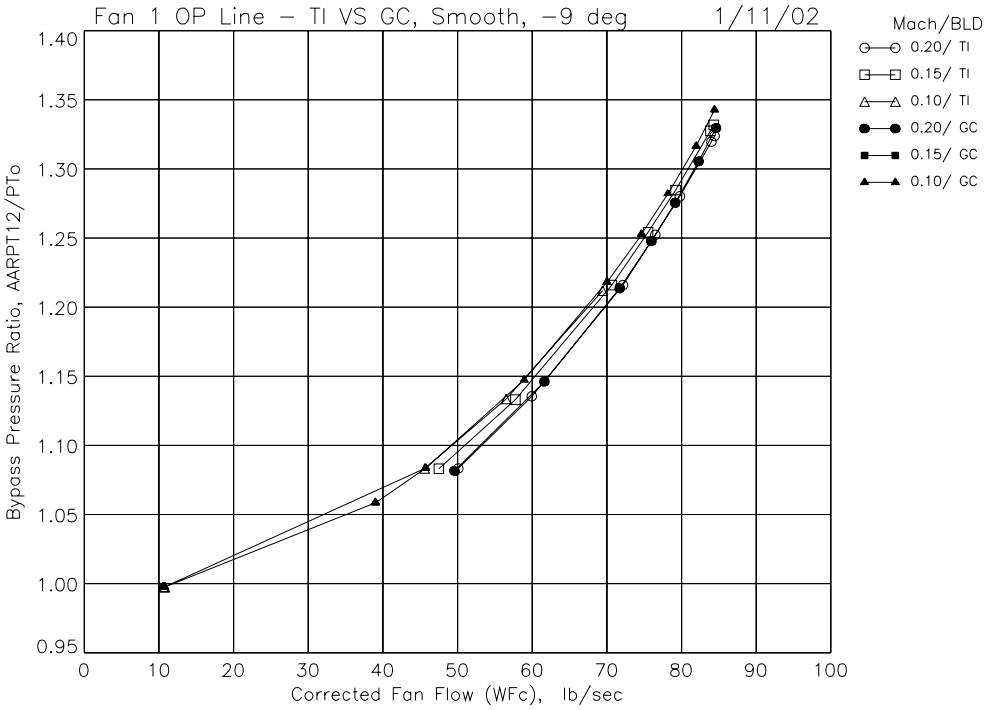

(a) Bypass total pressure ratio versus total fan corrected flow.

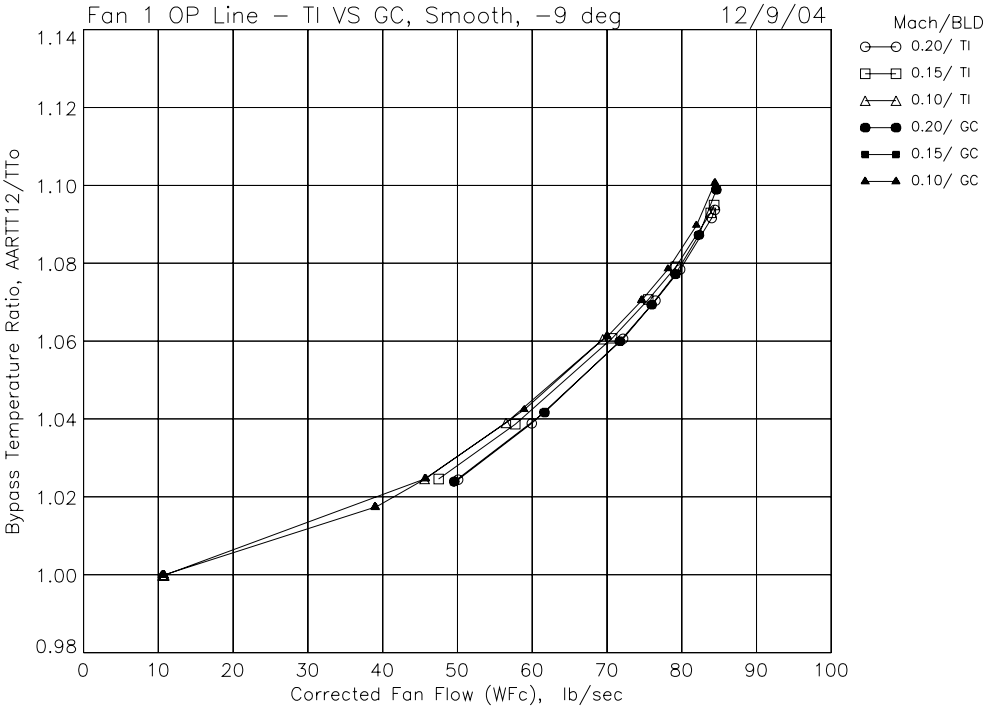

(b) Bypass total temperature ratio versus total fan corrected flow.

Figure 8.—TI and GC blade bypass operating line results with –9 deg blase angle, smooth rubstrip.

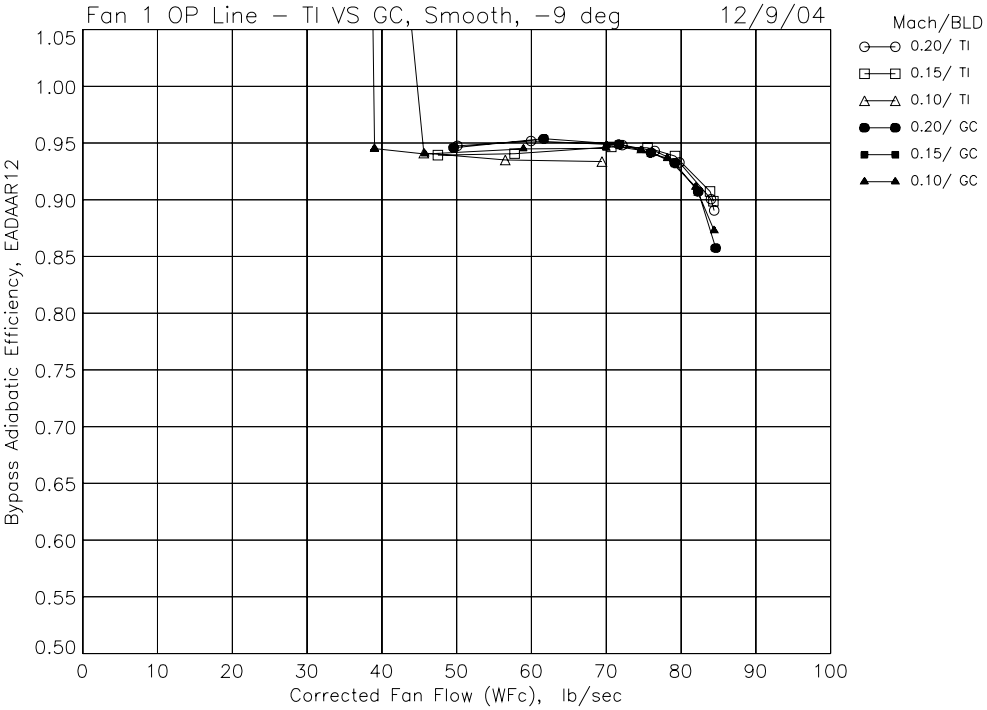

(c) Bypass adiabatic efficiency versus total fan corrected flow.

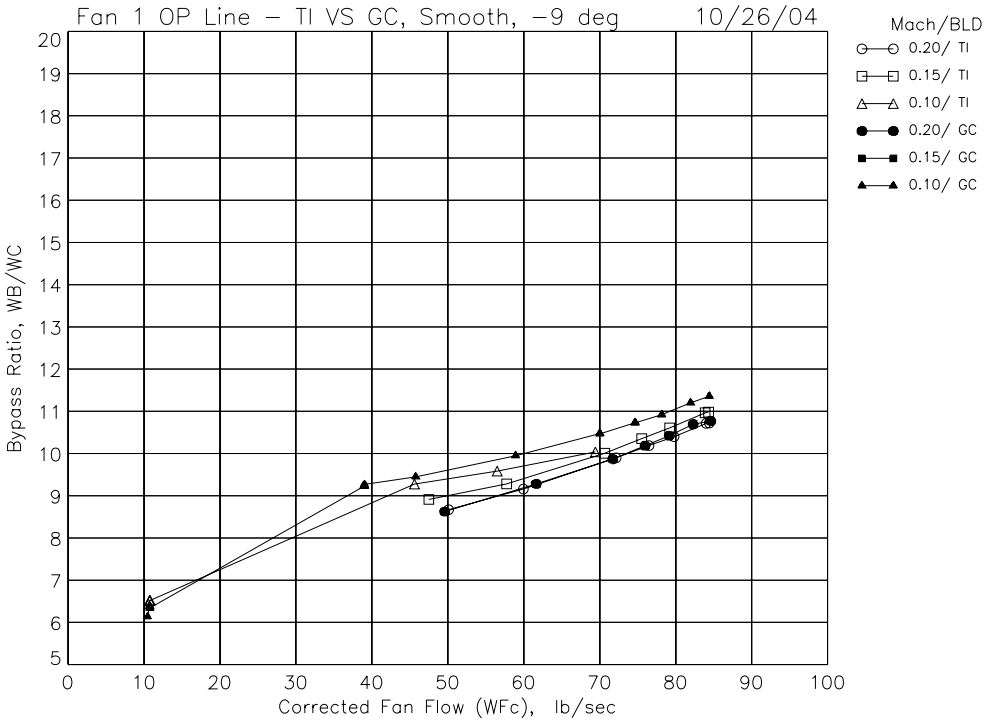

(d) Bypass ratio versus total fan corrected flow.

Figure 8.—TI and GC blade bypass operating line results with –9 deg blade angle, smooth rubstrip.

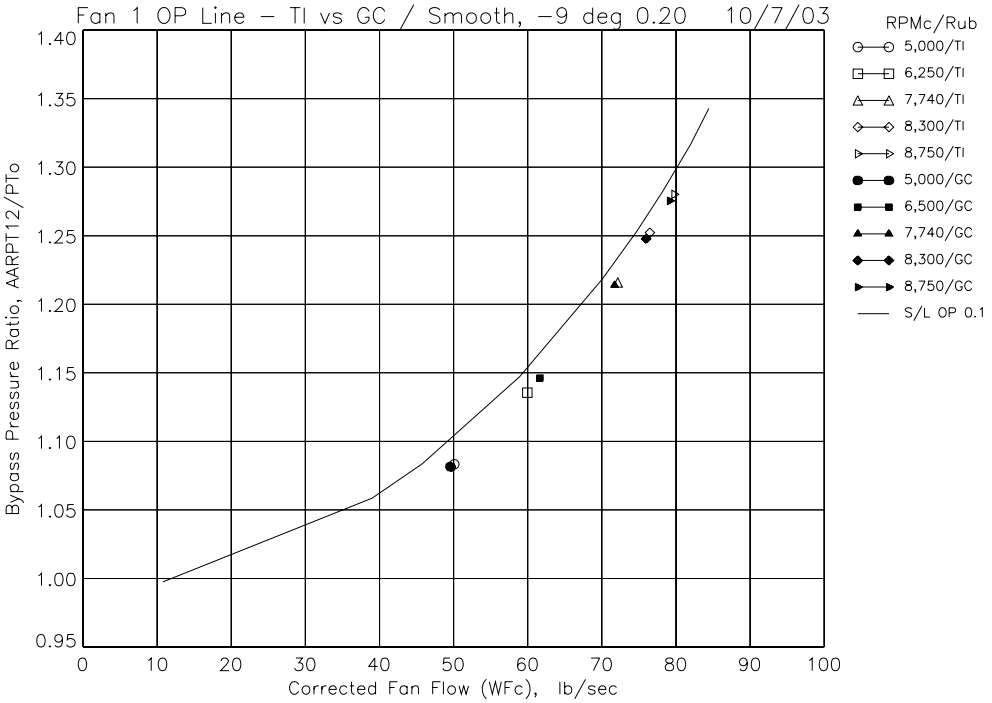

(a) Bypass total pressure ratio versus total fan corrected flow.

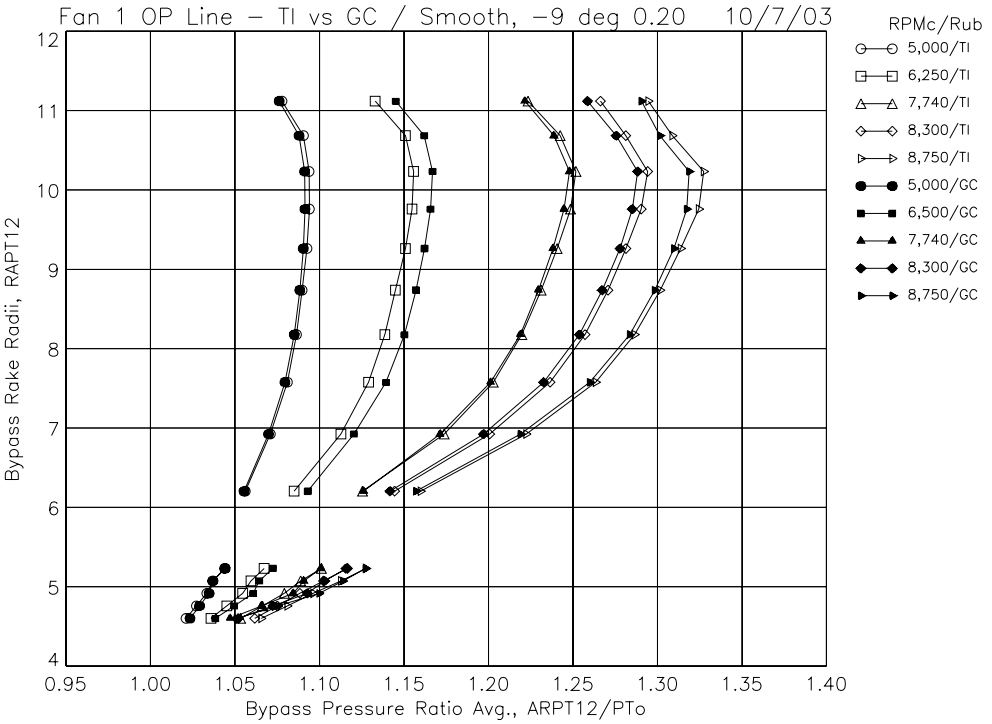

(b) Fan total pressure ratio radial profiles.

Figure 9.—TI and GC blade radial profiles on fan operating line, with –9 deg blade angle, smooth rubstrip, Mo = 0.20.

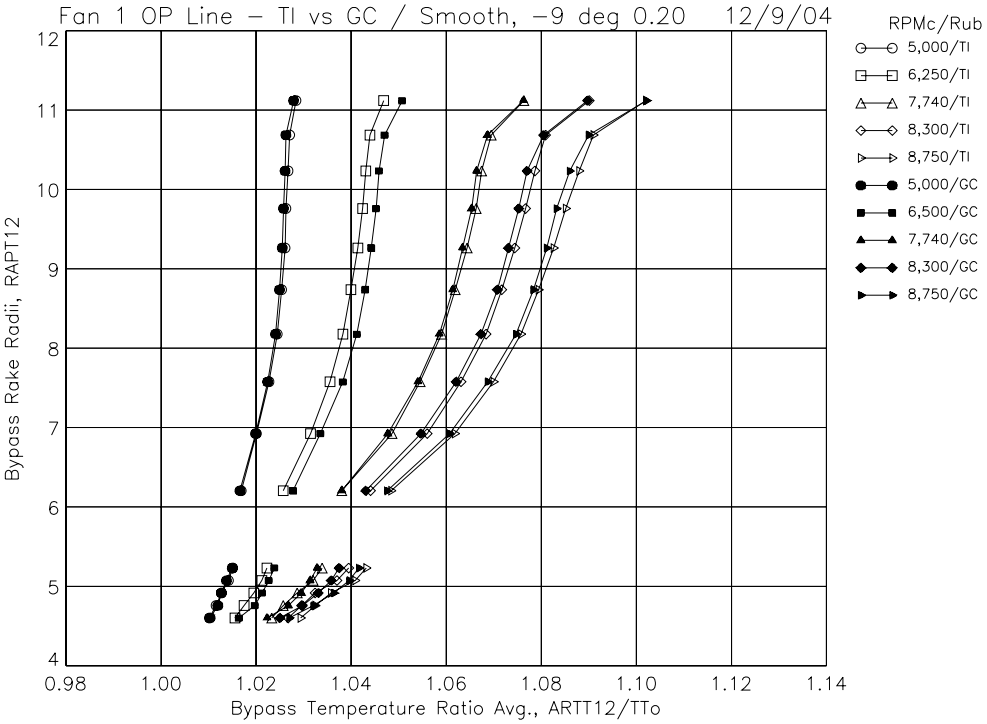

(c) Fan total temperature ratio radial profiles.

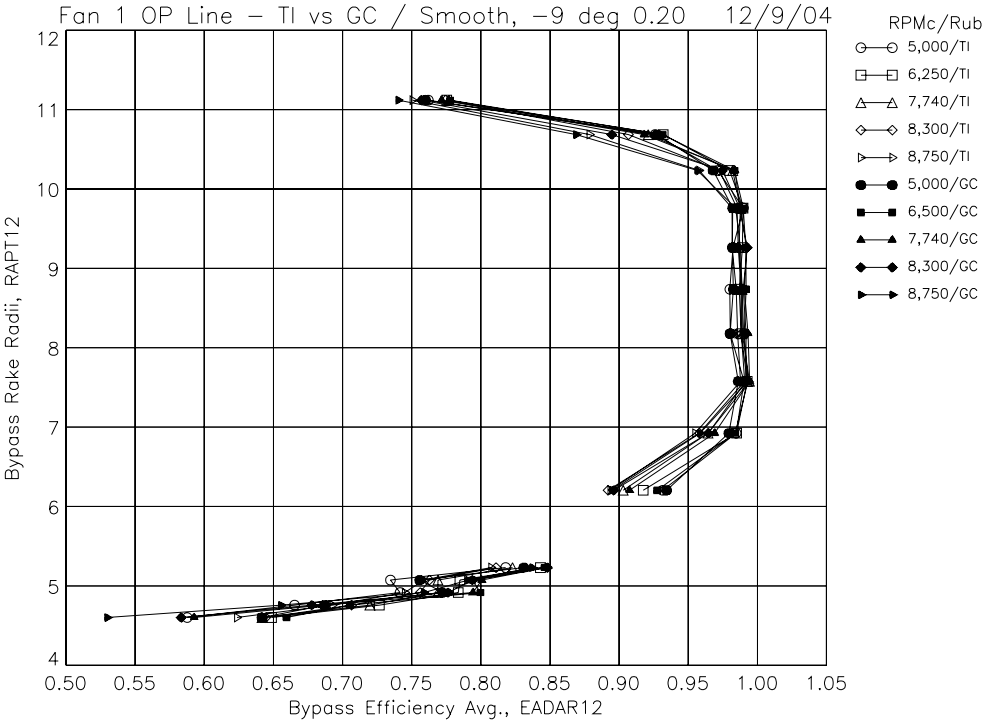

(d) Fan adiabatic efficiency radial profiles.

Figure 9.—TI and GC blade radial profiles on fan operating line, with –9 deg blade angle, smooth rubstrip, Mo = 0.20.

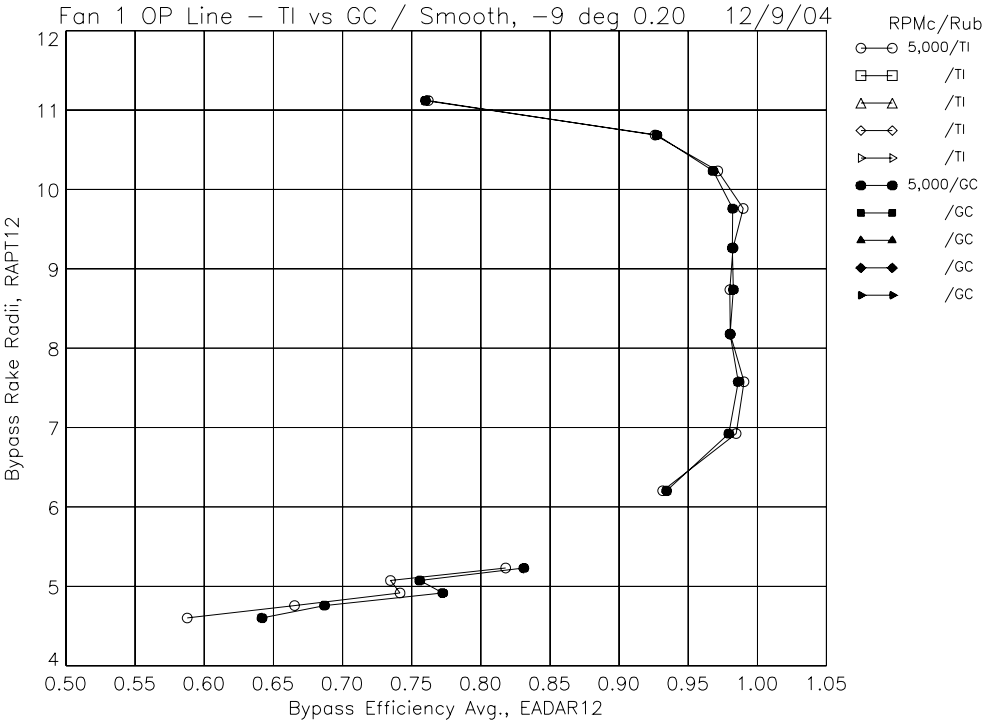

(e) Fan adiabatic efficiency radial profiles, 5,000 RPMc.

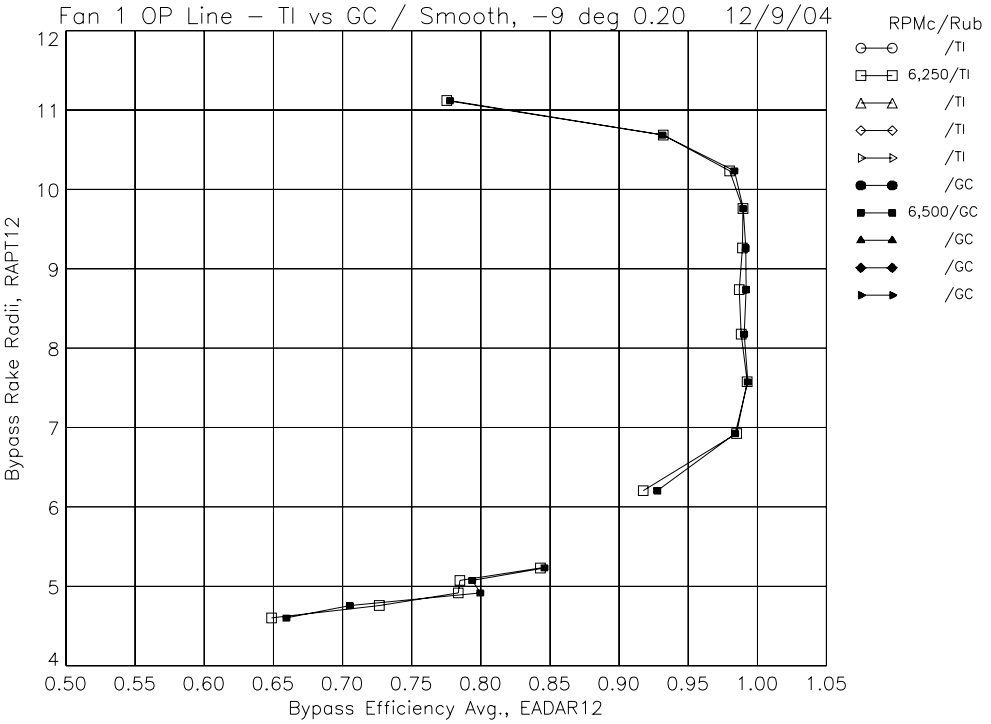

(f) Fan adiabatic efficiency radial profiles, 6,250 and 6,500 RPMc.

Figure 9.—TI and GC blade radial profiles on fan operating line, with –9 deg blade angle, smooth rubstrip, Mo = 0.20.

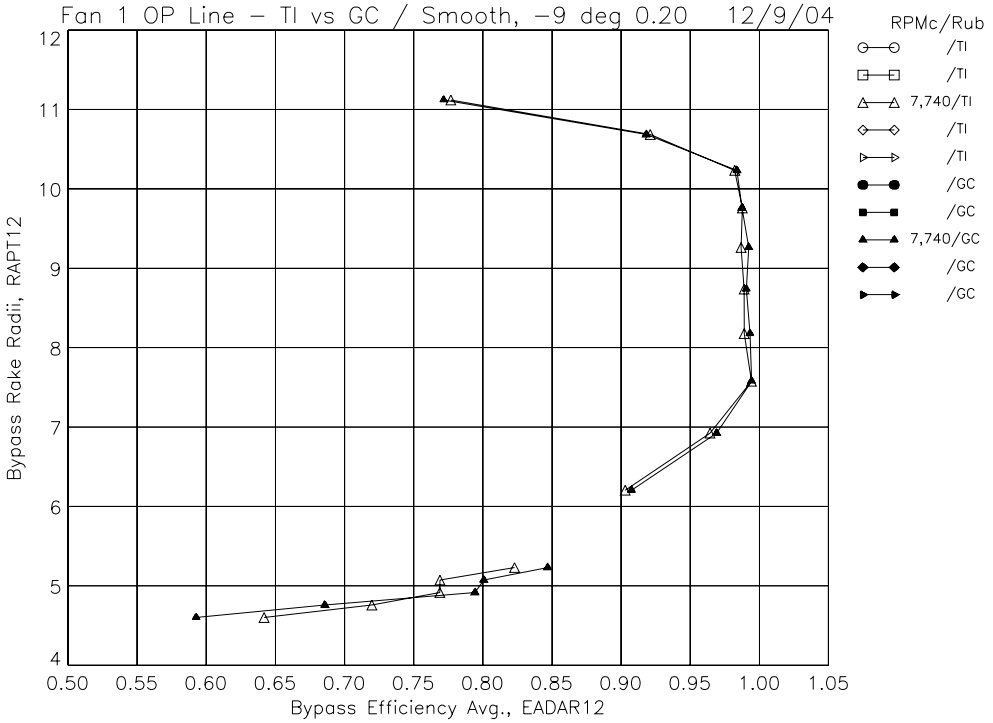

(g) Fan adiabatic efficiency radial profiles, 7,740 RPMc.

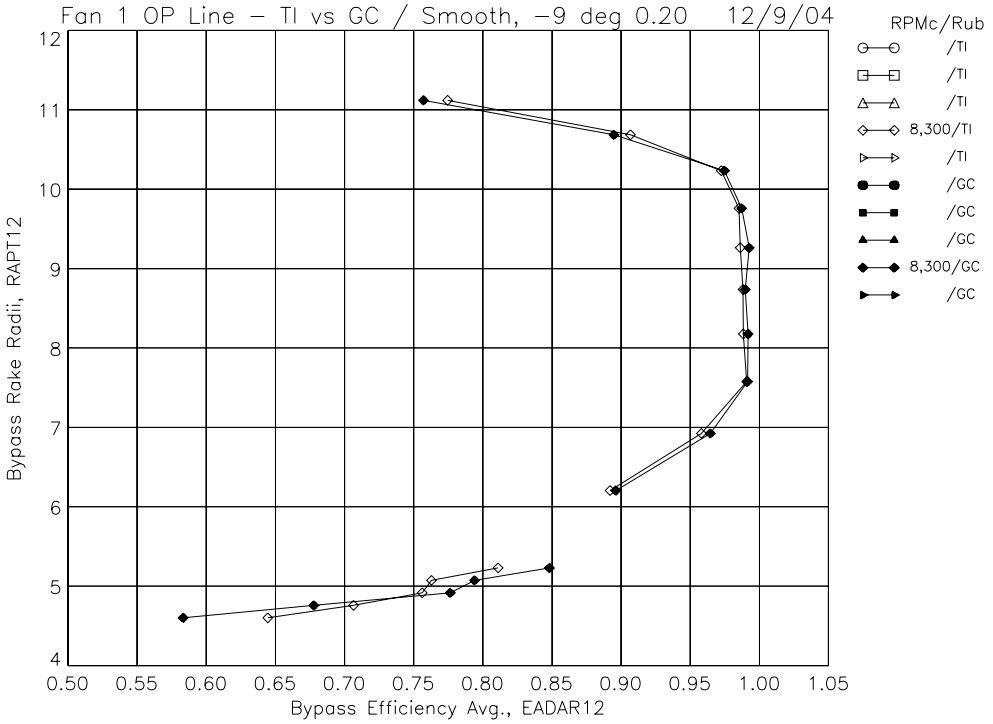

(h) Fan adiabatic efficiency radial profiles, 8,300 RPMc.

Figure 9.—TI and GC blade radial profiles on fan operating line, with –9 deg blade angle, smooth rubstrip, Mo = 0.20.

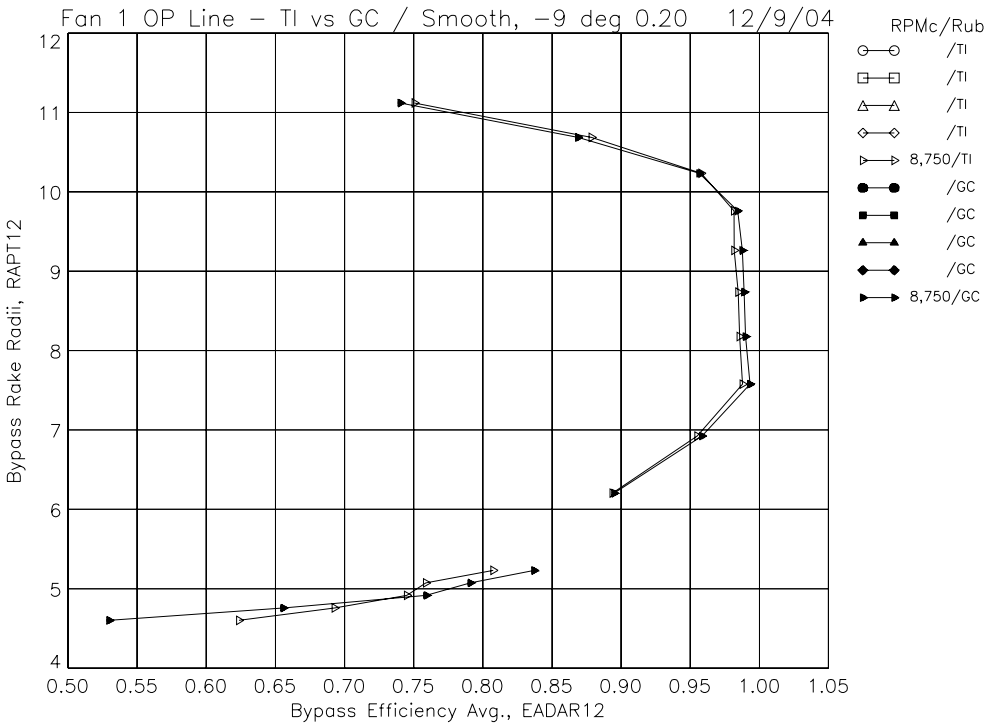

(i) Fan adiabatic efficiency radial profiles, 8,750 RPMc.

Figure 9.—TI and GC blade radial profiles on fan operating line, with –9 deg blade angle, smooth rubstrip, Mo = 0.20.

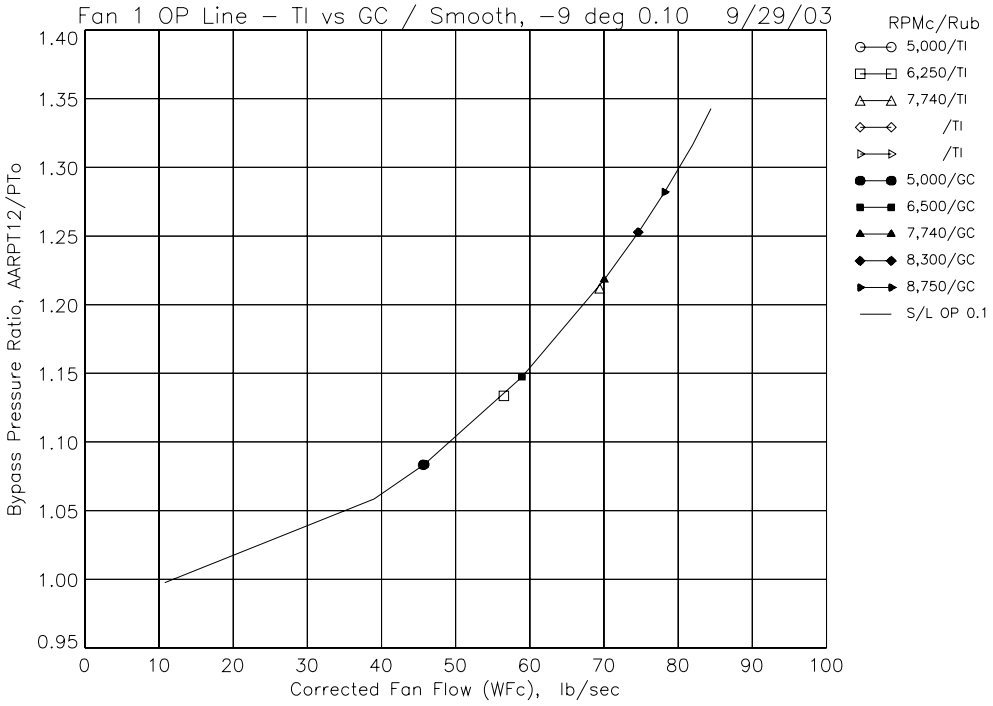

(a) Bypass total pressure ratio versus total fan corrected flow.

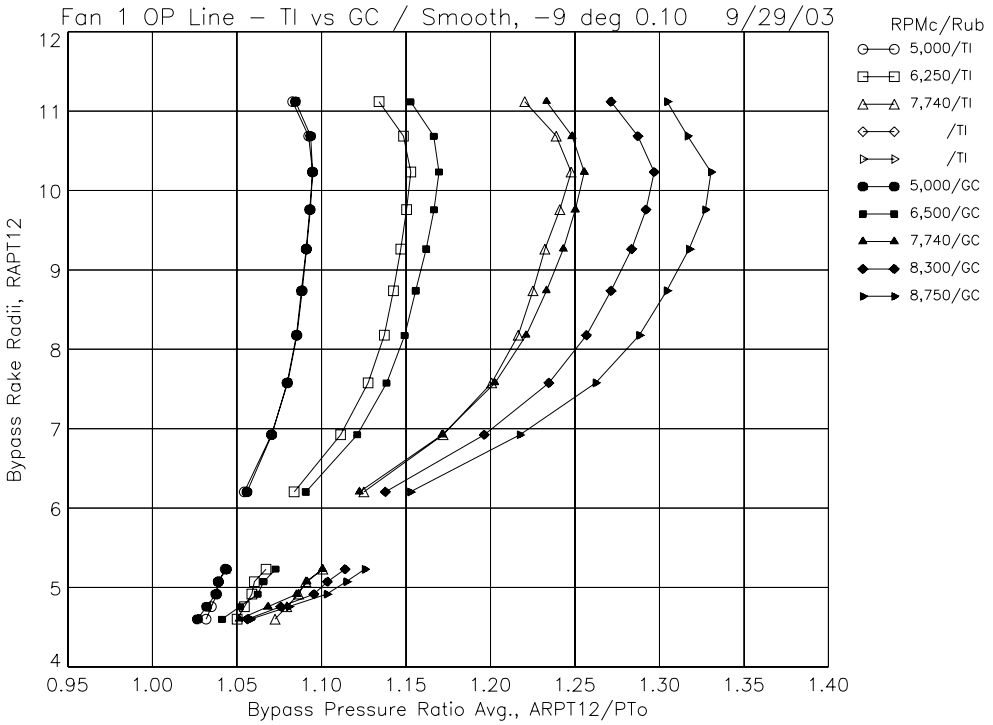

(b) Fan total pressure ratio radial profiles.

Figure 10.—TI and GC blade radial profiles on fan operating line, with –9 deg blade angle, smooth rubstrip, Mo = 0.10.

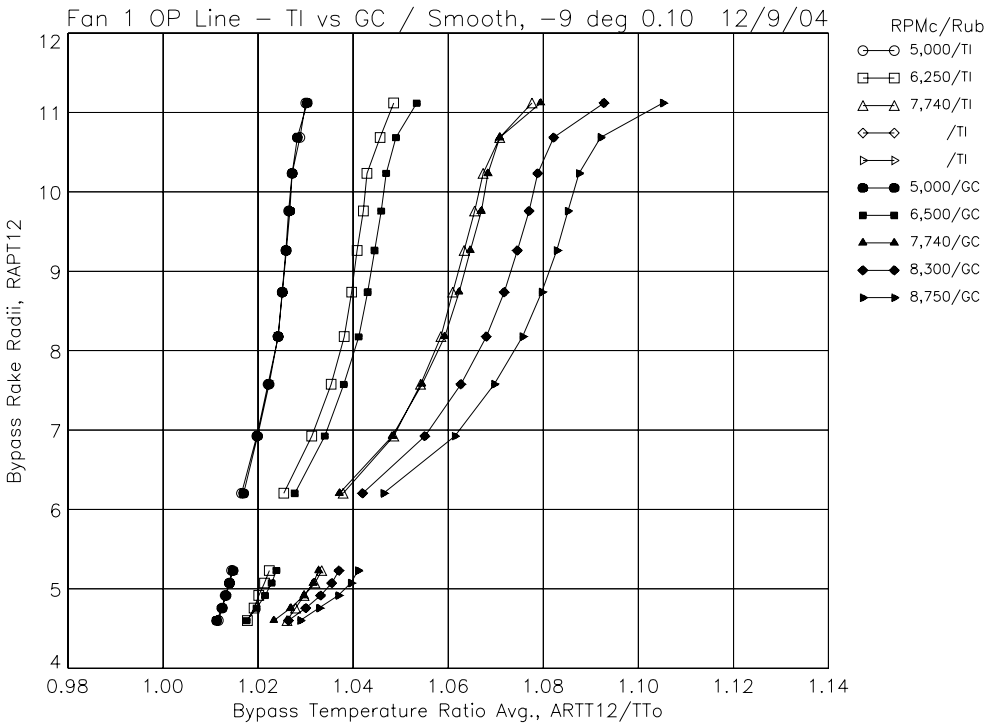

(c) Fan total temperature ratio radial profiles.

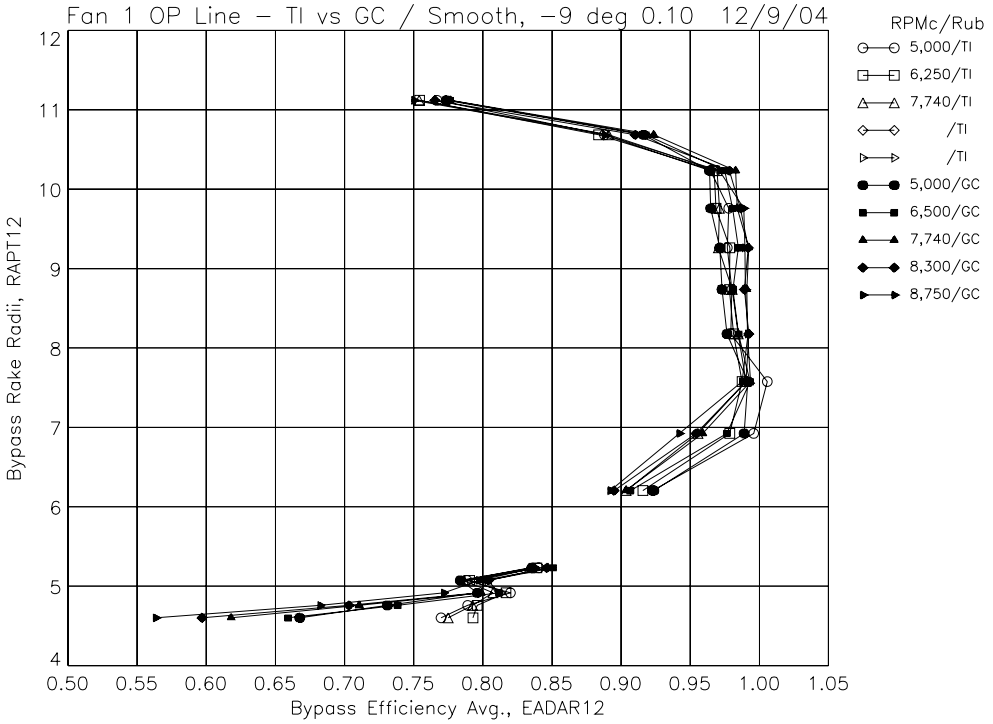

(d) Fan adiabatic efficiency radial profiles.

Figure 10.—TI and GC blade radial profiles on fan operating line, with –9 deg blade angle, smooth rubstrip, Mo = 0.10.

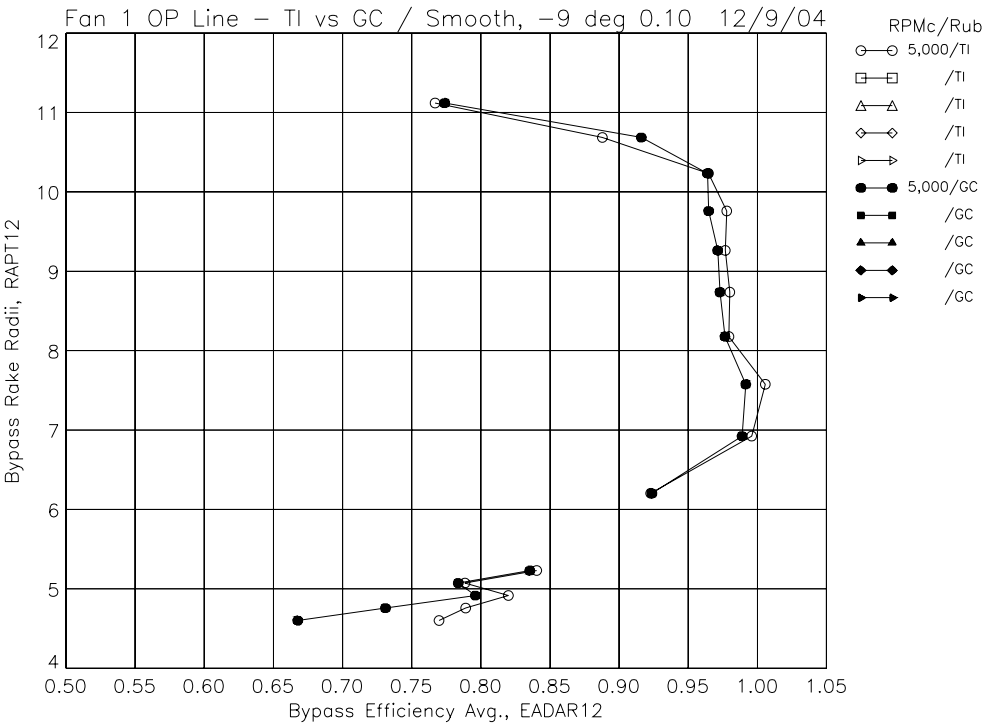

(e) Fan adiabatic efficiency radial profiles, 5,000 RPMc.

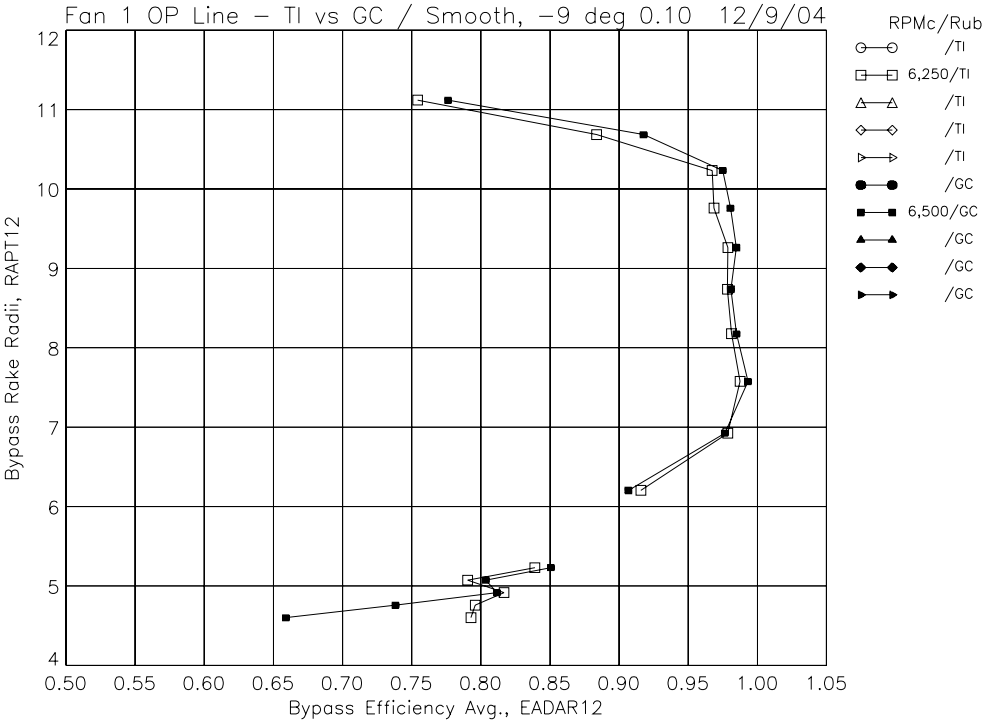

(f) Fan adiabatic efficiency radial profiles, 6,250 and 6,500 RPMc.

Figure 10.—TI and GC blade radial profiles on fan operating line, with –9 deg blade angle, smooth rubstrip, Mo = 0.10.

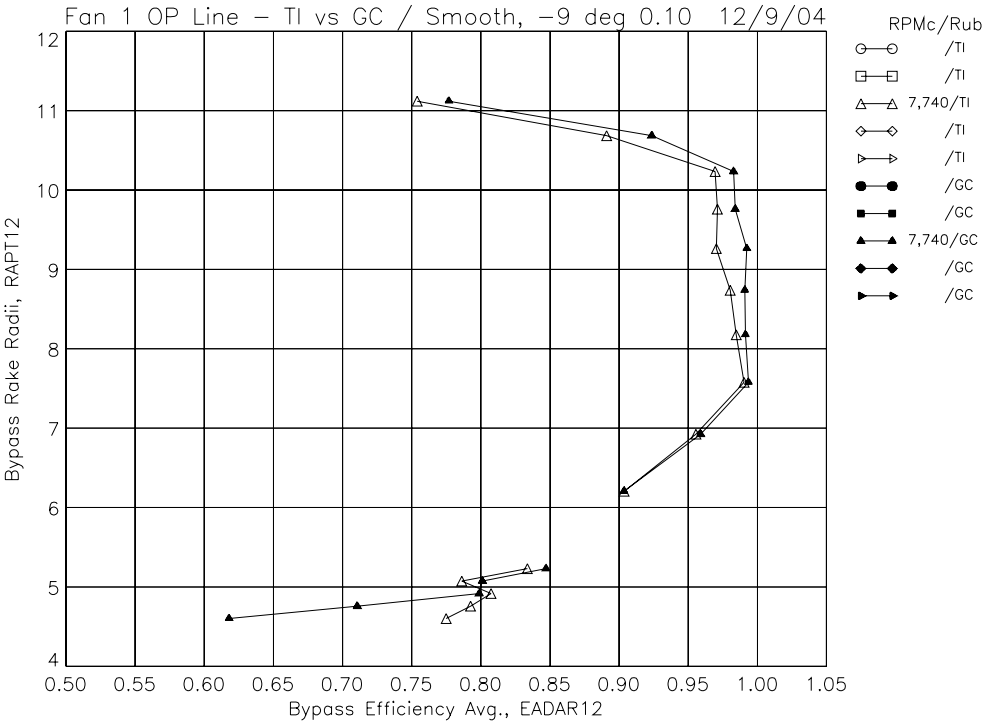

(g) Fan adiabatic efficiency radial profiles, 7,740 RPMc.

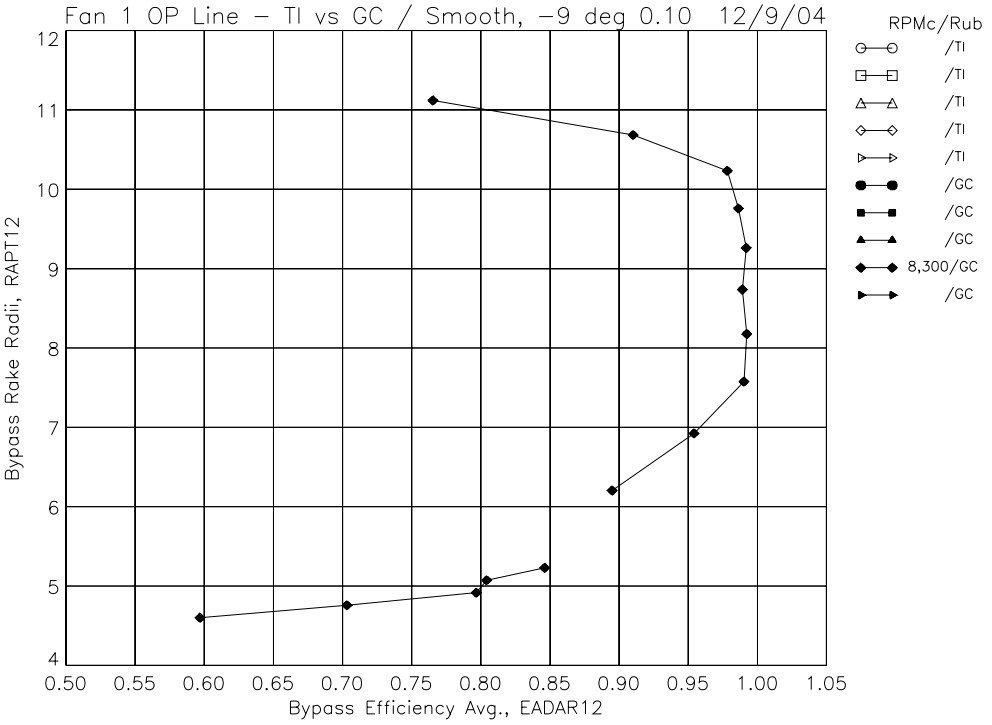

(h) Fan adiabatic efficiency radial profiles, 8,300 RPMc.

Figure 10.—TI and GC blade radial profiles on fan operating line, with –9 deg blade angle, smooth rubstrip, Mo = 0.10.

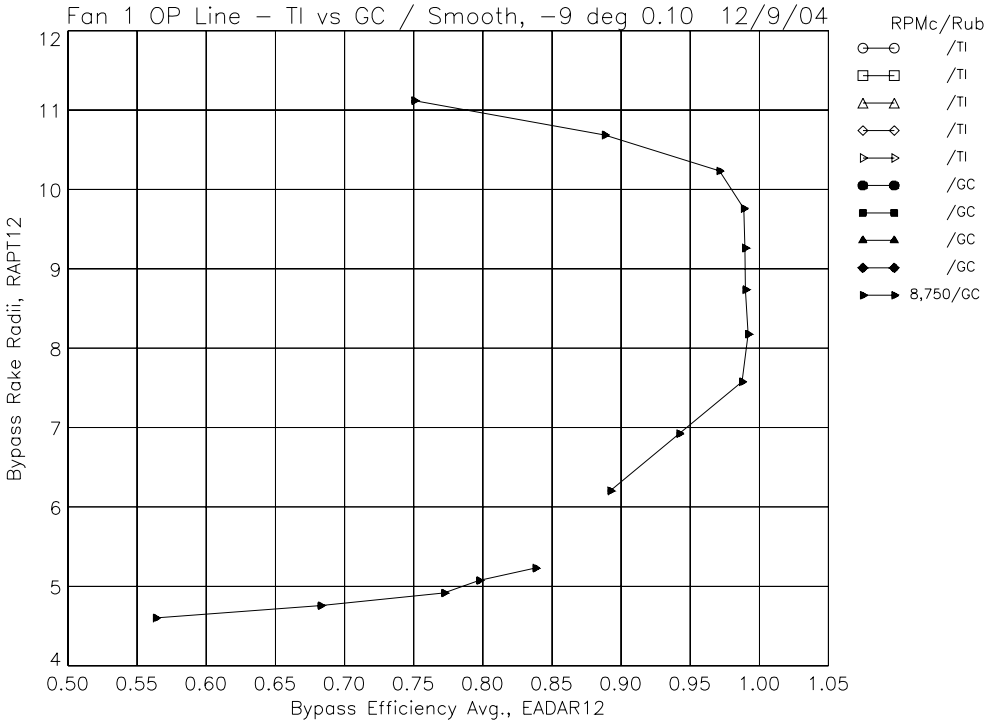

(i) Fan adiabatic efficiency radial profiles, 8,750 RPMc.

Figure 10.—TI and GC blade radial profiles on fan operating line, with –9 deg blade angle, smooth rubstrip, Mo = 0.10.

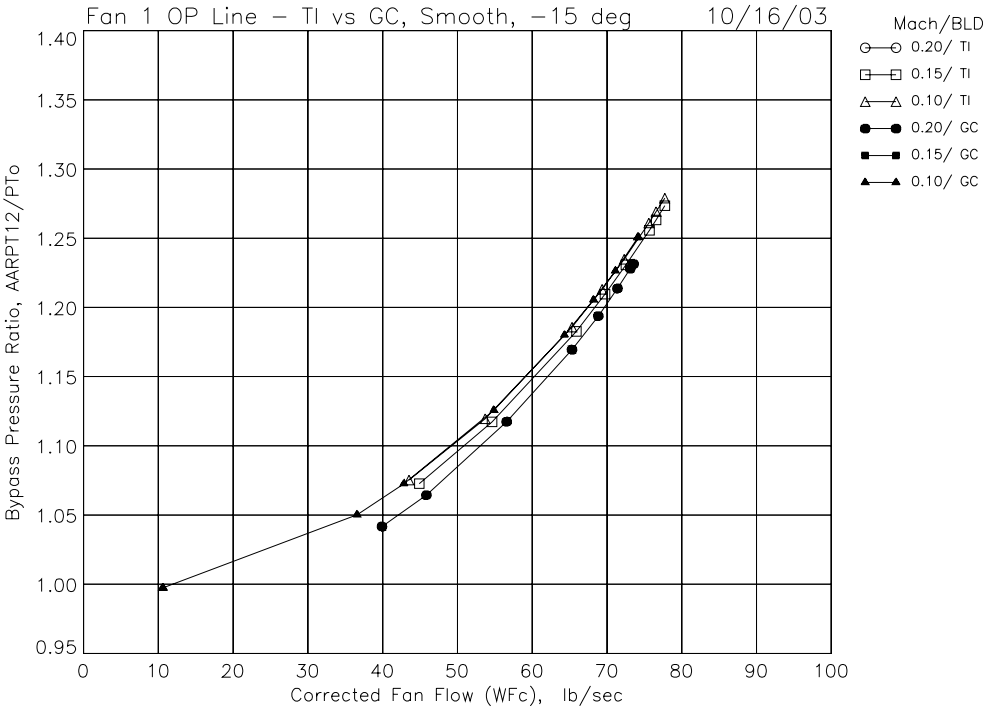

(a) Bypass total pressure ratio versus total fan corrected flow.

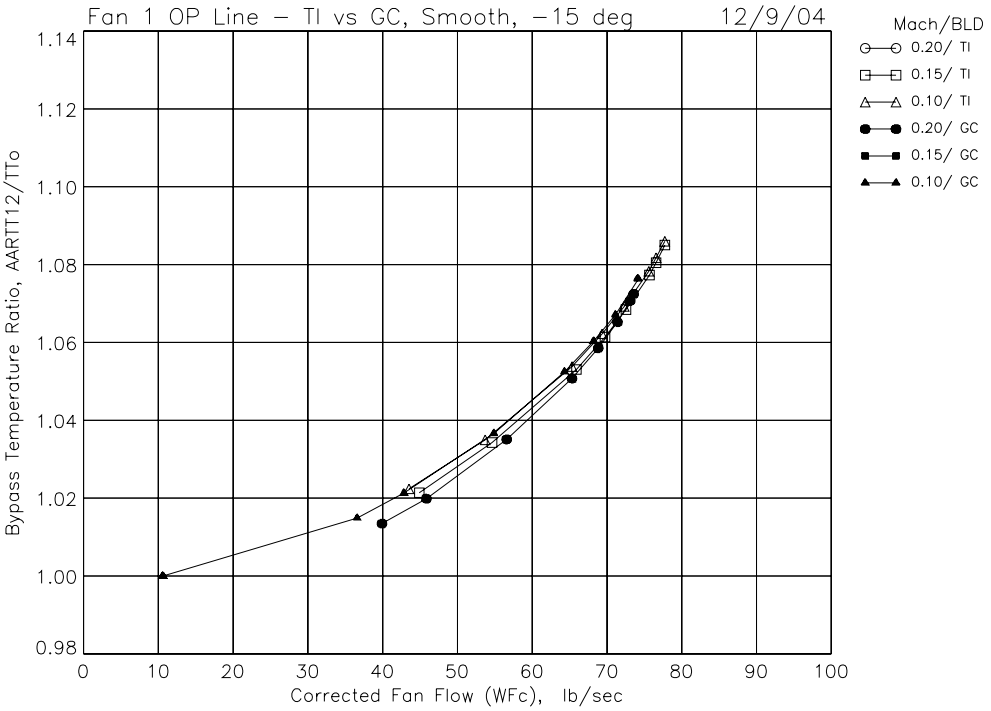

(b) Bypass total temperature ratio versus total fan corrected flow.

Figure 11.—TI and GC blade bypass operating line results with –15 deg blade angle, smooth rubstrip.

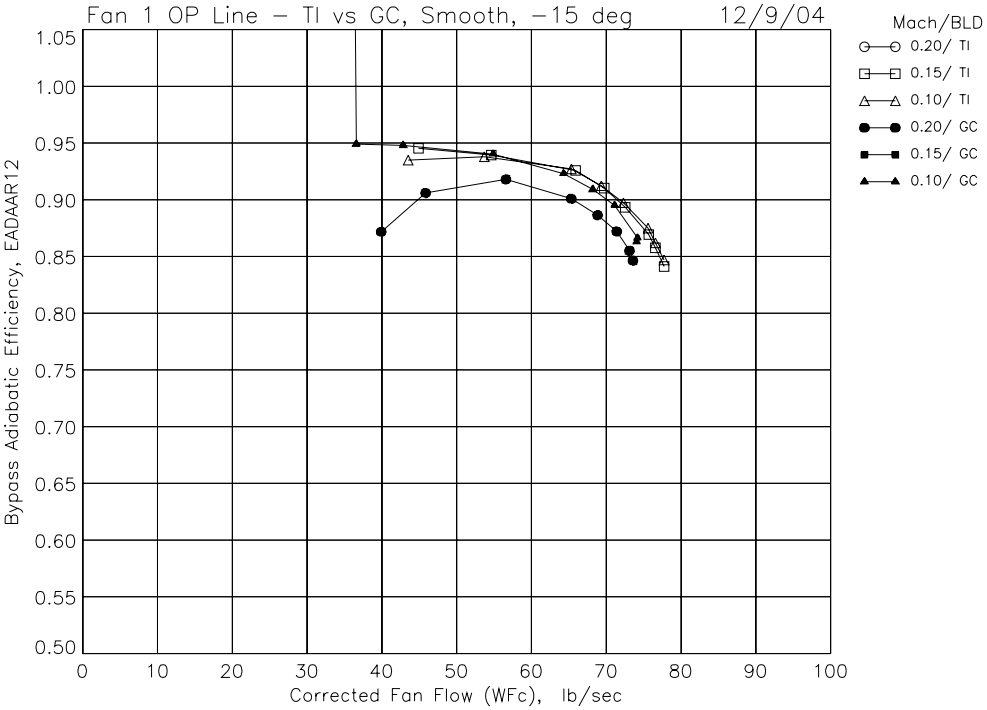

(c) Bypass adiabatic efficiency versus total fan corrected flow.

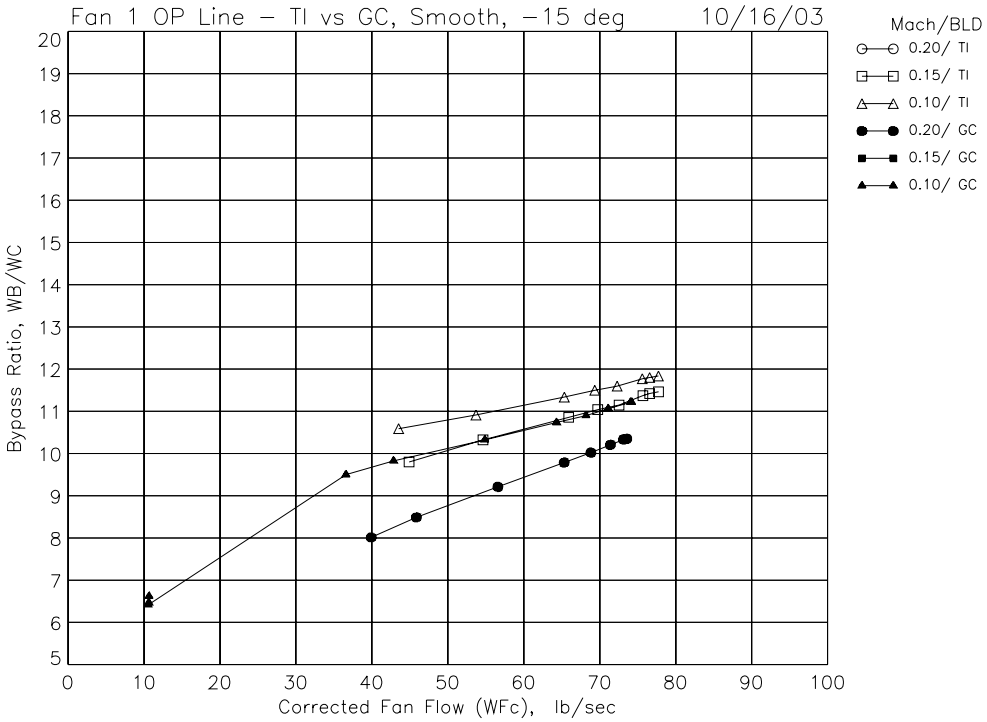

(d) Bypass ratio versus total fan corrected flow.

Figure 11.—TI and GC blade bypass operating line results with –15 deg blade angle, smooth rubstrip.

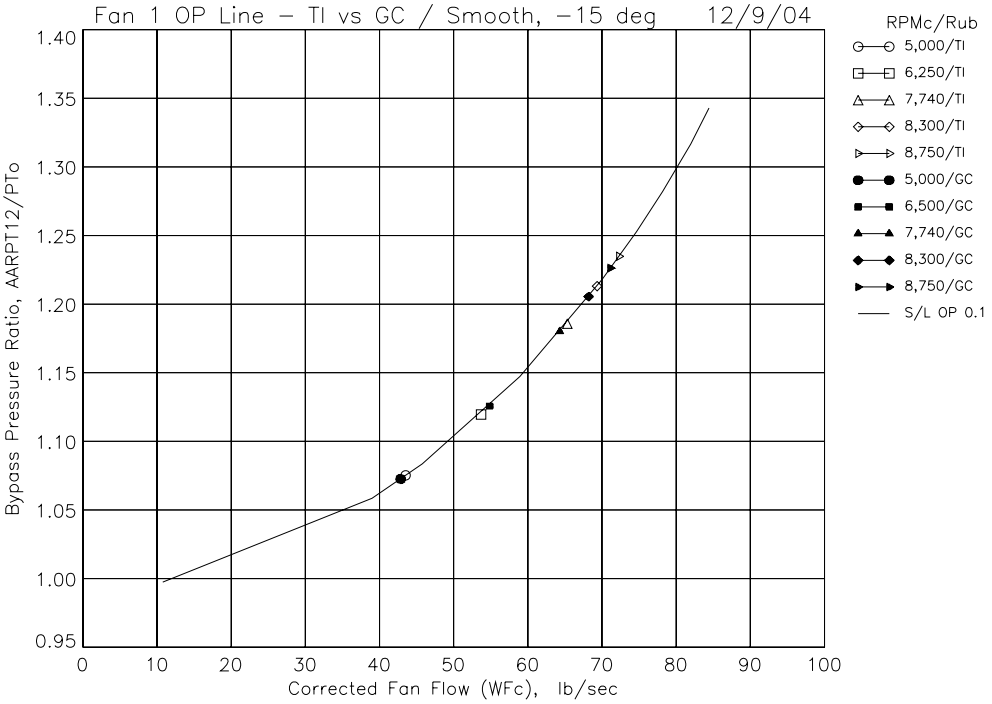

(a) Bypass total pressure ratio versus total fan corrected flow.

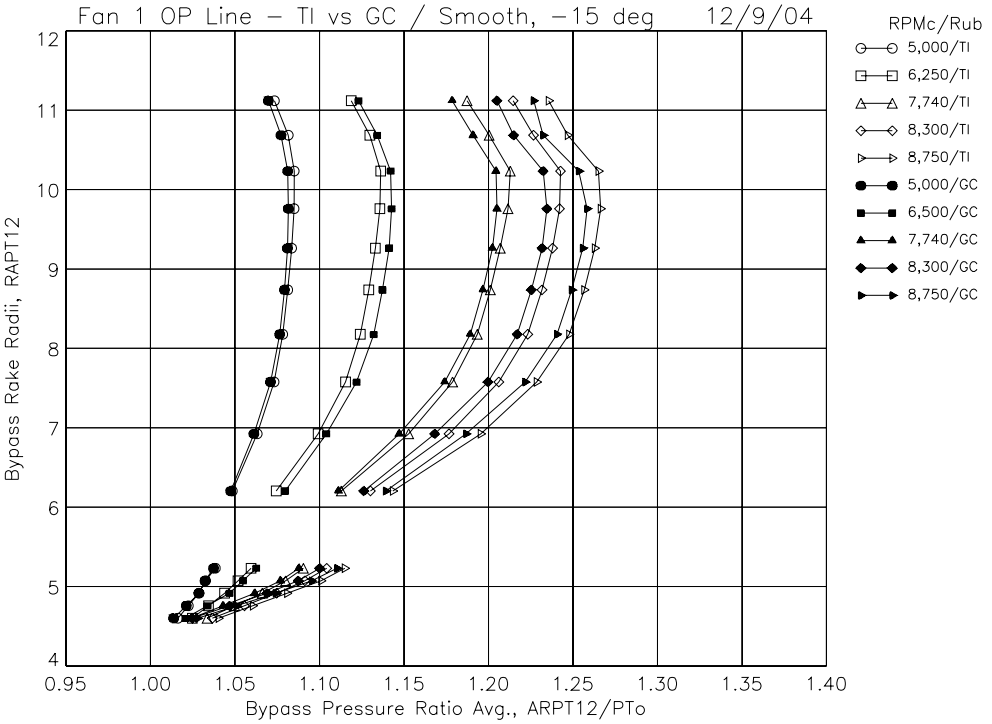

(b) Fan total pressure ratio radial profiles.

Figure 12.—TI and GC blade radial profiles on operating line with –15 deg blade angle, smooth rubstrip, Mo = 0.10.

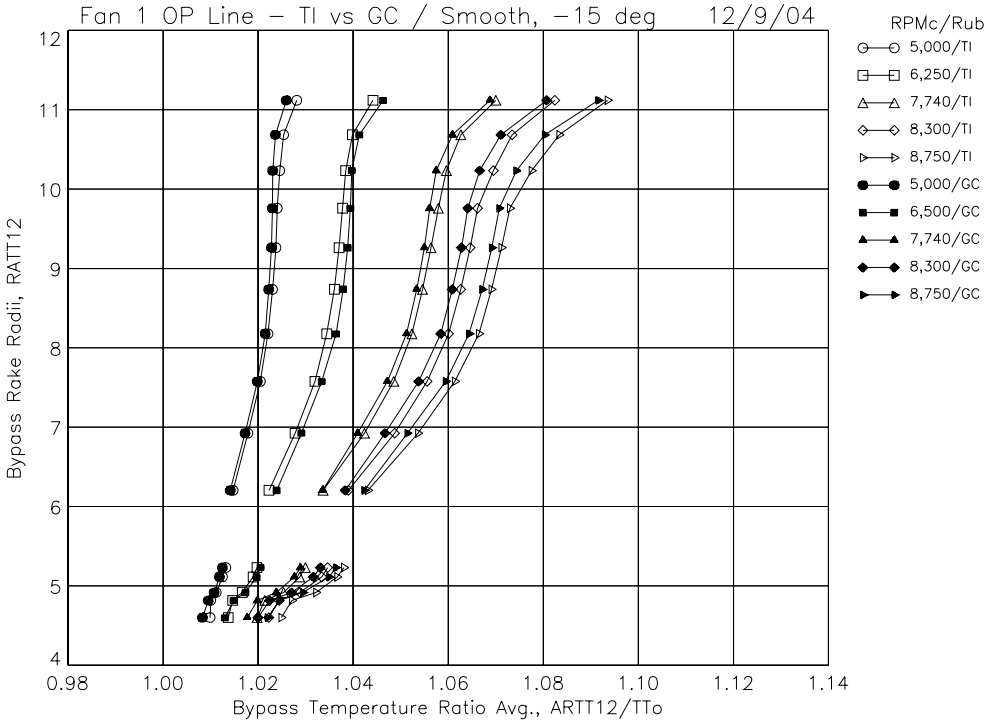

(c) Fan total temperature ratio radial profiles.

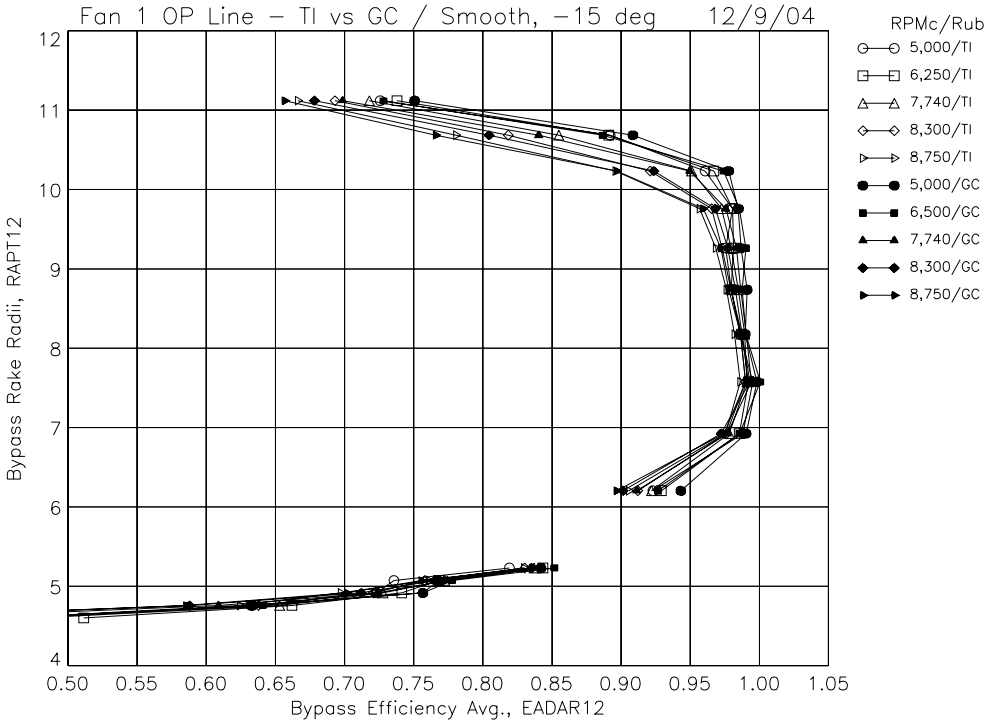

(d) Fan adiabatic efficiency radial profiles.

Figure 12.—TI and GC blade radial profiles on operating line with –15 deg blade angle, smooth rubstrip, Mo = 0.10.

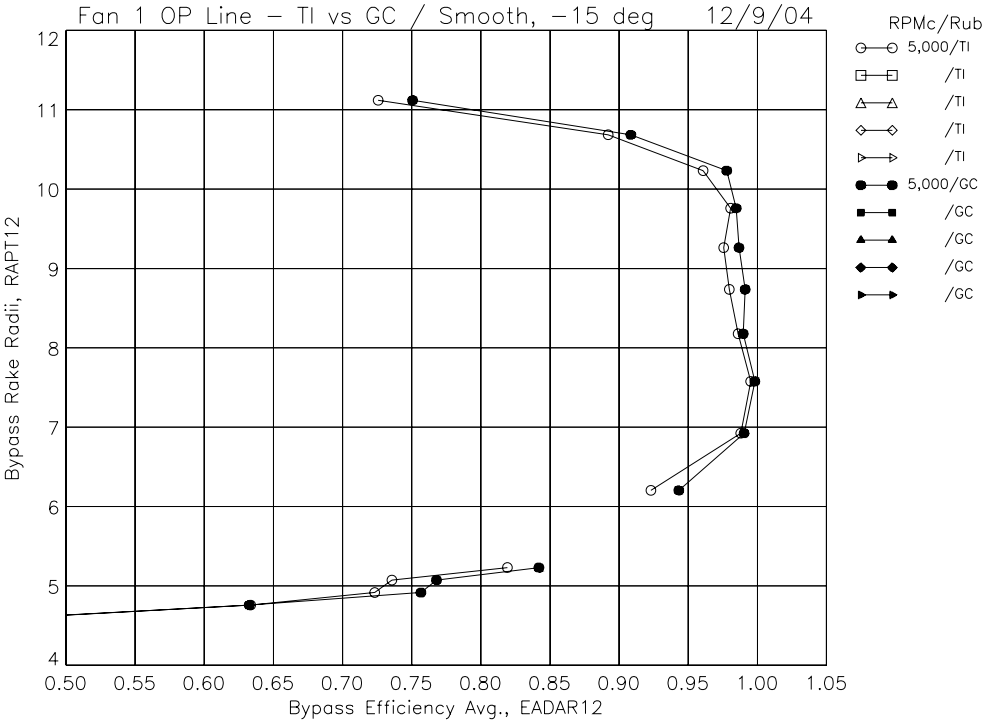

(e) Fan adiabatic efficiency radial profiles, 5,000 RPMc.

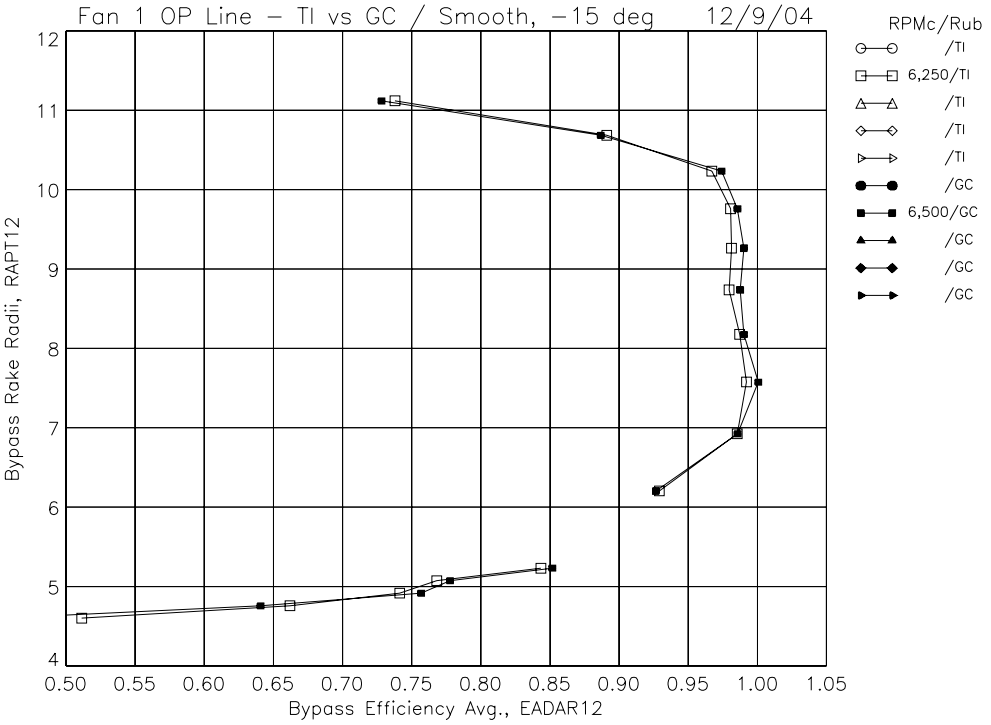

(f) Fan adiabatic efficiency radial profiles, 6,250 and 6,500 RPMc.

Figure 12.—TI and GC blade radial profiles on operating line with –15 deg blade angle, smooth rubstrip, Mo = 0.10.

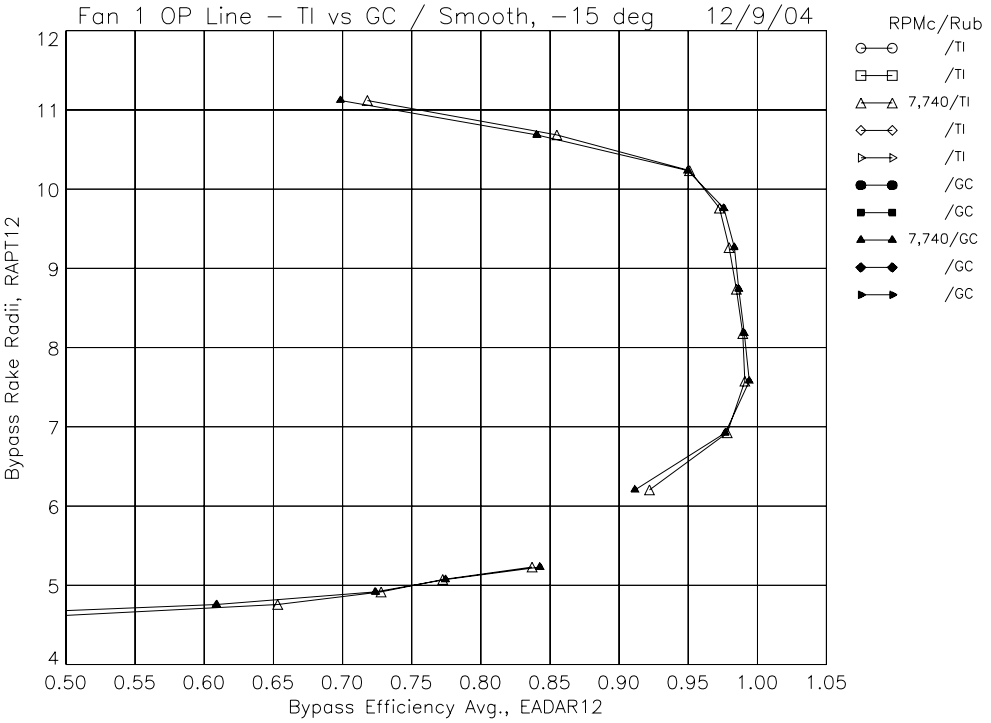

(g) Fan adiabatic efficiency radial profiles, 7,740 RPMc.

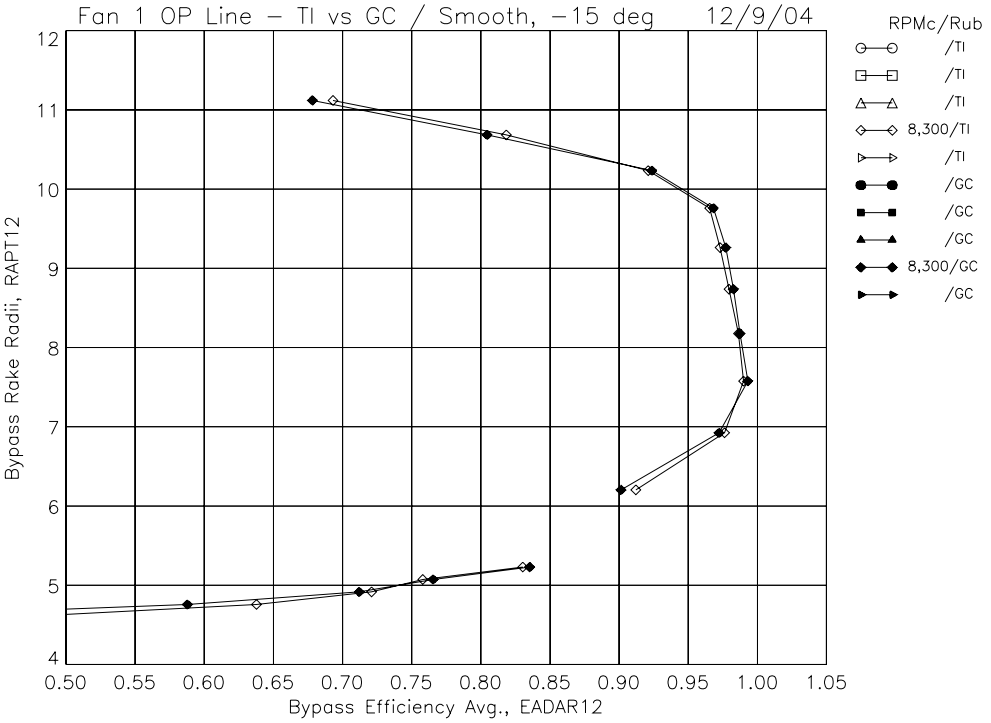

(h) Fan adiabatic efficiency radial profiles, 8,300 RPMc.

Figure 12.—TI and GC blade radial profiles on operating line with –15 deg blade angle, smooth rubstrip, Mo = 0.10.

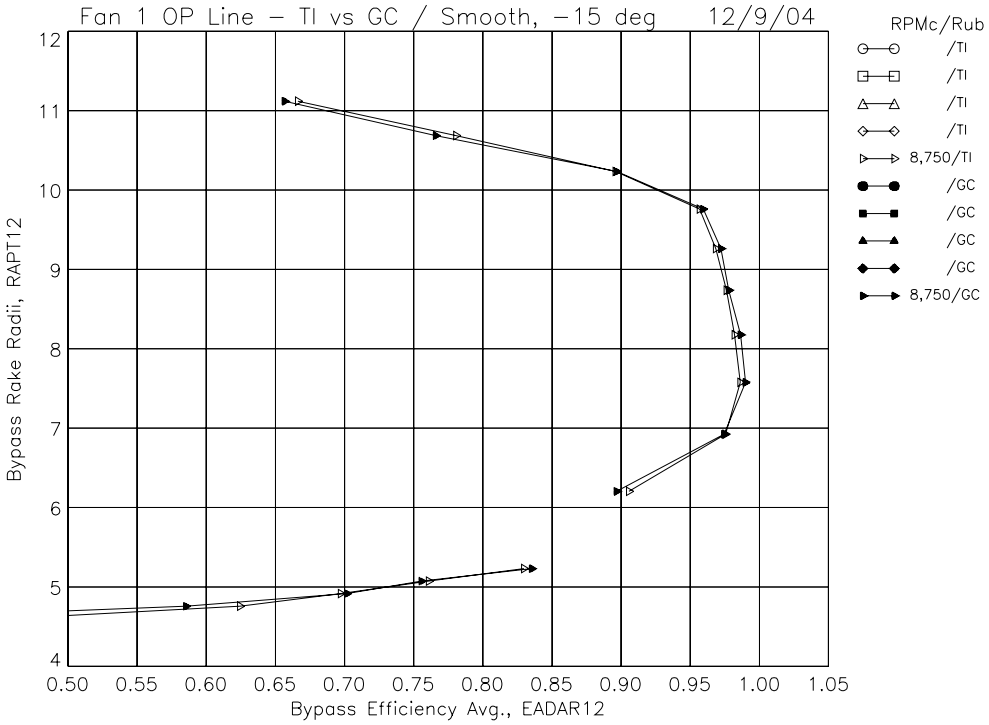

(i) Fan adiabatic efficiency radial profiles, 8,750 RPMc.

Figure 12.—TI and GC blade radial profiles on operating line with –15 deg blade angle, smooth rubstrip, Mo = 0.10.

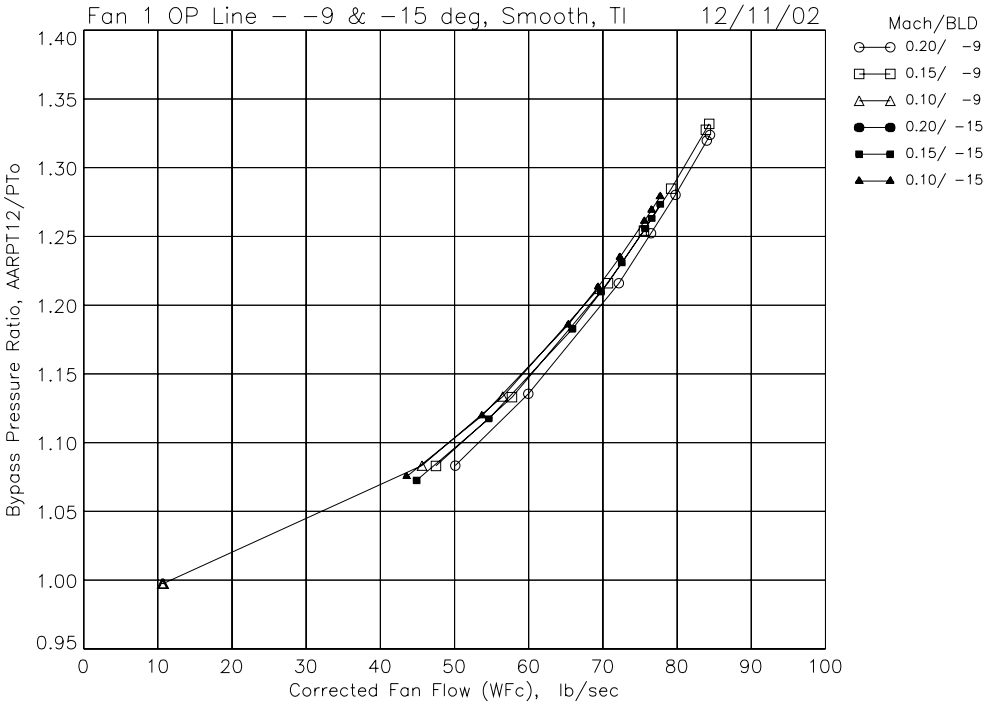

(a) Bypass total pressure ratio versus total fan corrected flow.

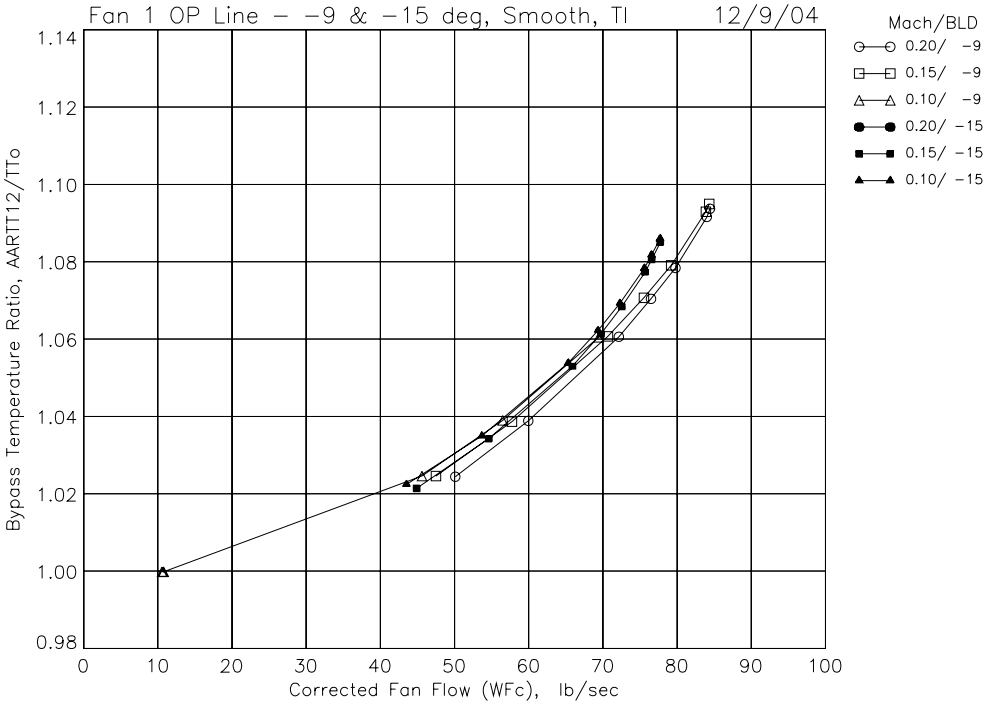

(b) Bypass total temperature ratio versus total fan corrected flow.

Figure 13.—The –9 and –15 deg blade angle bypass operating line results with TI blades, smooth rubstrip.

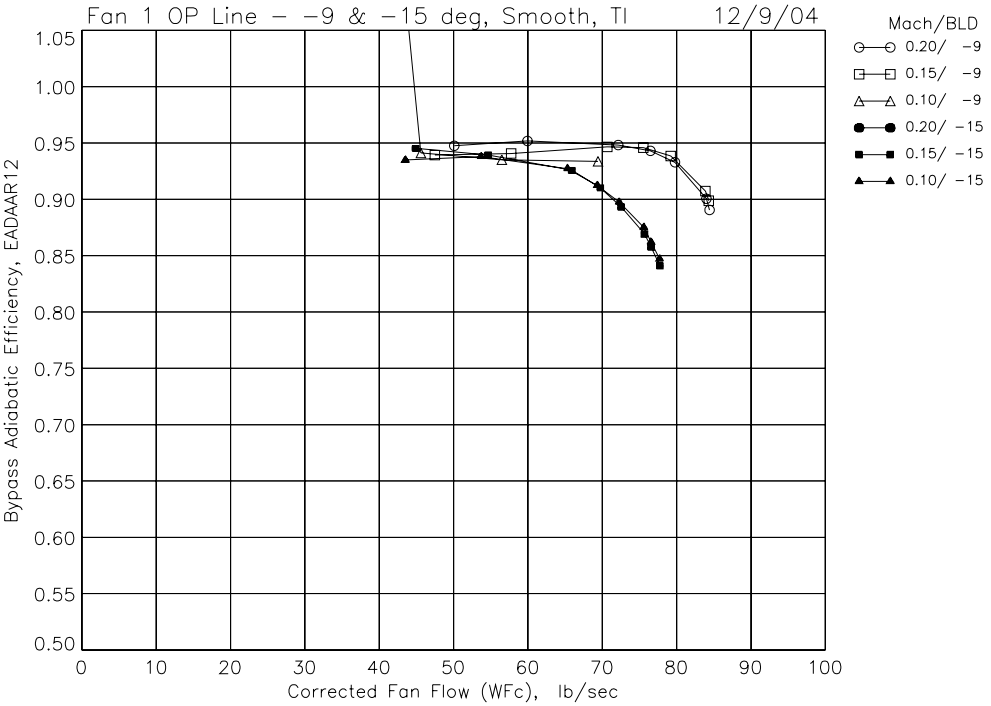

(c) Bypass adiabatic efficiency versus total fan corrected flow.

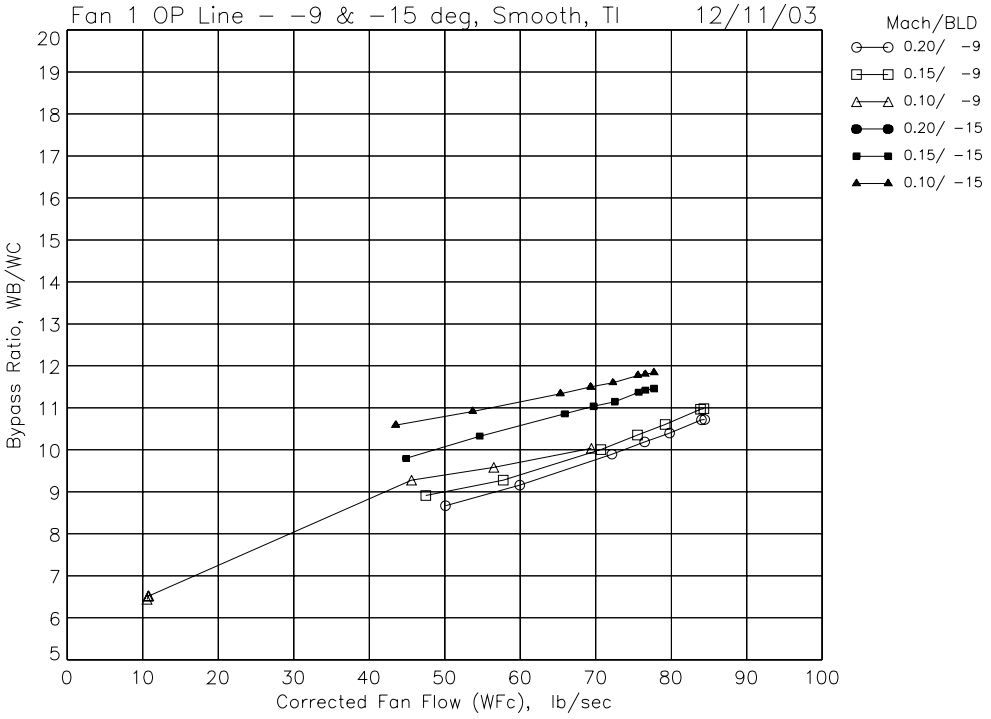

(d) Bypass ratio versus total fan corrected flow.

Figure 13.—The –9 and –15 deg blade angle bypass operating line results with TI blades, smooth rubstrip.

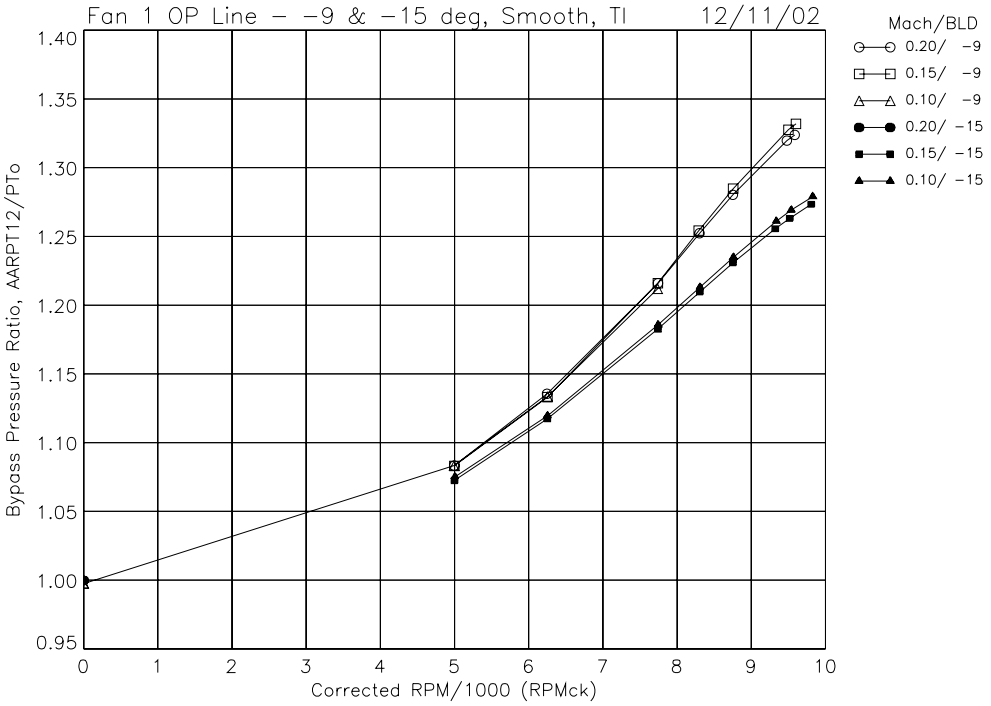

(e) Bypass total pressure ratio versus fan corrected speed.

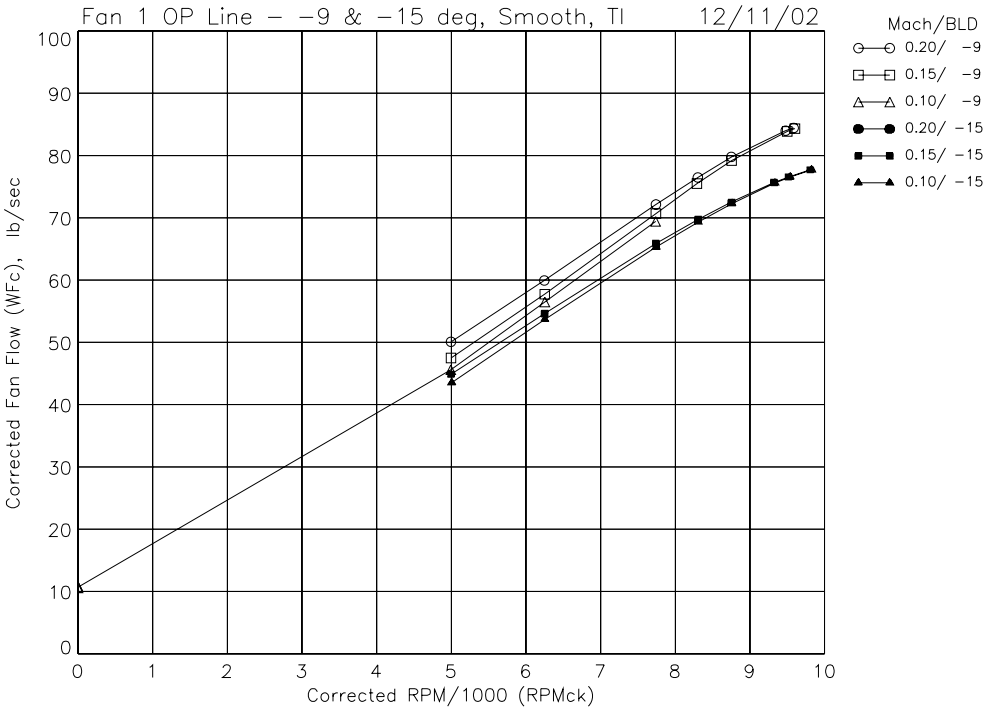

(f) Total fan corrected flow versus fan corrected speed.

Figure 13.—The –9 and –15 deg blade angle bypass operating line results with TI blades, smooth rubstrip.

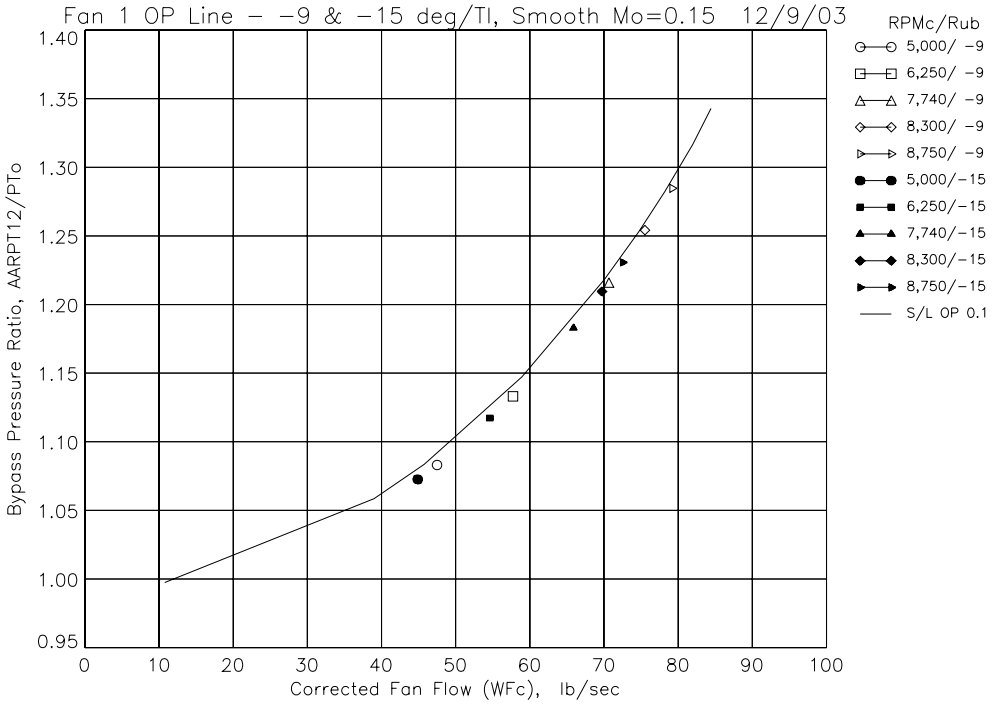

(a) Bypass total pressure ratio versus total fan corrected flow.

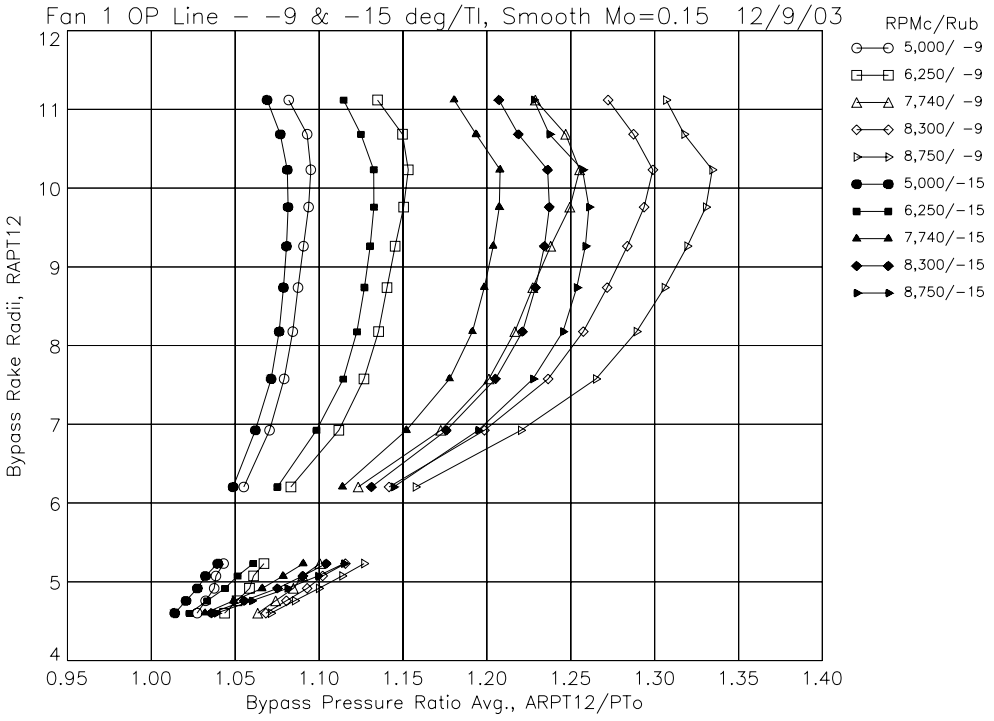

(b) Fan total pressure ratio radial profiles.

Figure 14.—The –9 and –15 deg blade angle radial profiles on operating line with TI blades, smooth rubstrip, Mo = 0.15.

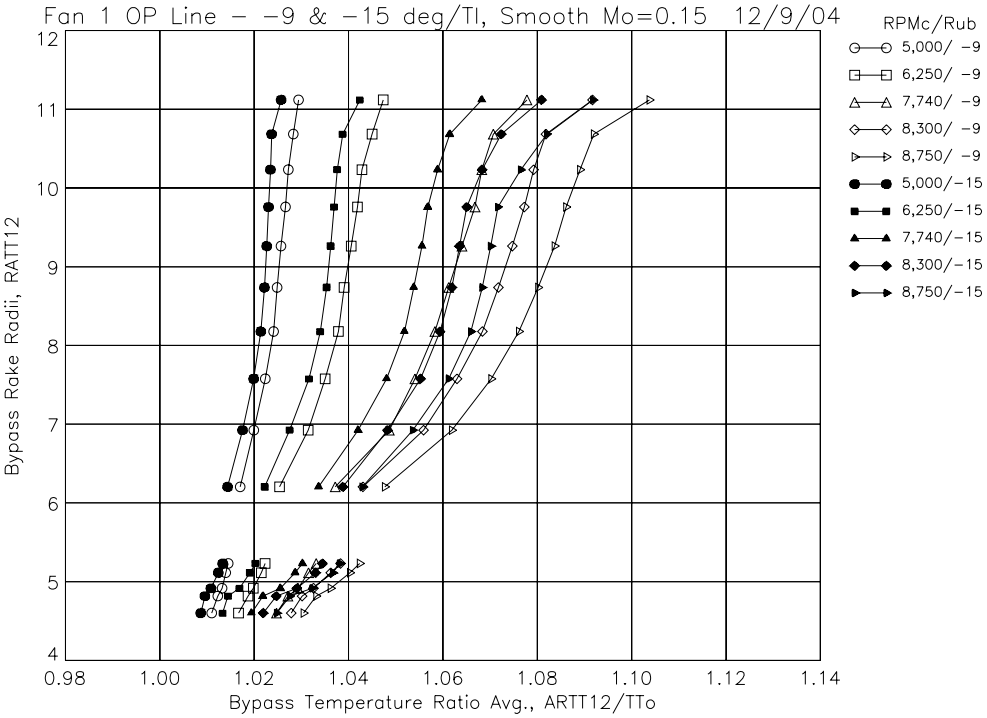

(c) Fan total temperature ratio radial profiles.

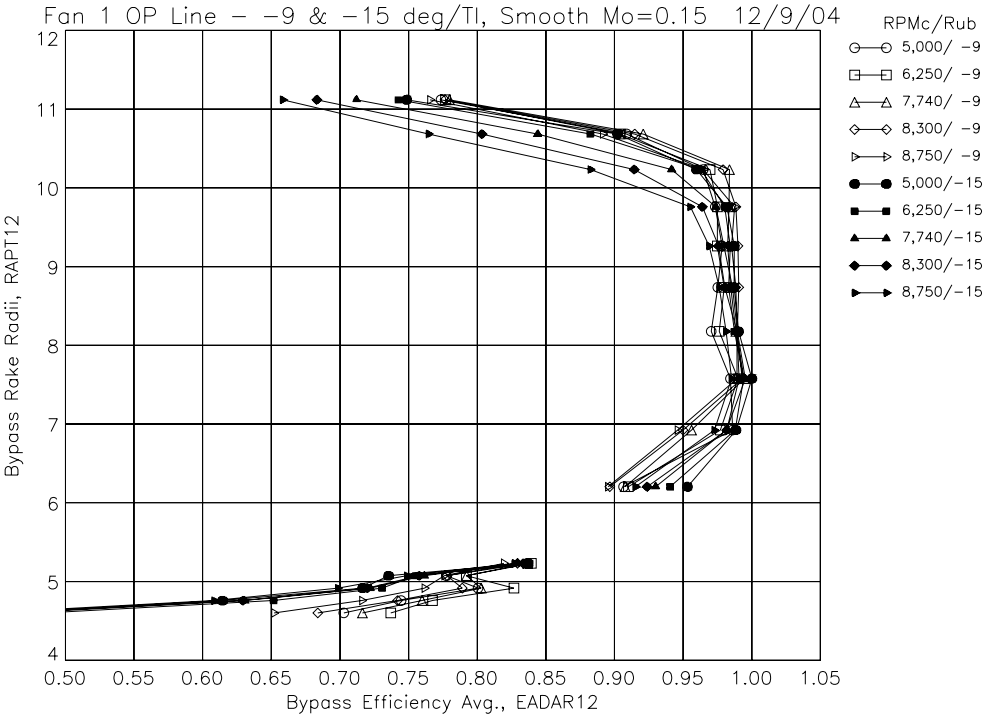

(d) Fan adiabatic efficiency radial profiles.

Figure 14.—The –9 and –15 deg blade angle radial profiles on operating line with TI blades, smooth rubstrip, Mo = 0.15.

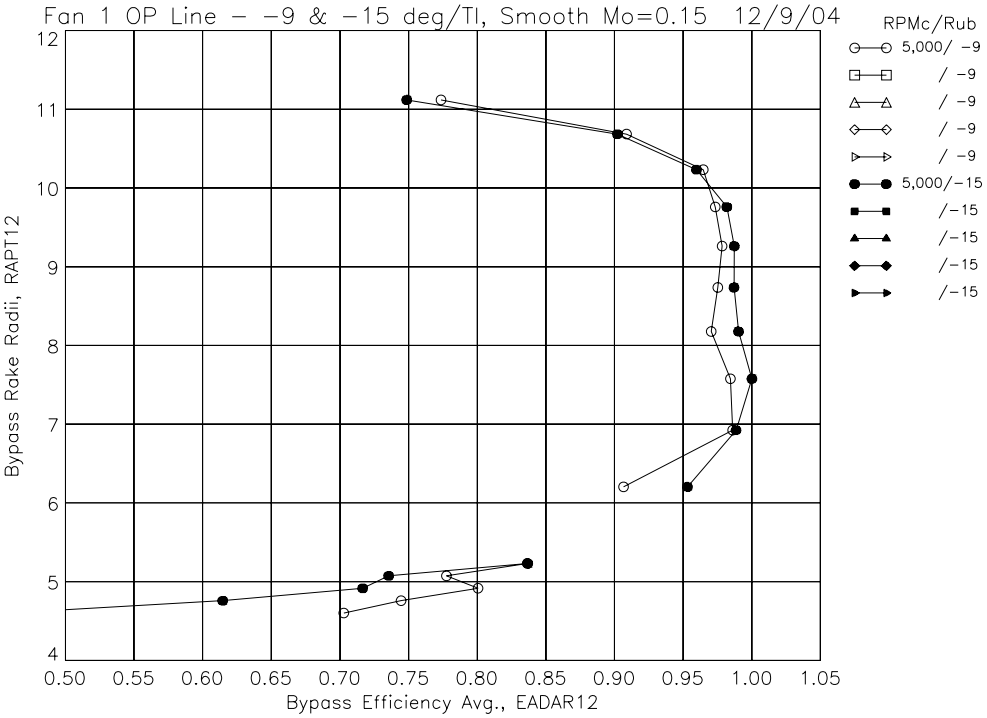

(e) Fan adiabatic efficiency radial profiles, 5,000 RPMc.

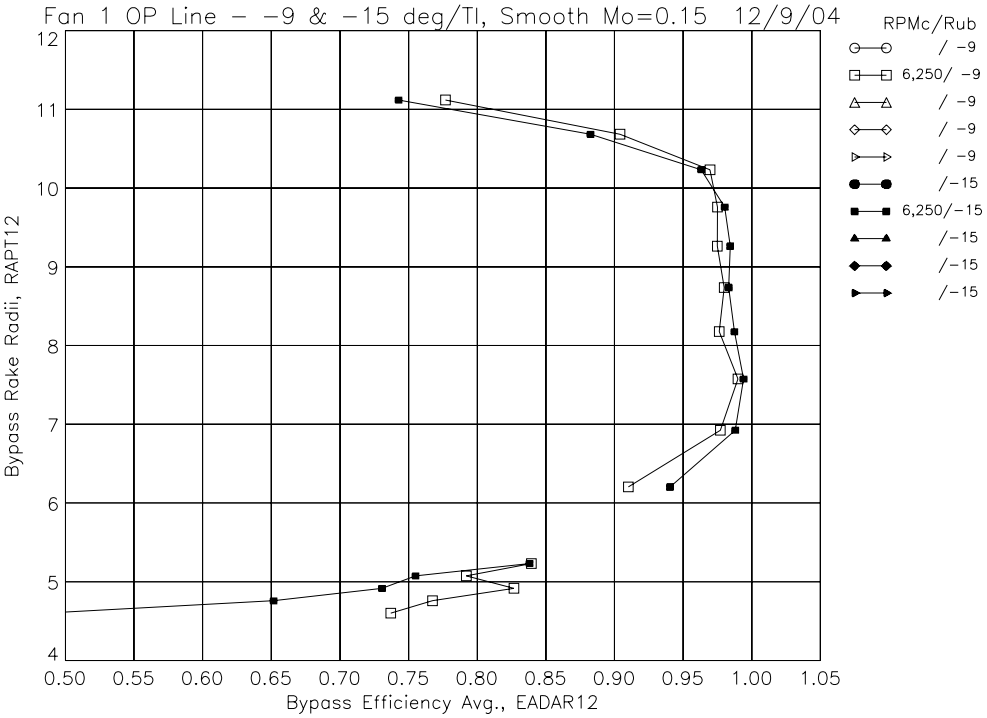

(f) Fan adiabatic efficiency radial profiles, 6,250 RPMc.

Figure 14.—The –9 and –15 deg blade angle radial profiles on operating line with TI blades, smooth rubstrip, Mo = 0.15.

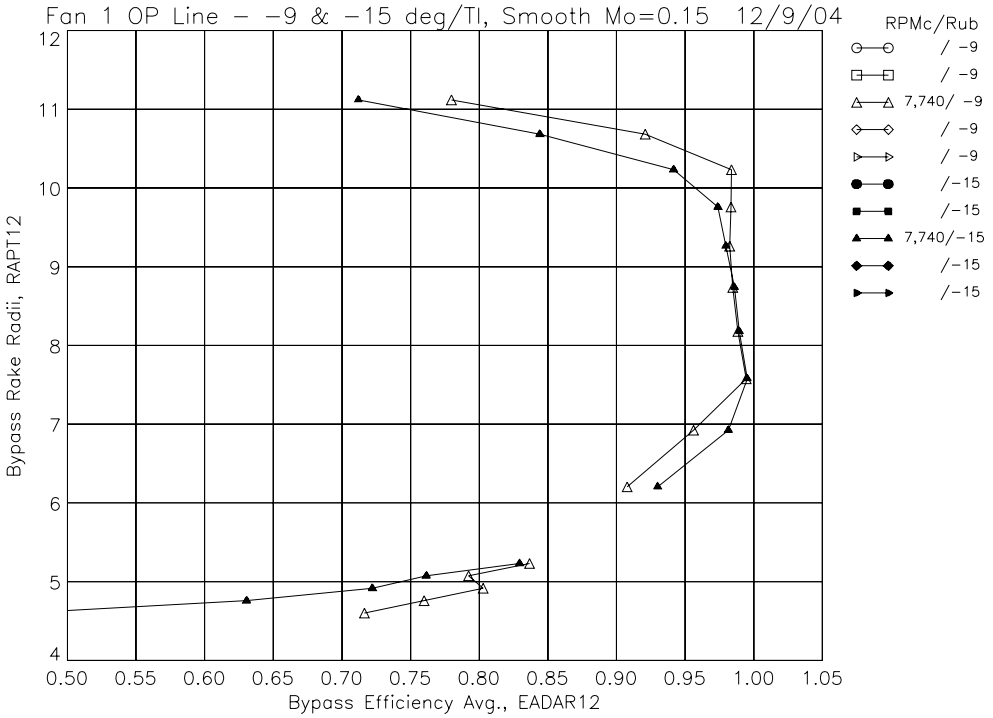

(g) Fan adiabatic efficiency radial profiles, 7,740 RPMc.

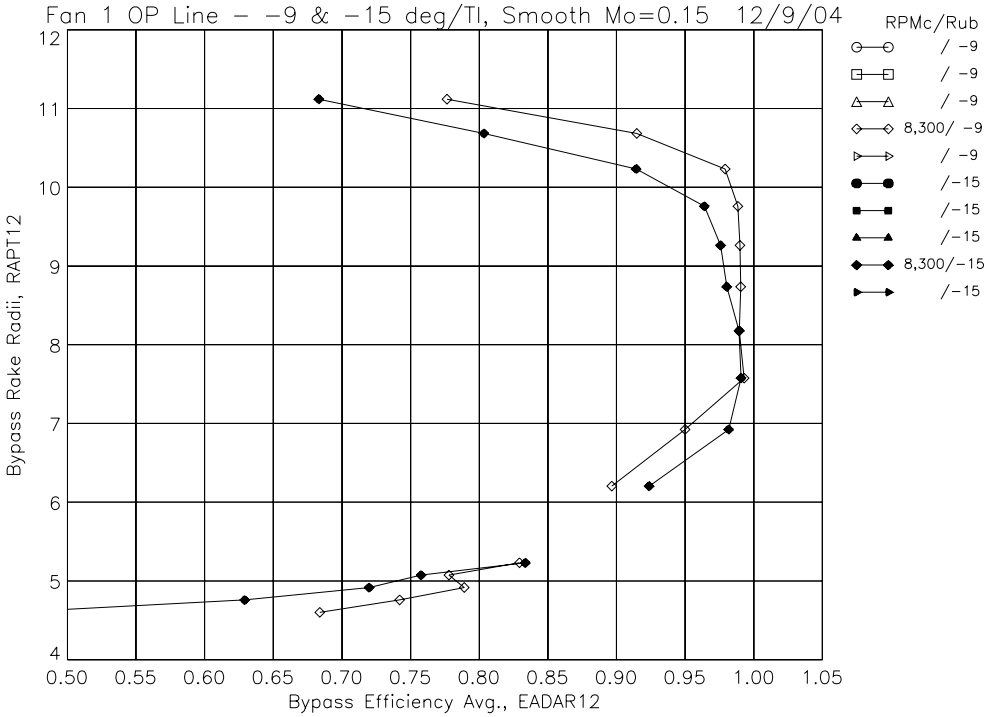

(h) Fan adiabatic efficiency radial profiles, 8,300 RPMc.

Figure 14.—The –9 and –15 deg blade angle radial profiles on operating line with TI blades, smooth rubstrip, Mo = 0.15.

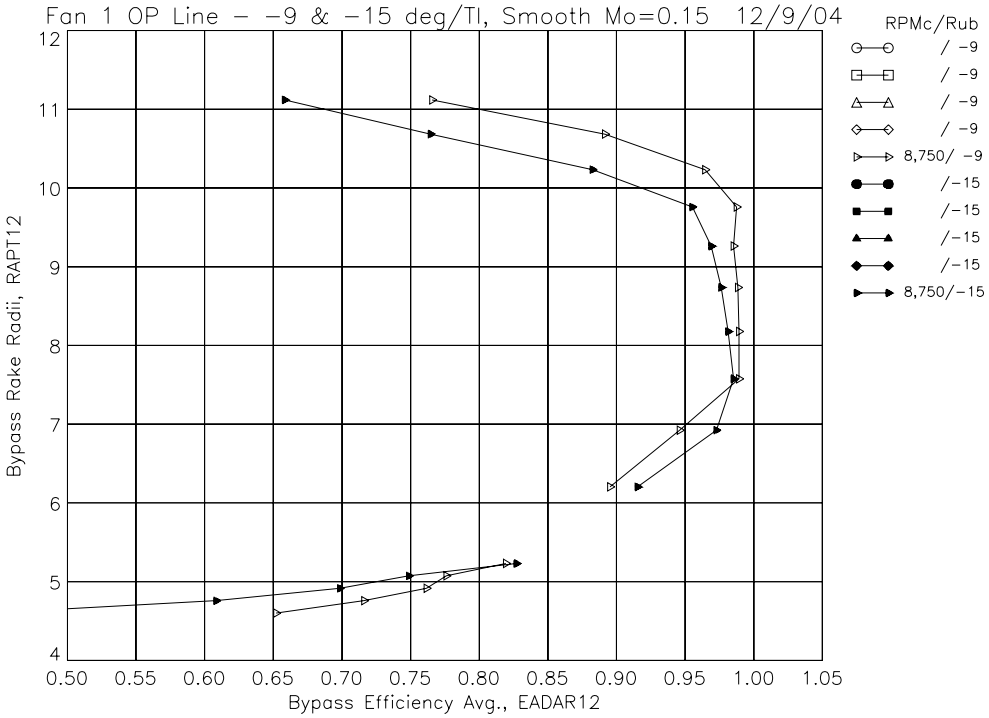

(i) Fan adiabatic efficiency radial profiles, 8,750 RPMc.

Figure 14.—The –9 and –15 deg blade angle radial profiles on operating line with TI blades, smooth rubstrip, Mo = 0.15.

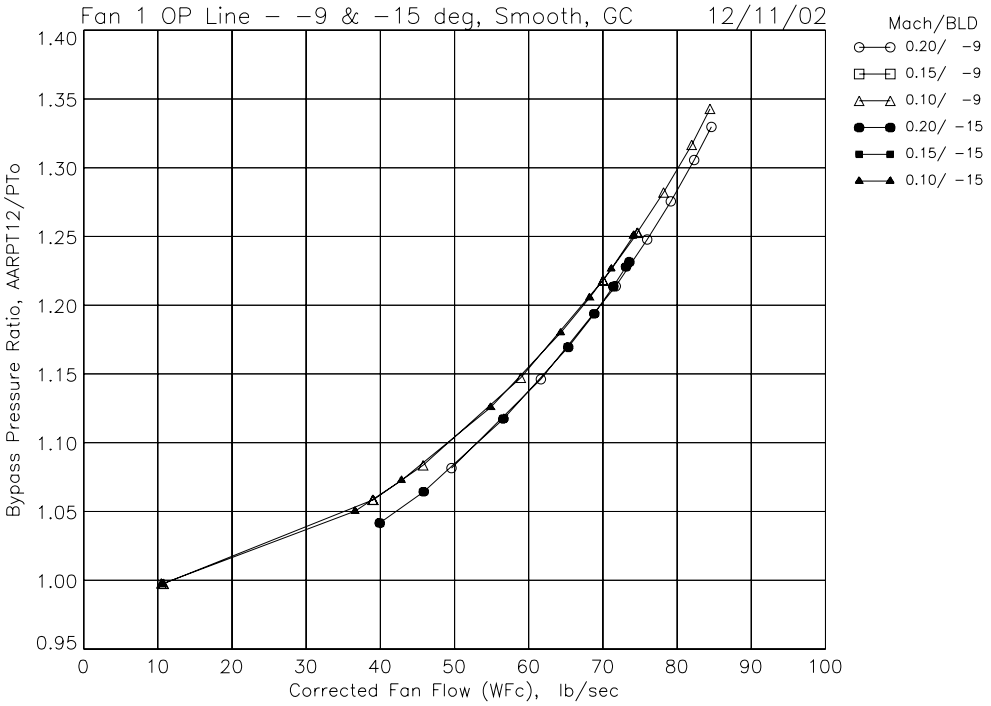

(a) Bypass total pressure ratio versus total fan corrected flow.

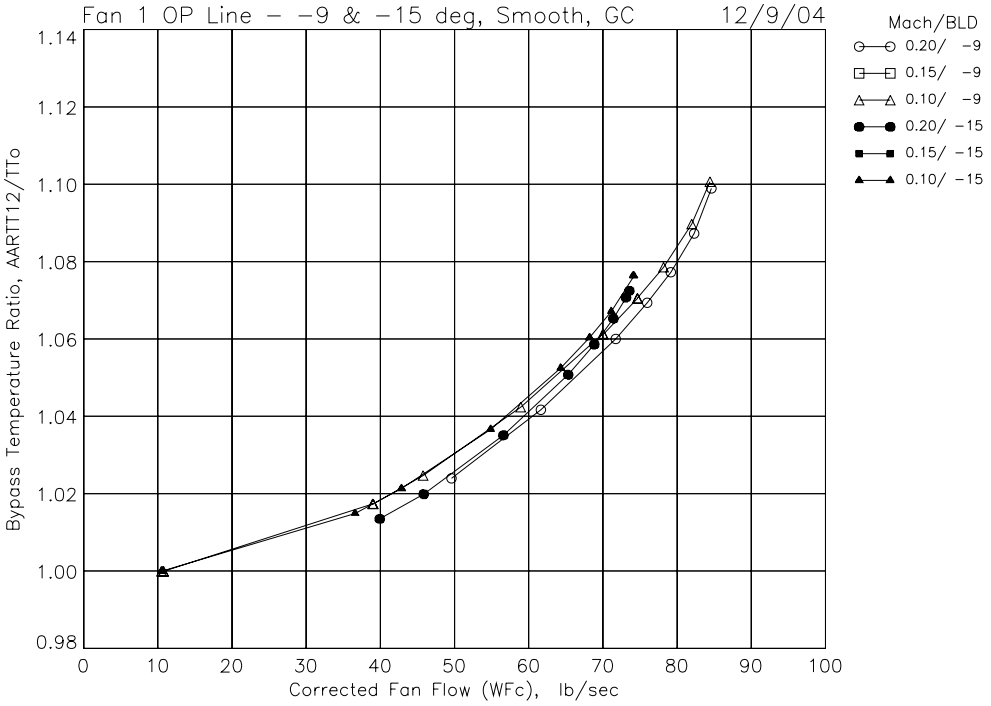

(b) Bypass total temperature ratio versus total fan corrected flow.

Figure 15.—The –9 and –15 deg blade angle bypass operating line results with GC blades, smooth rubstrip.

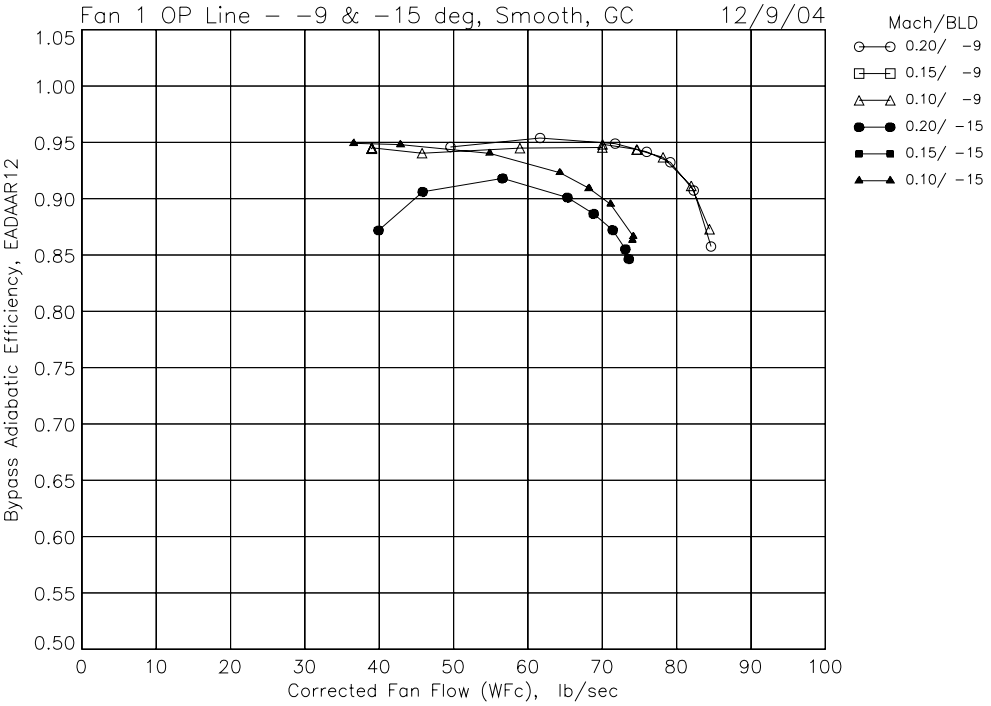

(c) Bypass adiabatic efficiency versus total fan corrected flow.

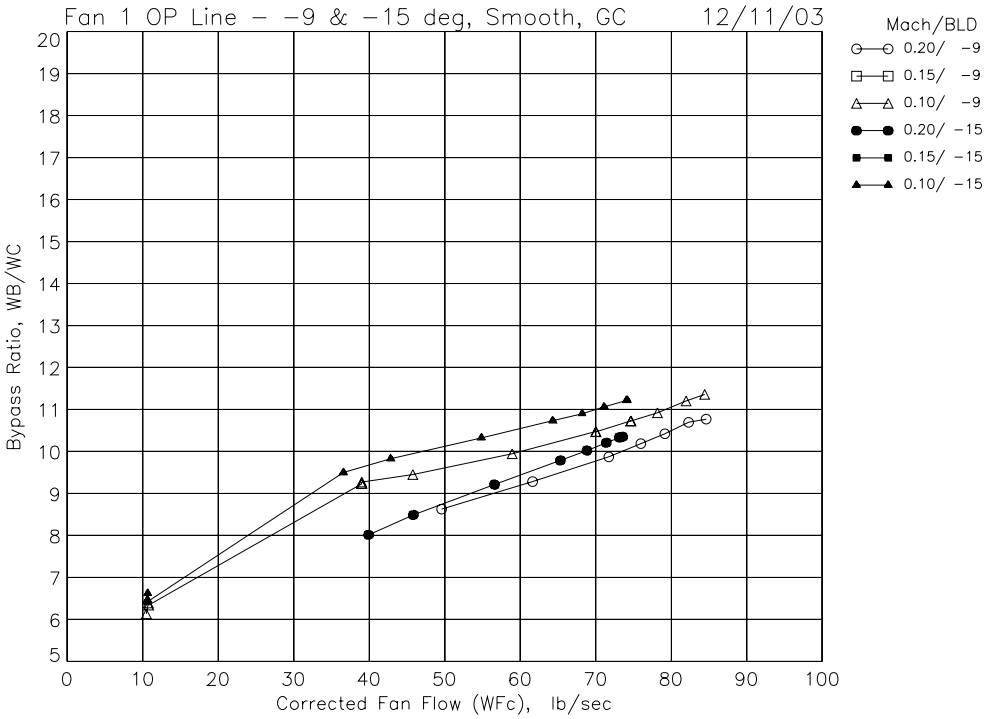

(d) Bypass ratio versus total fan corrected flow.

Figure 15.—The –9 and –15 deg blade angle bypass operating line results with GC blades, smooth rubstrip.

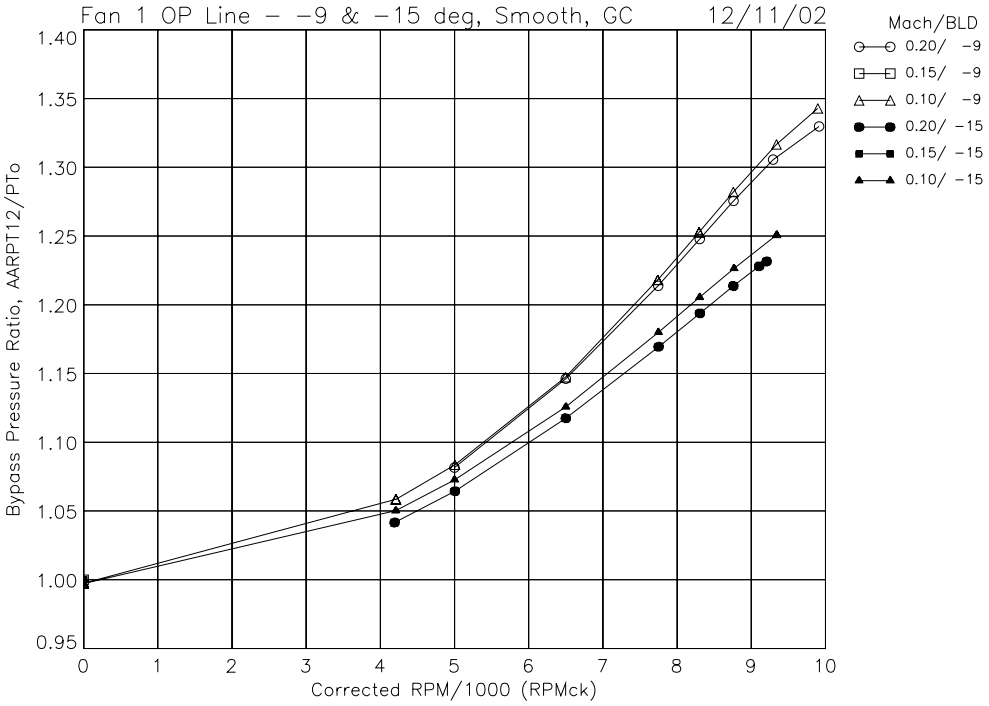

(e) Bypass total pressure ratio versus fan corrected speed.

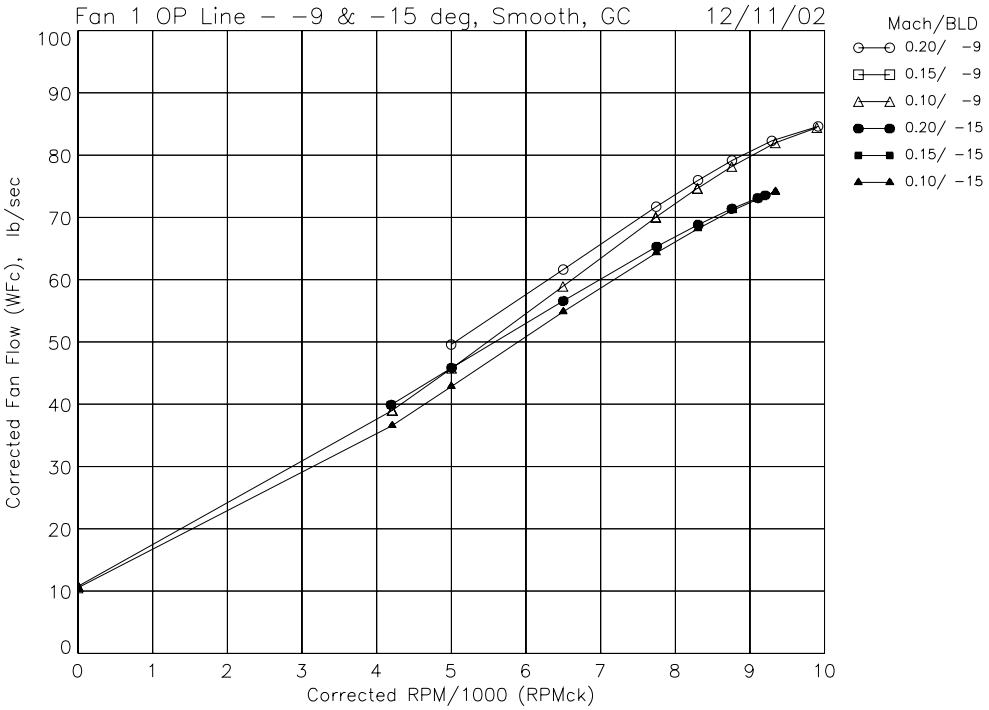

(f) Total fan corrected flow versus fan corrected speed.

Figure 15.—The –9 and –15 deg blade angle bypass operating line results with GC blades, smooth rubstrip.

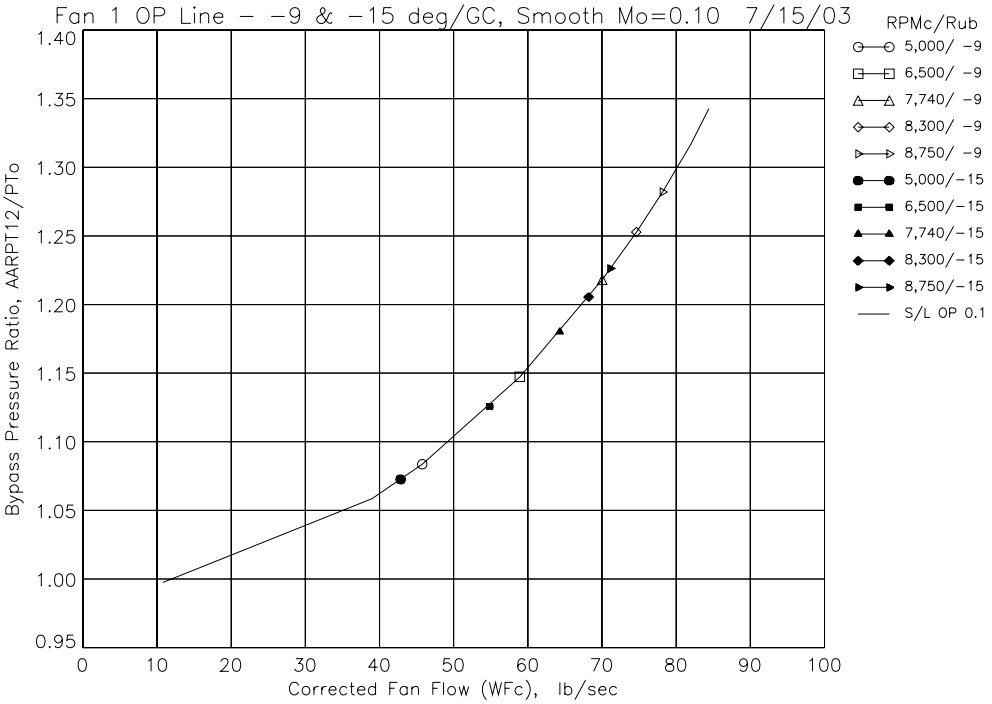

(a) Bypass total pressure ratio versus total fan corrected flow.

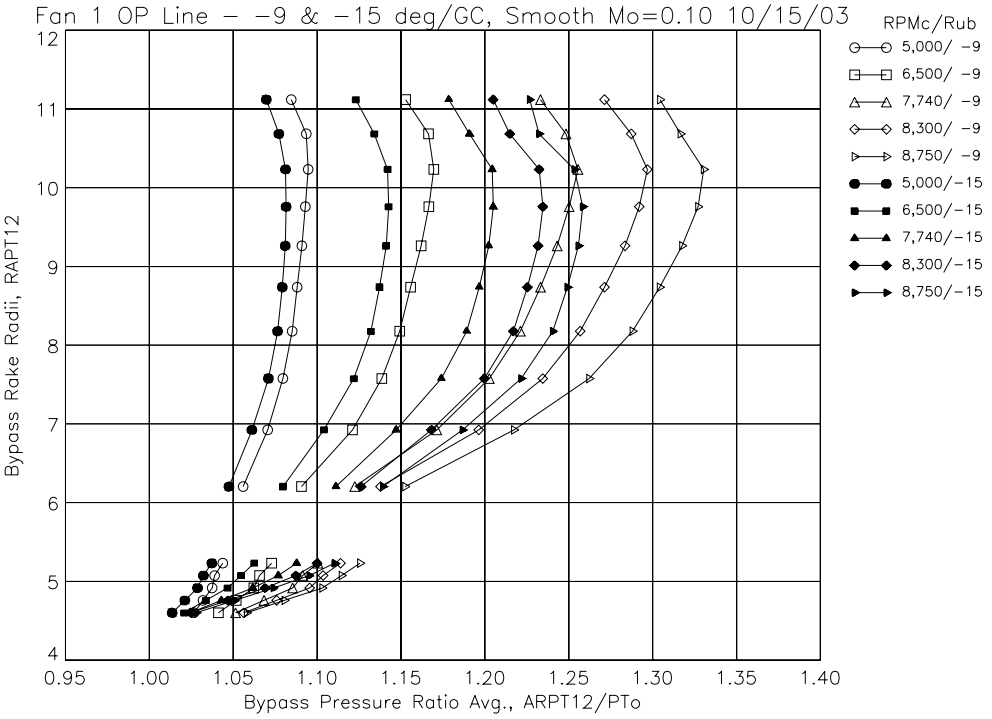

(b) Fan total pressure ratio radial profiles.

Figure 16.—The –9 and –15 deg blade angle radial profiles on operating line with GC blades, smooth rubstrip, Mo = 0.10.

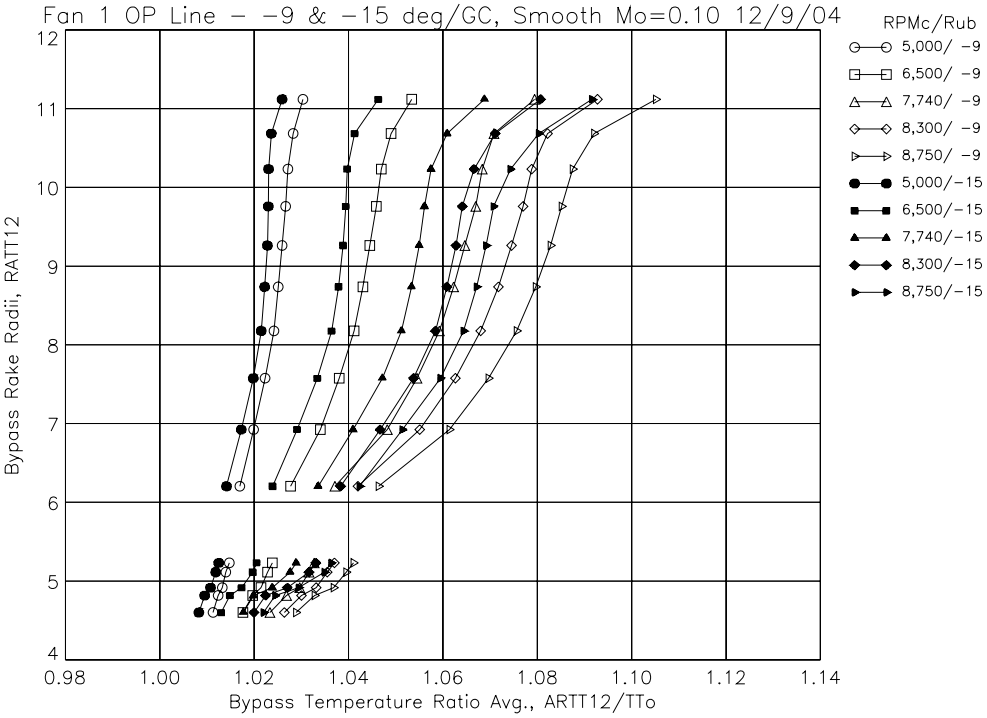

(c) Fan total temperature ratio radial profiles.

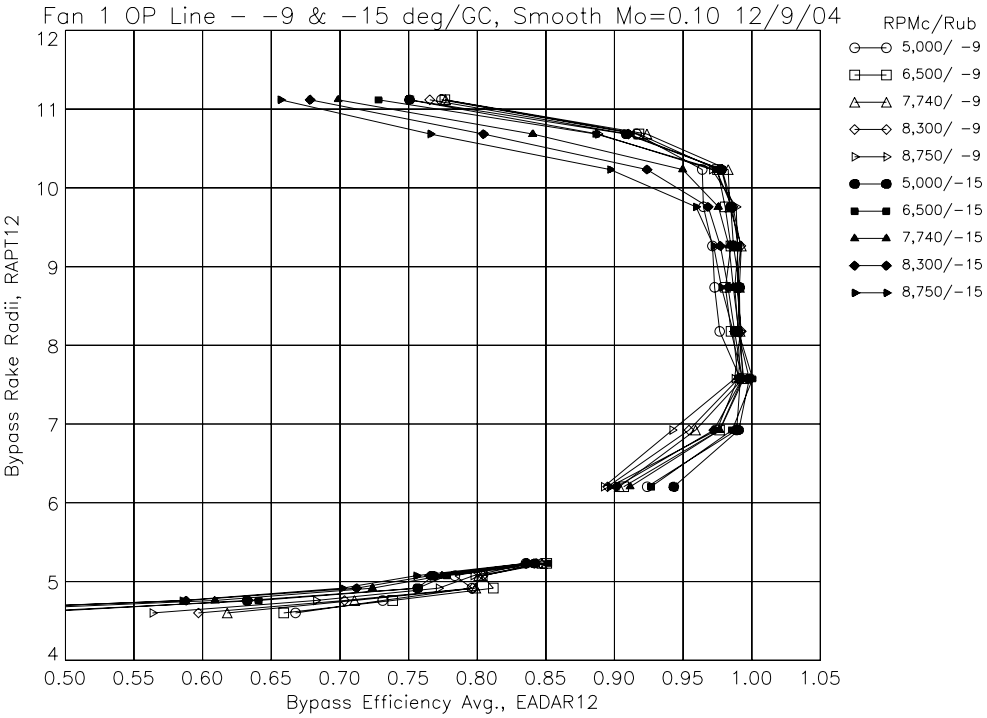

(d) Fan adiabatic efficiency radial profiles.

Figure 16.—The –9 and –15 deg blade angle radial profiles on operating line with GC blades, smooth rubstrip, Mo = 0.10.

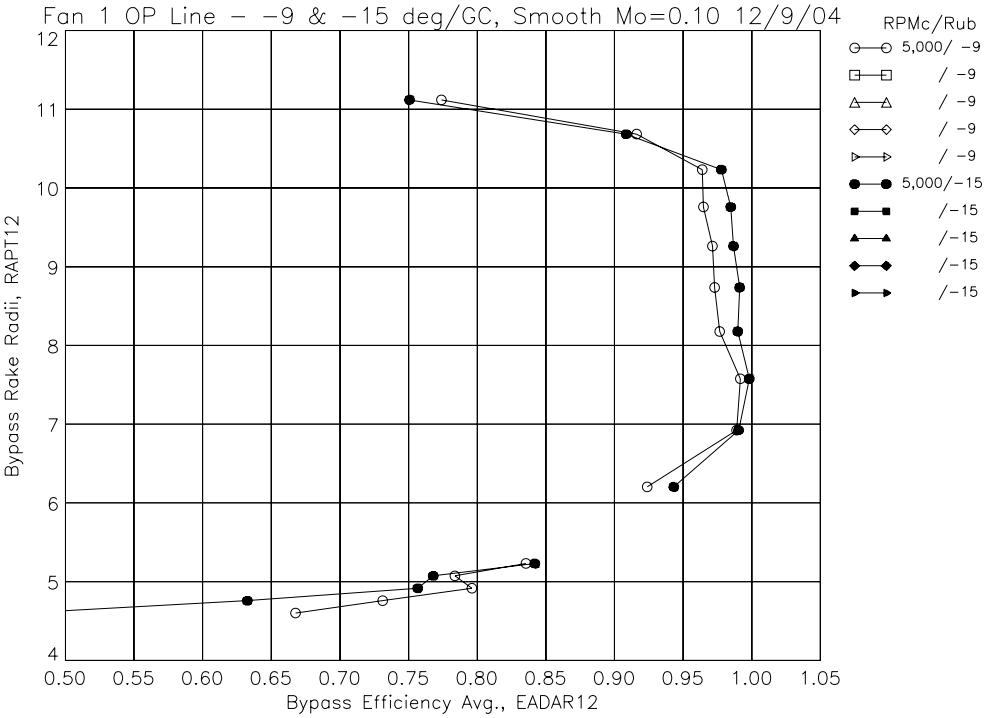

(e) Fan adiabatic efficiency radial profiles, 5,000 RPMc.

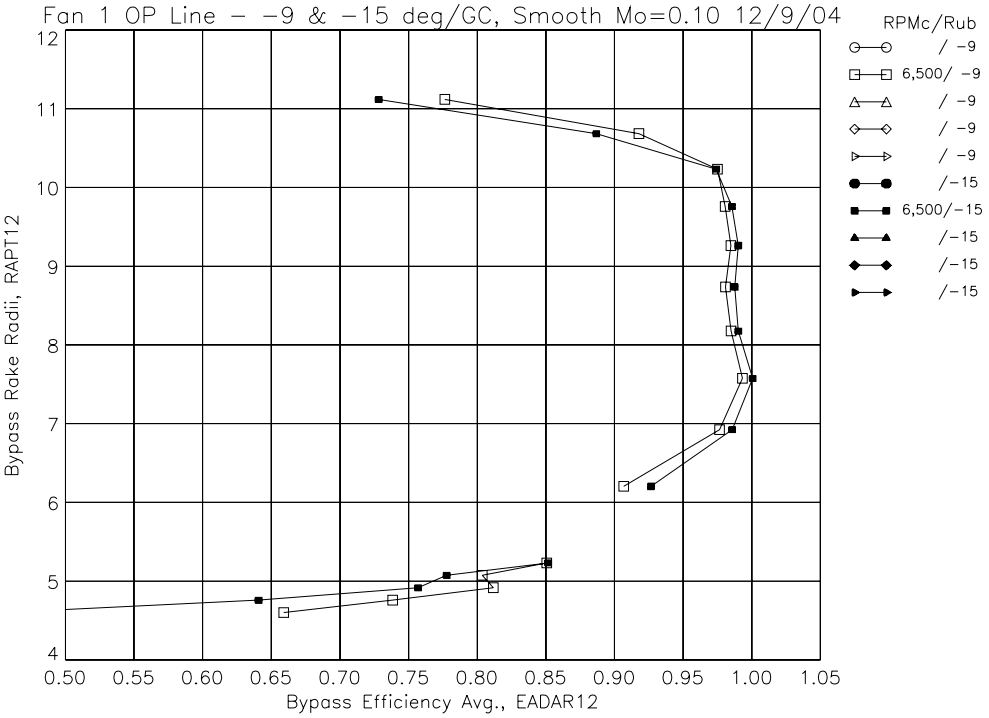

(f) Fan adiabatic efficiency radial profiles, 6,500 RPMc.

Figure 16.—The –9 and –15 deg blade angle radial profiles on operating line with GC blades, smooth rubstrip, Mo = 0.10.

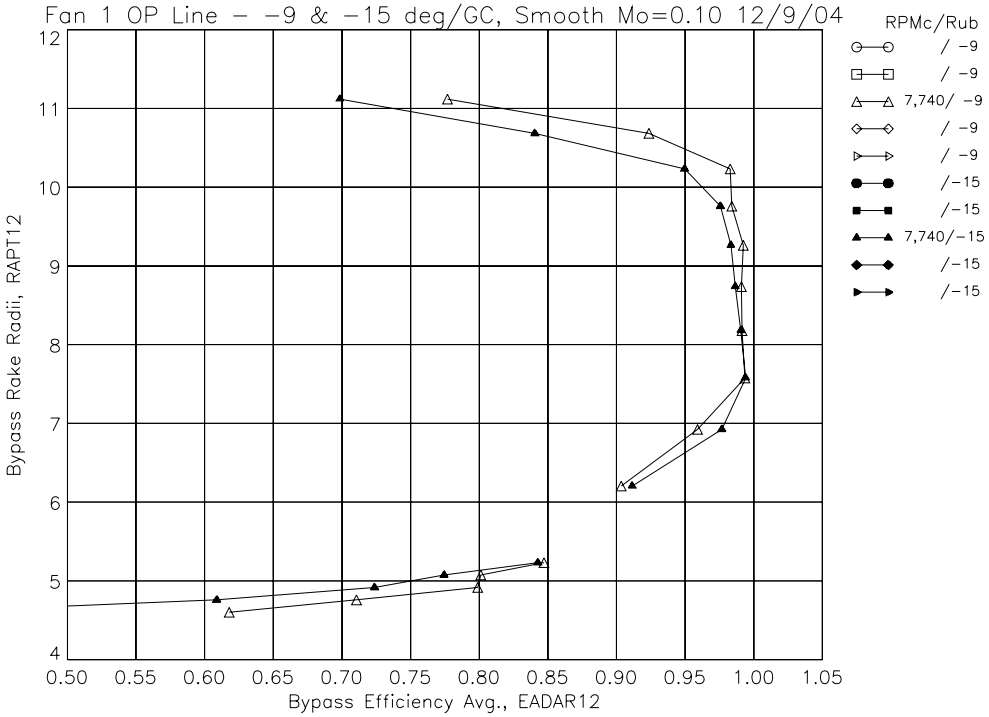

(g) Fan adiabatic efficiency radial profiles, 7,740 RPMc.

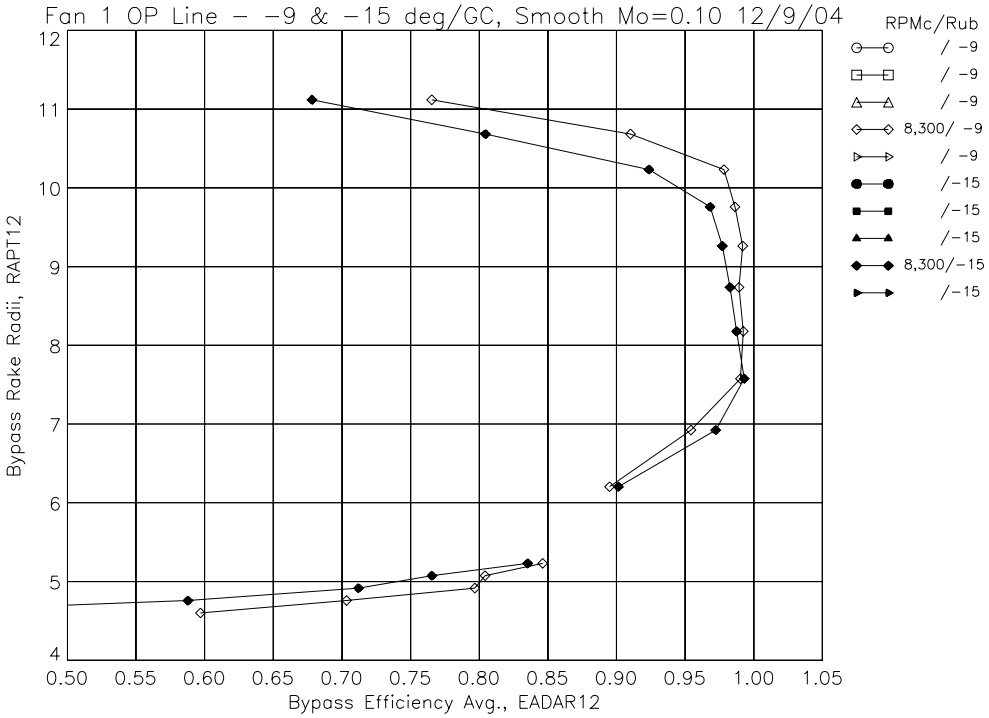

(h) Fan adiabatic efficiency radial profiles, 8,300 RPMc.

Figure 16.—The –9 and –15 deg blade angle radial profiles on operating line with GC blades, smooth rubstrip, Mo = 0.10.

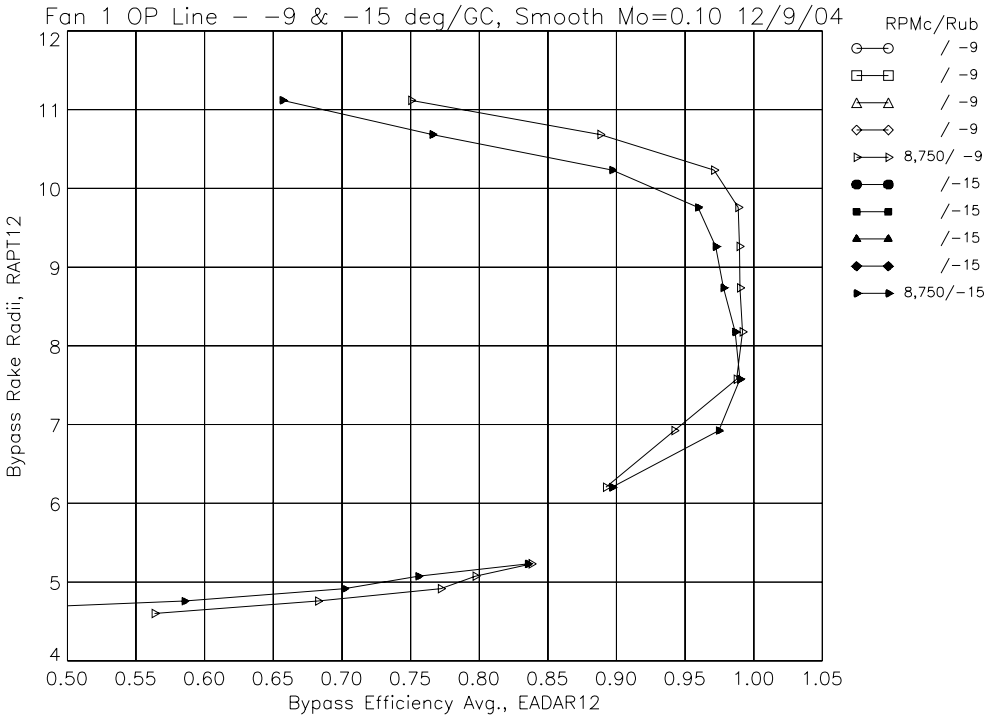

(i) Fan adiabatic efficiency radial profiles, 8,750 RPMc.

Figure 16.—The –9 and –15 deg blade angle radial profiles on operating line with GC blades, smooth rubstrip, Mo = 0.10.

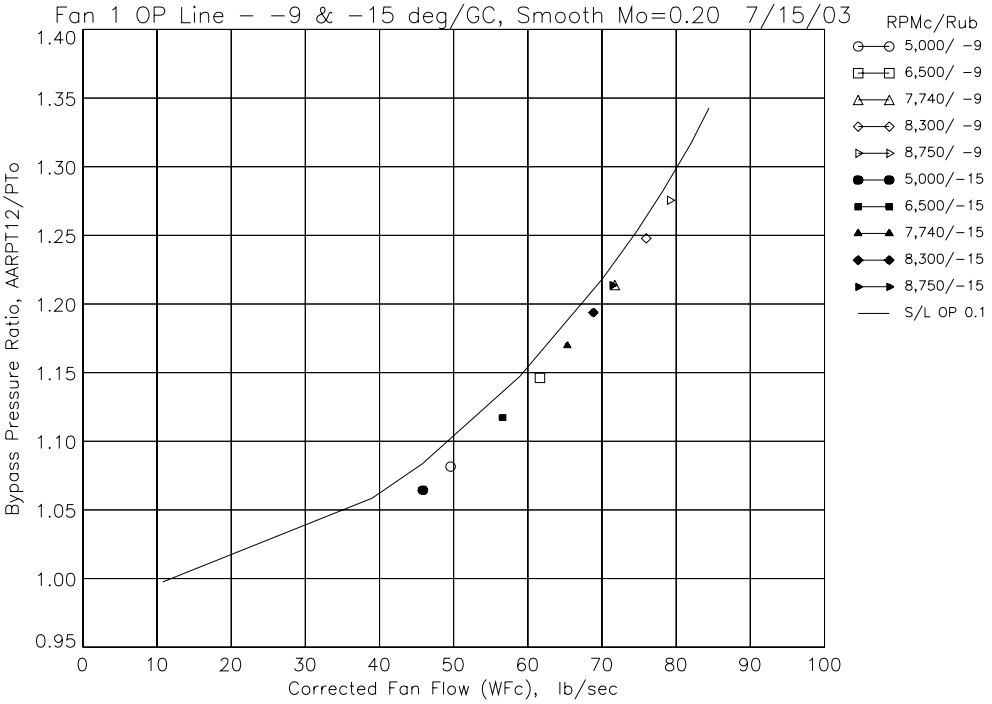

(a) Bypass total pressure ratio versus total fan corrected flow.

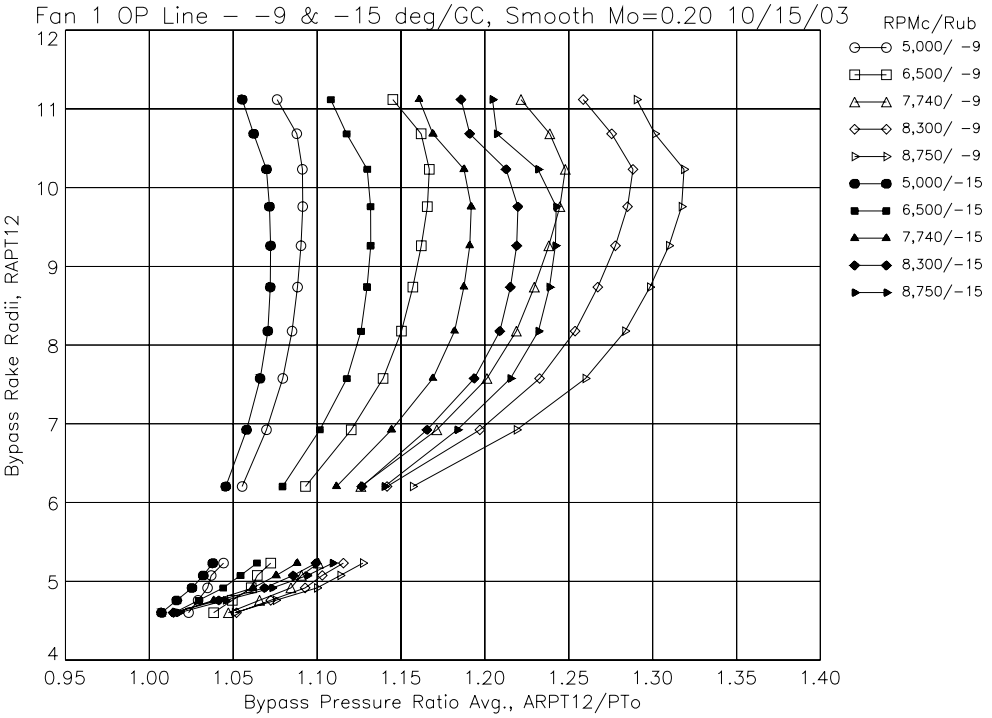

(b) Fan total pressure ratio radial profiles.

Figure 17.—The –9 and –15 deg blade angle radial profiles on operating line with GC blades, smooth rubstrip, Mo = 0.20.

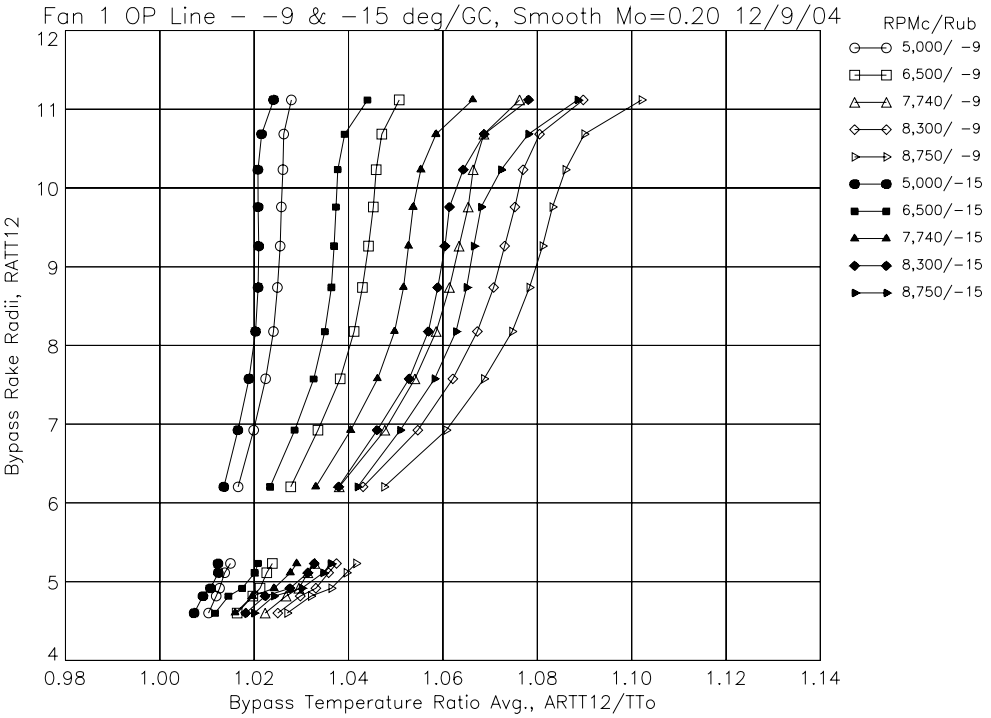

(c) Fan total temperature ratio radial profiles.

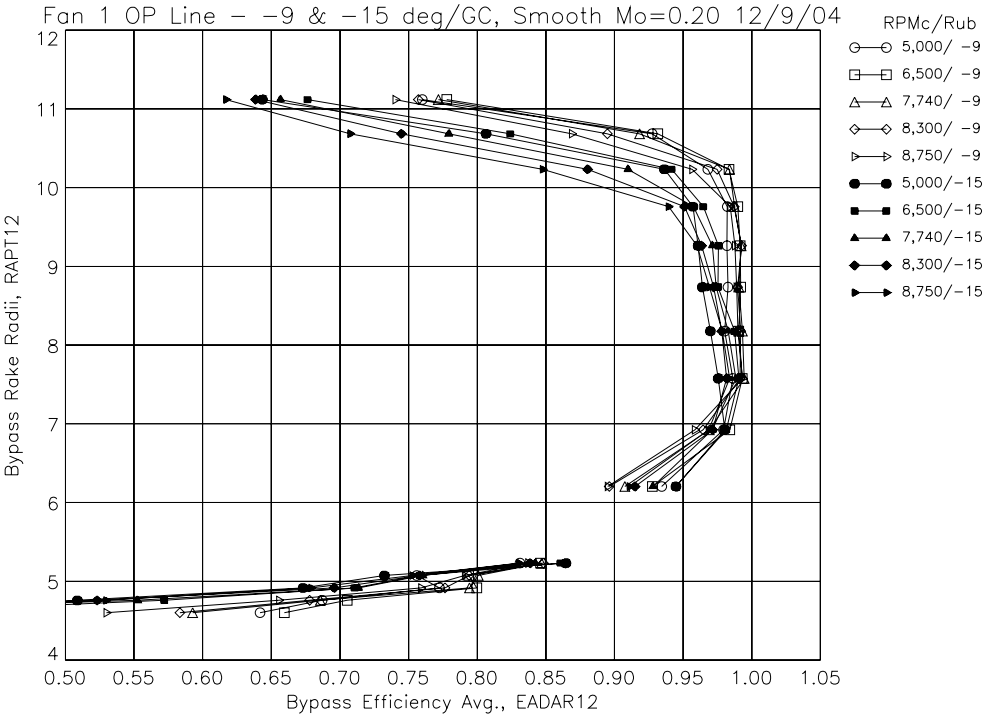

(d) Fan adiabatic efficiency radial profiles.

Figure 17.—The –9 and –15 deg blade angle radial profiles on operating line with GC blades, smooth rubstrip, Mo = 0.20.

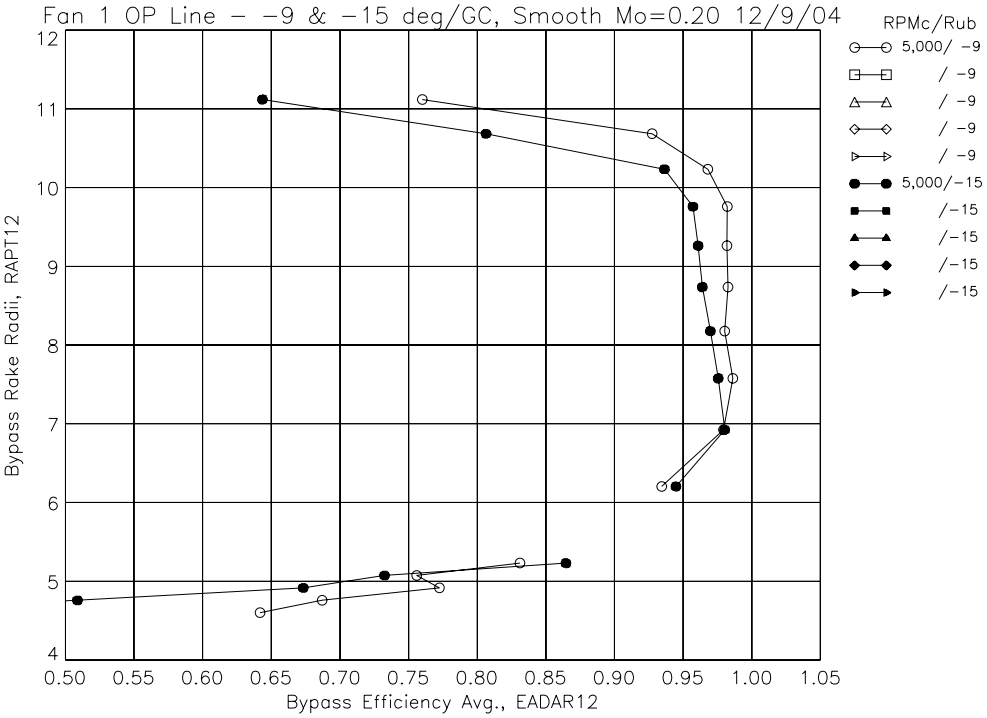

(e) Fan adiabatic efficiency radial profiles, 5,000 RPMc.

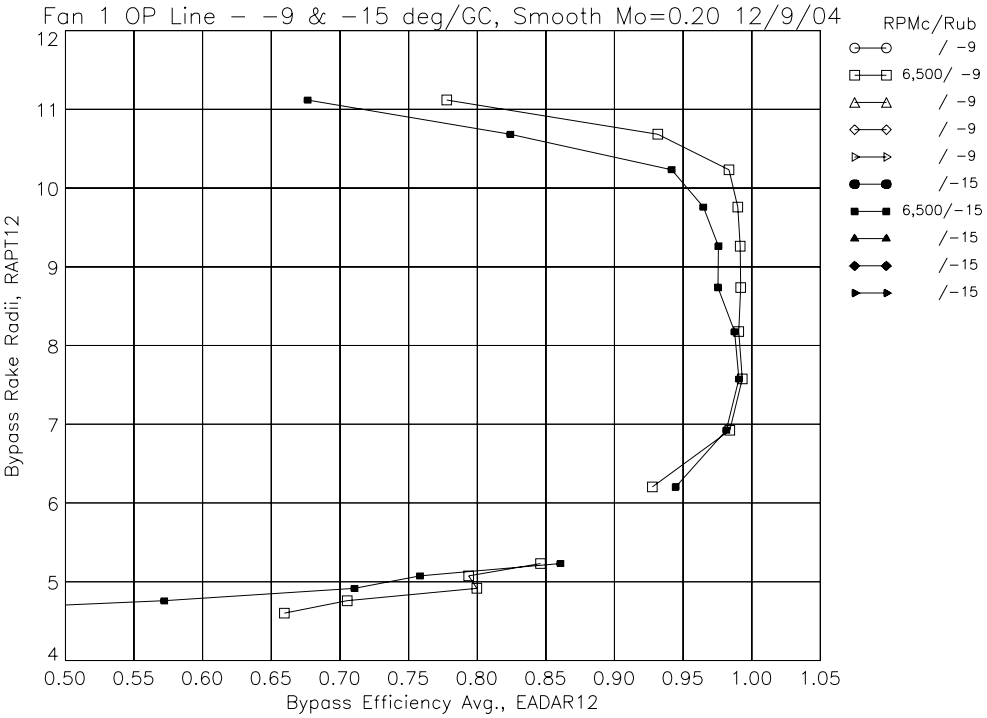

(f) Fan adiabatic efficiency radial profiles, 6,500 RPMc.

Figure 17.—The –9 and –15 deg blade angle radial profiles on operating line with GC blades, smooth rubstrip, Mo = 0.20.

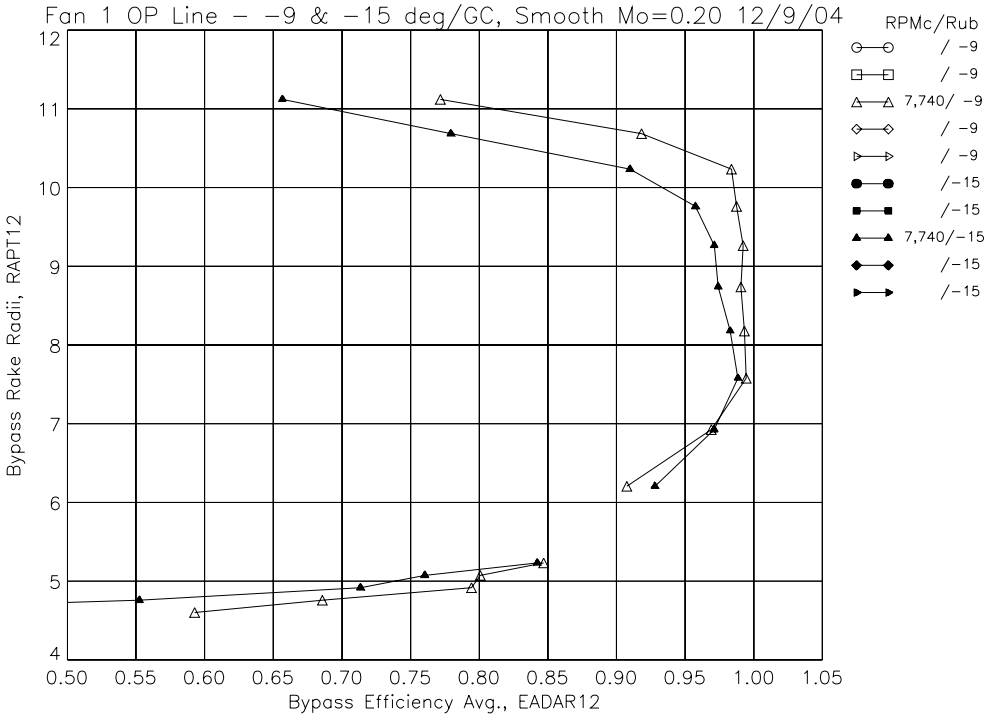

(g) Fan adiabatic efficiency radial profiles, 7,740 RPMc.

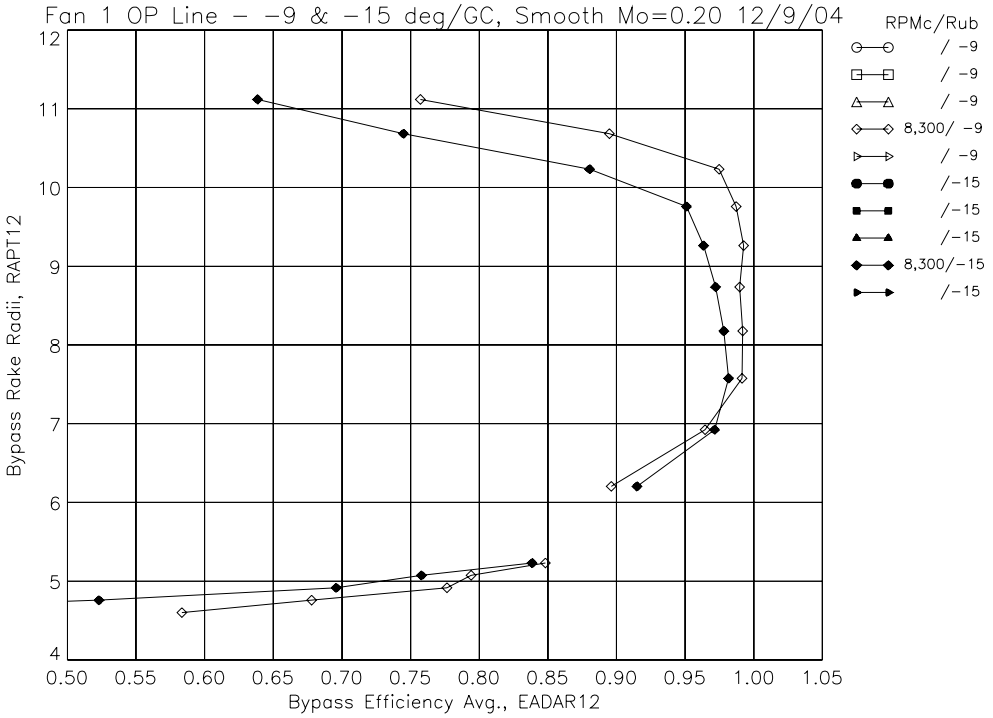

(h) Fan adiabatic efficiency radial profiles, 8,300 RPMc.

Figure 17.—The –9 and –15 deg blade angle radial profiles on operating line with GC blades, smooth rubstrip, Mo = 0.20.

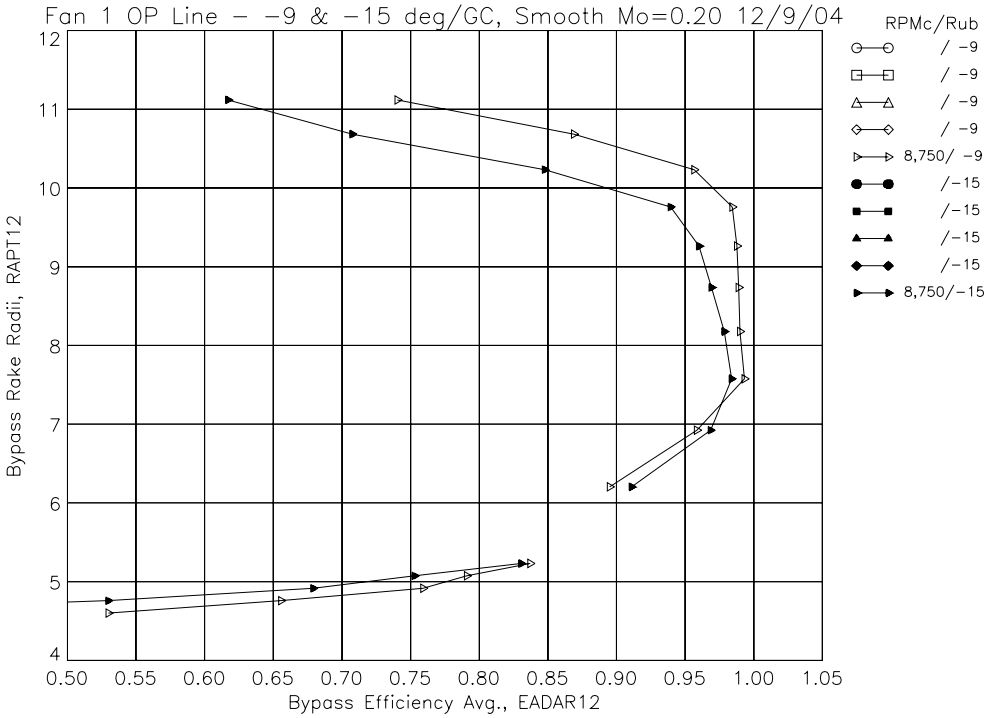

(i) Fan adiabatic efficiency radial profiles, 8,750 RPMc.

Figure 17.—The –9 and –15 deg blade angle radial profiles on operating line with GC blades, smooth rubstrip, Mo = 0.20.

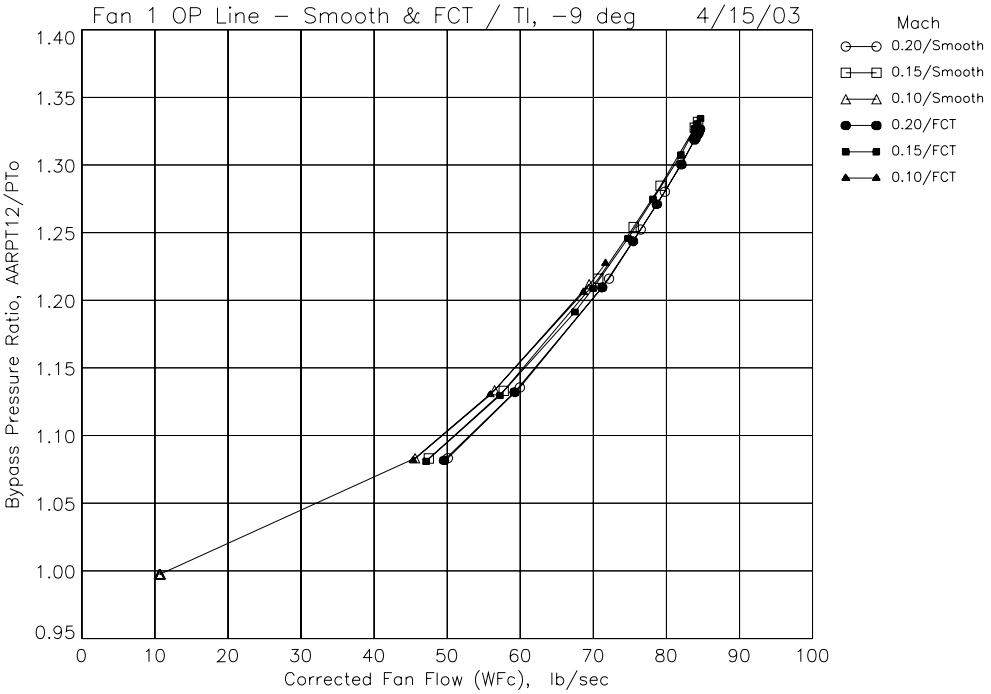

(a) Bypass total pressure ratio versus total fan corrected flow.

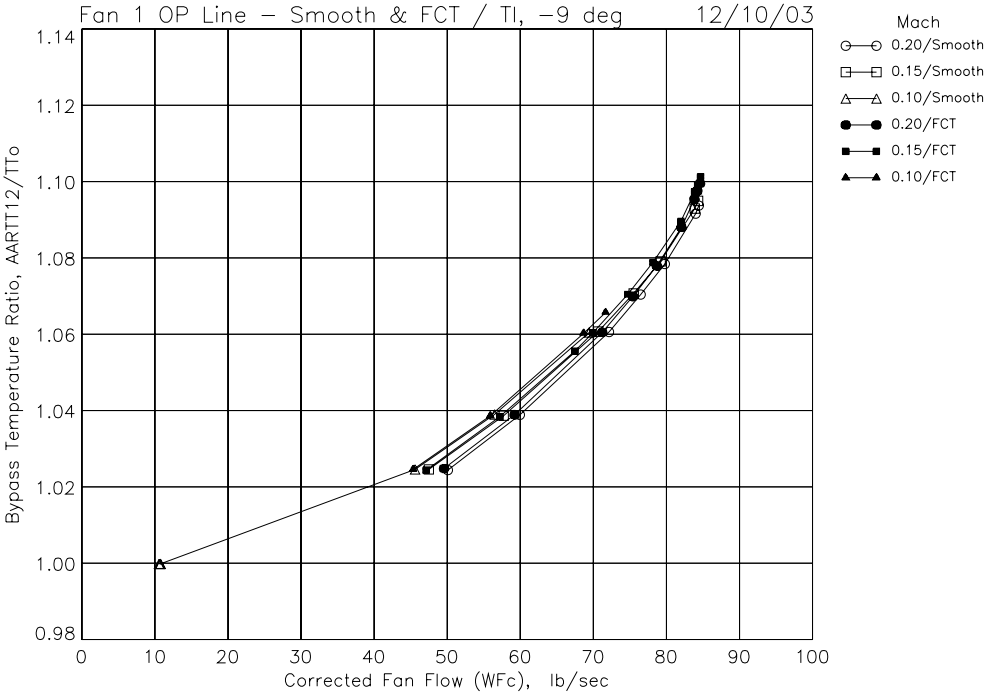

(b) Fan total temperature ratio radial profiles.

Figure 18.—Smooth and FCT rubstrip bypass operating line results, –9 deg blade angle, TI blade.

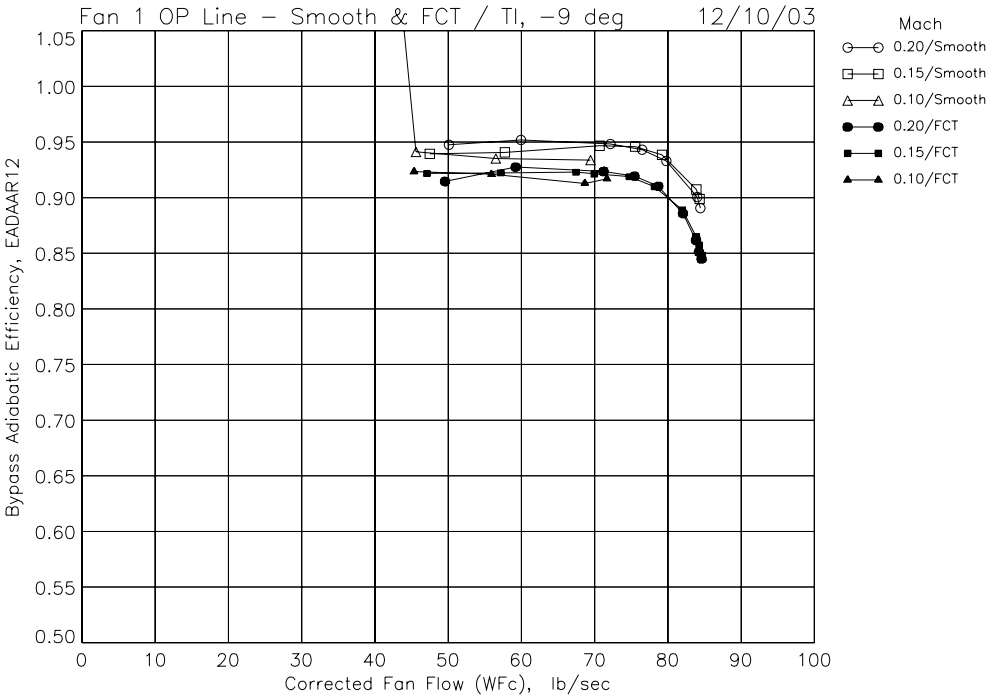

(c) Bypass adiabatic efficiency versus total fan corrected flow.

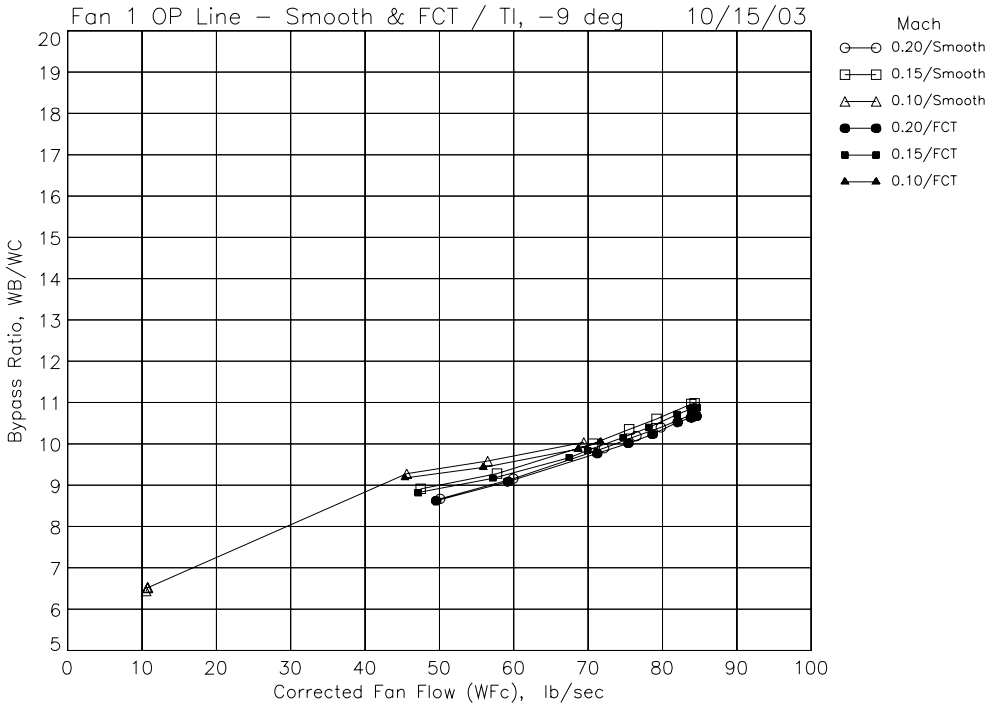

(d) Bypass ratio versus total fan corrected flow.

Figure 18.—Smooth and FCT rubstrip bypass operating line results, –9 deg blade angle, TI blade.

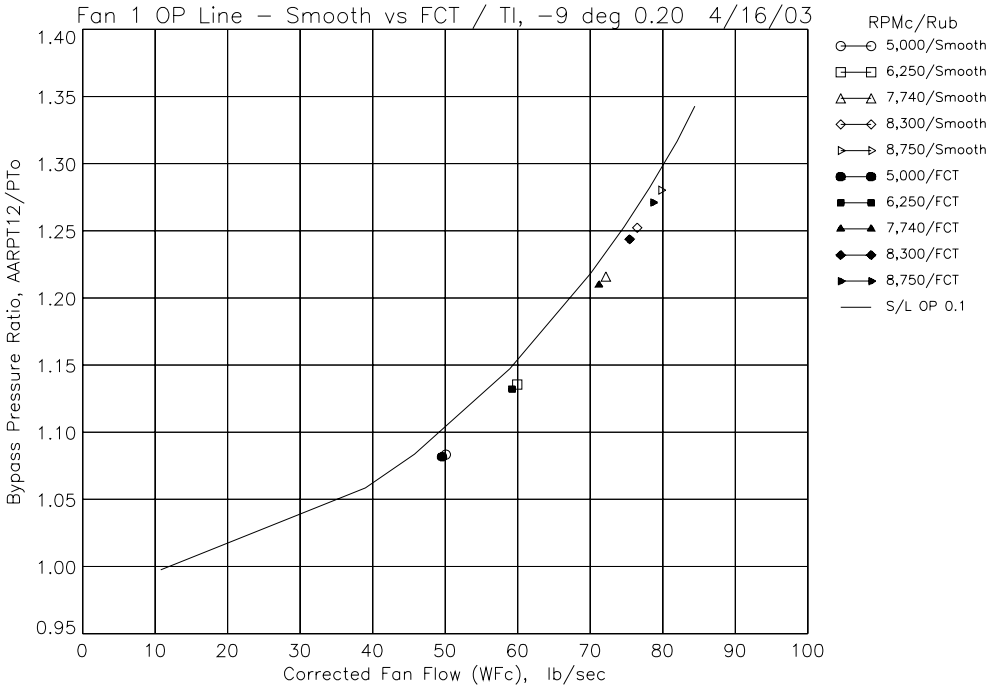

(a) Bypass total pressure ratio versus total fan corrected flow.

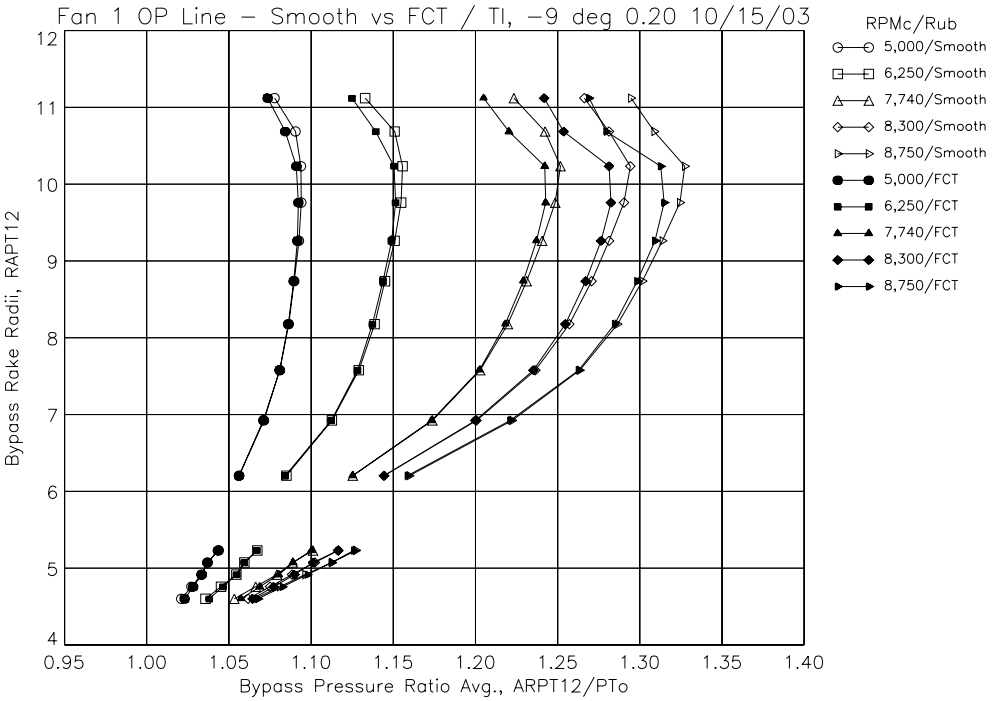

(b) Fan total pressure ratio radial profiles.

Figure19.—Smooth and FCT rubstrip radial profiles on fan operating line, –9 deg blade angle, TI blade, Mo = 0.20.

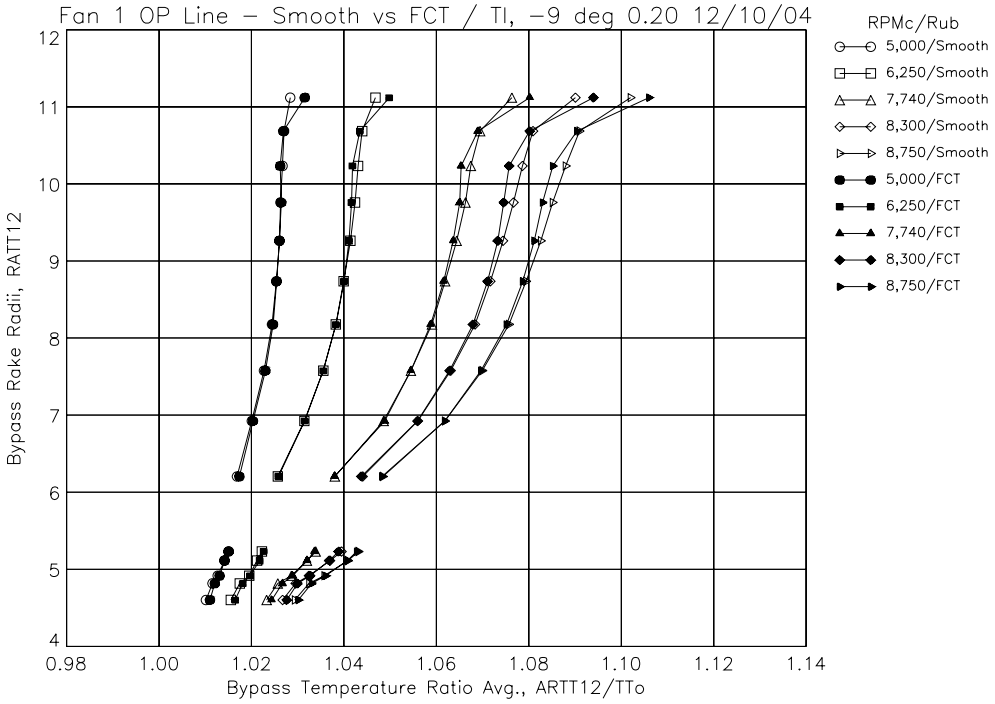

(c) Fan total temperature ratio radial profiles.

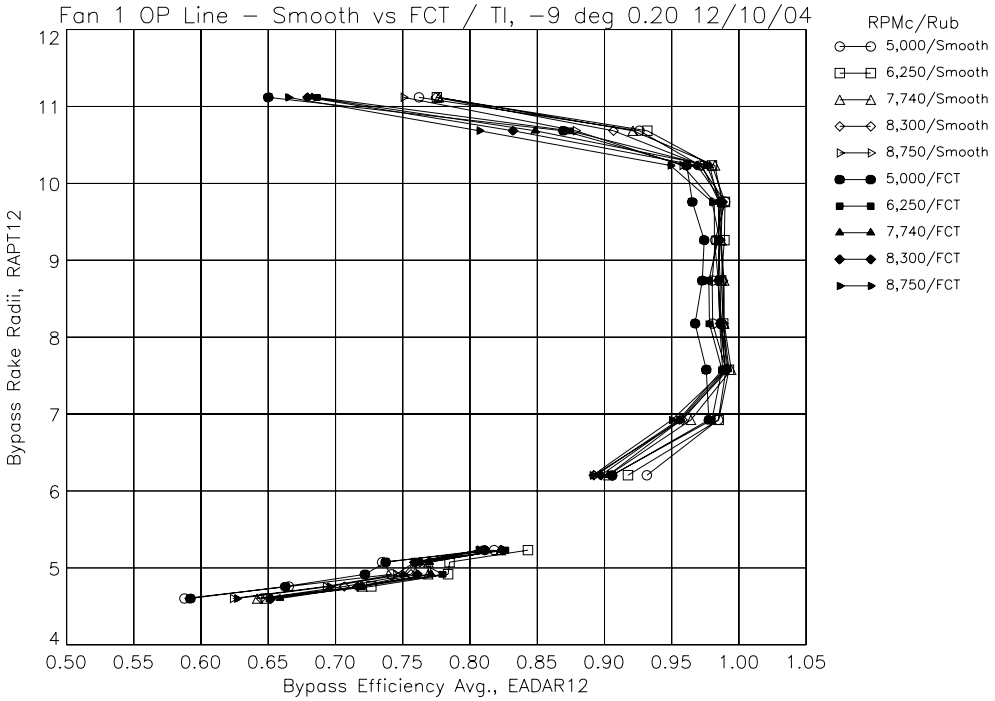

(d) Fan adiabatic efficiency radial profiles.

Figure19.—Smooth and FCT rubstrip radial profiles on fan operating line, –9 deg blade angle, TI blade, Mo = 0.20.

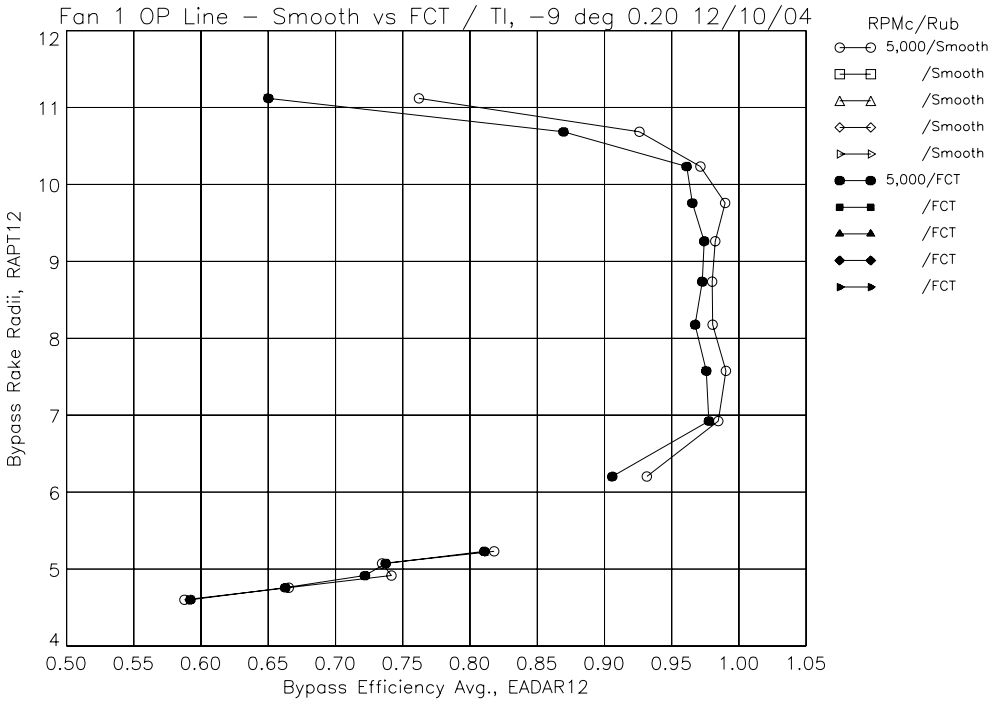

(e) Fan adiabatic efficiency radial profiles, 5,000 RPMc.

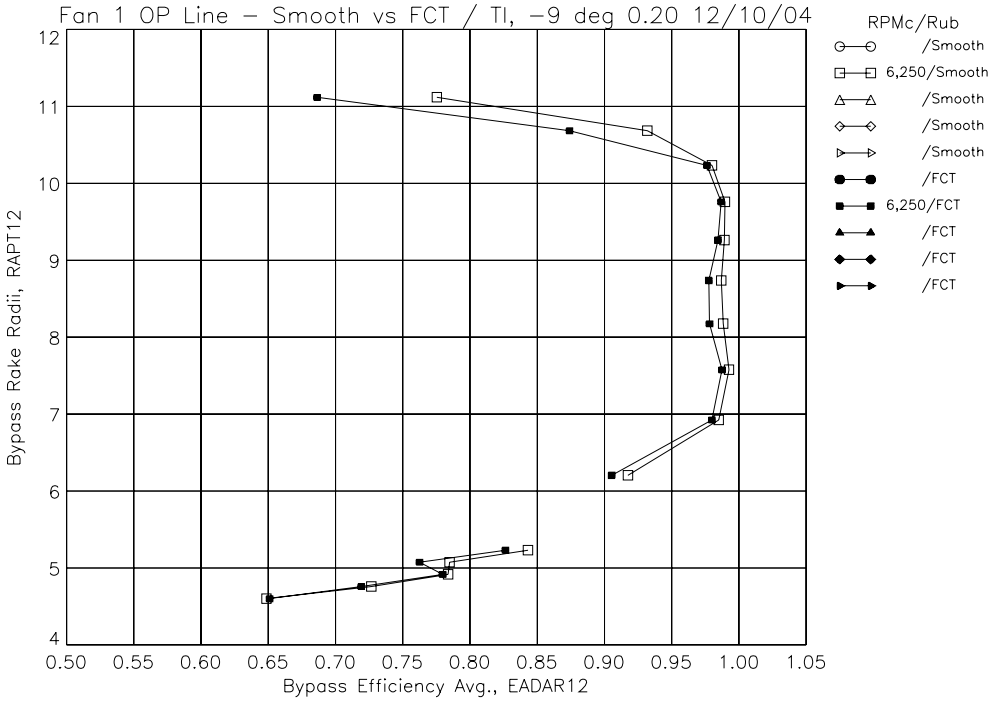

(f) Fan adiabatic efficiency radial profiles, 6,250 RPMc.

Figure19.—Smooth and FCT rubstrip radial profiles on fan operating line, –9 deg blade angle, TI blade, Mo = 0.20.

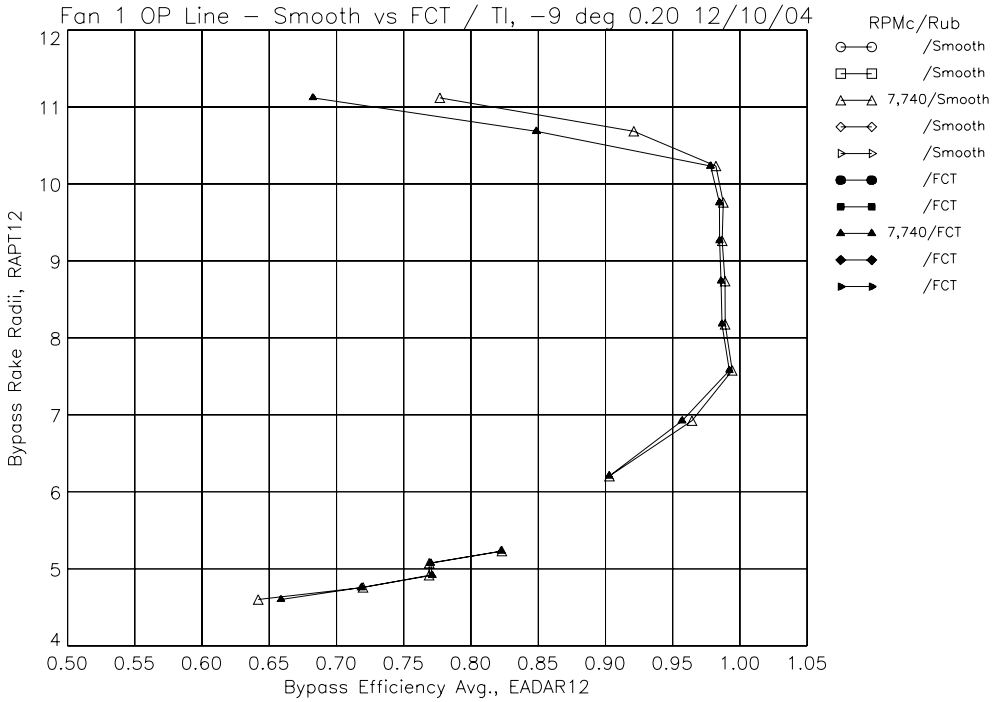

(g) Fan adiabatic efficiency radial profiles, 7,740 RPMc.

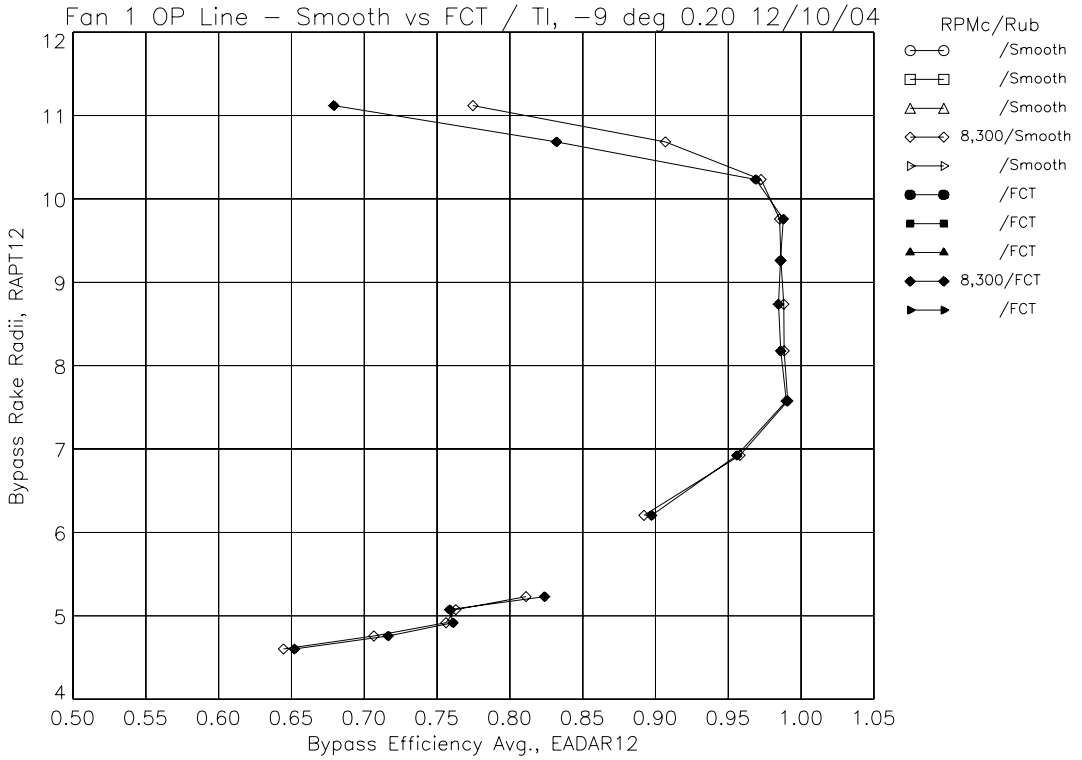

(h) Fan adiabatic efficiency radial profiles, 8,300 RPMc.

Figure19.—Smooth and FCT rubstrip radial profiles on fan operating line, –9 deg blade angle, TI blade, Mo = 0.20.

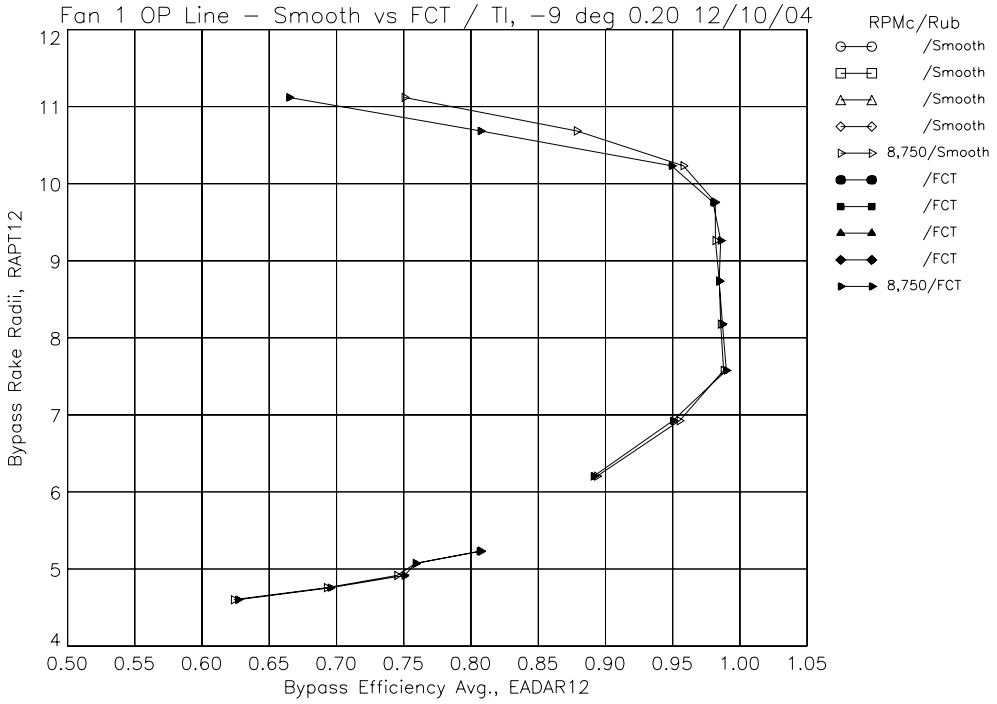

(i) Fan adiabatic efficiency radial profiles, 8,750 RPMc.

Figure19.—Smooth and FCT rubstrip radial profiles on fan operating line, –9 deg blade angle, TI blade, Mo = 0.20.

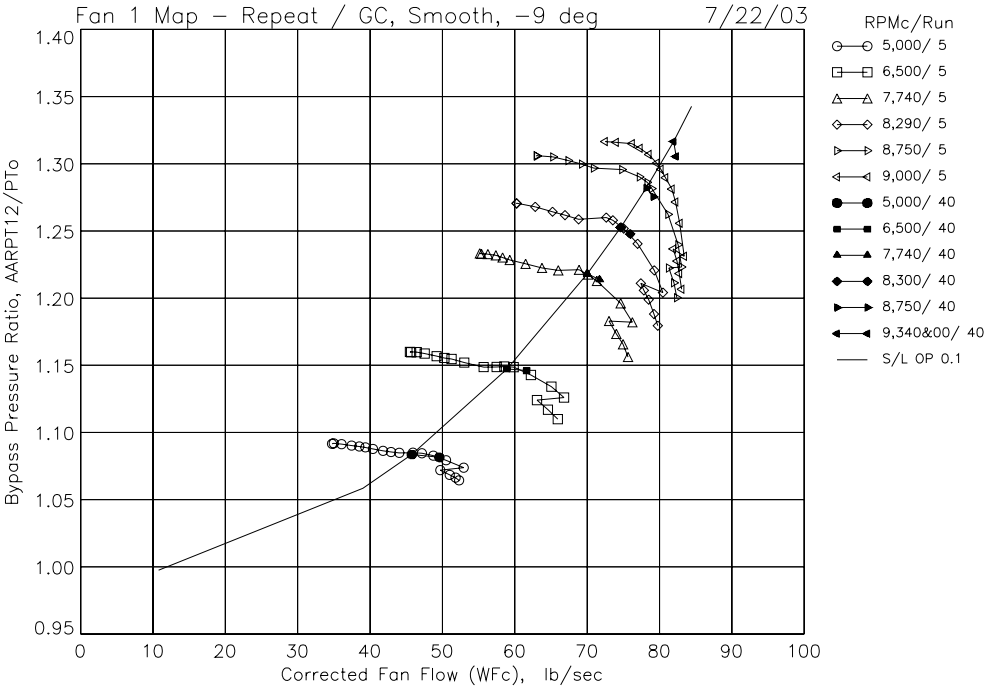

(a) Bypass total pressure ratio versus total fan corrected flow.

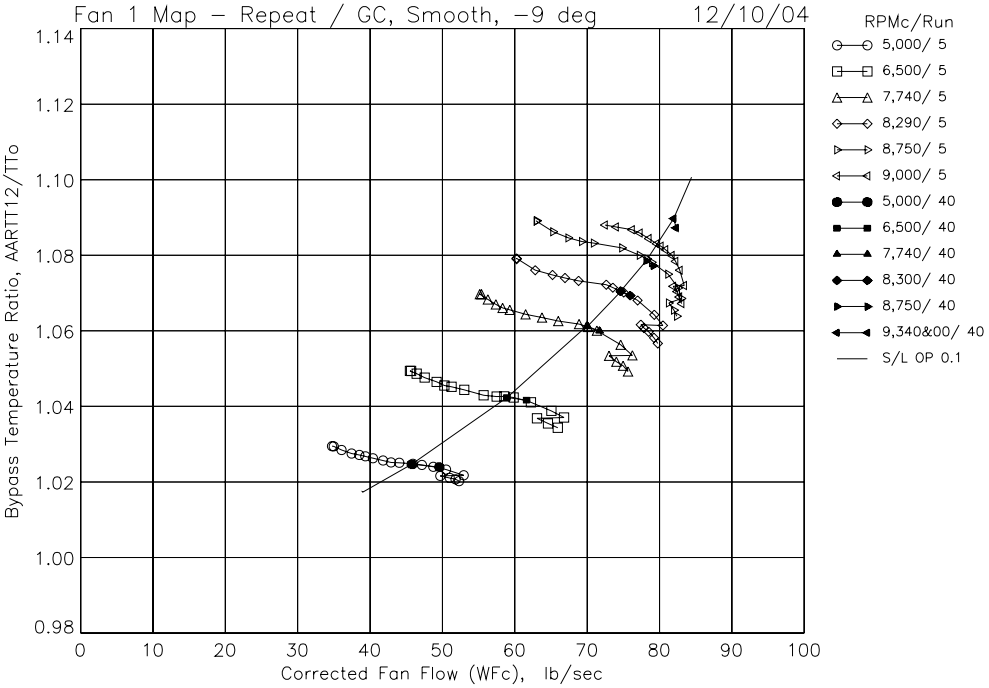

(b) Bypass total temperature ratio versus total fan corrected flow.

Figure 20.—Bypass performance map results and repeatability with –9 deg blade angle, smooth rubstrip.

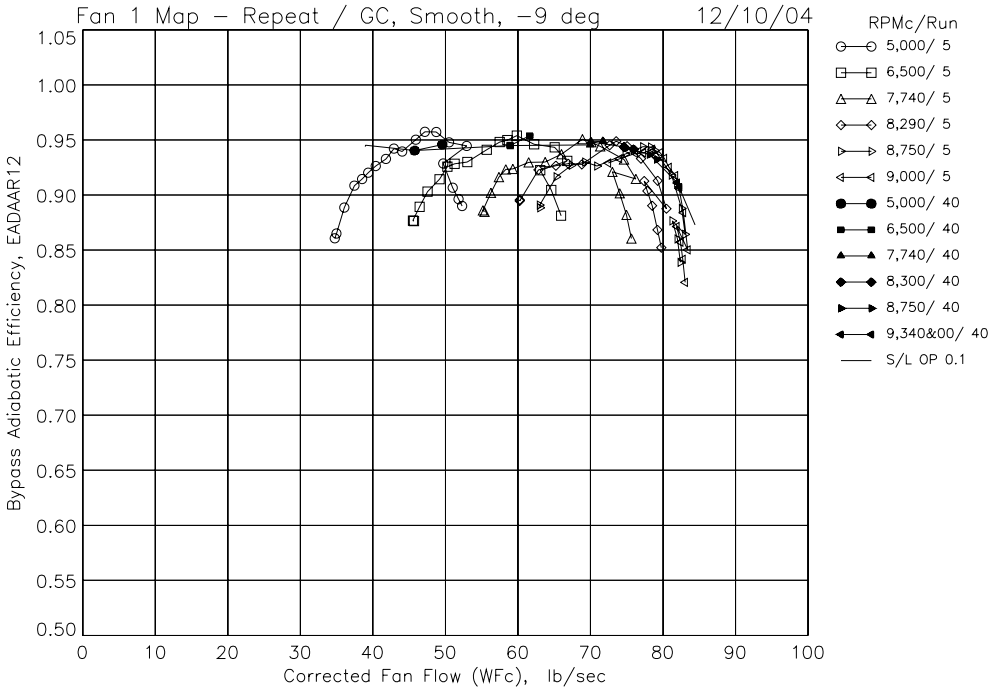

(c) Bypass adiabatic efficiency versus total fan corrected flow.

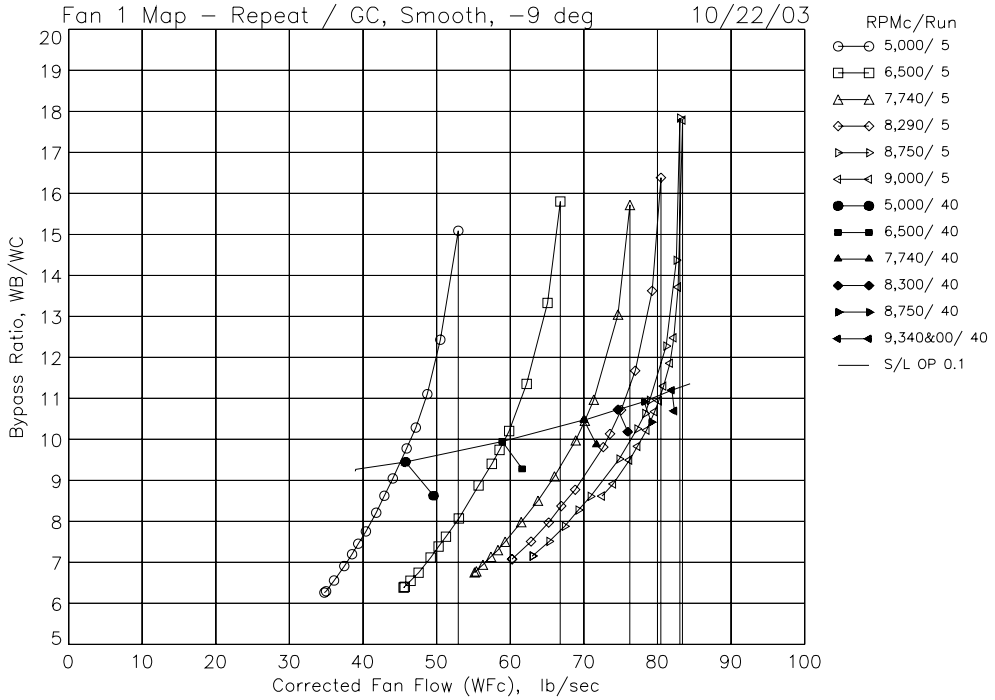

(d) Bypass ratio versus total fan corrected flow.

Figure 20.—Bypass performance map results and repeatability with –9 deg blade angle, smooth rubstrip.

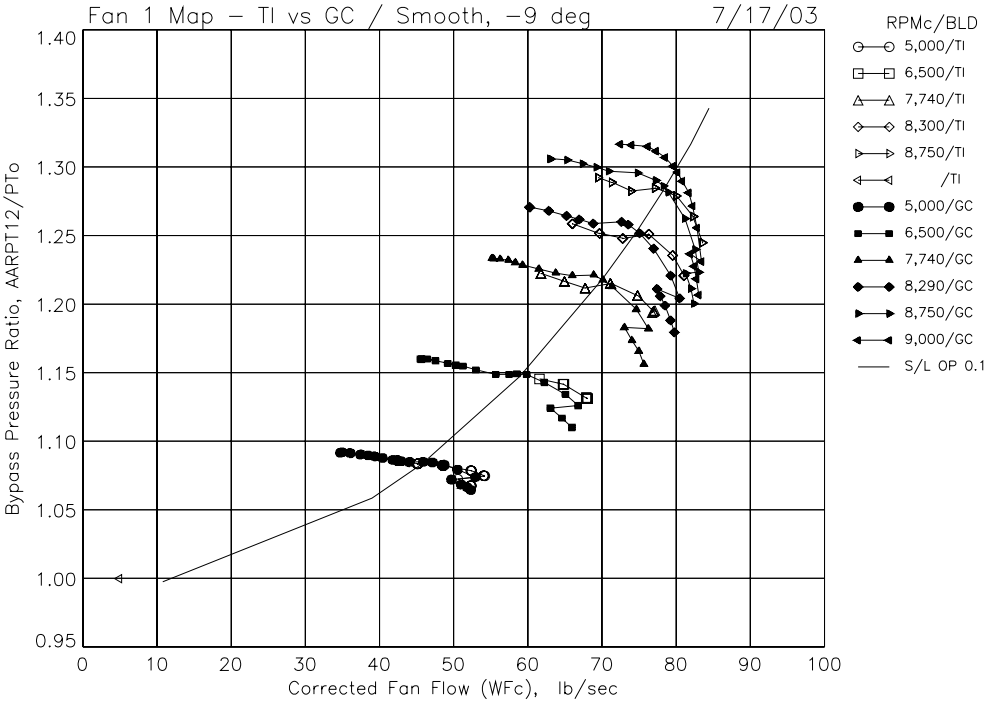

(a) Bypass total pressure ratio versus total fan corrected flow.

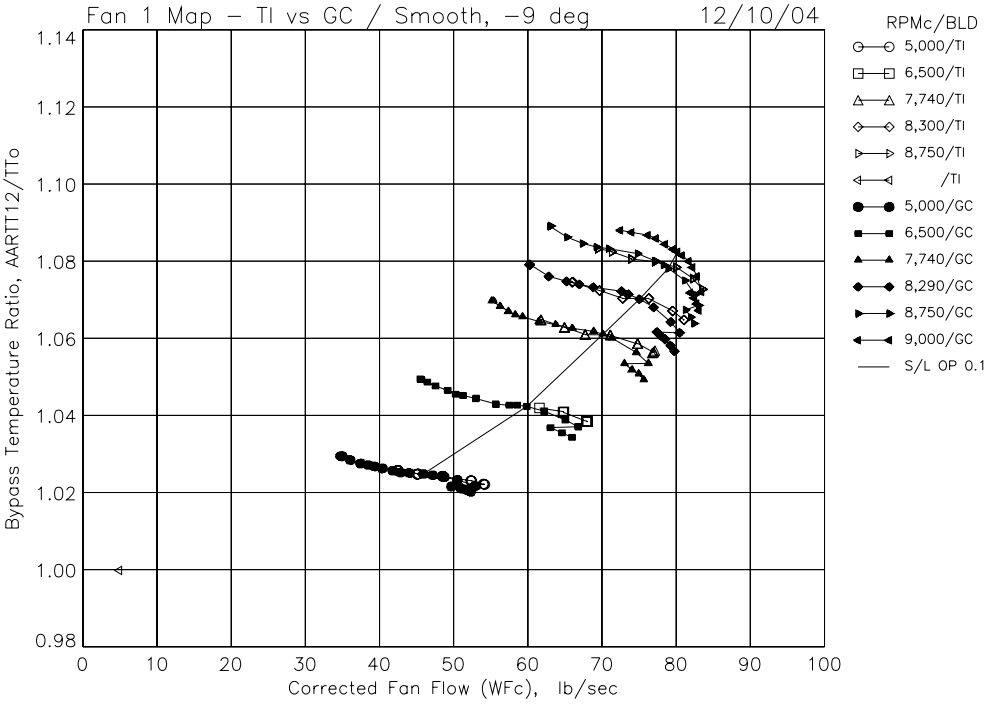

(b) Bypass total temperature ratio versus total fan corrected flow.

Figure 21.—TI and GC blade bypass performance map results with –9 deg blade angle, smooth rubstrip.

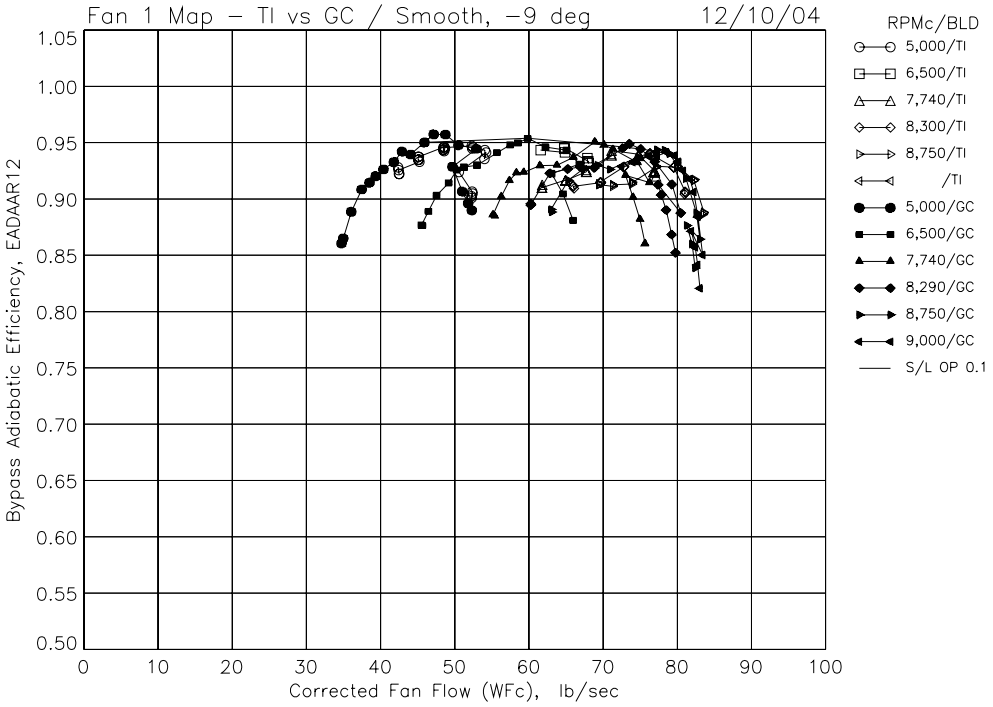

(c) Bypass adiabatic efficiency versus total fan corrected flow.

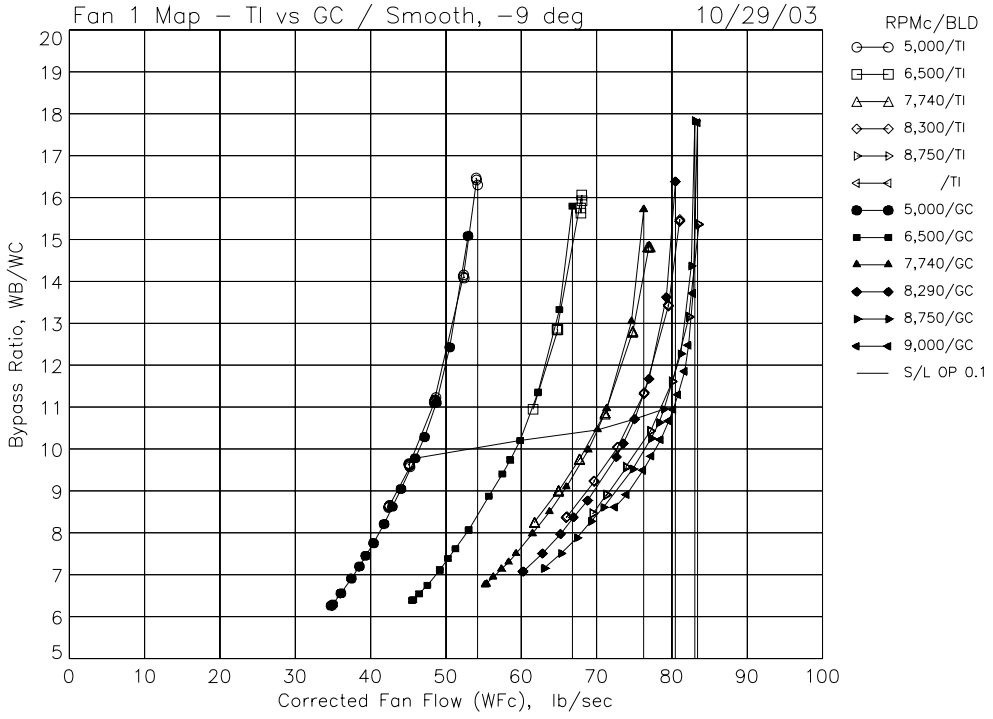

(d) Bypass ratio versus total fan corrected flow.

Figure 21.—TI and GC blade bypass performance map results with –9 deg blade angle, smooth rubstrip.

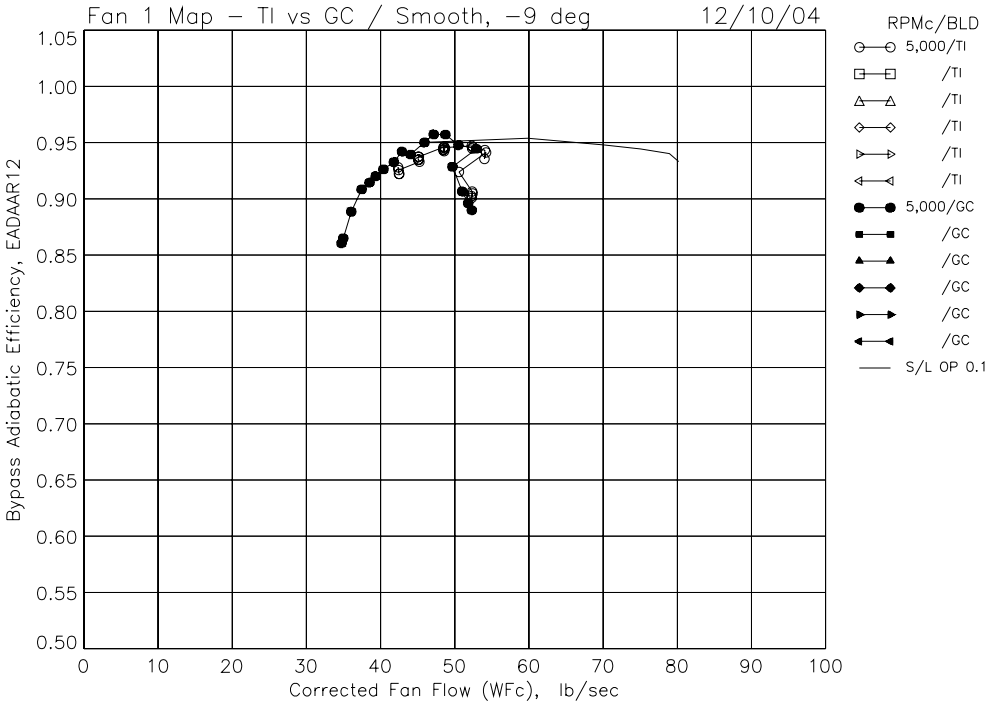

(a) Bypass adiabatic efficiency versus total fan corrected flow.

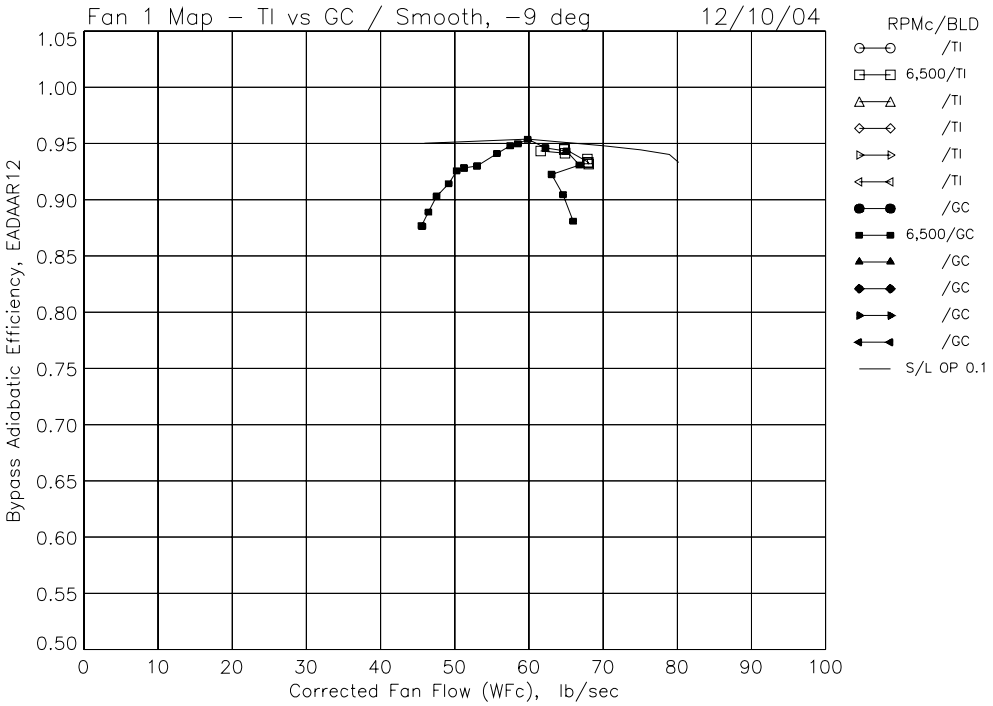

(b) Bypass adiabatic efficiency versus total fan corrected flow.

Figure 22.—TI and GC blade single-speed bypass efficiency results with –9 deg blade angle, smooth rubstrip.

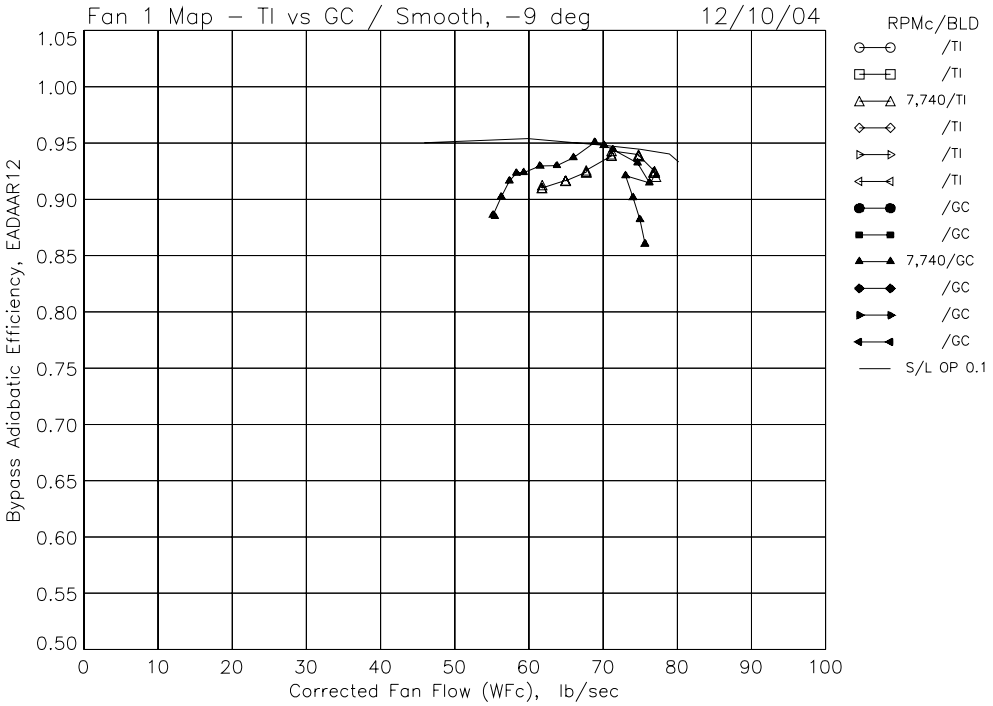

(c) Bypass adiabatic efficiency versus total fan corrected flow.

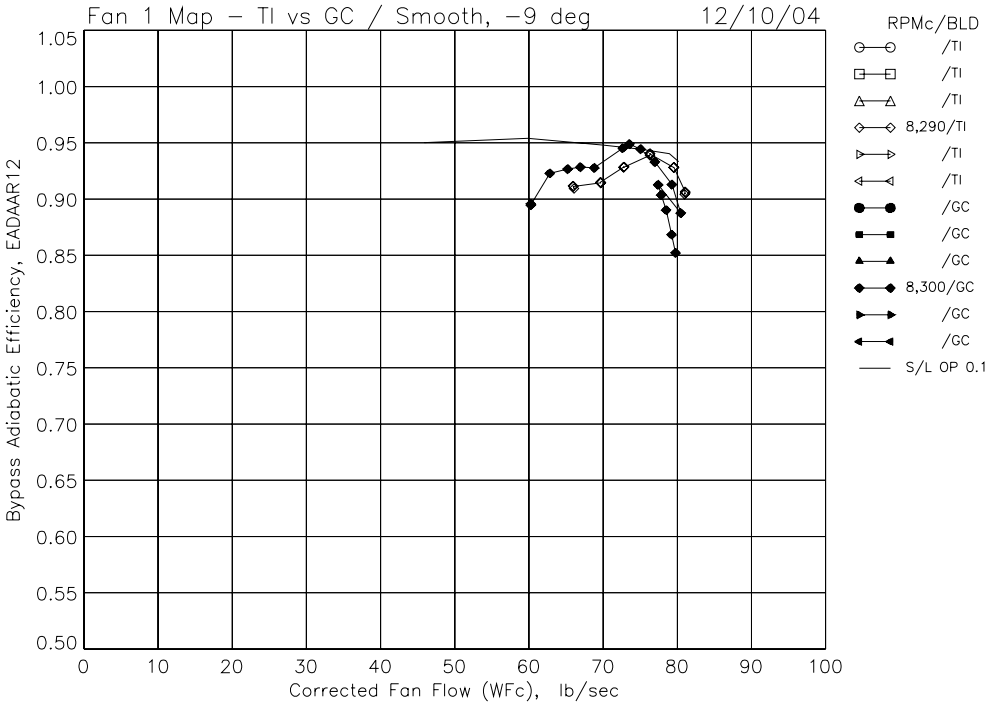

(d) Bypass adiabatic efficiency versus total fan corrected flow.

Figure 22.—TI and GC blade single-speed bypass efficiency results with –9 deg blade angle, smooth rubstrip.

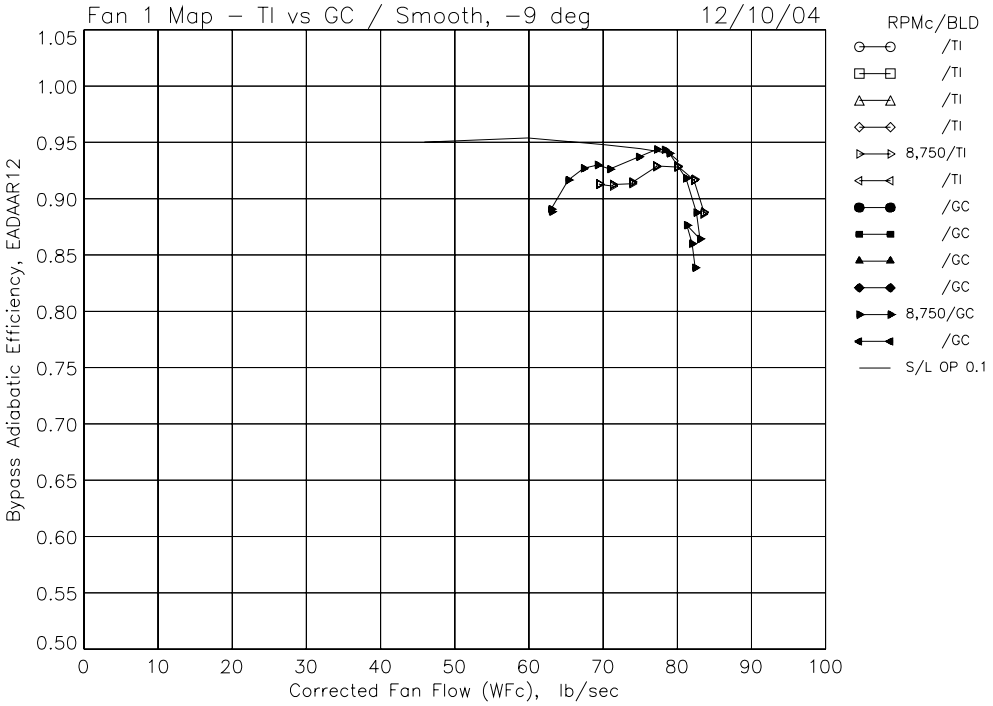

(e) Bypass adiabatic efficiency versus total fan corrected flow.

Figure 22.—TI and GC blade single-speed bypass efficiency results with –9 deg blade angle, smooth rubstrip.

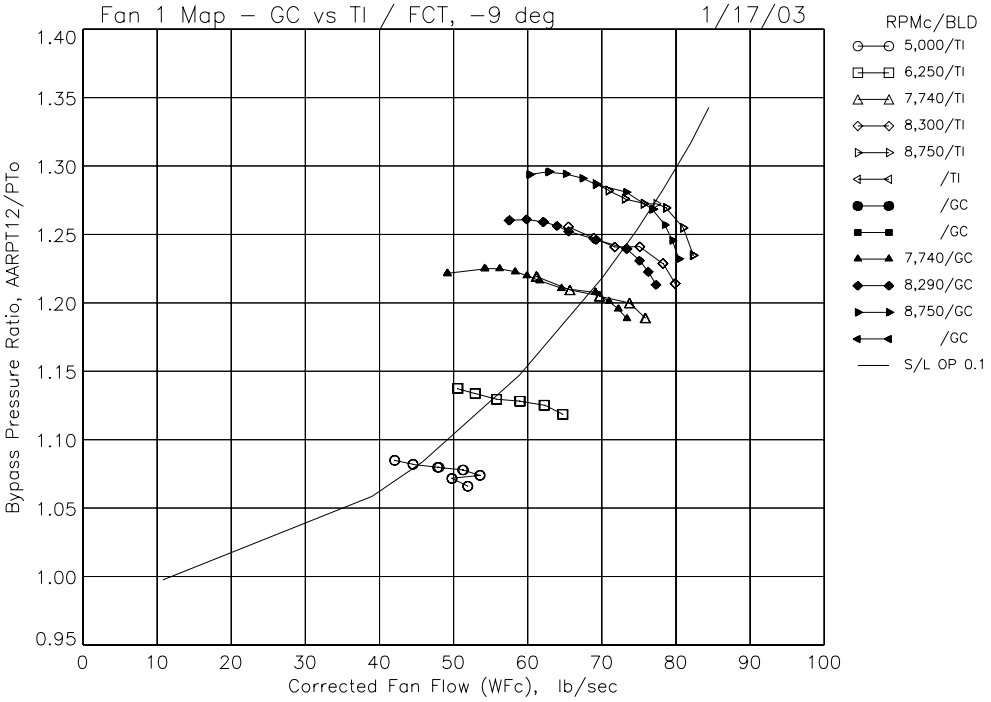

(a) Bypass total pressure ratio versus total fan corrected flow.

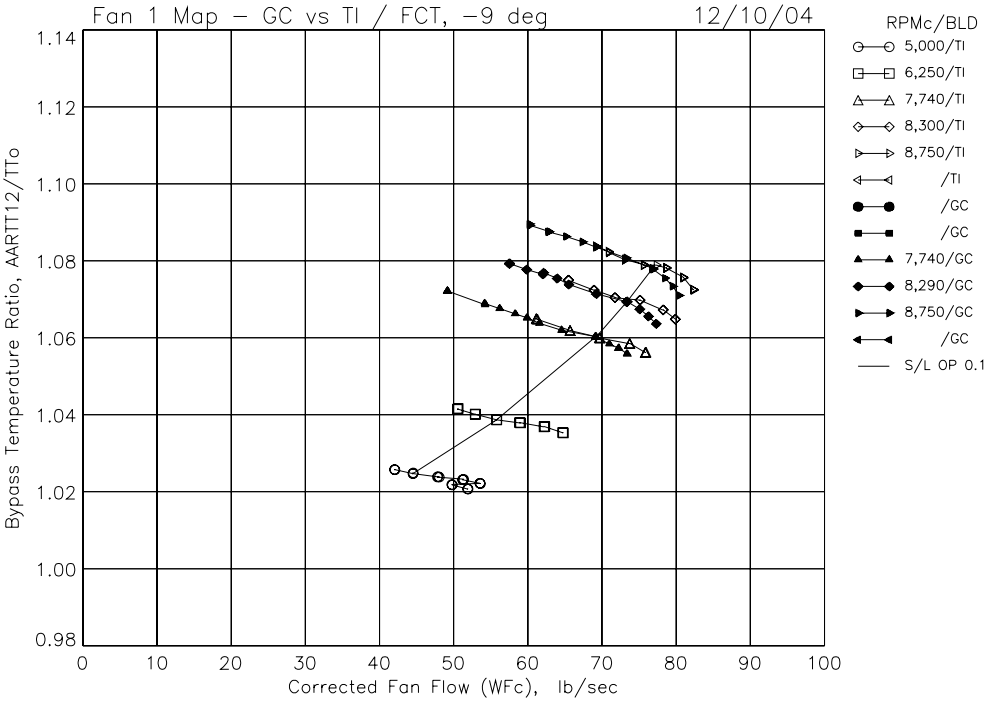

(b) Bypass total temperature ratio versus total fan corrected flow.

Figure 23.—TI and GC blade bypass performance map results with –9 deg blade angle, FCT rubstrip.

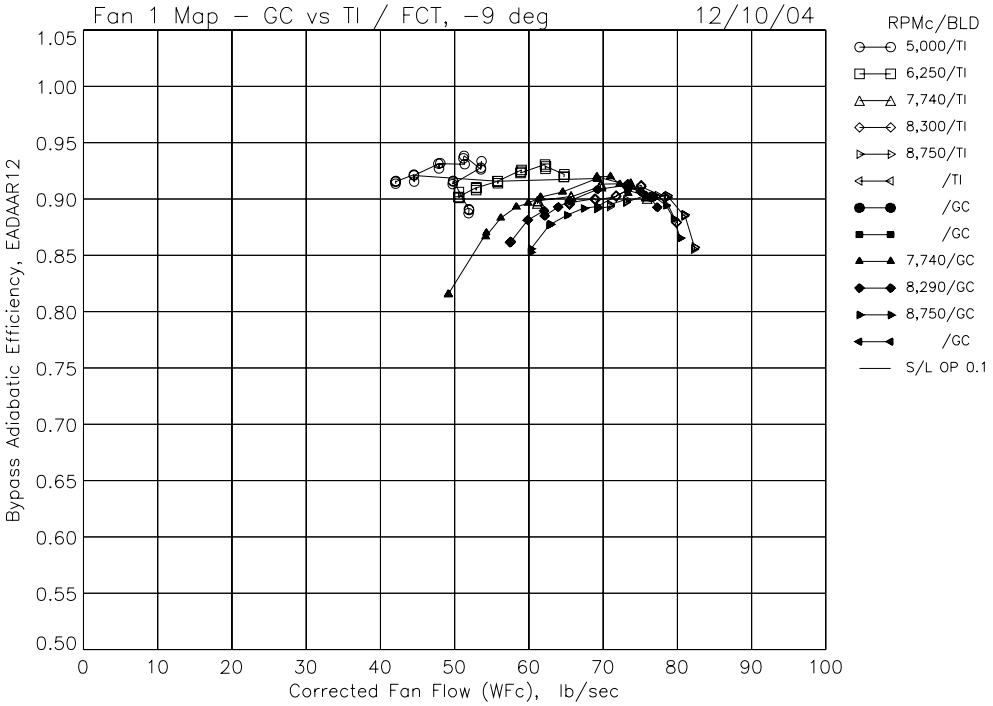

(c) Bypass adiabatic efficiency versus total fan corrected flow.

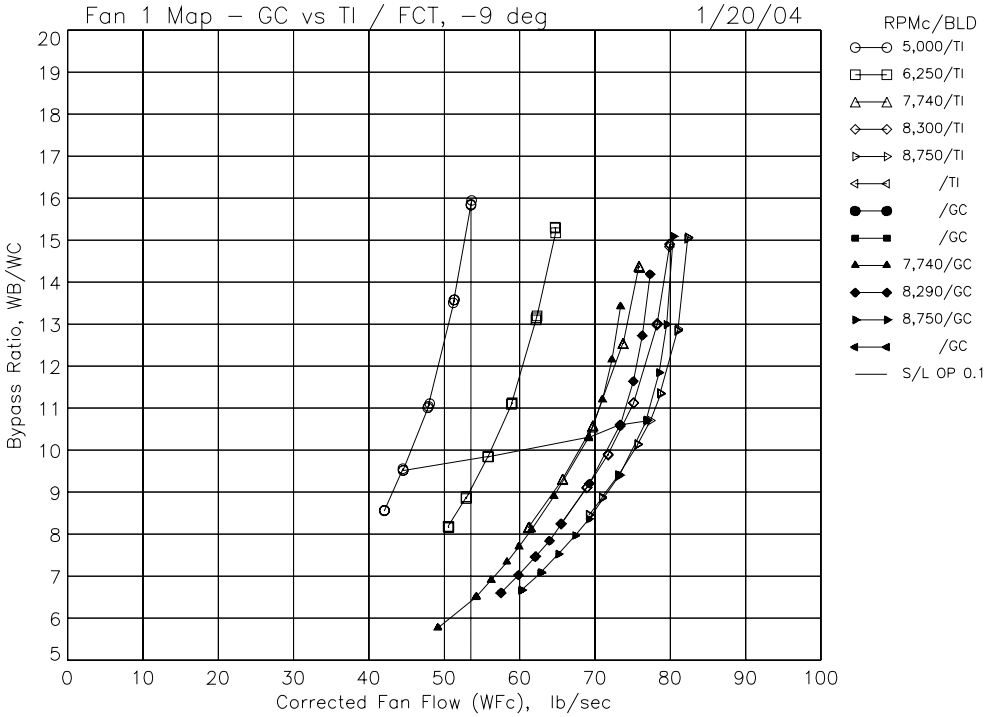

(d) Bypass ratio versus total fan corrected flow.

Figure 23.—TI and GC blade bypass performance map results with –9 deg blade angle, FCT rubstrip.

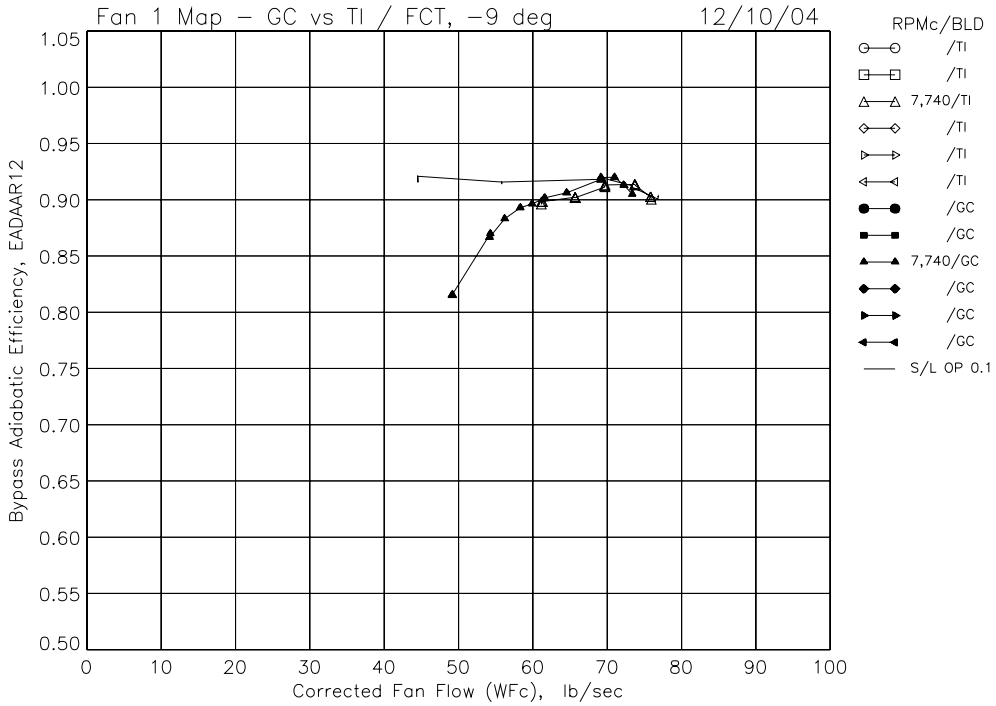

(a) Bypass adiabatic efficiency versus total fan corrected flow.

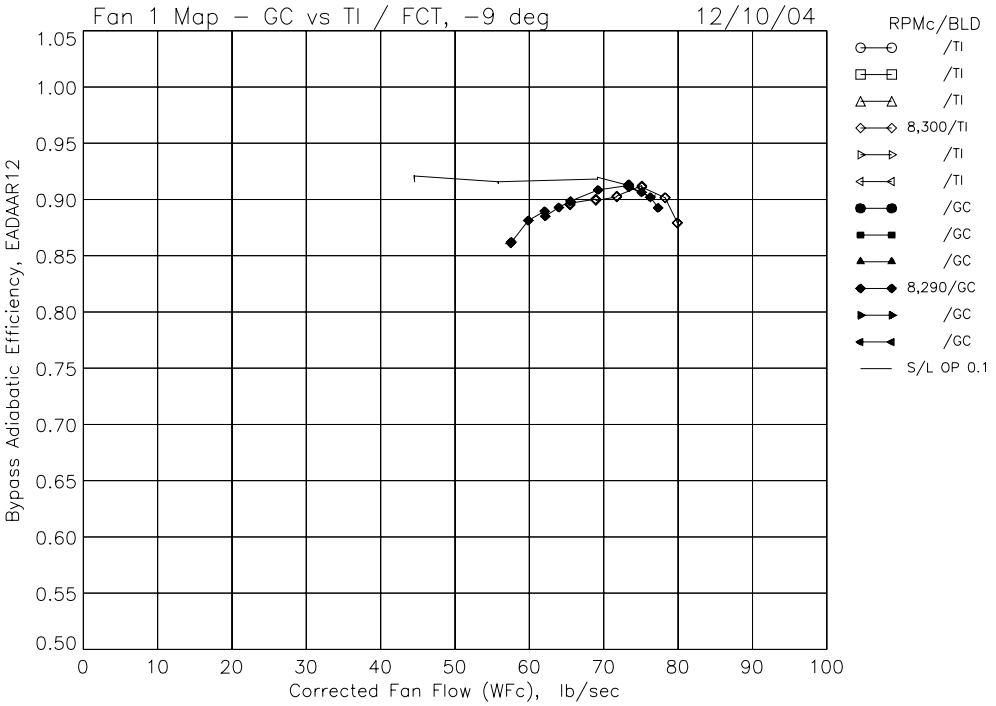

(b) Bypass adiabatic efficiency versus total fan corrected flow.

Figure 24.—TI and GC blade single-speed bypass efficiency results with –9 deg blade angle, FCT rubstrip.

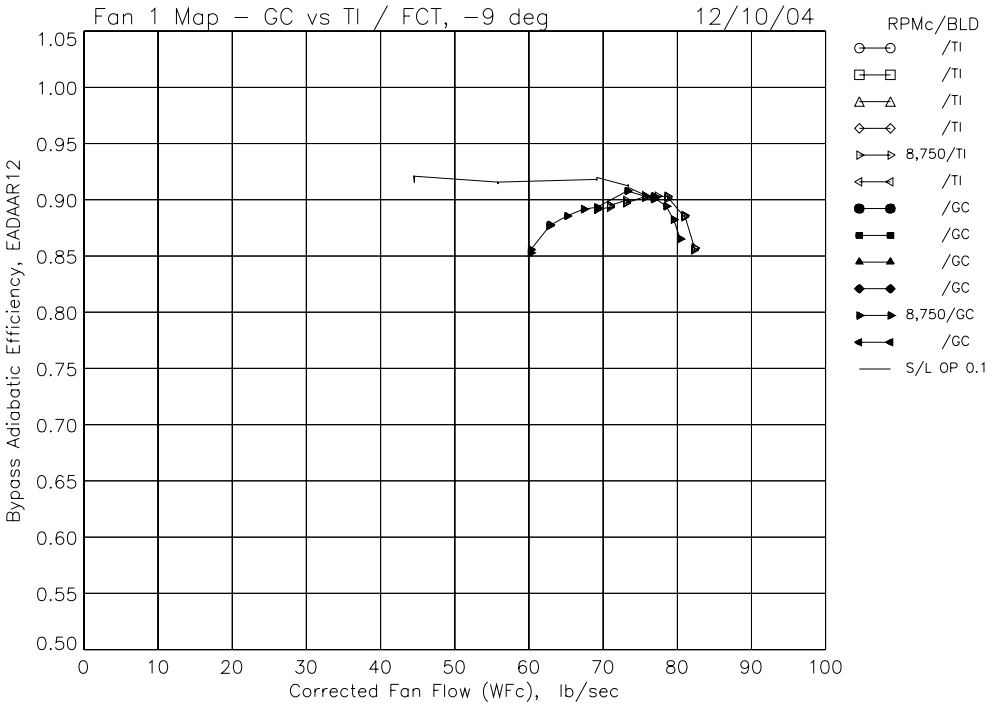

(c) Bypass adiabatic efficiency versus total fan corrected flow.

Figure 24.—TI and GC blade single-speed bypass efficiency results with –9 deg blade angle, FCT rubstrip.

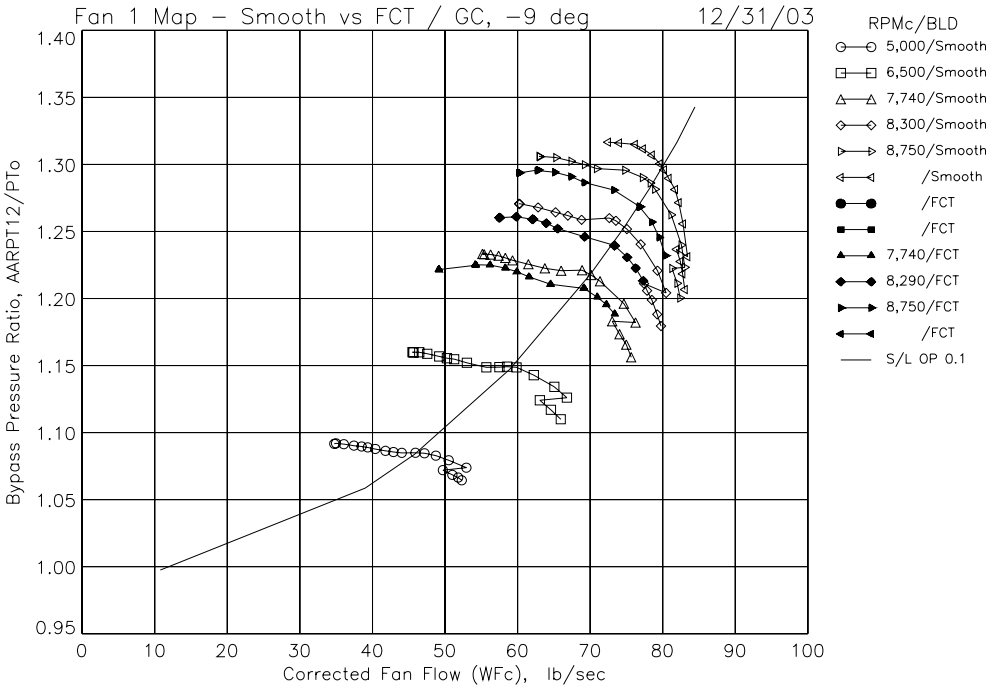

(a) Bypass total pressure ratio versus total fan corrected flow.

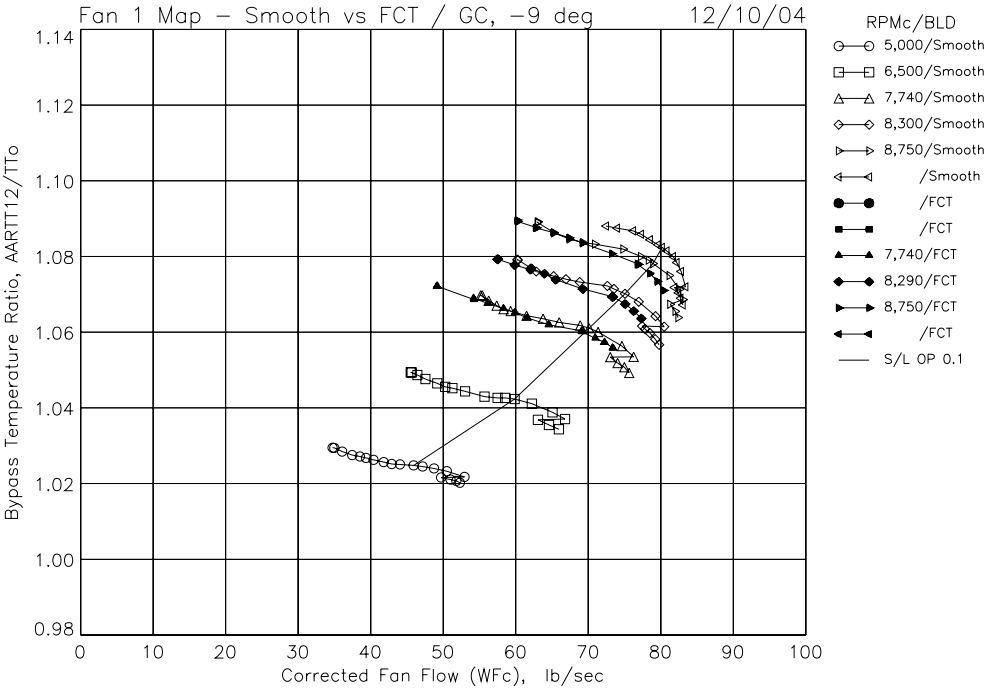

(b) Bypass total temperature ratio versus total fan corrected flow.

Figure 25.—Smooth and FCT bypass performance map results with –9 deg blade angle, GC blades.

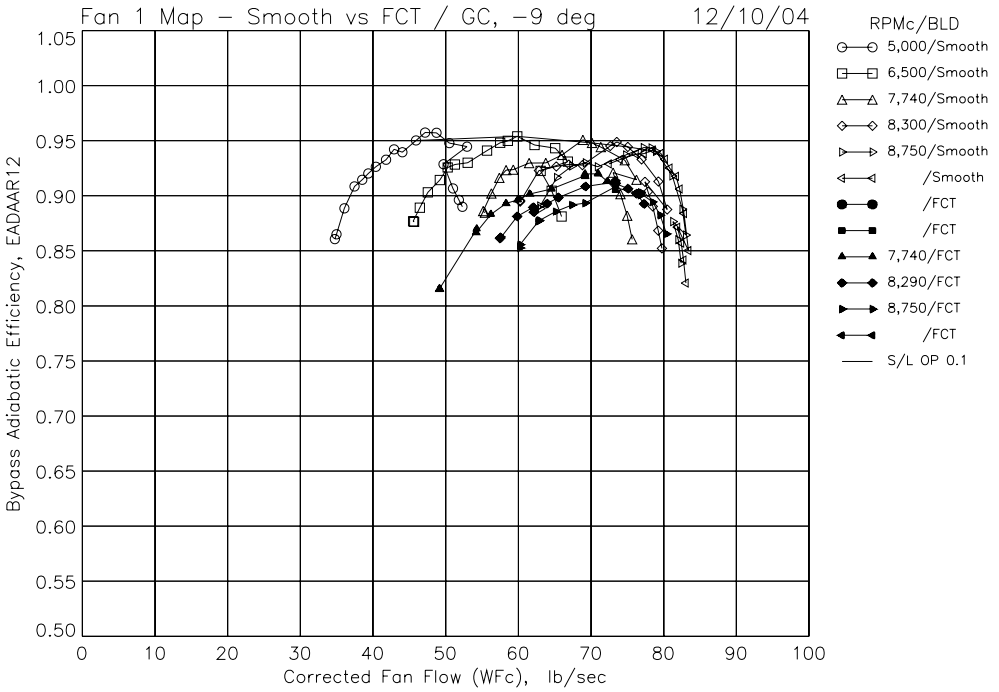

(c) Bypass adiabatic efficiency versus total fan corrected flow.

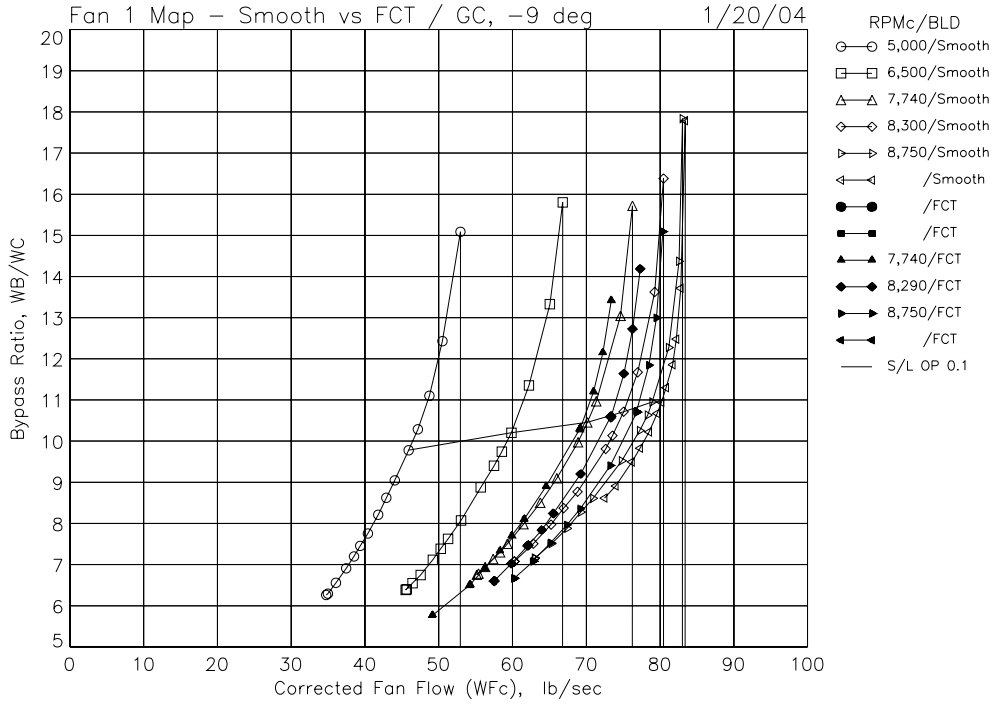

(d) Bypass ratio versus total fan corrected flow.

Figure 25.—Smooth and FCT bypass performance map results with –9 deg blade angle, GC blades.

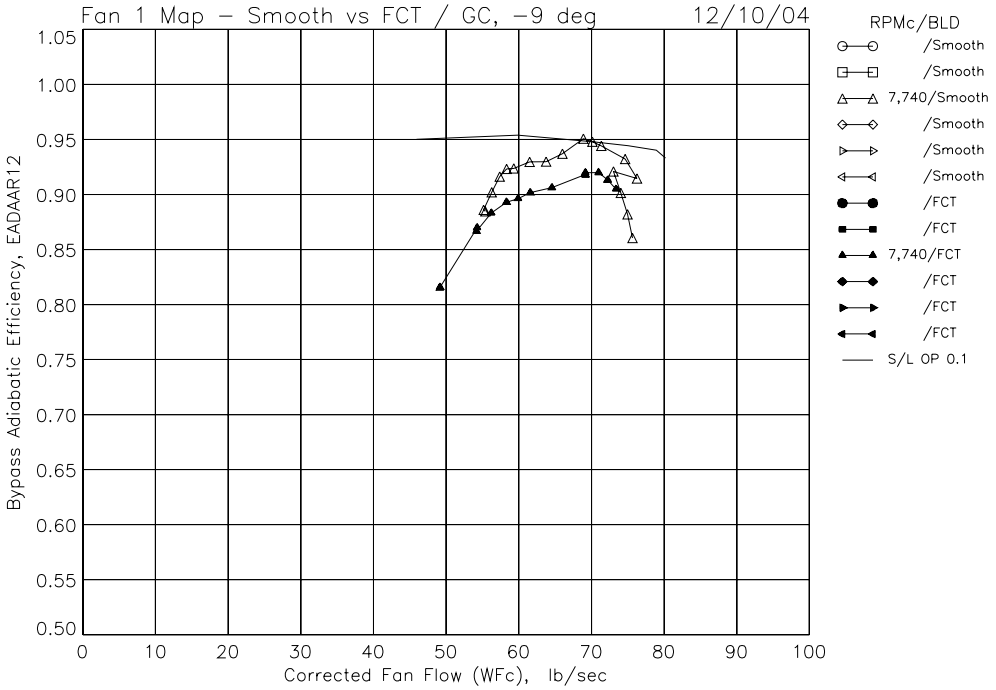

(a) Bypass adiabatic efficiency versus total fan corrected flow.

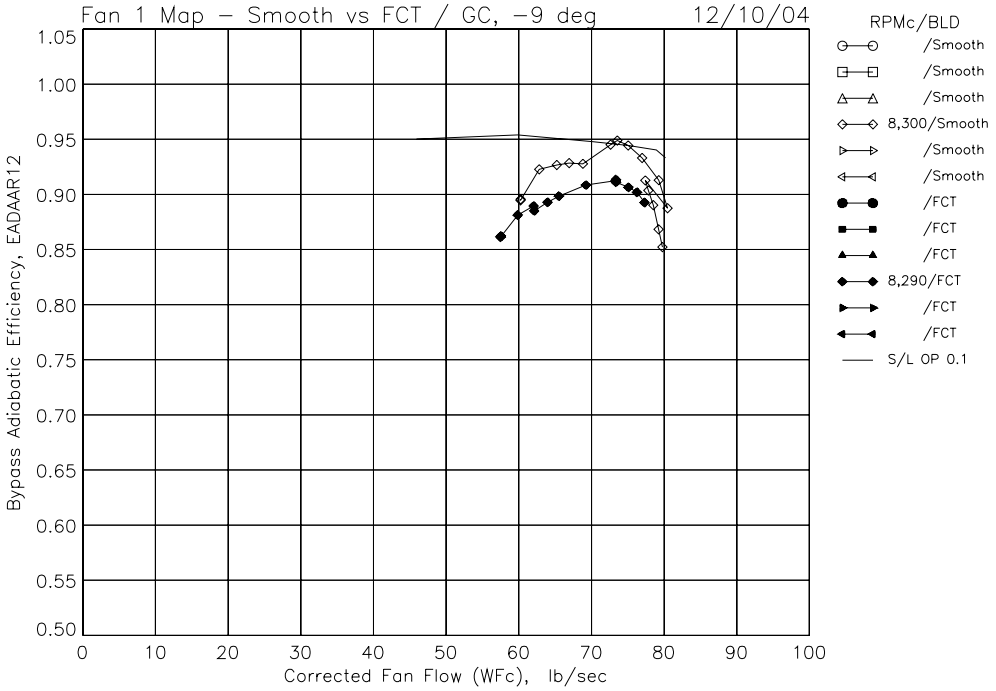

(b) Bypass adiabatic efficiency versus total fan corrected flow.

Figure 26.—Smooth and FCT single-speed bypass efficiency results with –9 deg blade angle, GC blades.

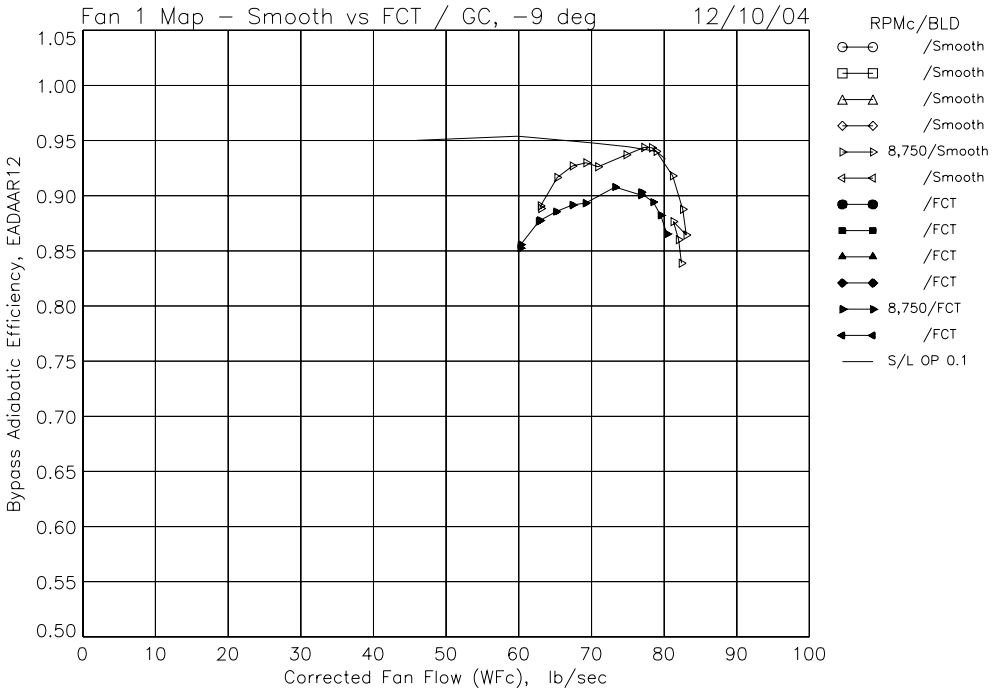

(c) Bypass adiabatic efficiency versus total fan corrected flow.

Figure 26.—Smooth and FCT single-speed bypass efficiency results with –9 deg blade angle, GC blades.

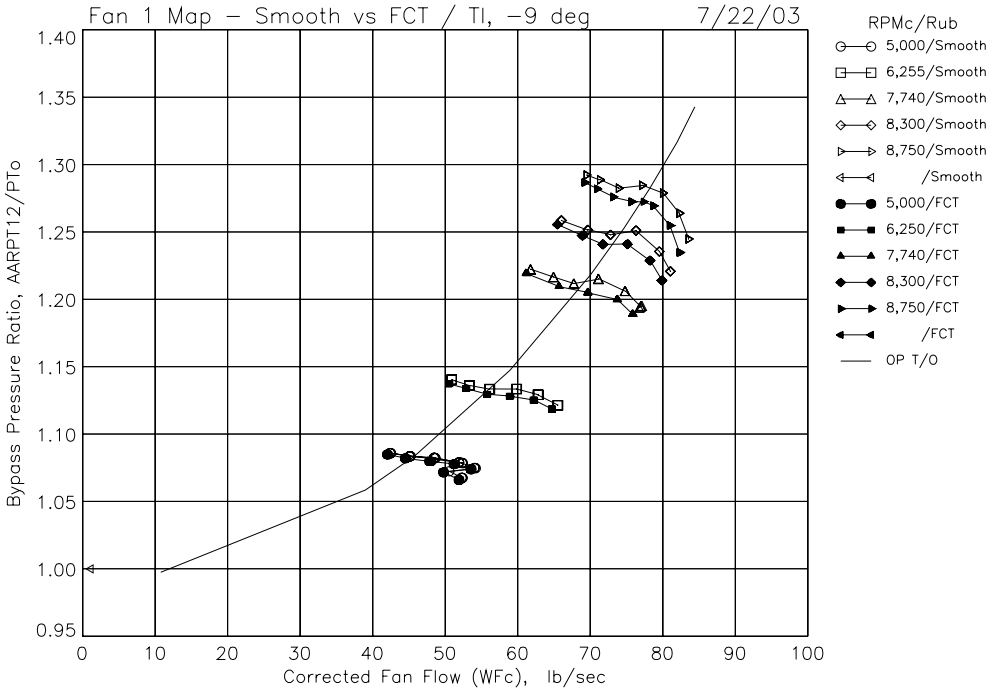

(a) Bypass total pressure ratio versus total fan corrected flow.

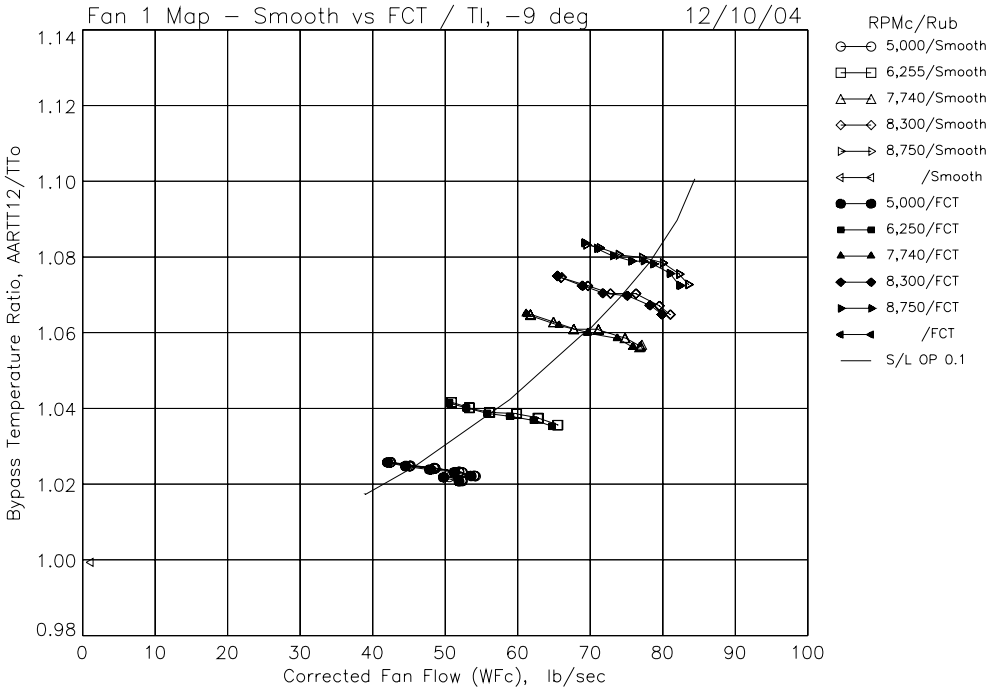

(b) Bypass total temperature ratio versus total fan corrected flow.

Figure 27.—Smooth and FCT bypass performance map results with –9 deg blade angle, TI blades.

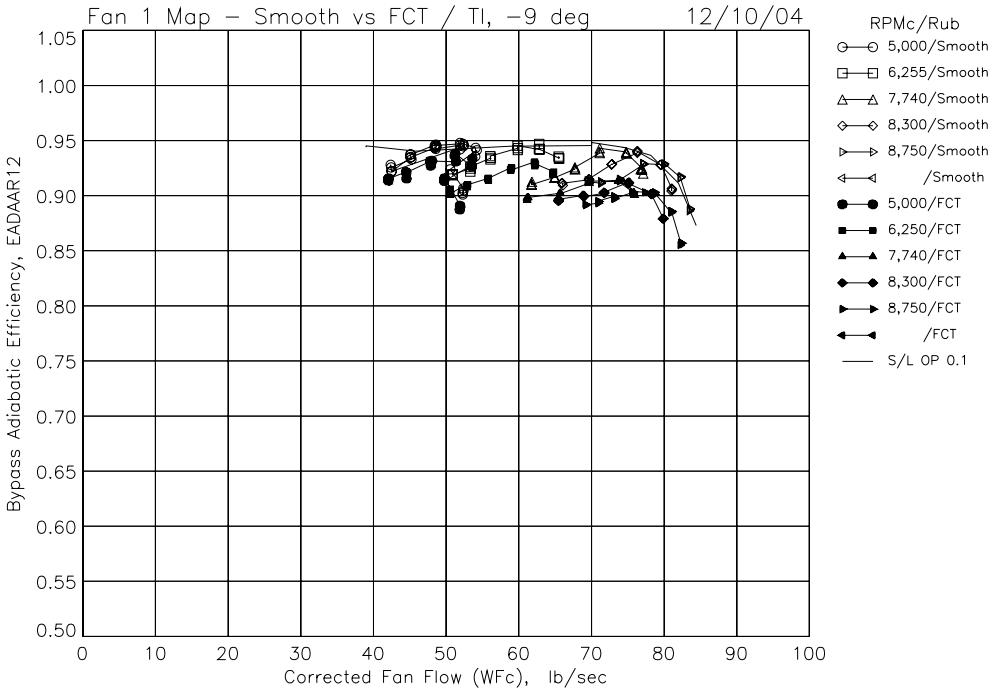

(c) Bypass adiabatic efficiency versus total fan corrected flow.

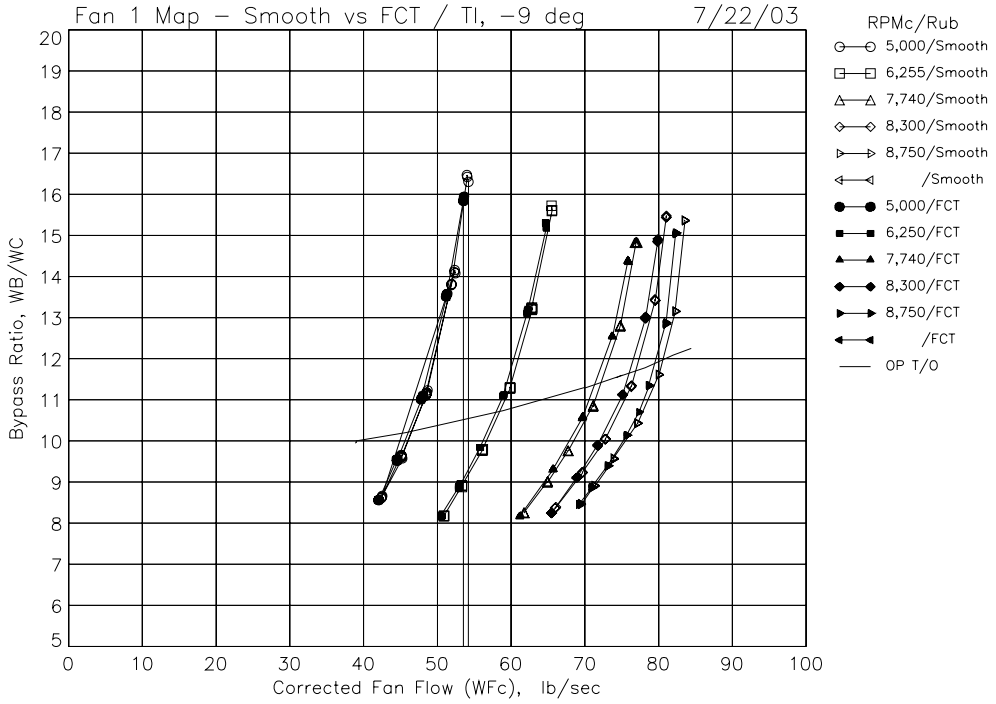

(d) Bypass ratio versus total fan corrected flow.

Figure 27.—Smooth and FCT bypass performance map results with –9 deg blade angle, TI blades.

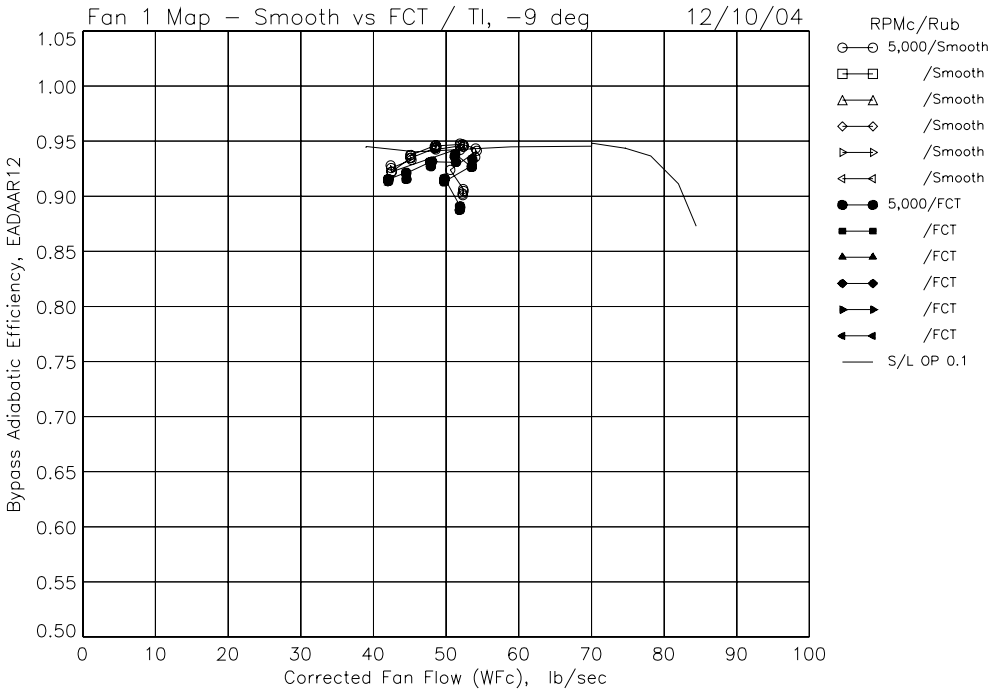

(a) Bypass adiabatic efficiency versus total fan corrected flow.

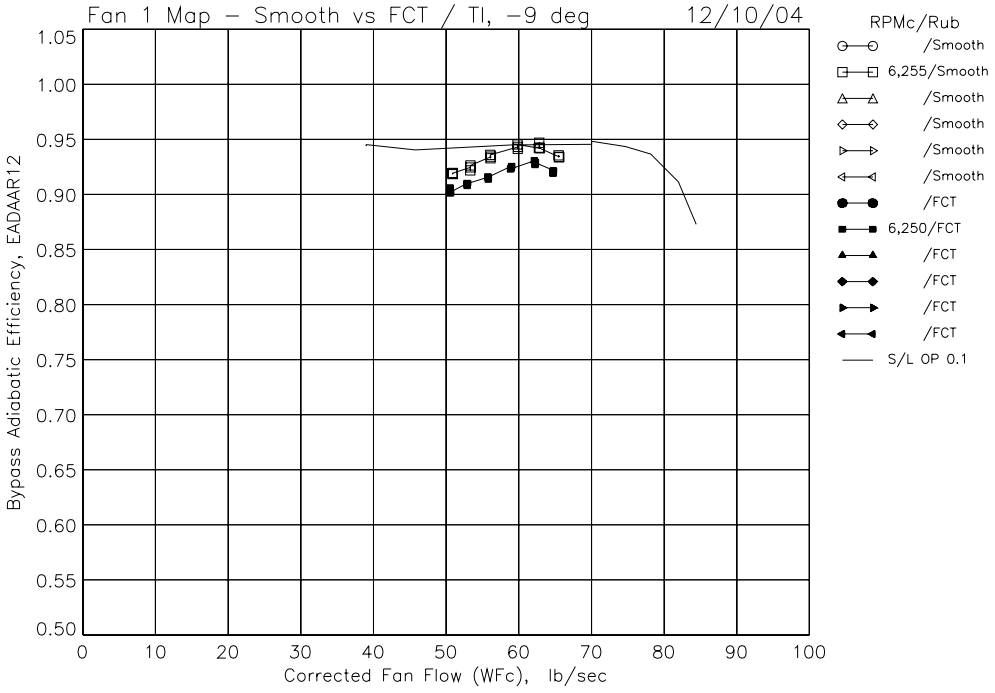

(b) Bypass adiabatic efficiency versus total fan corrected flow.

Figure 28.—Smooth and FCT single-speed bypass efficiency results with –9 deg blade angle, TI blades.

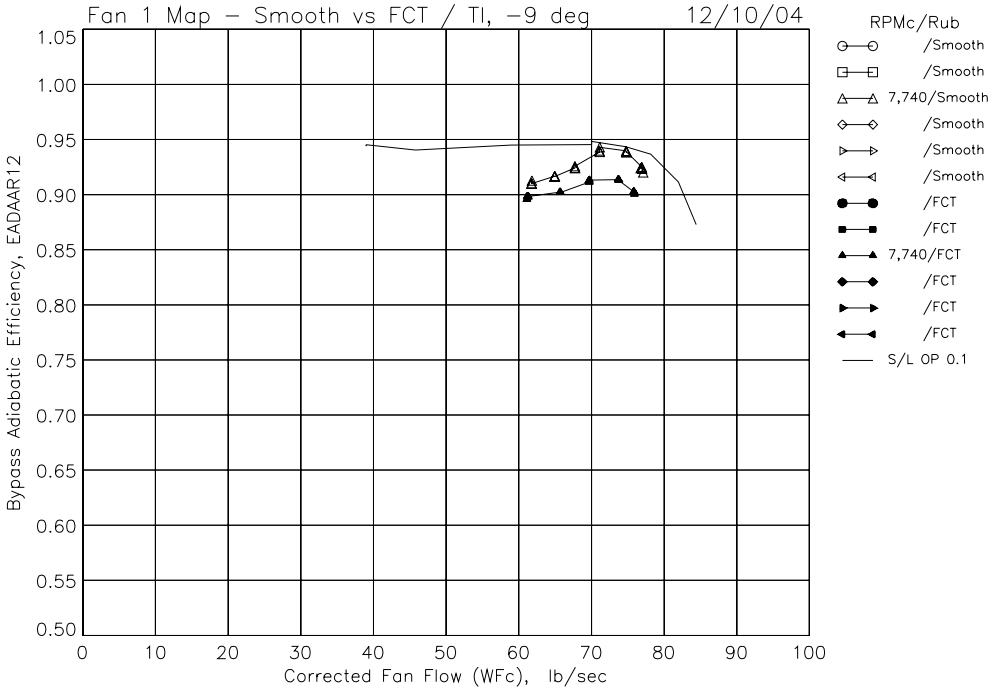

(c) Bypass adiabatic efficiency versus total fan corrected flow.

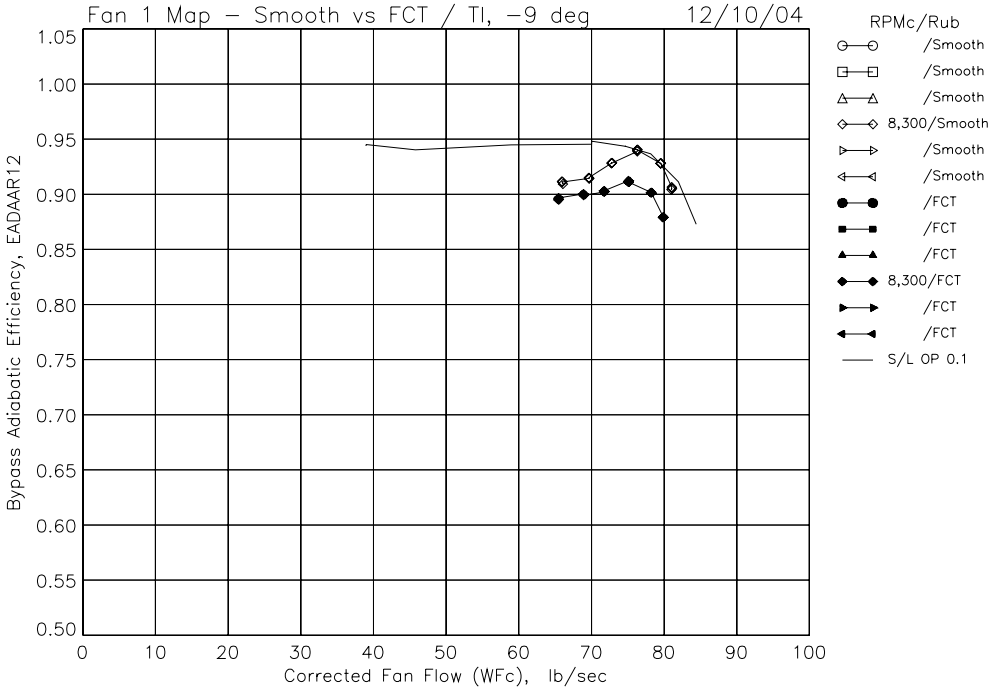

(d) Bypass adiabatic efficiency versus total fan corrected flow.

Figure 28.—Smooth and FCT single-speed bypass efficiency results with –9 deg blade angle, TI blades.

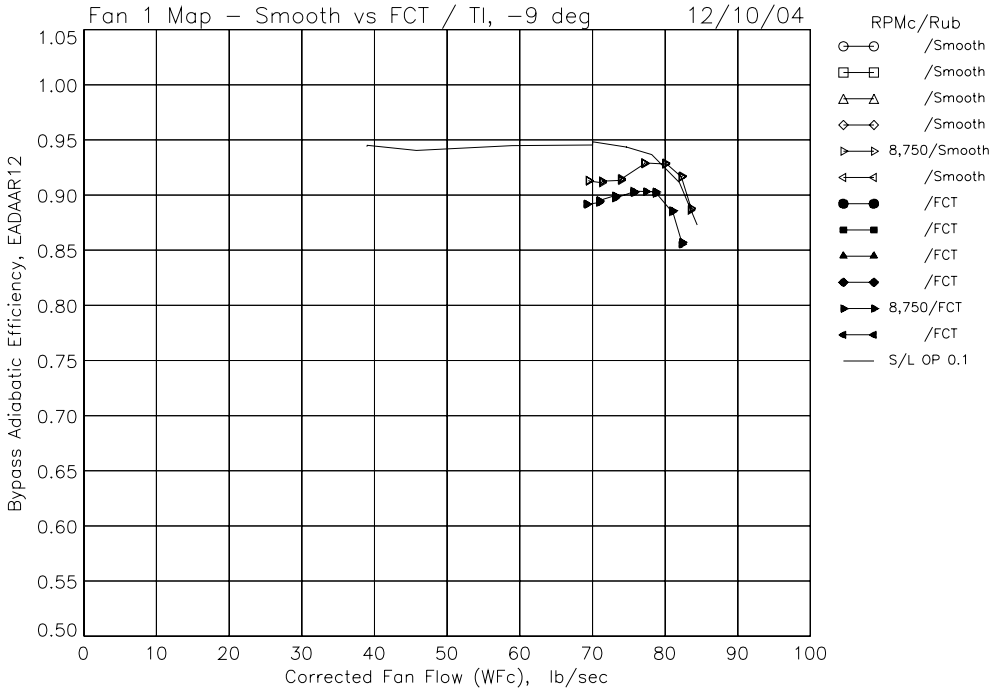

(e) Bypass adiabatic efficiency versus total fan corrected flow.

Figure 28.—Smooth and FCT single-speed bypass efficiency results with –9 deg blade angle, TI blades.

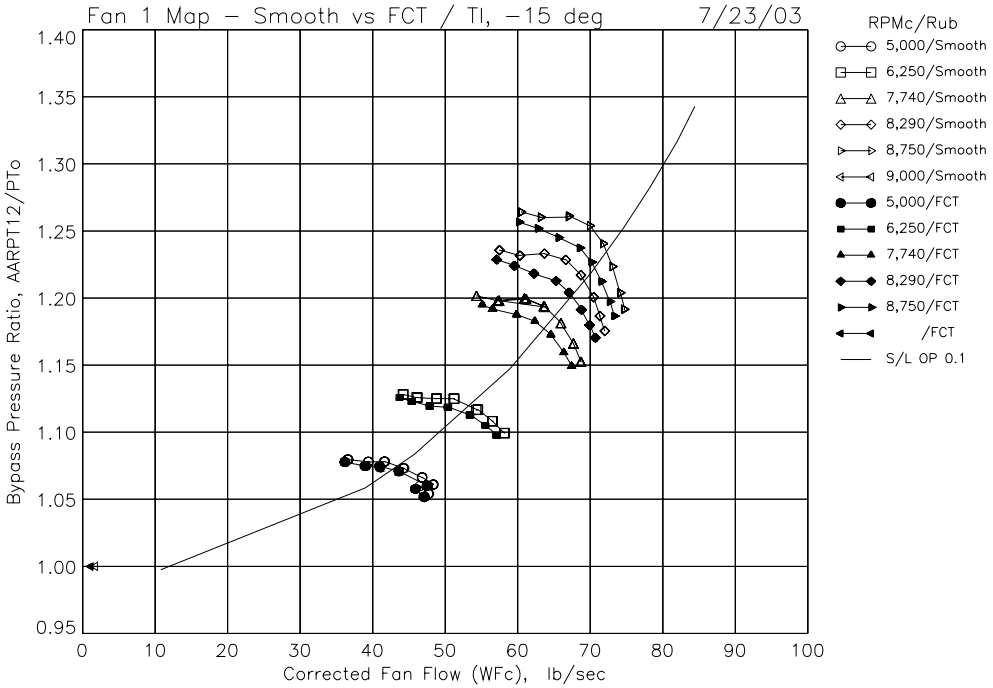

(a) Bypass total pressure ratio versus total fan corrected flow.

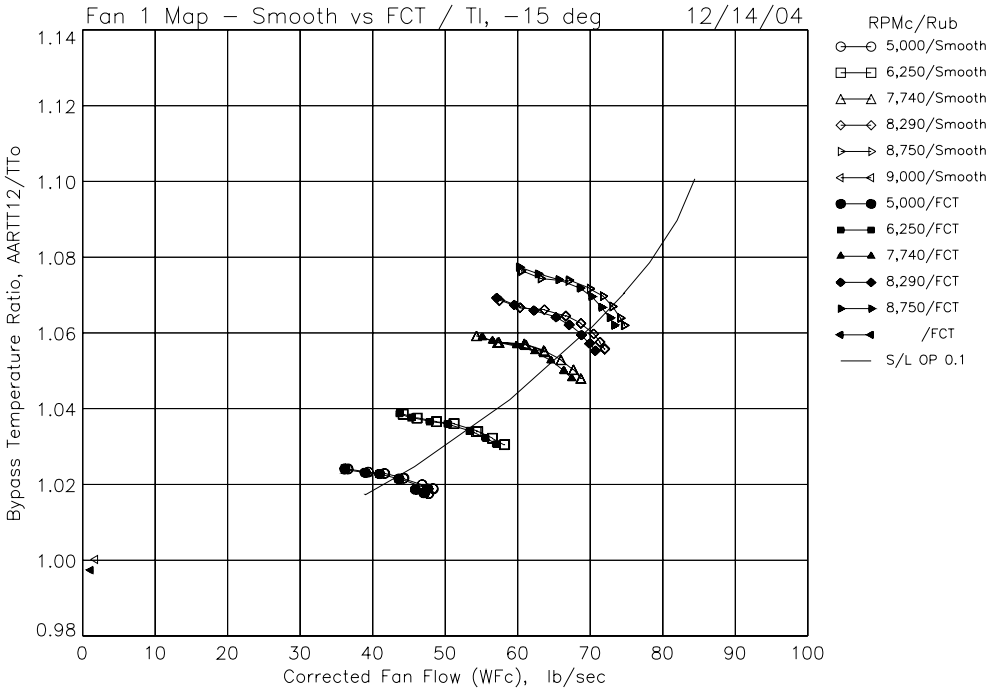

(b) Bypass total temperature ratio versus total fan corrected flow.

Figure 29.—Smooth and FCT bypass performance map TI blades.

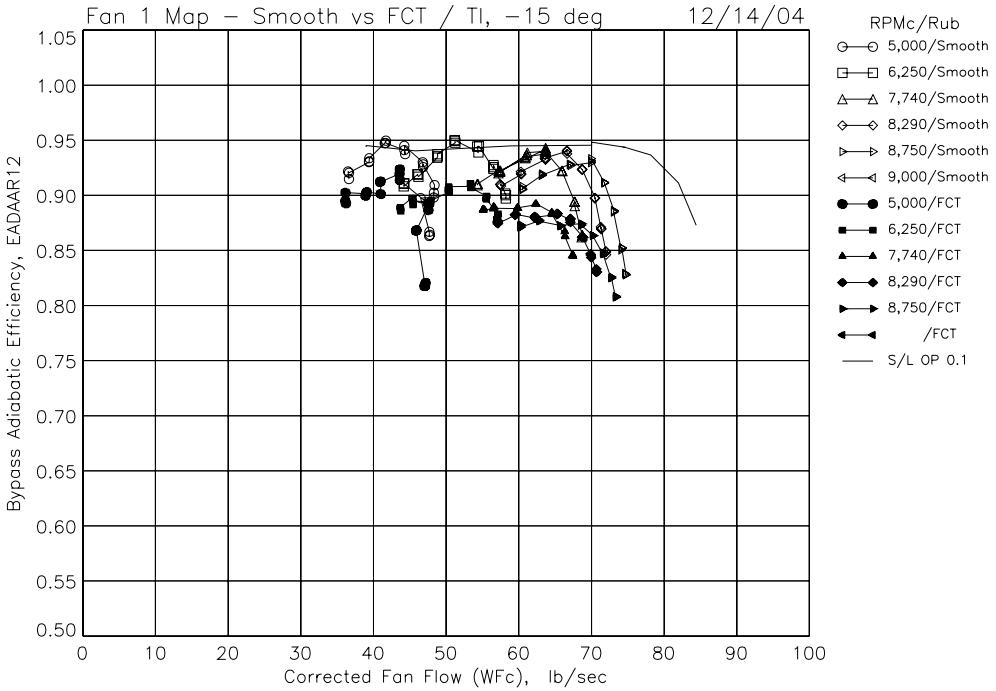

(c) Bypass adiabatic efficiency versus total fan corrected flow.

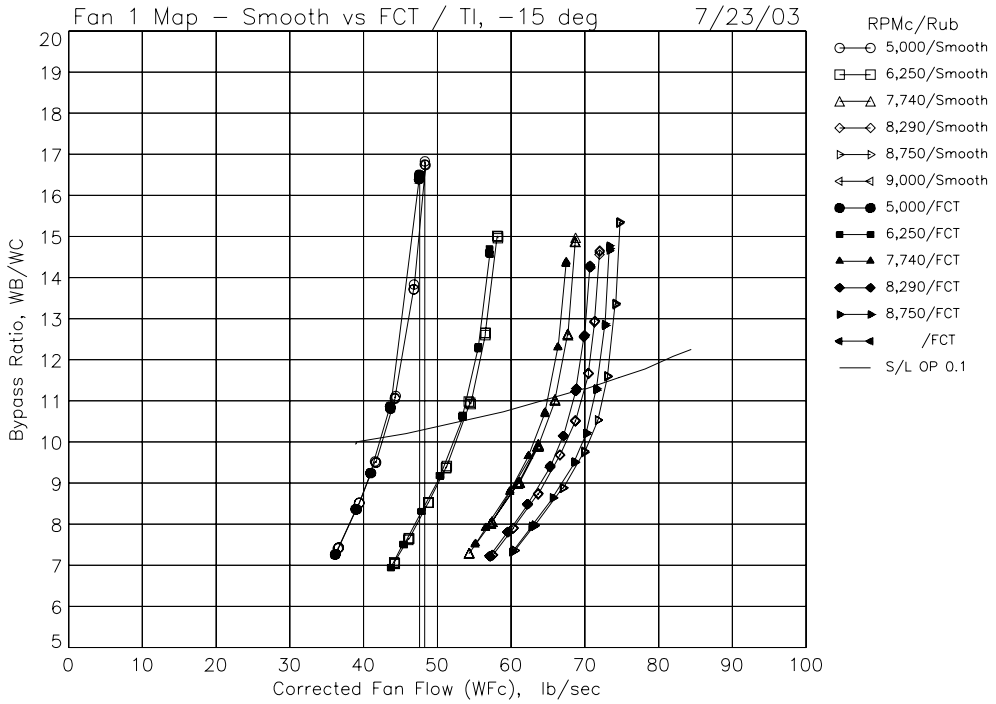

(d) Bypass ratio versus total fan corrected flow.

Figure 29.—Smooth and FCT bypass performance map results with –15 deg blade angle, TI blades.

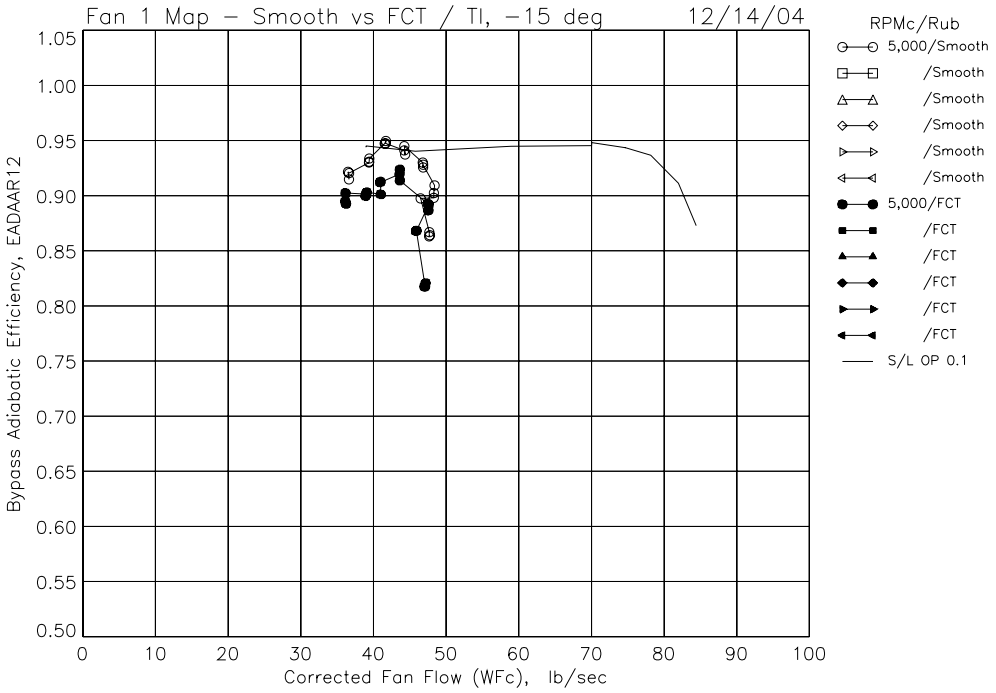

(a) Bypass adiabatic efficiency versus total fan corrected flow.

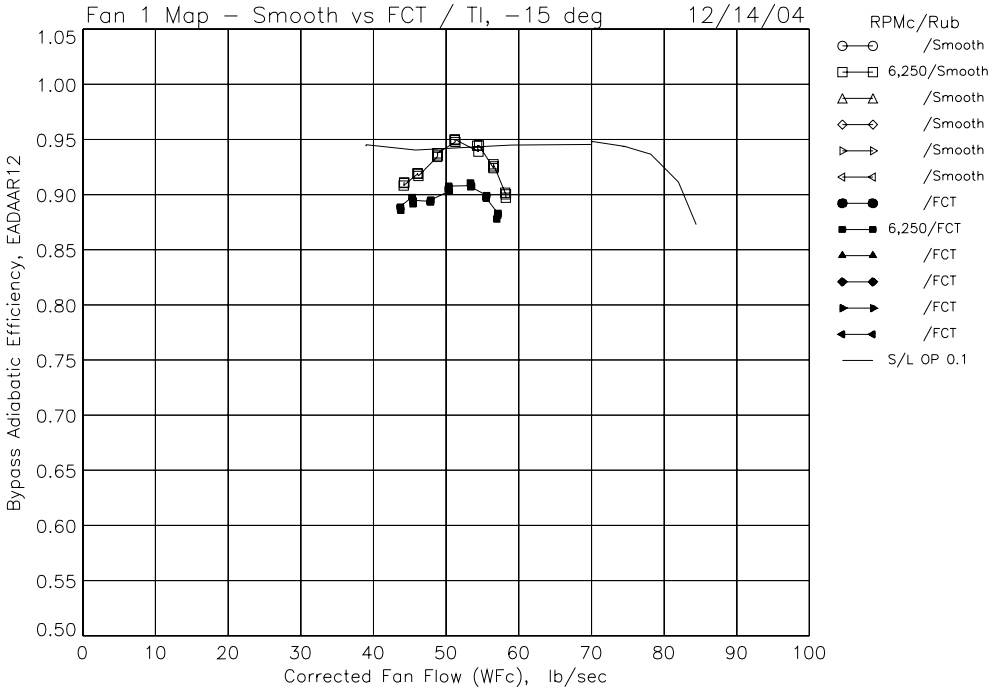

(b) Bypass adiabatic efficiency versus total fan corrected flow.

Figure 30.—Smooth and FCT single-speed bypass efficiency results with –15 deg blade angle, TI blades.

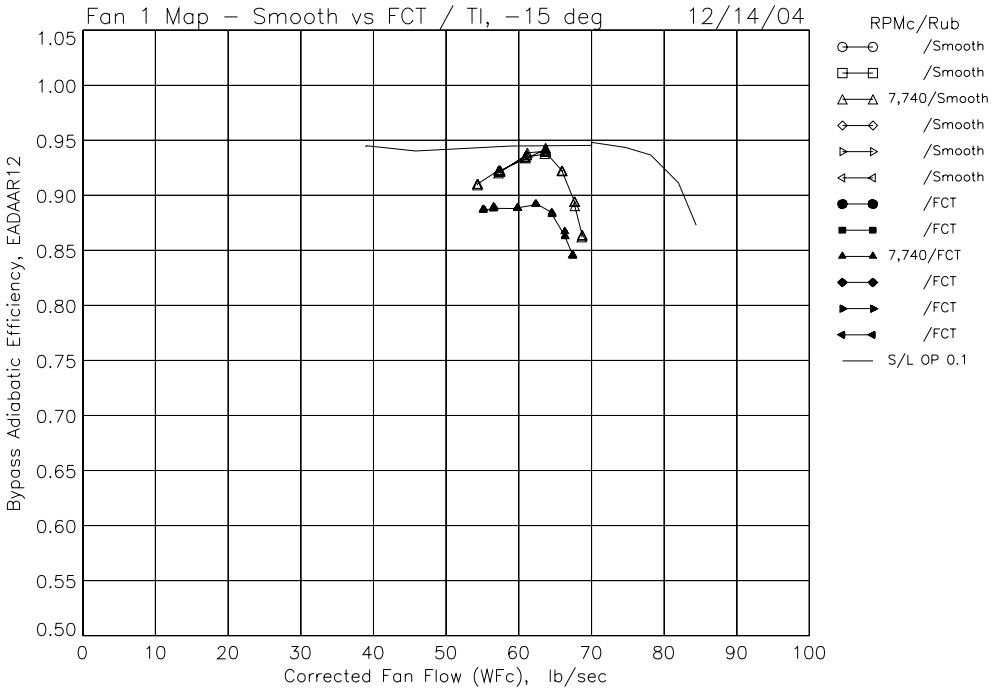

(c) Bypass adiabatic efficiency versus total fan corrected flow.

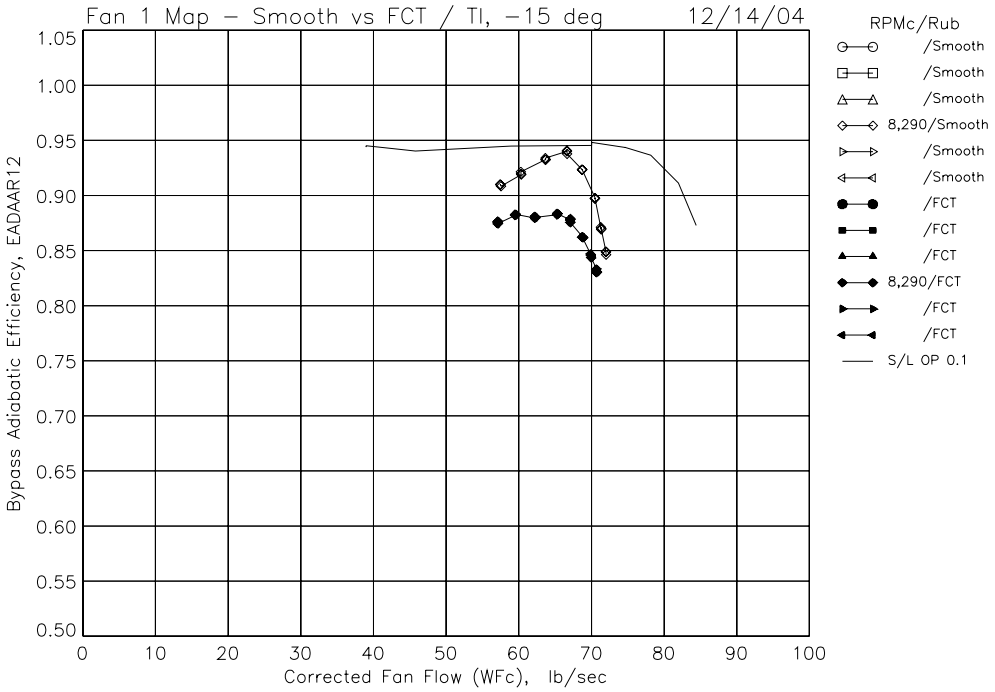

(d) Bypass adiabatic efficiency versus total fan corrected flow.

Figure 30.—Smooth and FCT single-speed bypass efficiency results with –15 deg blade angle, TI blades.

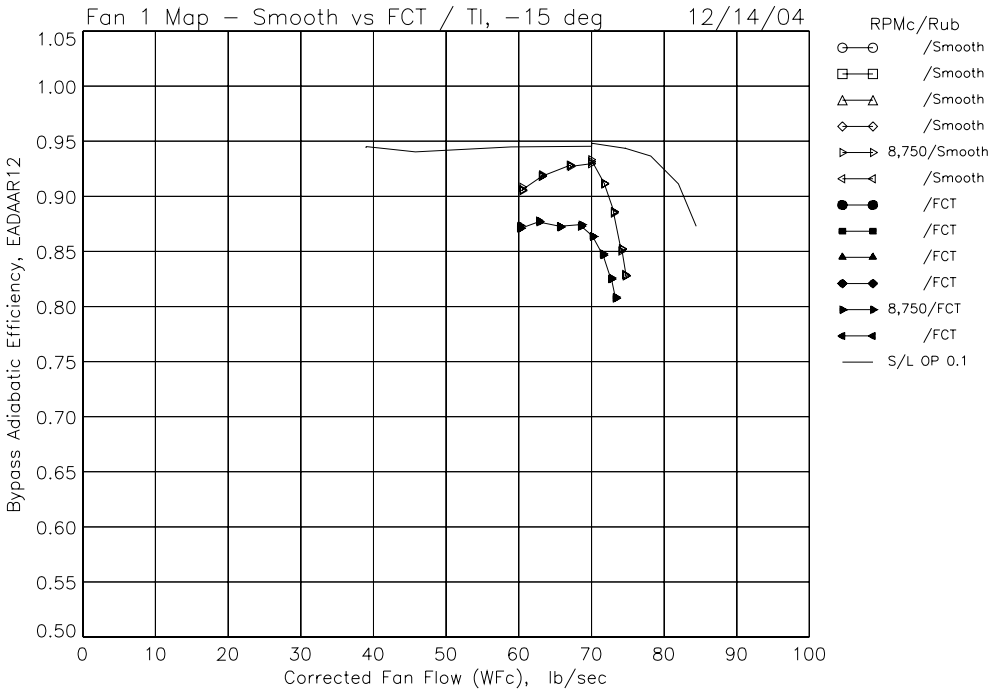

(e) Bypass adiabatic efficiency versus total fan corrected flow.

Figure 30.—Smooth and FCT single-speed bypass efficiency results with –15 deg blade angle, TI blades.

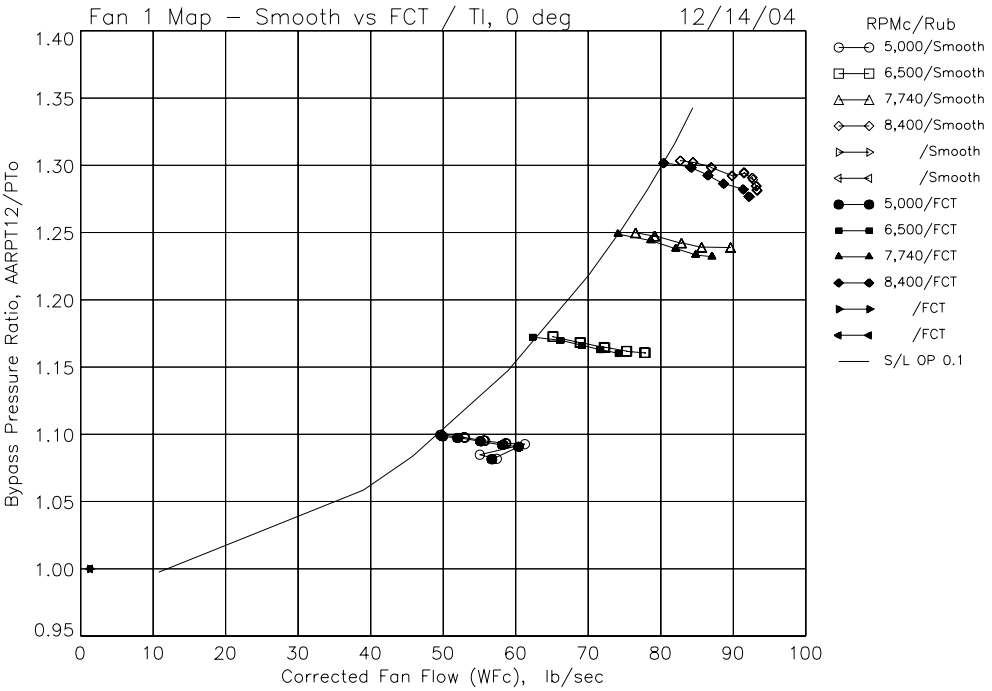

(a) Bypass total pressure ratio versus total fan corrected flow.

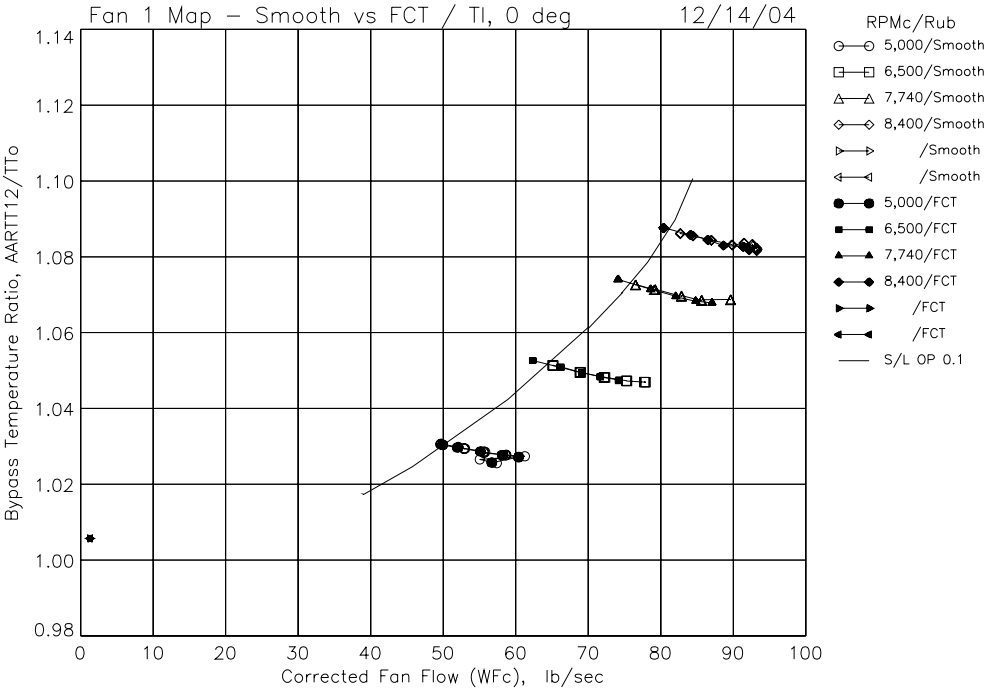

(b) Bypass total temperature ratio versus total fan corrected flow.

Figure 31.—Smooth and FCT bypass performance map results with zero blade angle, TI blades.

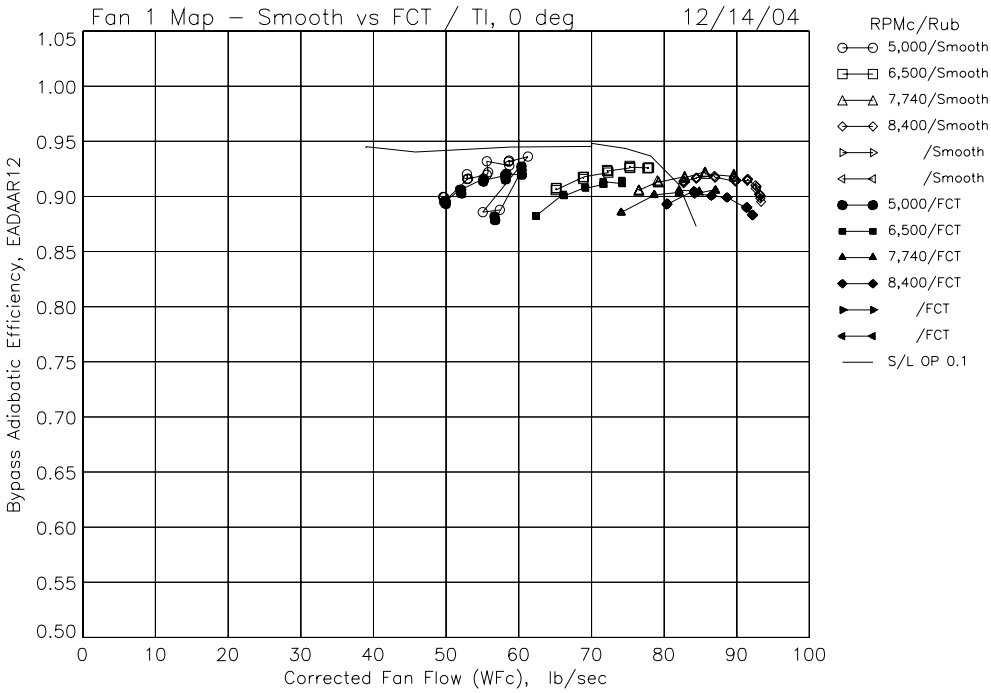

(c) Bypass adiabatic efficiency versus total fan corrected flow.

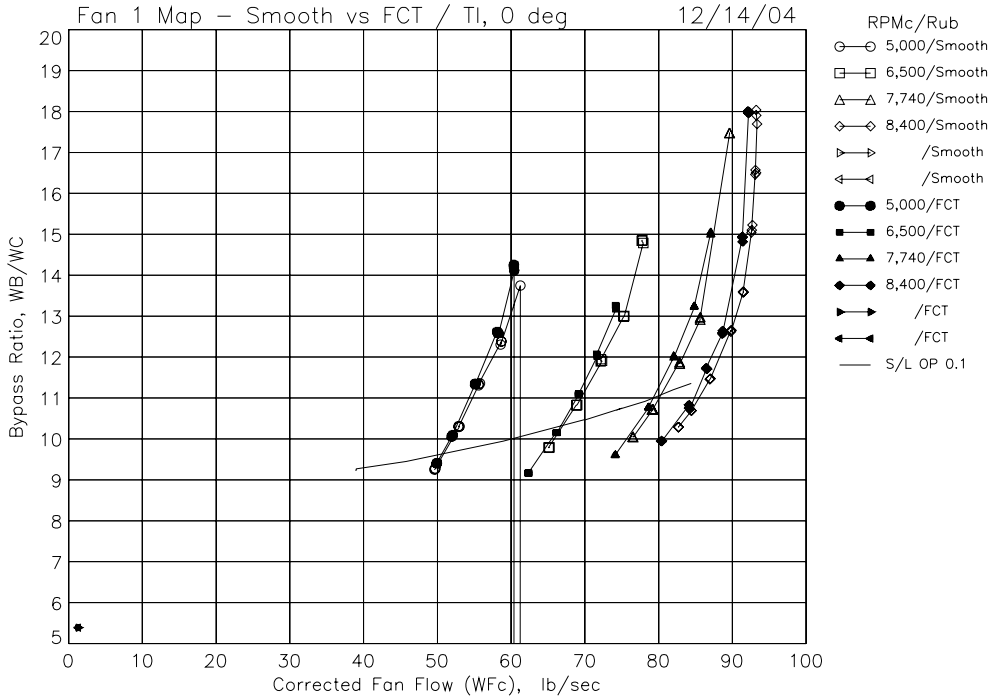

(d) Bypass ratio versus total fan corrected flow.

Figure 31.—Smooth and FCT bypass performance map results with zero blade angle, TI blades.

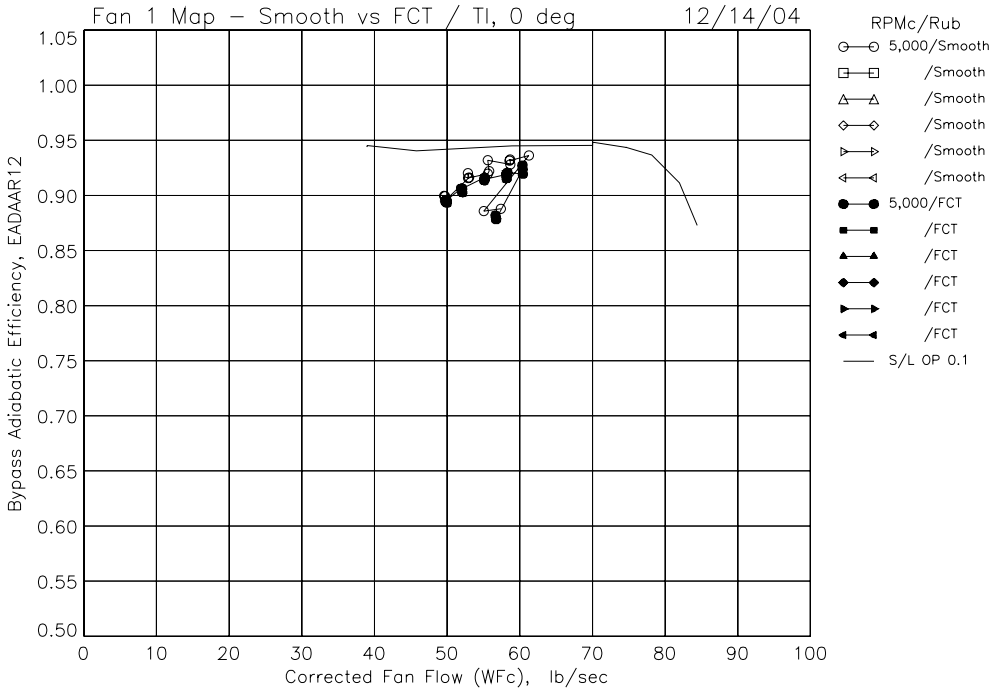

(a) Bypass adiabatic efficiency versus total fan corrected flow, RPMc = 5,000.

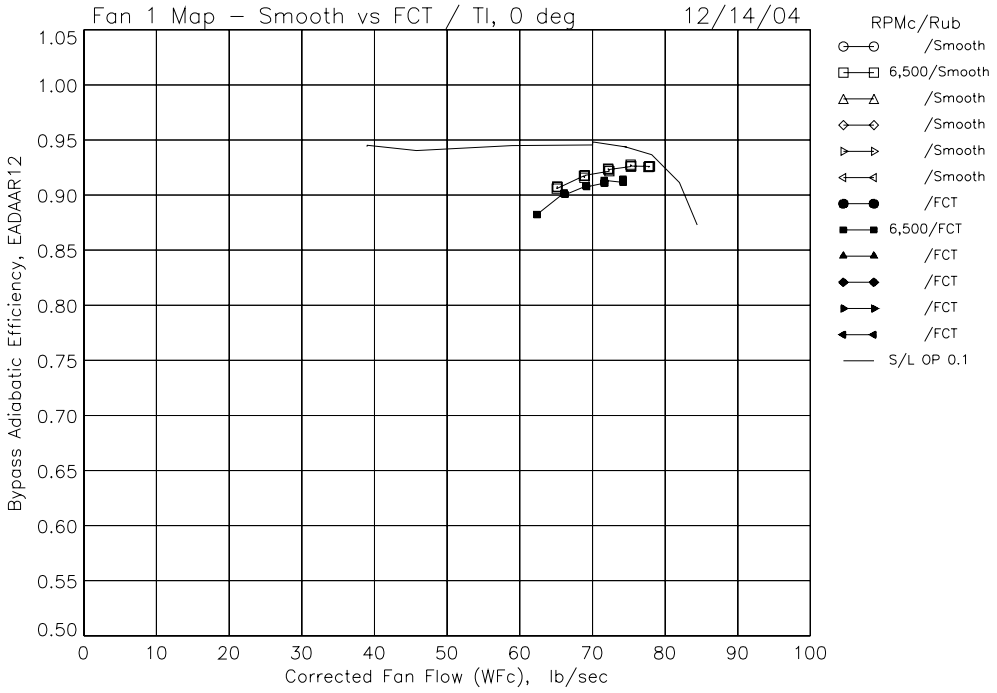

(b) Bypass adiabatic efficiency versus total fan corrected flow, RPMc = 6,500.

Figure 32.—Smooth and FCT single-speed bypass efficiency results with 0 degree blade angle, TI blades.

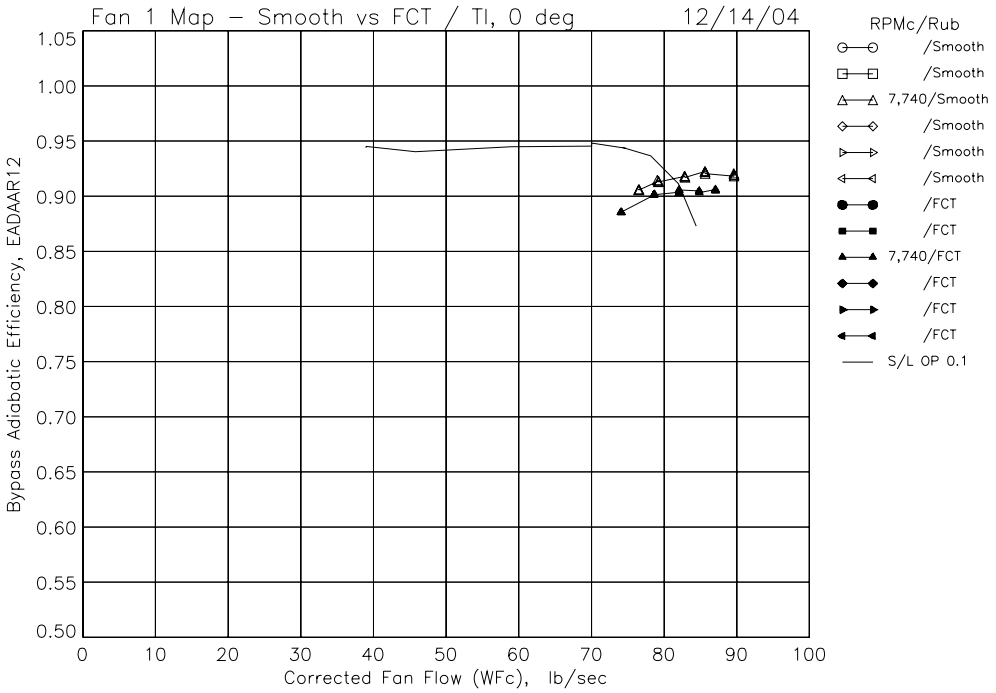

(c) Bypass adiabatic efficiency versus total fan corrected flow, RPMc = 7,740.

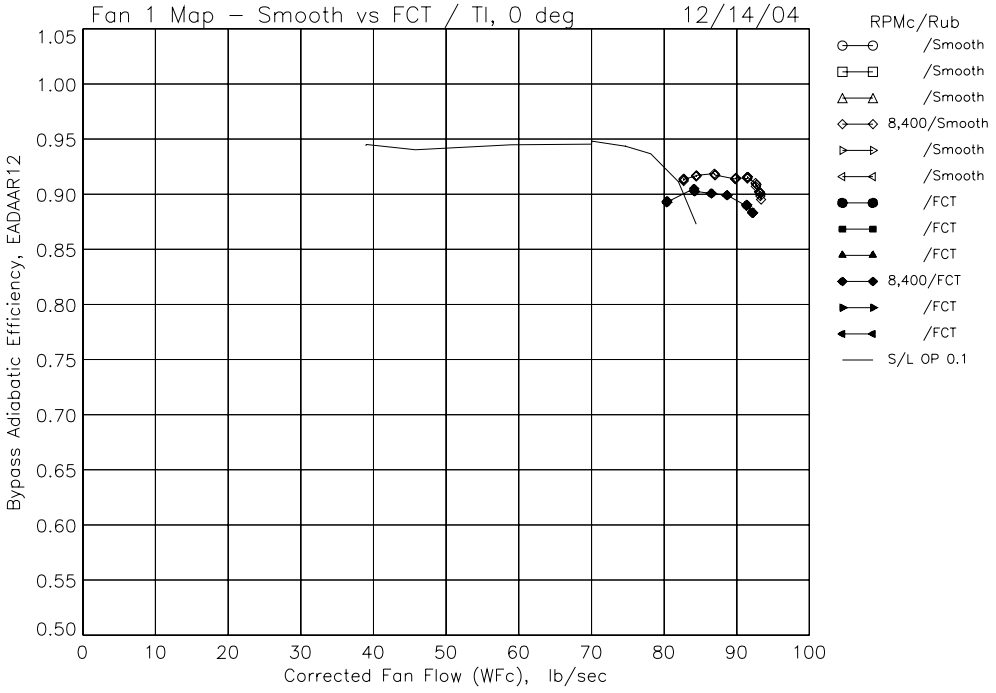

(d) Bypass adiabatic efficiency versus total fan corrected flow, RPMc = 8,400.

Figure 32.—Smooth and FCT single-speed bypass efficiency results with 0 degree blade angle, TI blades.

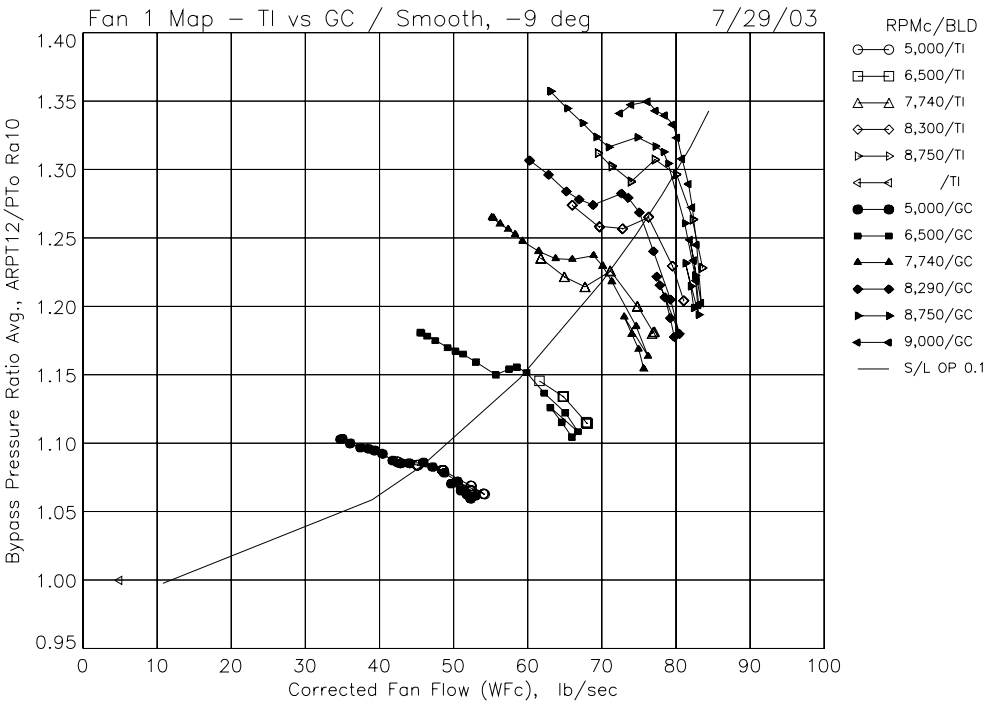

(a) Bypass 10th radius total pressure ratio versus total fan corrected flow.

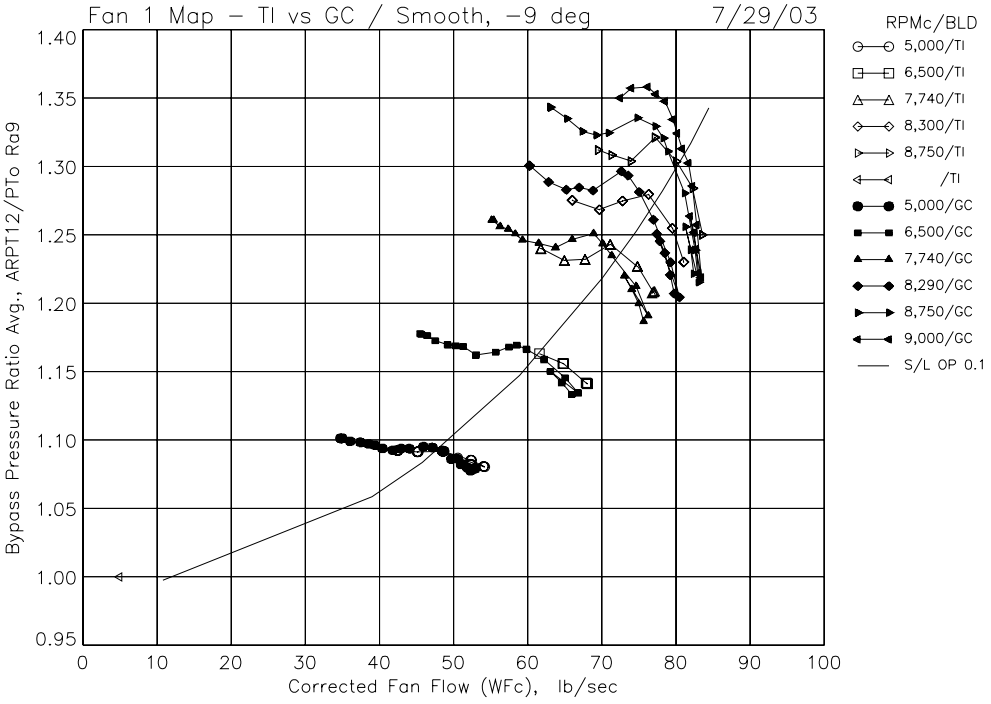

(b) Bypass 9th radius total pressure ratio versus total fan corrected flow.

Figure 33.—TI and GC blade single-radius pressure ratio map results with –9 deg blade angle, smooth rubstrip.

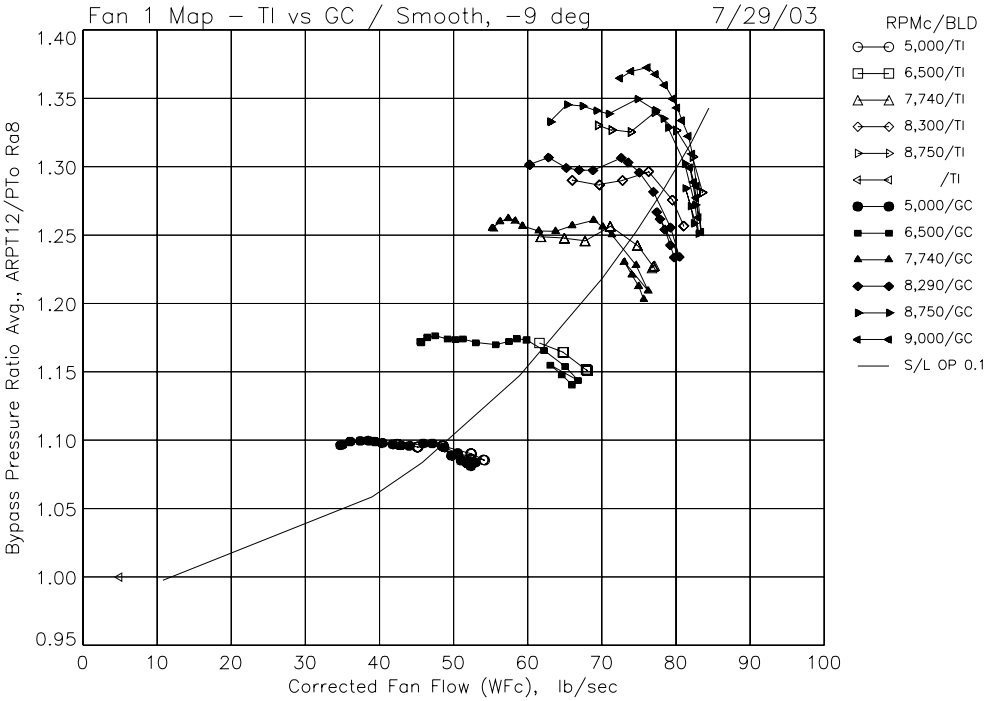

(c) Bypass 8th radius total pressure ratio versus total fan corrected flow.

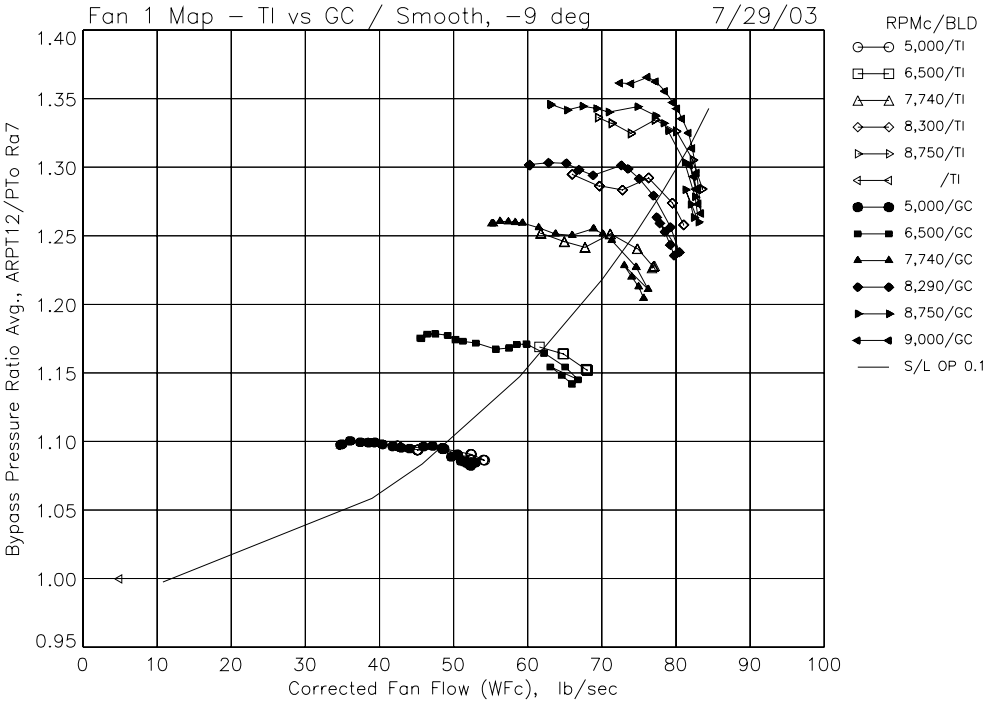

(d) Bypass 7th radius total pressure ratio versus total fan corrected flow.

Figure 33.—TI and GC blade single-radius pressure ratio map results with –9 deg blade angle, smooth rubstrip.

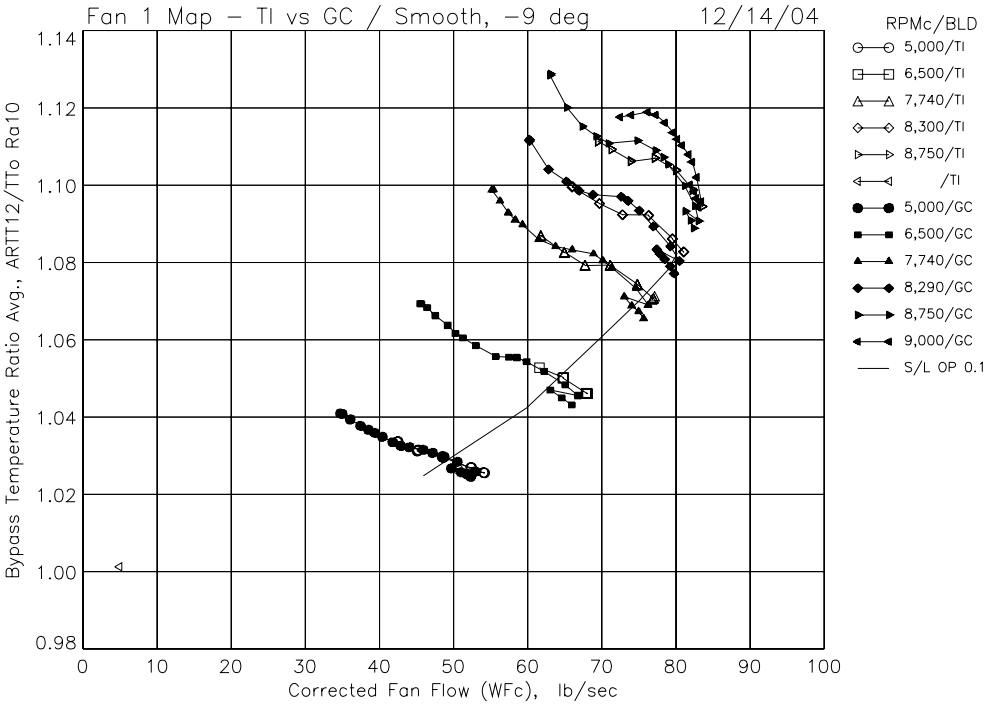

(a) Bypass 10th radius total temperature ratio versus total fan corrected flow.

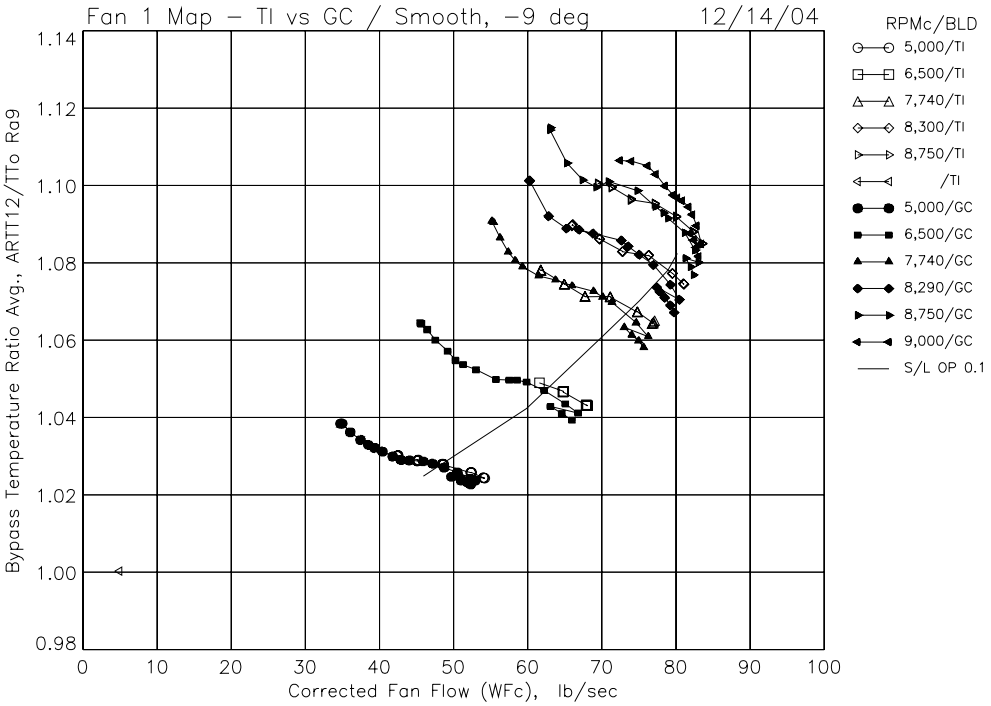

(b) Bypass 9th radius total temperature ratio versus total fan corrected flow.

Figure 34.—TI and GC blade single-radius temperature ratio map results with –9 deg blade angle, smooth rubstrip.

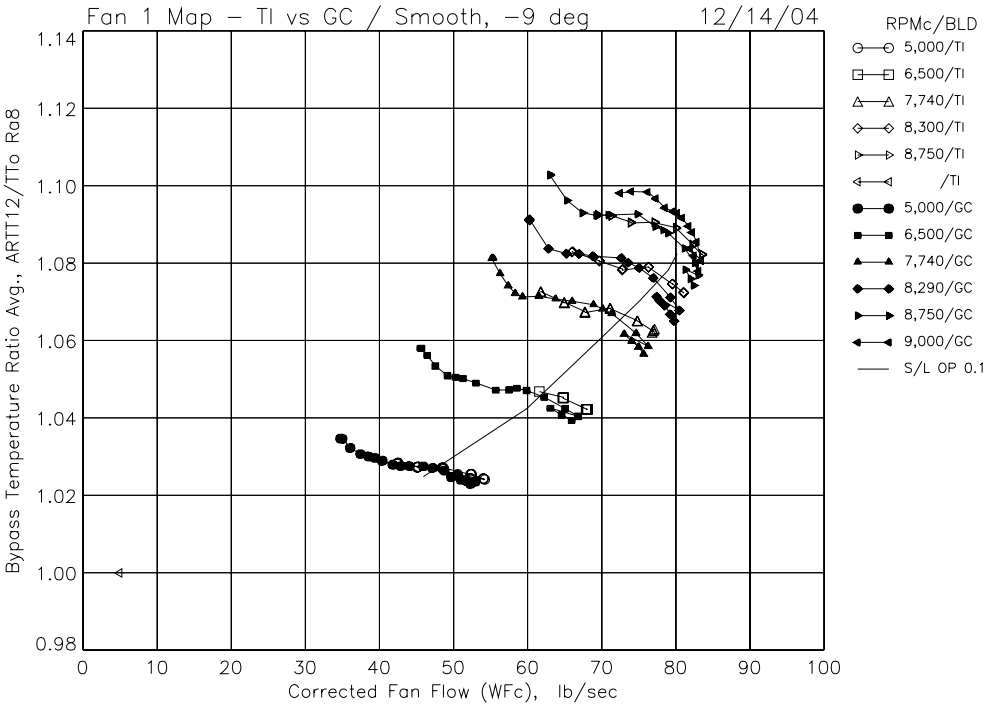

(c) Bypass 8th radius total temperature ratio versus total fan corrected flow.

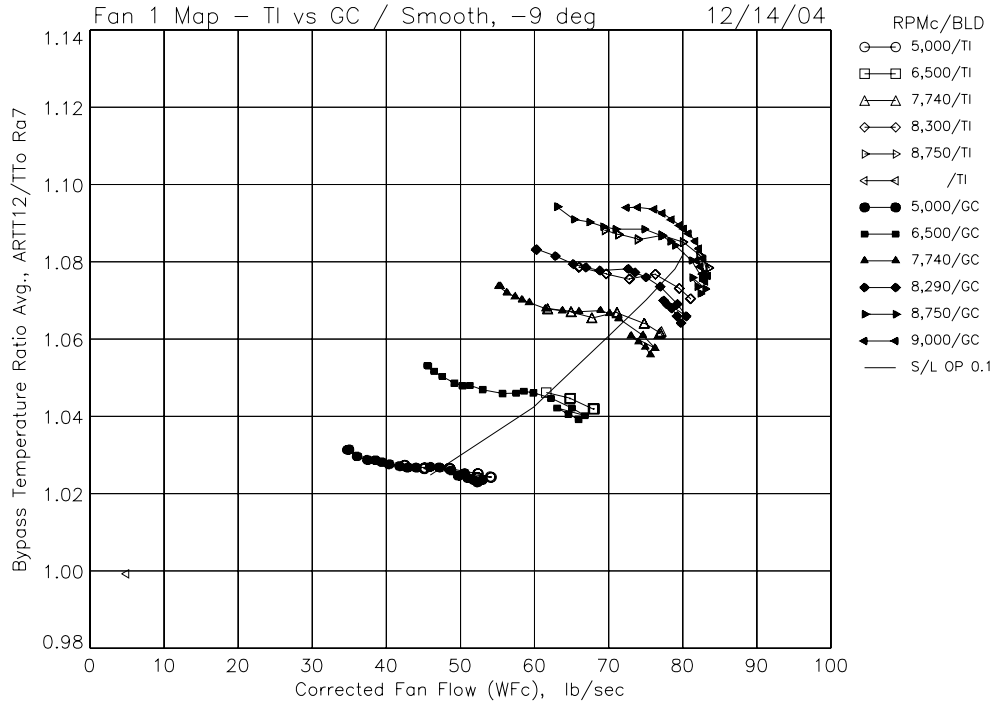

(d) Bypass 7th radius total temperature ratio versus total fan corrected flow.

Figure 34.—TI and GC blade single-radius temperature ratio map results with –9 deg blade angle, smooth rubstrip.

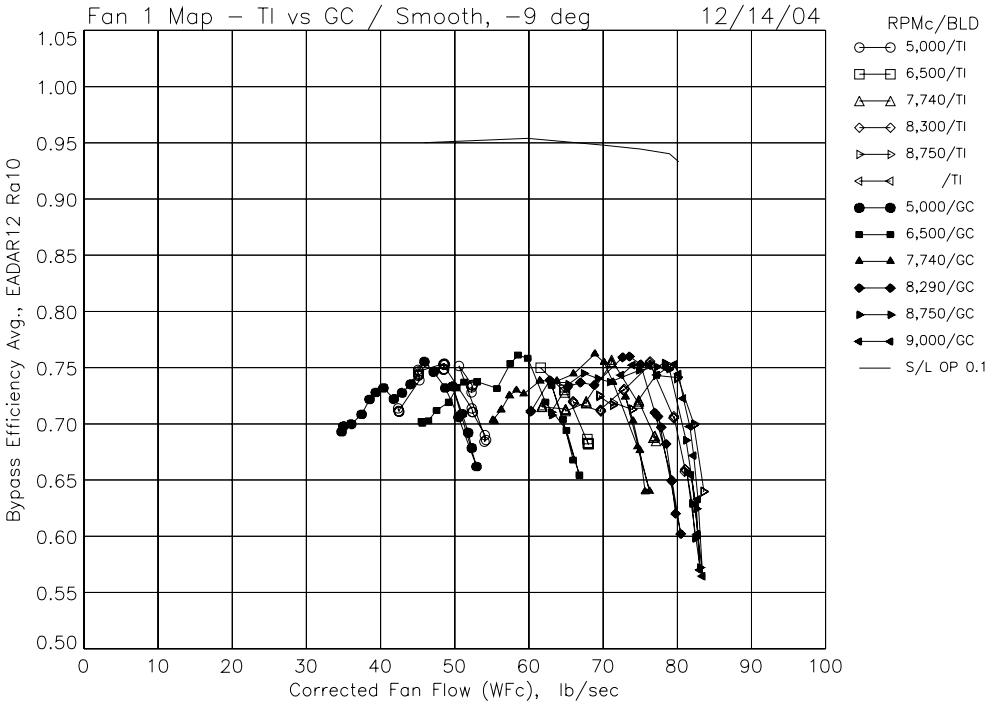

(a) Bypass 10th radius adiabatic efficiency versus total fan corrected flow.

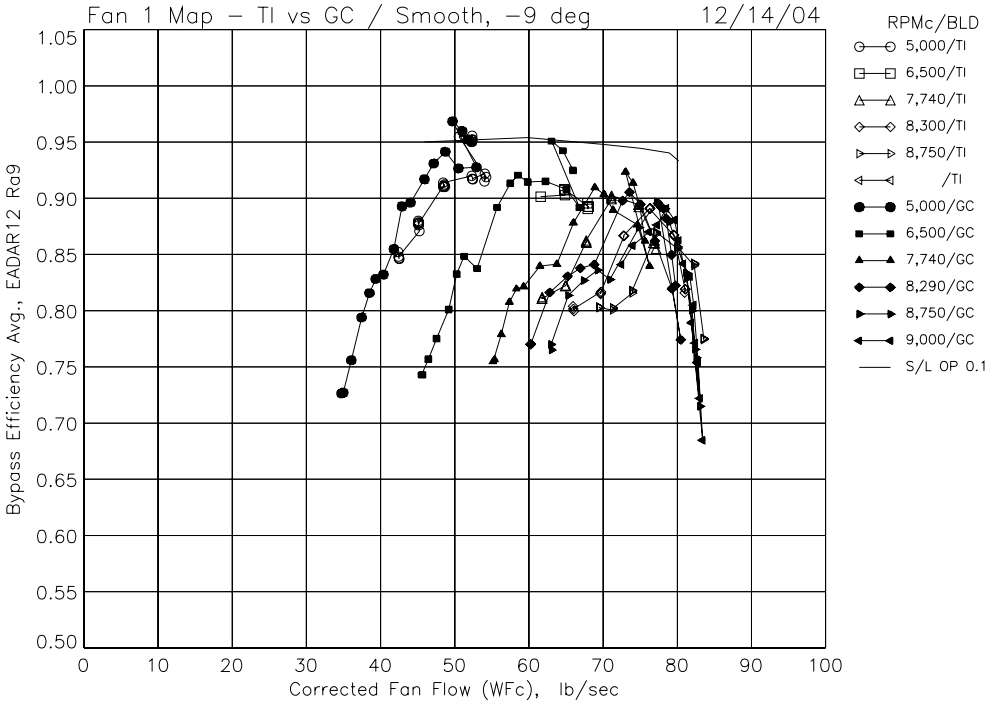

(b) Bypass 9th radius adiabatic efficiency versus total fan corrected flow.

Figure 35.—TI and GC blade single-radius adiabatic efficiency map results with –9 deg blade angle, smooth rubstrip.

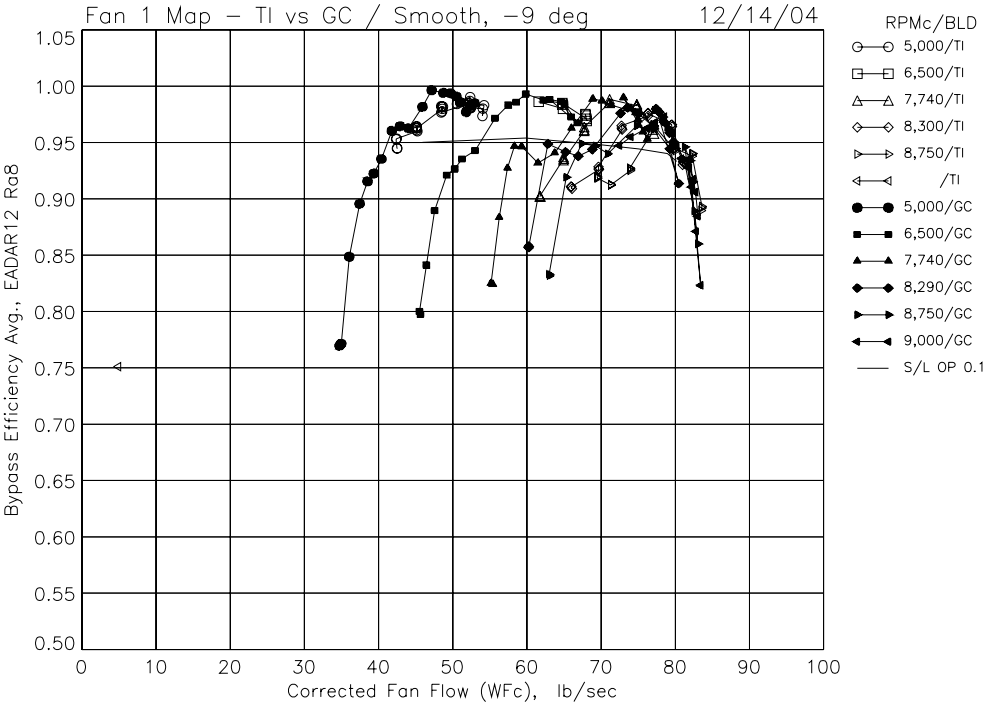

(c) Bypass 8th radius adiabatic efficiency versus total fan corrected flow.

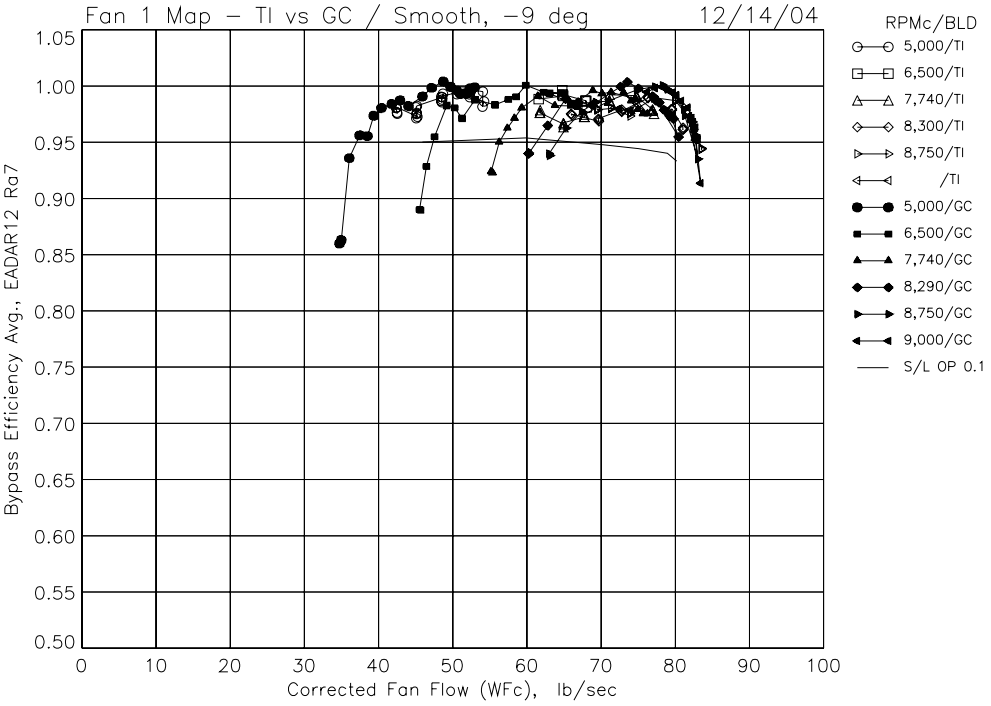

(d) Bypass 7th radius adiabatic efficiency versus total fan corrected flow.

Figure 35.—TI and GC blade single-radius adiabatic efficiency map results with –9 deg blade angle, smooth rubstrip.

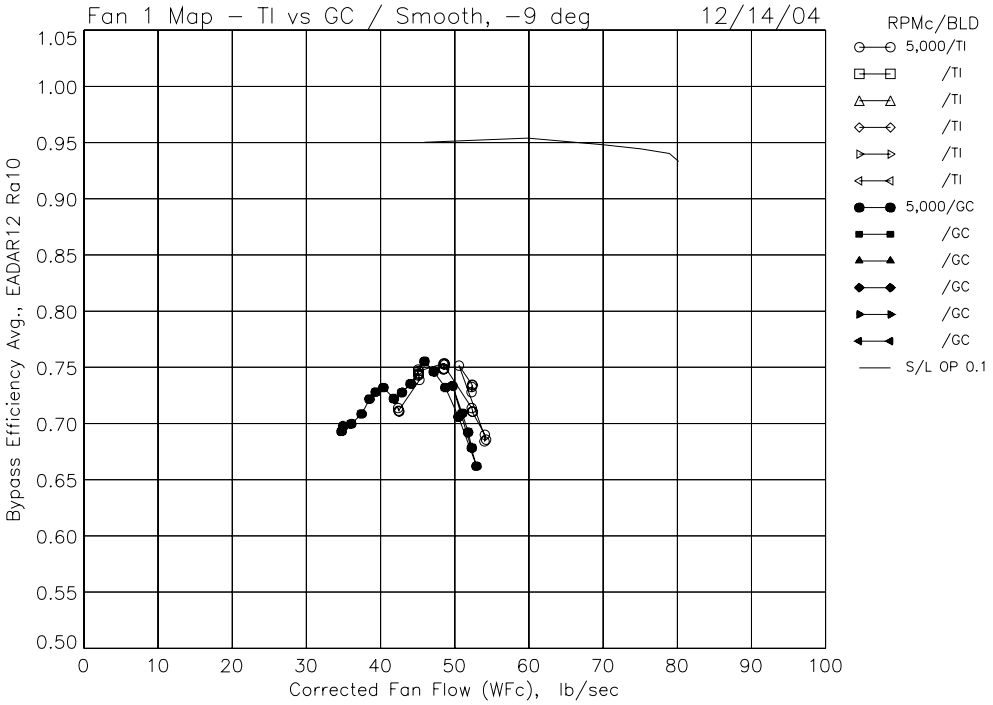

(a) Bypass 10th radius adiabatic efficiency versus total fan corrected flow, RPMc = 5,000.

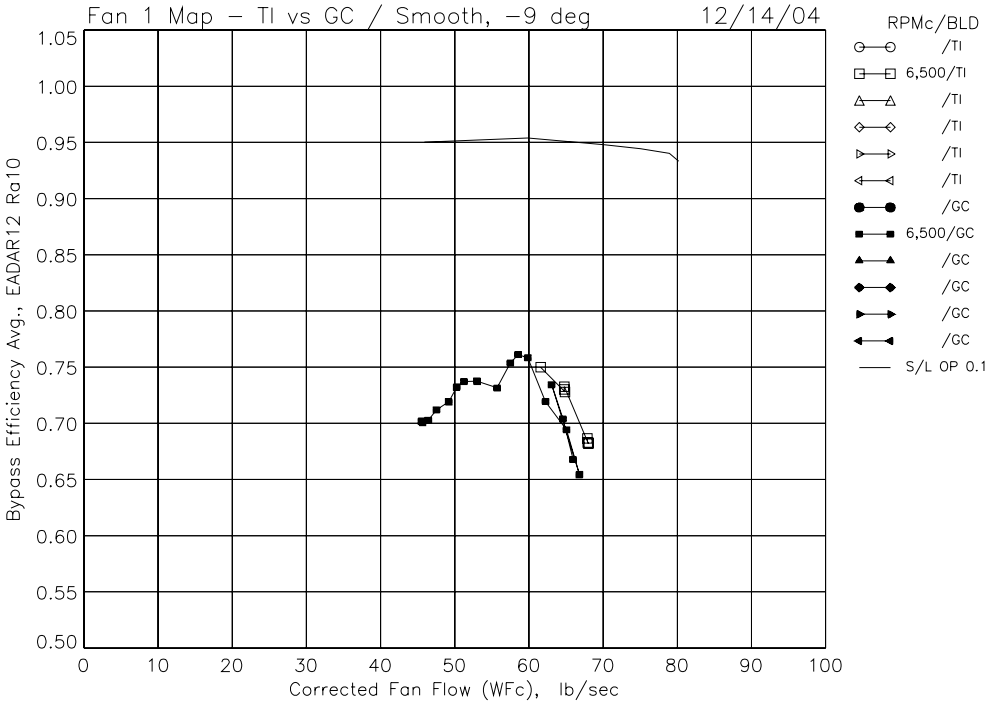

(b) Bypass 10th radius adiabatic efficiency versus total fan corrected flow, RPMc = 6,500.

Figure 36.—TI and GC blade single-speed, single-radius, efficiency results with –9 deg blade angle, smooth rubstrip.

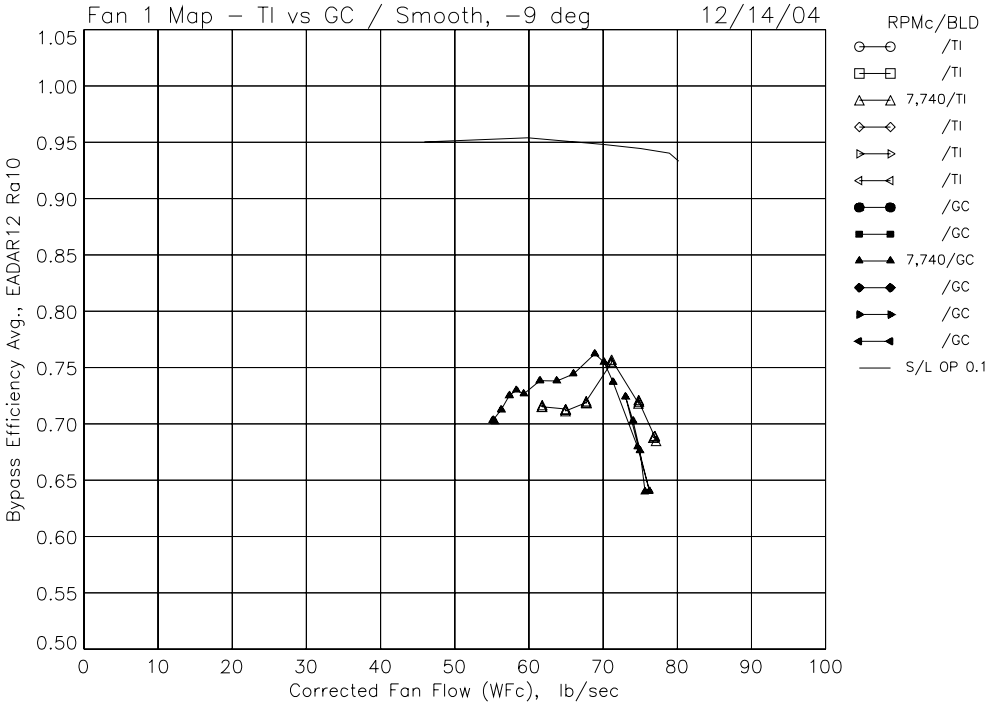

(c) Bypass 10th radius adiabatic efficiency versus total fan corrected flow, RPMc = 7,740.

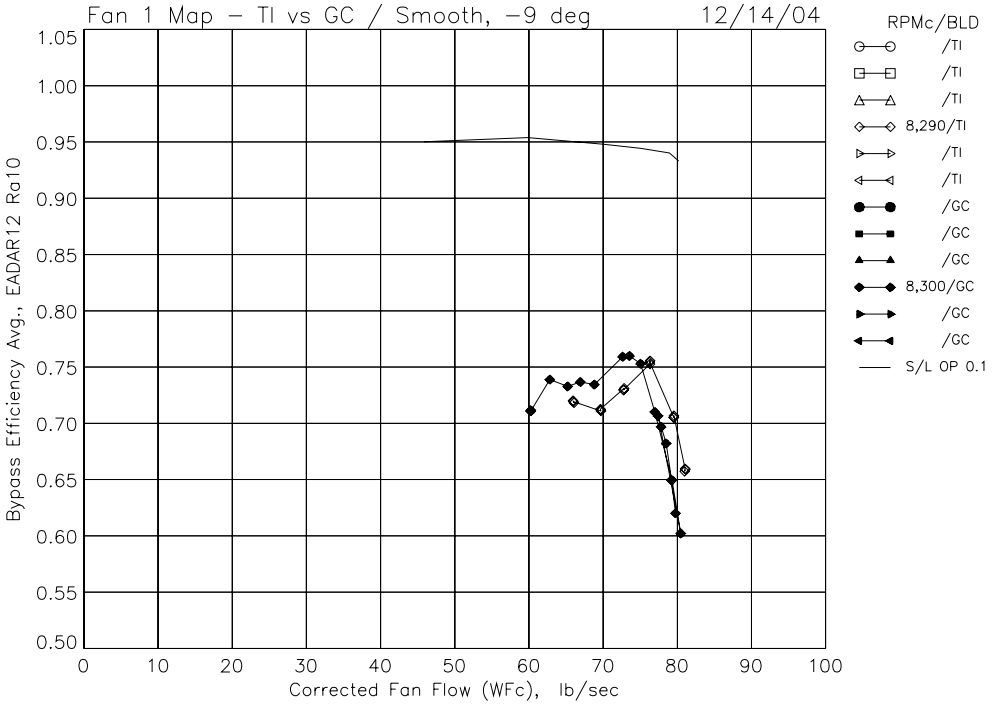

(d) Bypass 10th radius adiabatic efficiency versus total fan corrected flow, RPMc = 8,300.

Figure 36.—TI and GC blade single-speed, single-radius, efficiency results with –9 deg blade angle, smooth rubstrip.

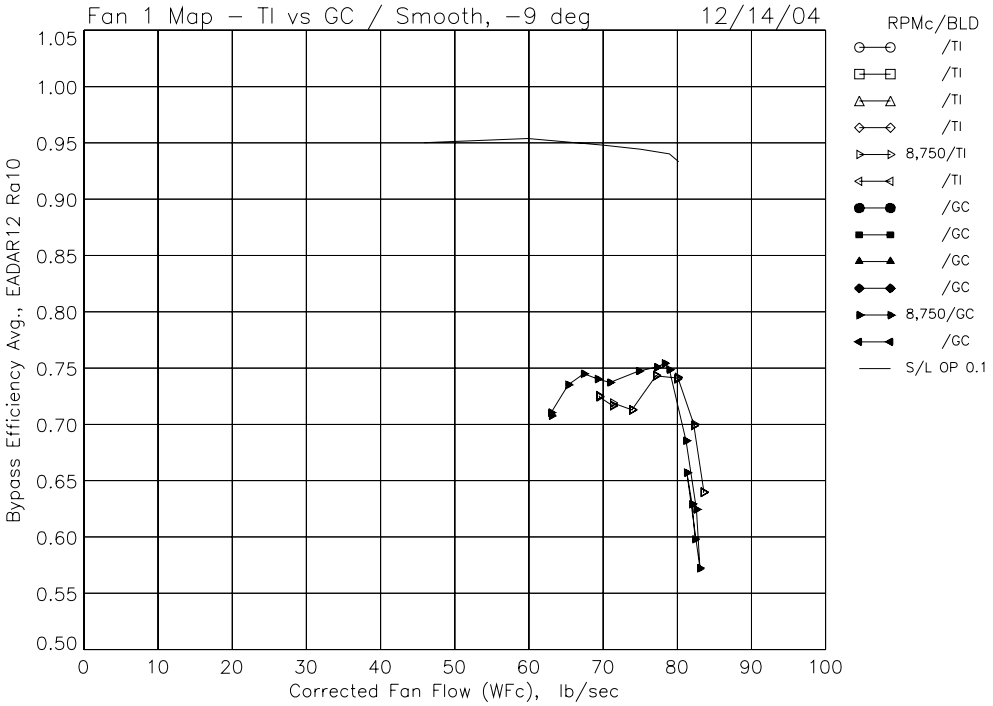

(e) Bypass 10th radius adiabatic efficiency versus total fan corrected flow, RPMc = 8,750.

Figure 36.—TI and GC blade single-speed, single-radius, efficiency results with –9 deg blade angle, smooth rubstrip.

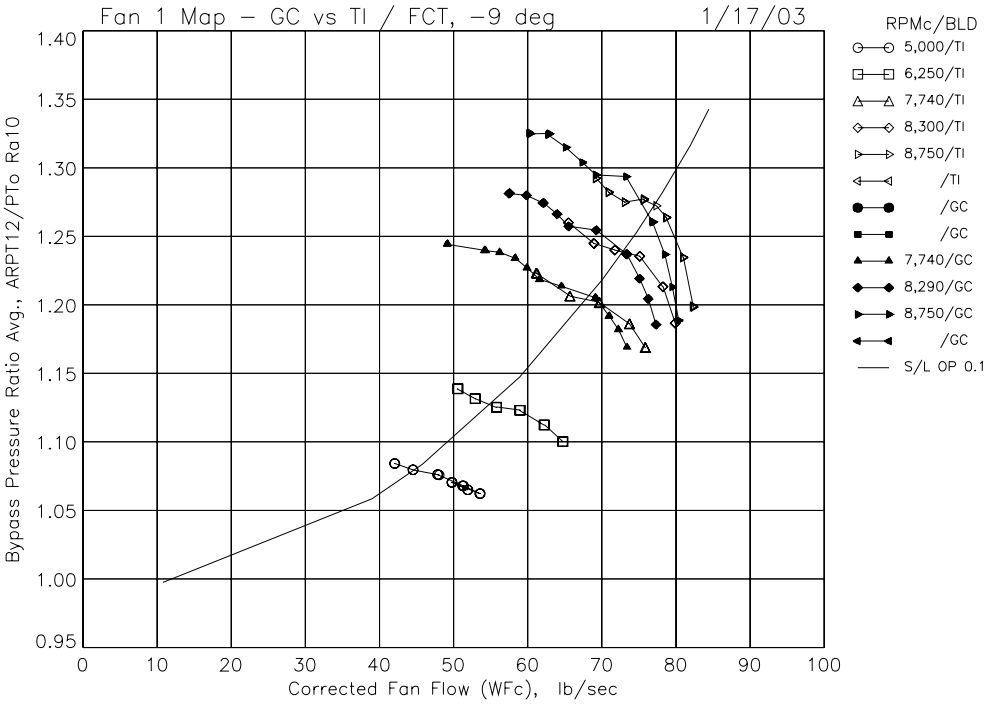

(a) Bypass 10th radius total pressure ratio versus total fan corrected flow.

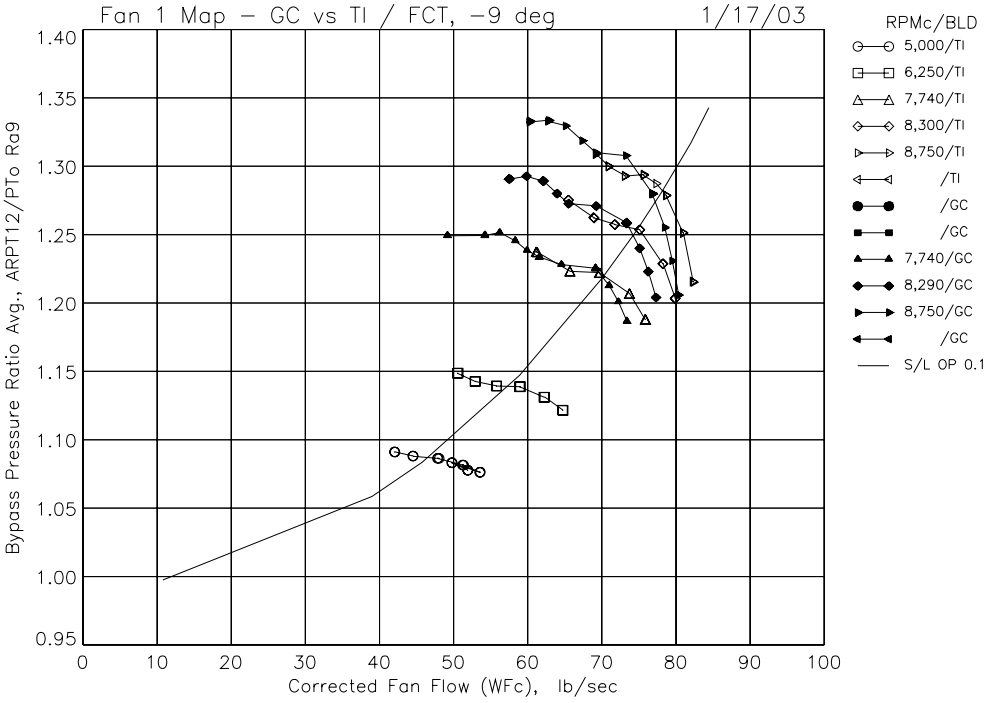

(b) Bypass 9th radius total pressure ratio versus total fan corrected flow.

Figure 37.—TI and GC blade single-radius pressure ratio map results with –9 deg blade angle, FCT rubstrip.

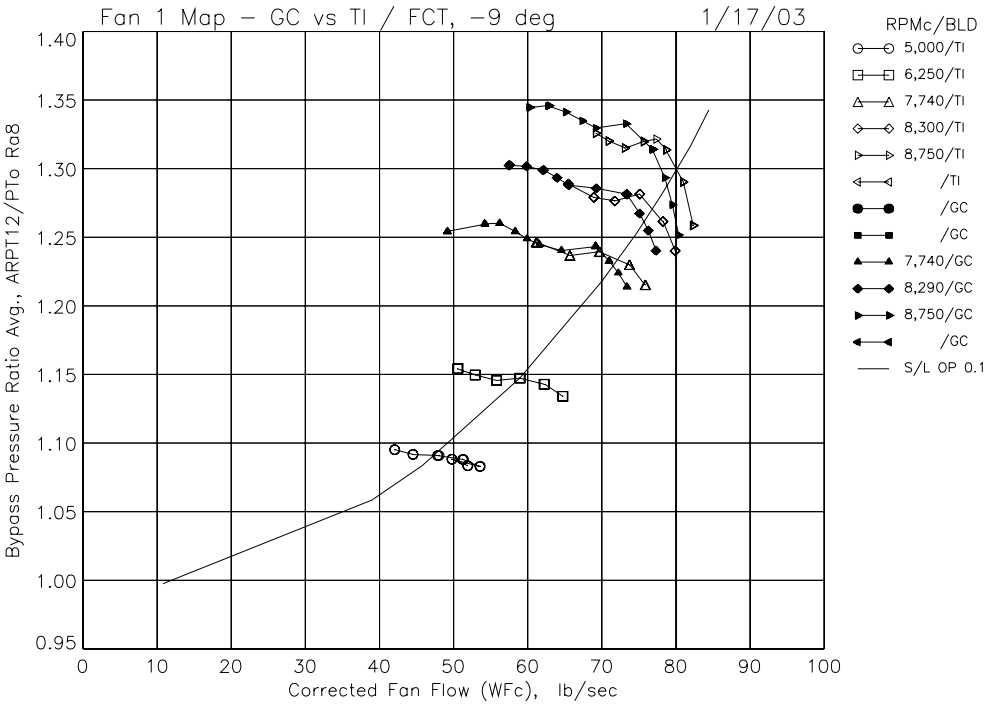

(c) Bypass 8th radius total pressure ratio versus total fan corrected flow.

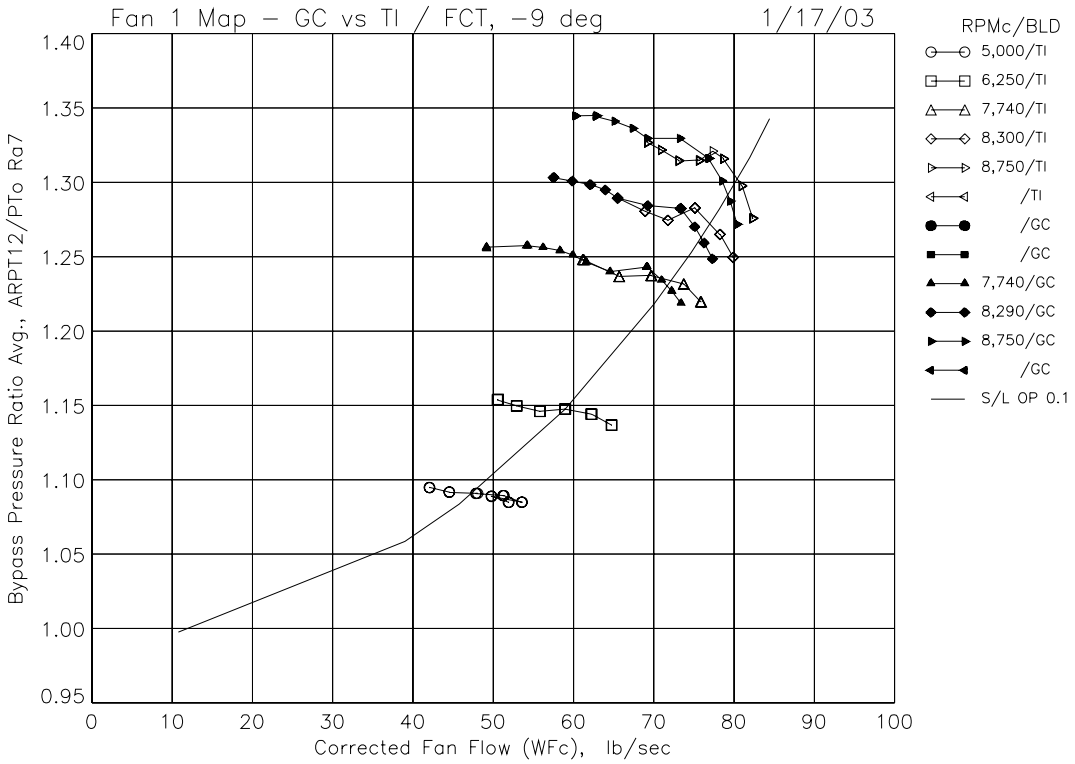

(d) Bypass 7th radius total pressure ratio versus total fan corrected flow.

Figure 37.—TI and GC blade single-radius pressure ratio map results with –9 deg blade angle, FCT rubstrip.

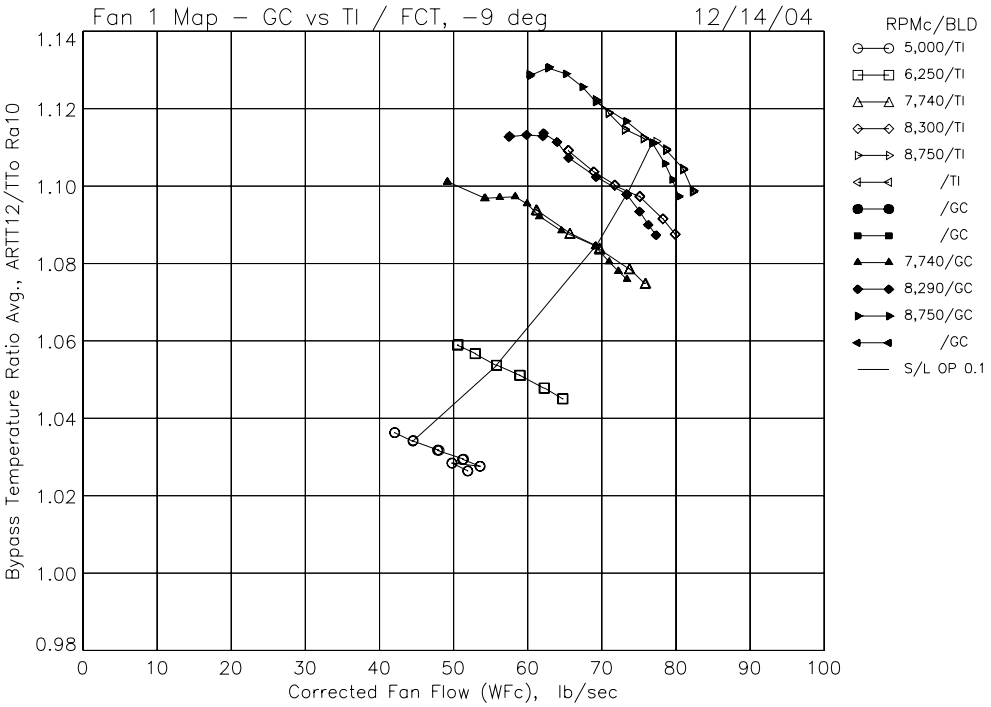

(a) Bypass 10th radius total temperature ratio versus total fan corrected flow.

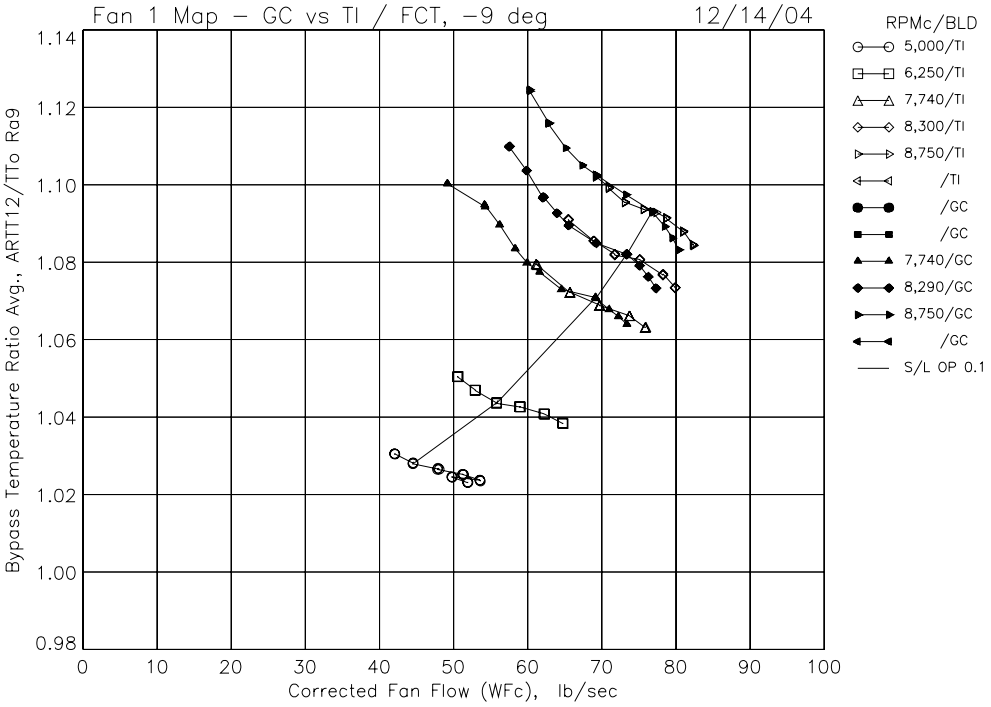

(b) Bypass 9th radius total temperature ratio versus total fan corrected flow.

Figure 38.—TI and GC blade single-radius temperature ratio map results with –9 deg blade angle, FCT rubstrip.

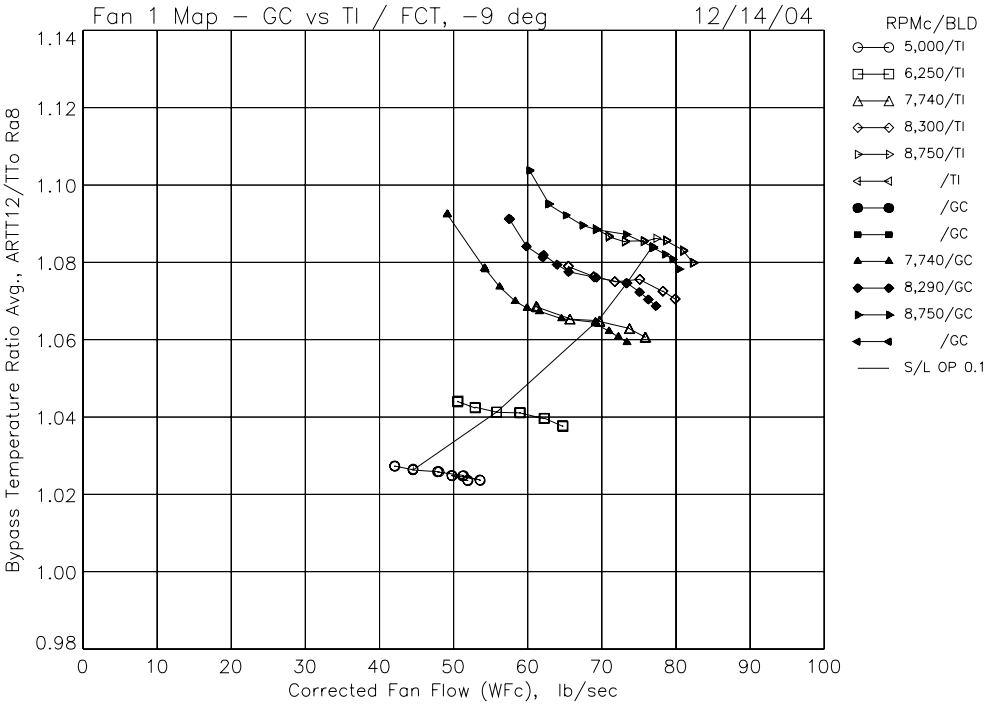

(c) Bypass 8th radius total temperature ratio versus total fan corrected flow.

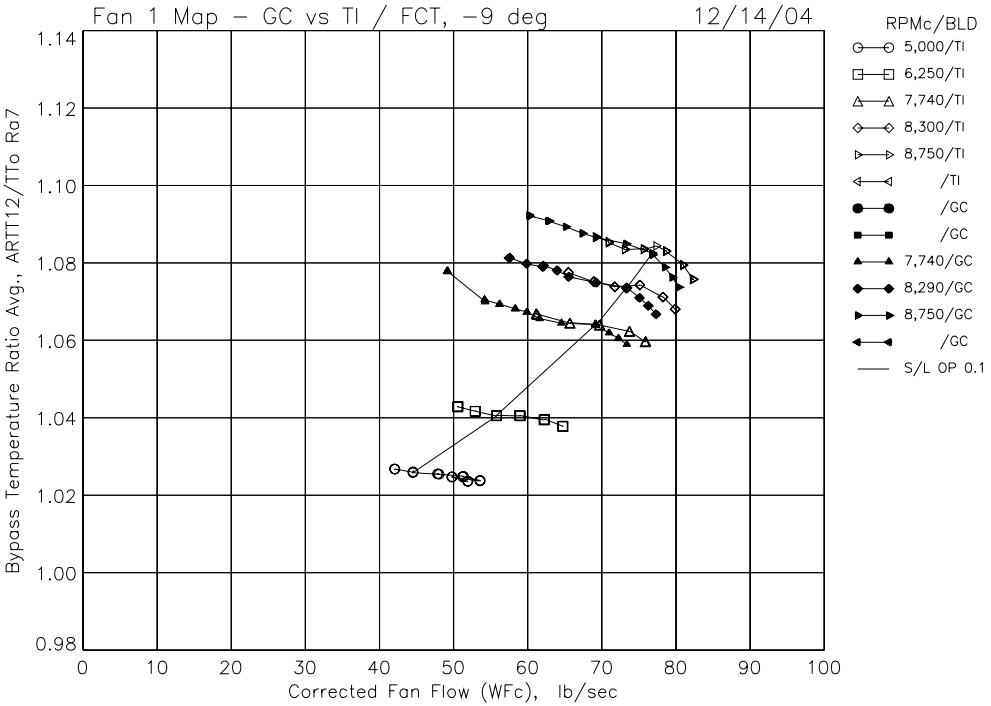

(d) Bypass 7th radius total temperature ratio versus total fan corrected flow.

Figure 38.—TI and GC blade single-radius temperature ratio map results with –9 deg blade angle, FCT rubstrip.

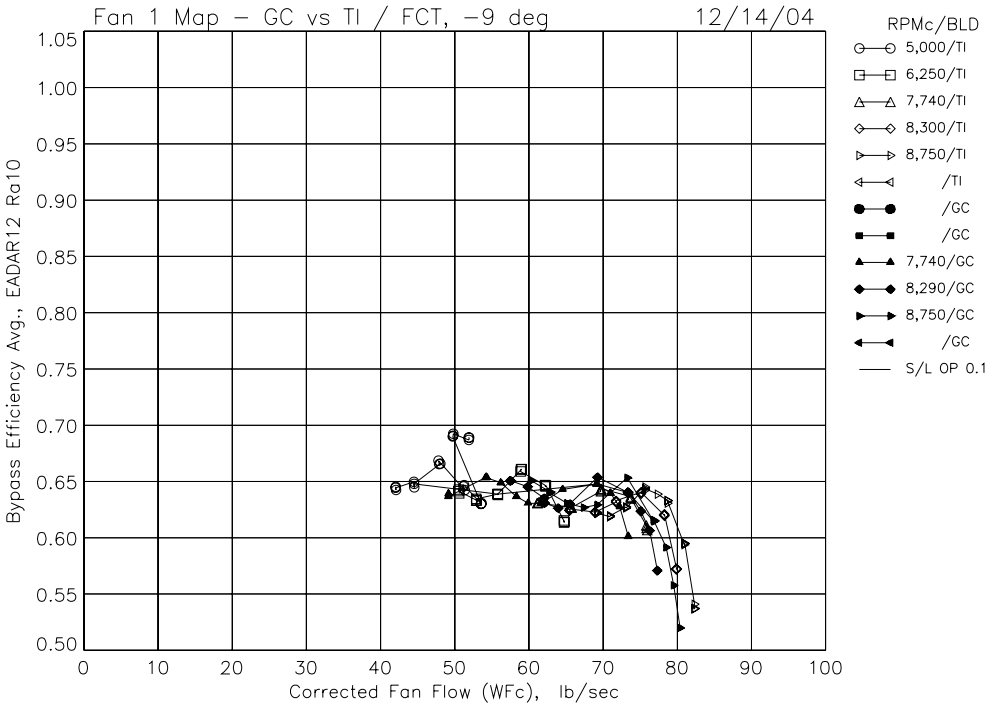

(a) Bypass 10th radius adiabatic efficiency versus total fan corrected flow.

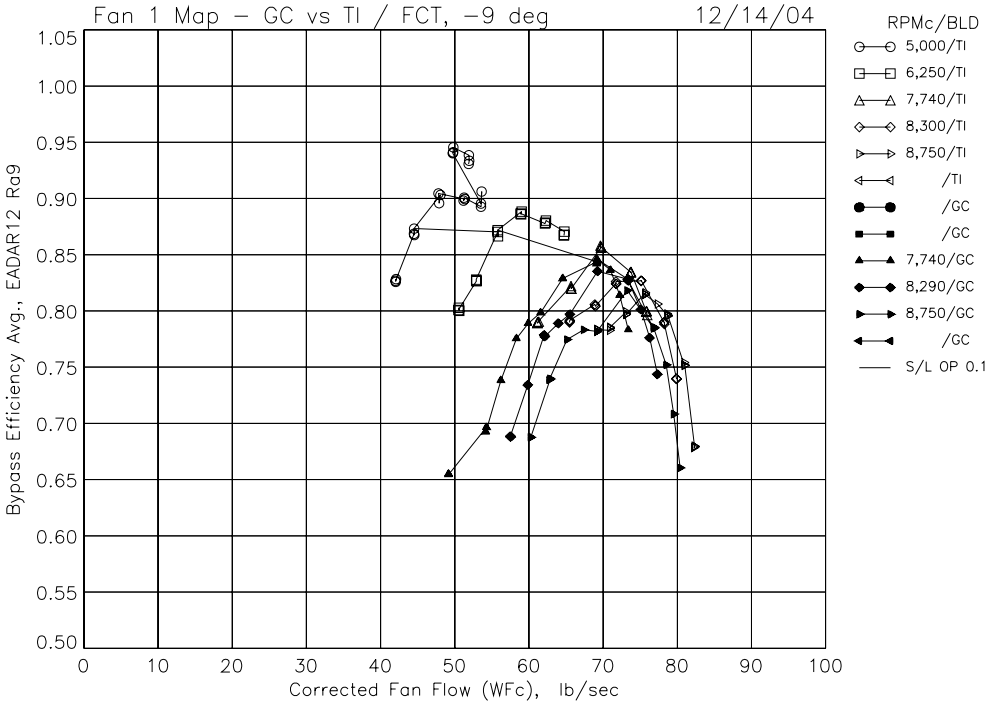

(b) Bypass 9th radius adiabatic efficiency versus total fan corrected flow.

Figure 39.—TI and GC blade single-radius adiabatic efficiency map results with –9 deg blade angle, FCT rubstrip.

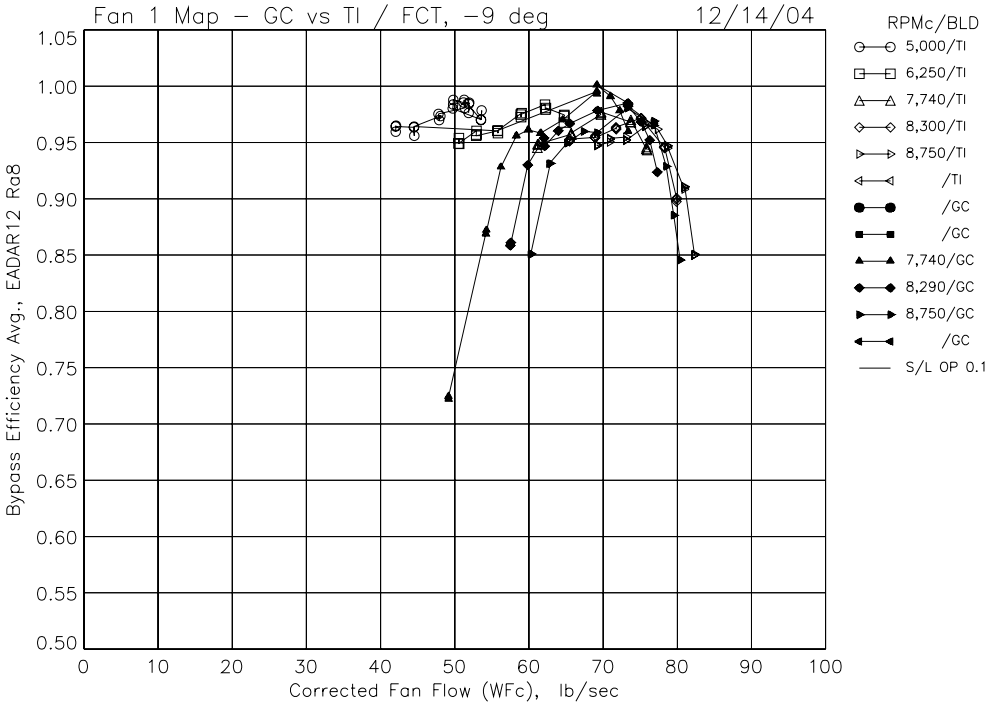

(c) Bypass 8th radius adiabatic efficiency versus total fan corrected flow.

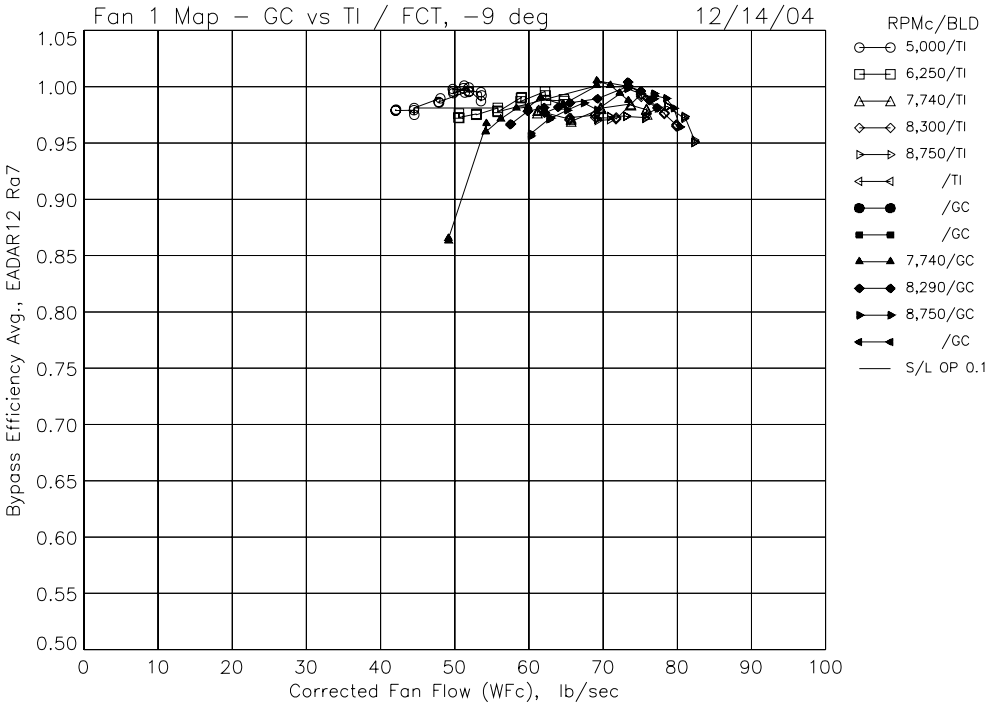

(d) Bypass 7th radius adiabatic efficiency versus total fan corrected flow.

Figure 39.—TI and GC blade single-radius adiabatic efficiency map results with –9 deg blade angle, FCT rubstrip.

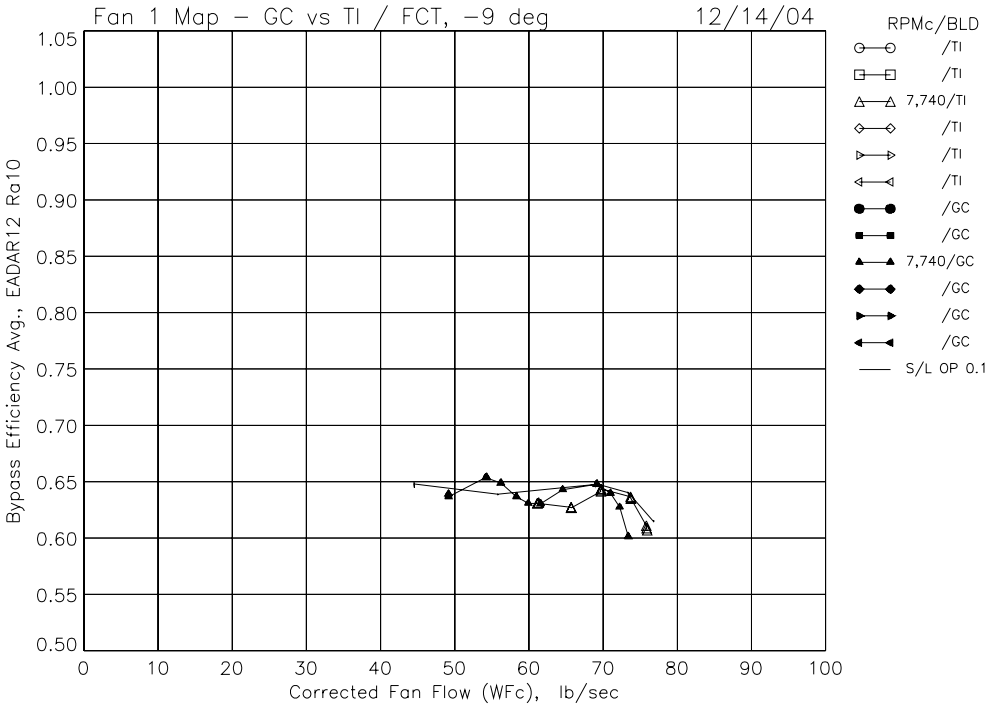

(a) Bypass 10th radius adiabatic efficiency versus total fan corrected flow, RPMc = 7,740.

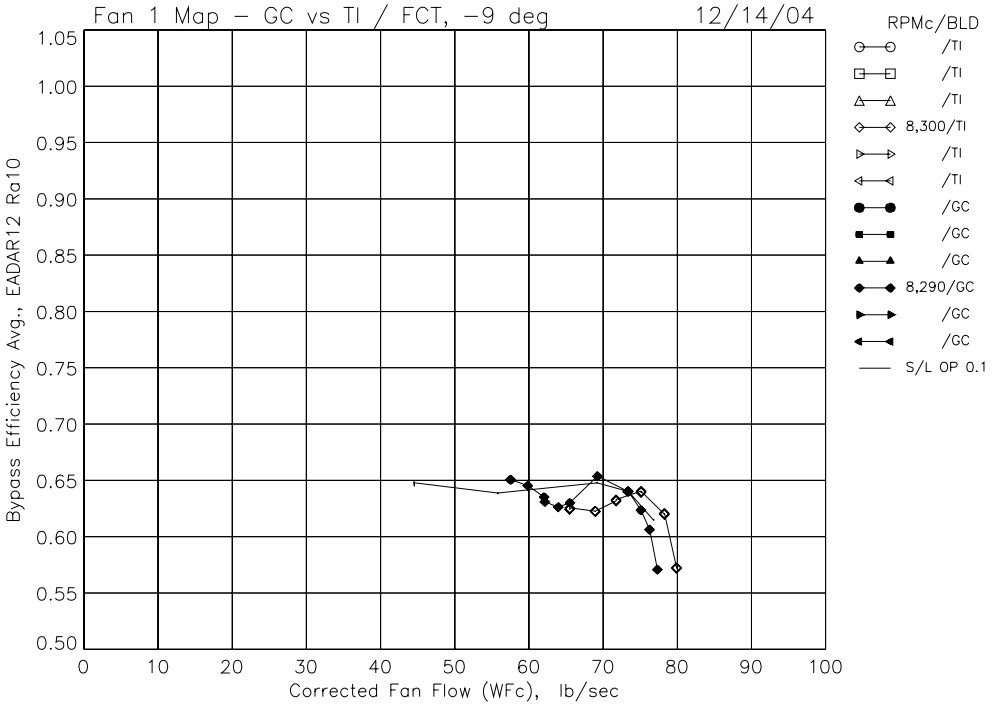

(b) Bypass 10th radius adiabatic efficiency versus total fan corrected flow, RPMc = 8,300.

Figure 40.—TI and GC blade single-speed, single-radius, efficiency results with –9 deg blade angle, FCT rubstrip.

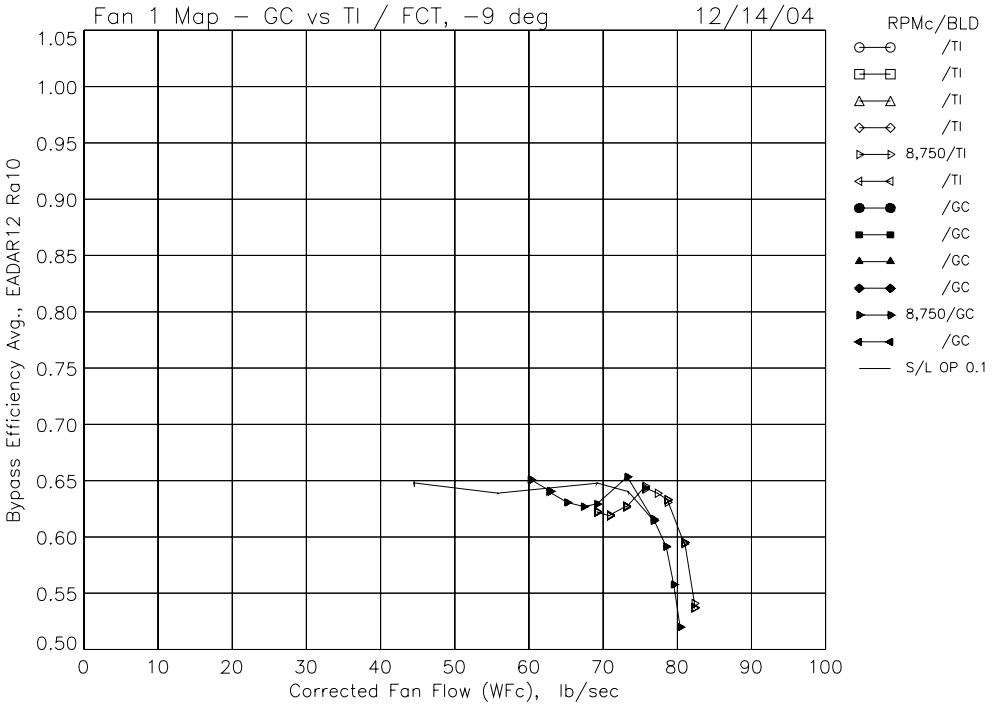

(c) Bypass 10th radius adiabatic efficiency versus total fan corrected flow, RPMc = 8,750.

Figure 40.—TI and GC blade single-speed, single-radius, efficiency results with –9 deg blade angle, FCT rubstrip.

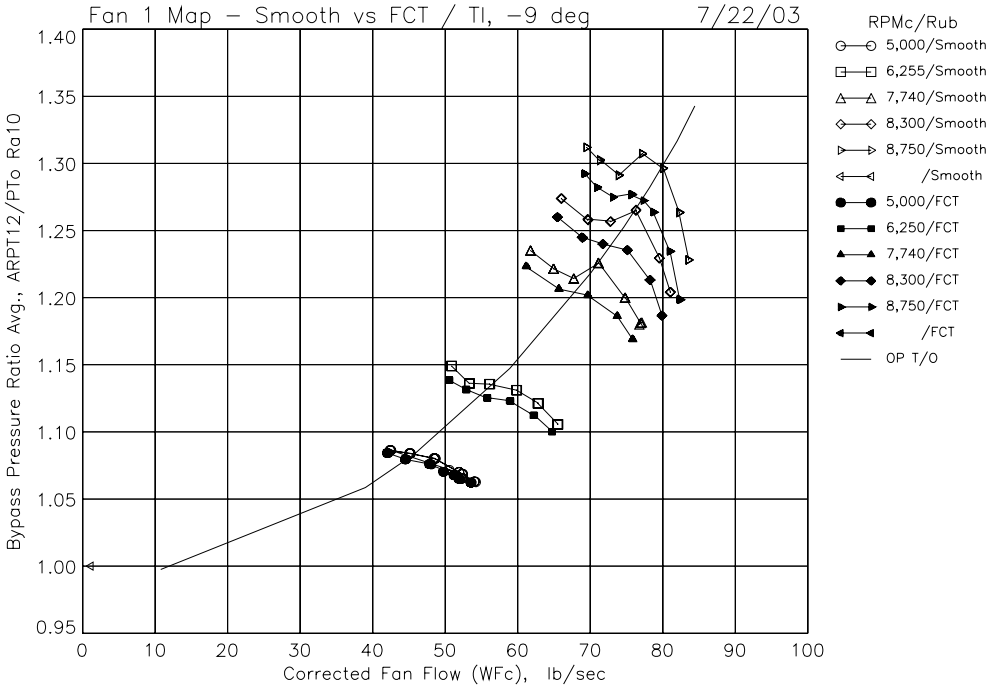

(a) Bypass 10th radius total pressure ratio versus total fan corrected flow.

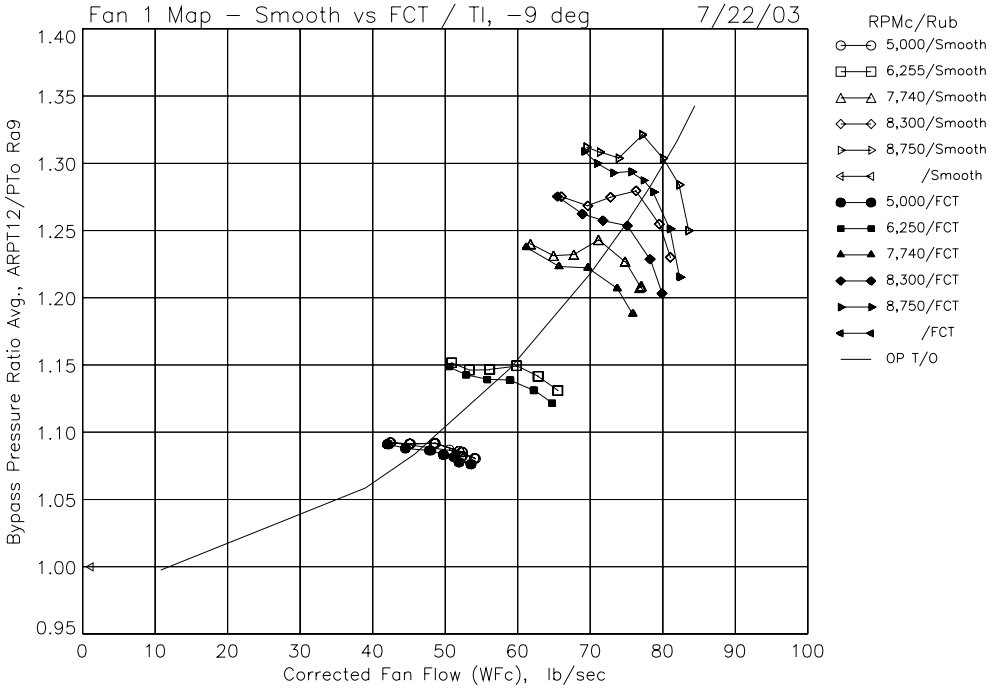

(b) Bypass 9th radius total pressure ratio versus total fan corrected flow.

Figure 41.—Smooth and FCT rubstrip single-radius pressure ratio map results with –9 deg blade angle, TI blades.

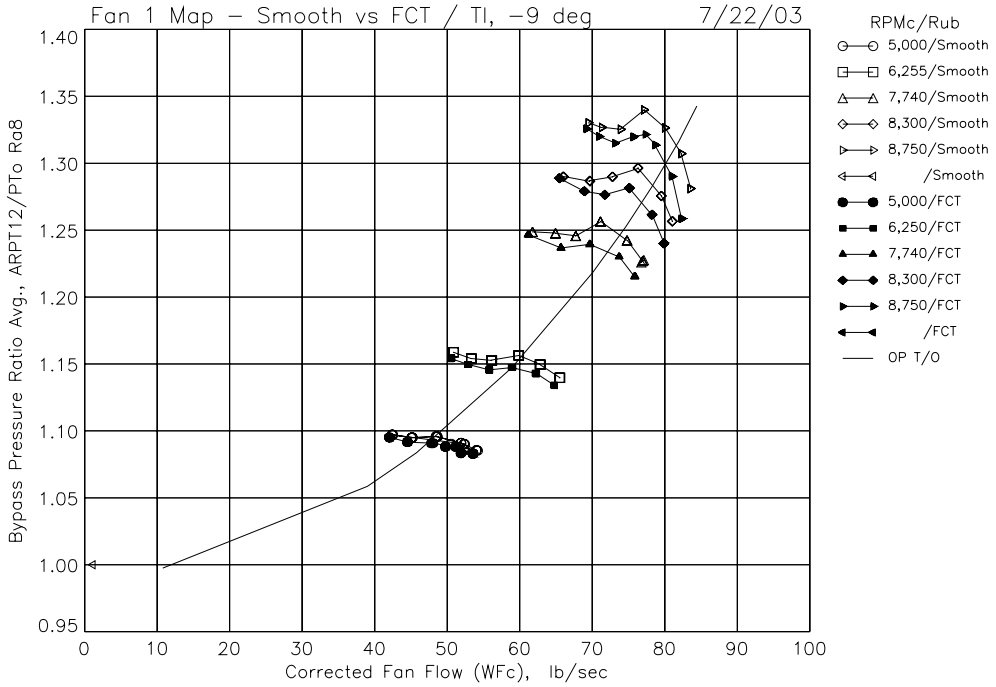

(c) Bypass 8th radius total pressure ratio versus total fan corrected flow.

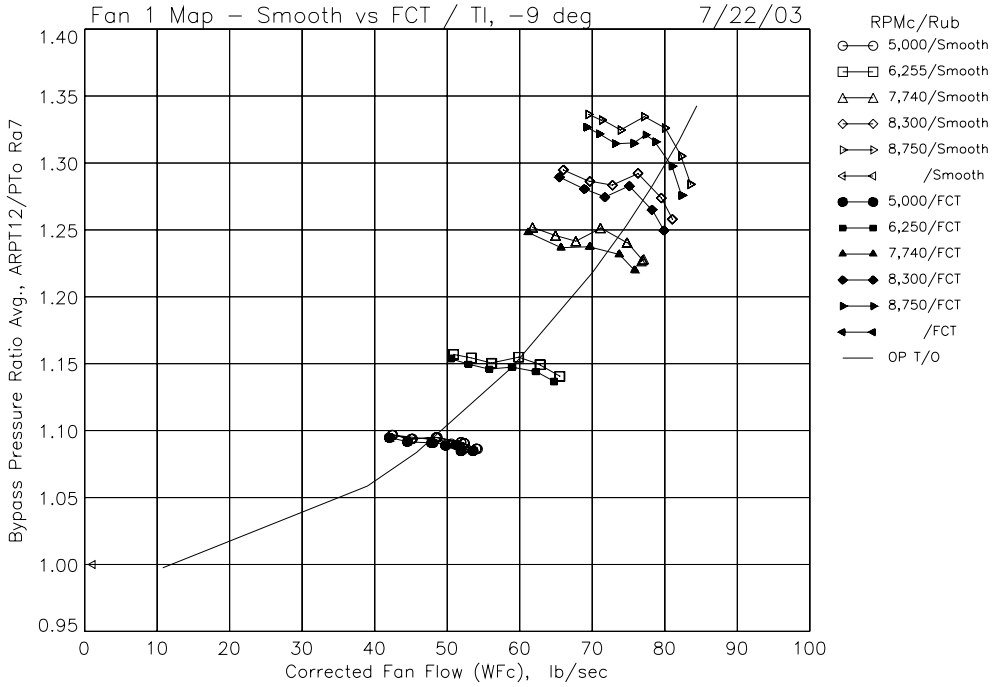

(d) Bypass 7th radius total pressure ratio versus total fan corrected flow.

Figure 41.—Smooth and FCT rubstrip single-radius pressure ratio map results with –9 deg blade angle, TI blades.

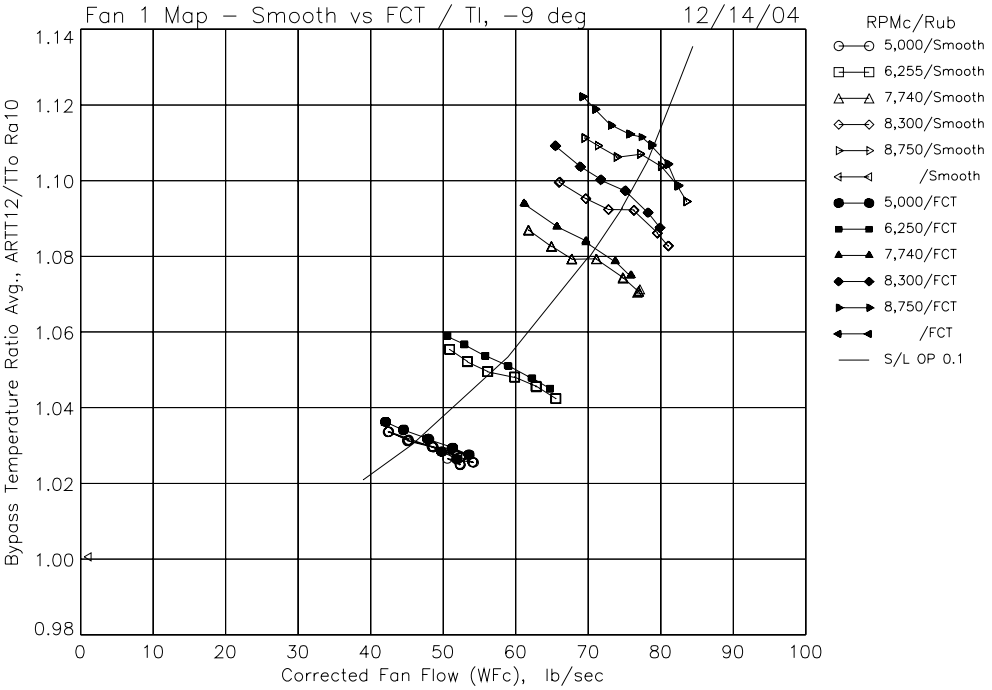

(a) Bypass 10th radius total temperature ratio versus total fan corrected flow.

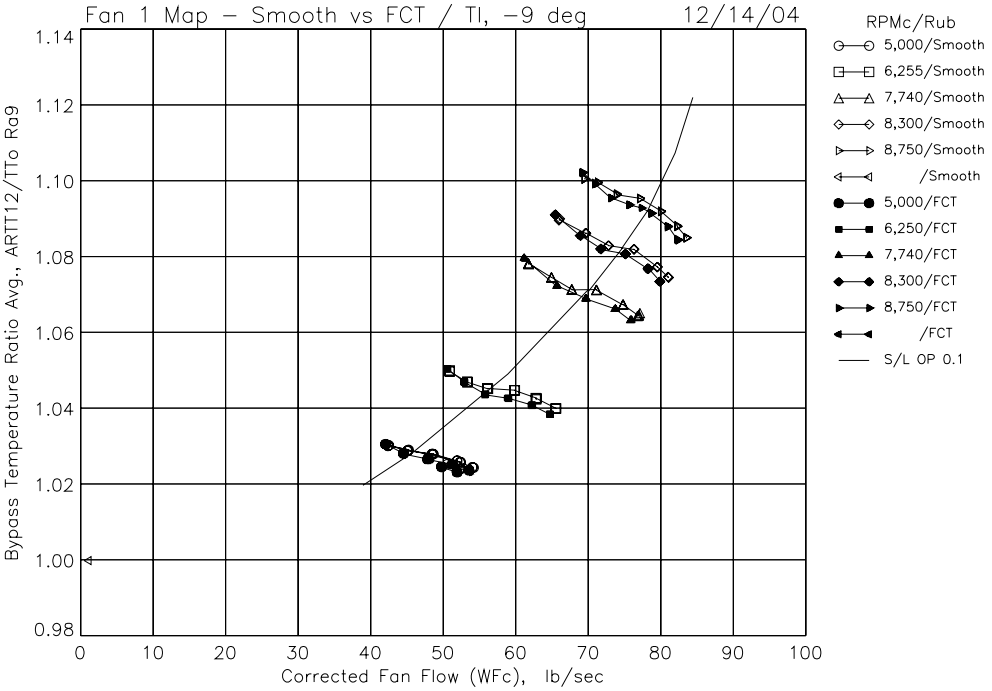

(b) Bypass 9th radius total temperature ratio versus total fan corrected flow.

Figure 42.—Smooth and FCT rubstrip single-radius temperature ratio map results with –9 deg blade angle, TI blades.

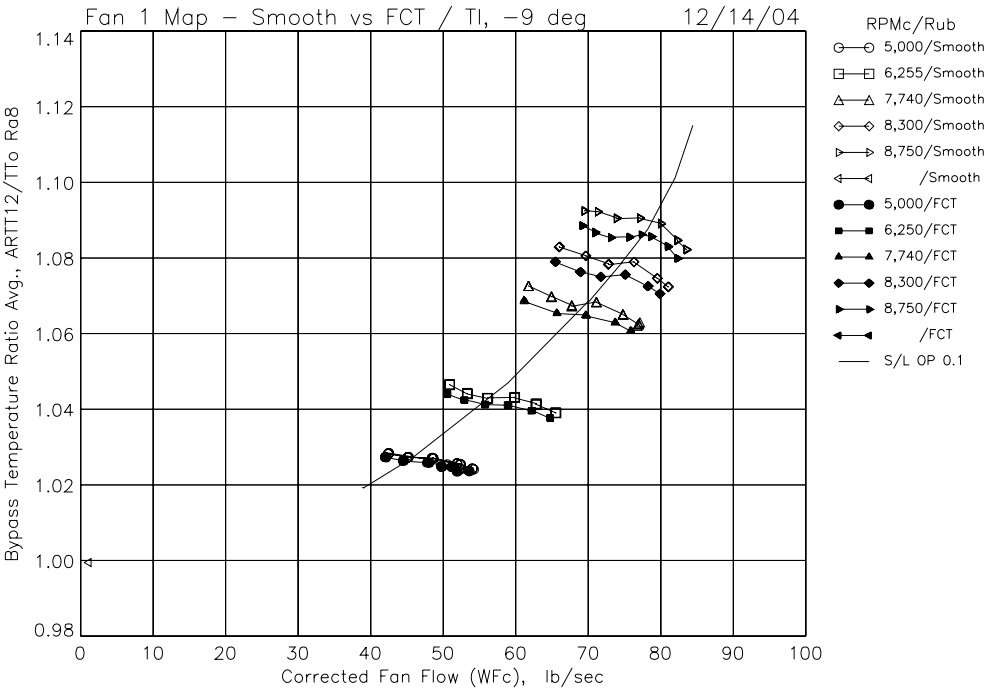

(c) Bypass 8th radius total temperature ratio versus total fan corrected flow.

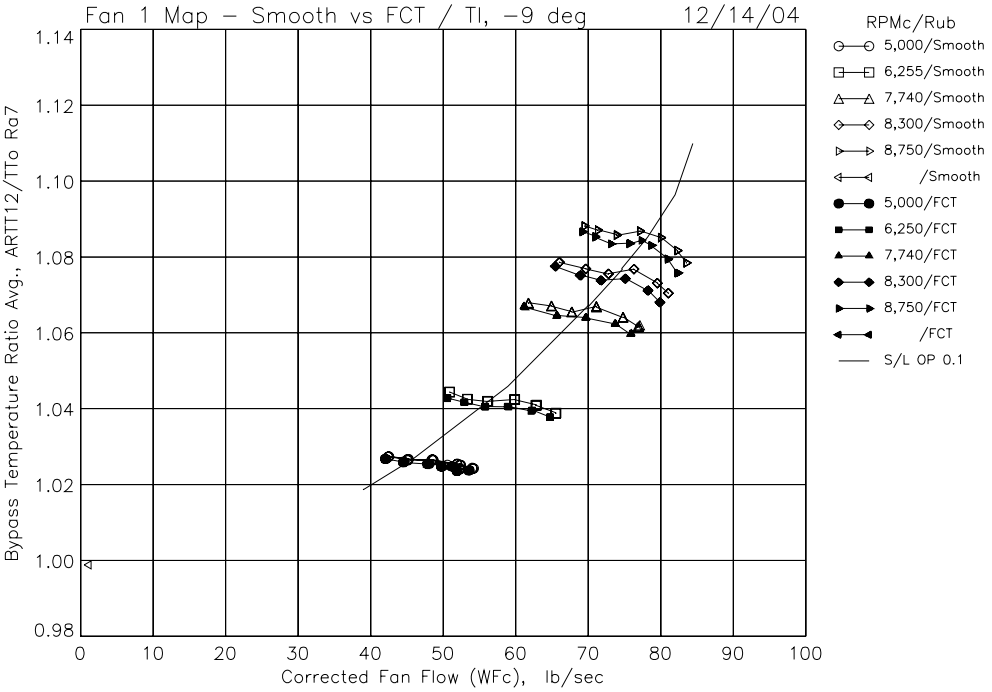

(d) Bypass 7th radius total temperature ratio versus total fan corrected flow.

Figure 42.—Smooth and FCT rubstrip single-radius temperature ratio map results with –9 deg blade angle, TI blades.

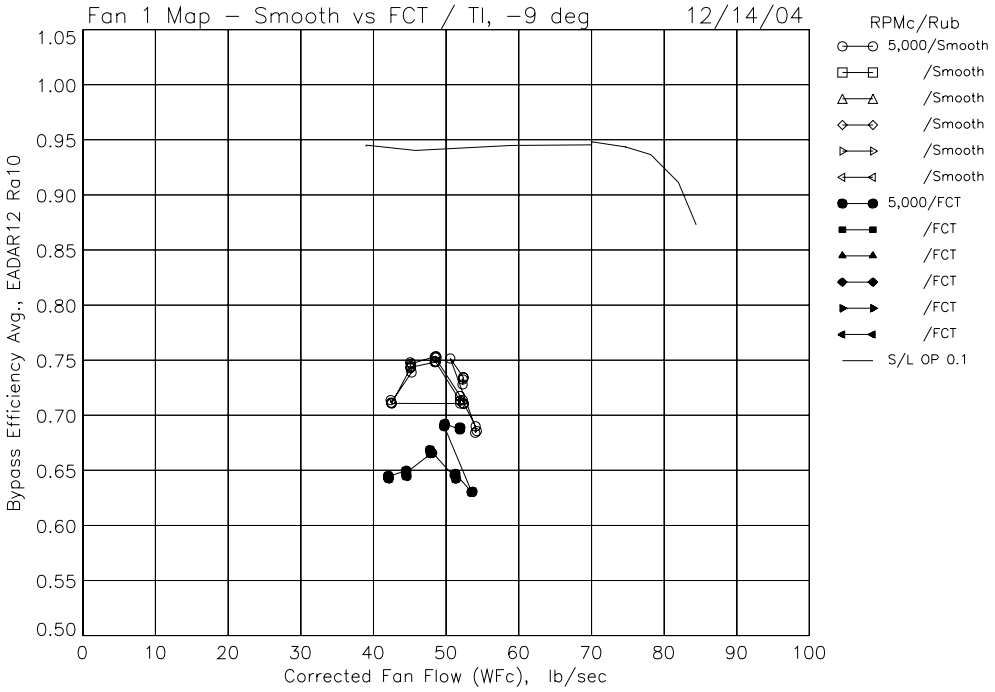

(a) Bypass 10th radius adiabatic efficiency versus total fan corrected flow, RPMc = 5,000.

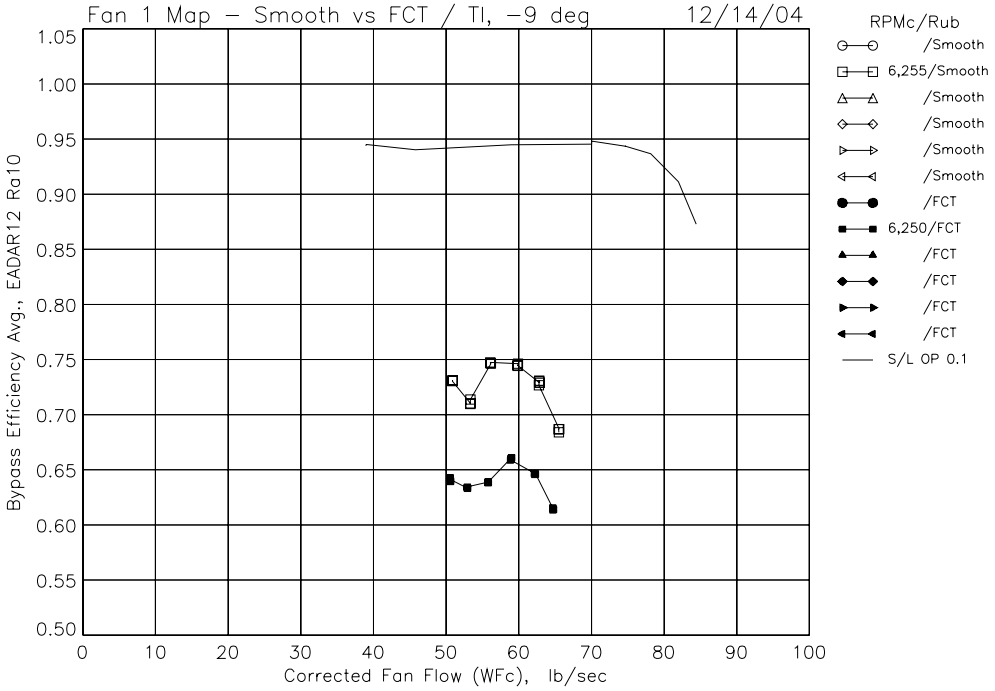

(b) Bypass 10th radius adiabatic efficiency versus total fan corrected flow, RPMc = 6,250.

Figure 43.—Smooth and FCT rubstrip single-speed, single-radius efficiency results with –9 deg blade angle, TI blades.

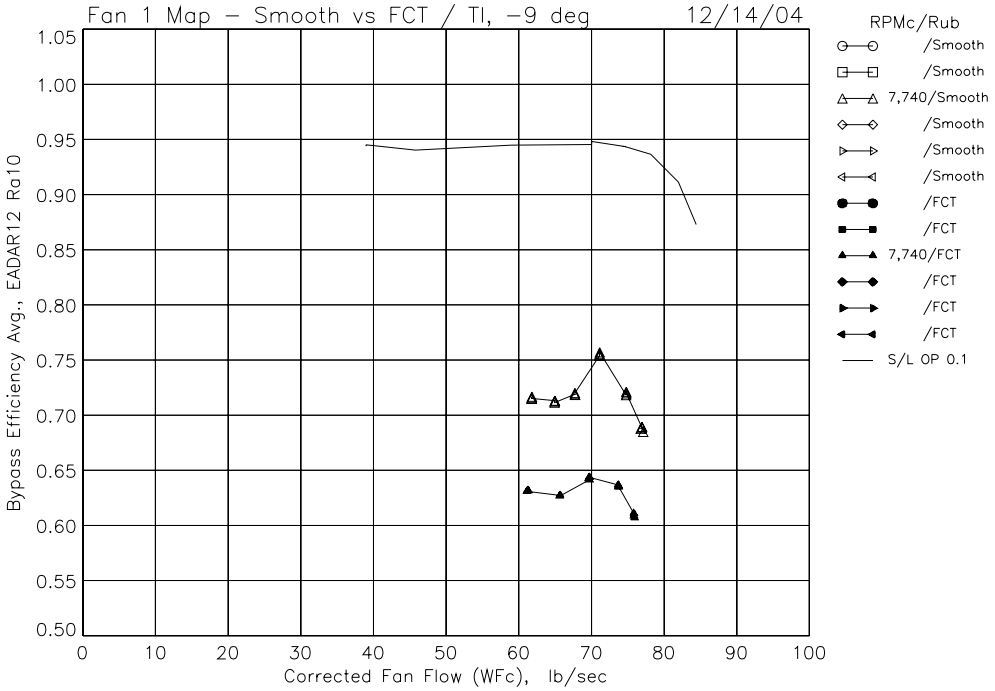

(c) Bypass 10th radius adiabatic efficiency versus total fan corrected flow, RPMc = 7,740.

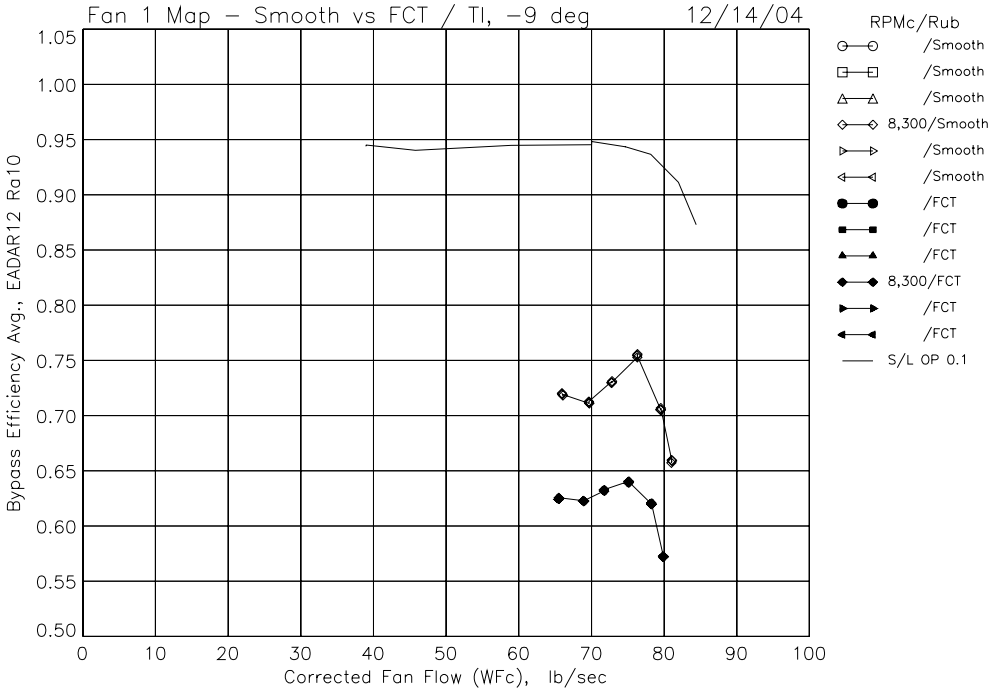

(d) Bypass 10th radius adiabatic efficiency versus total fan corrected flow, RPMc = 8,300.

Figure 43.—Smooth and FCT rubstrip single-speed, single-radius efficiency results with –9 deg blade angle, TI blades.

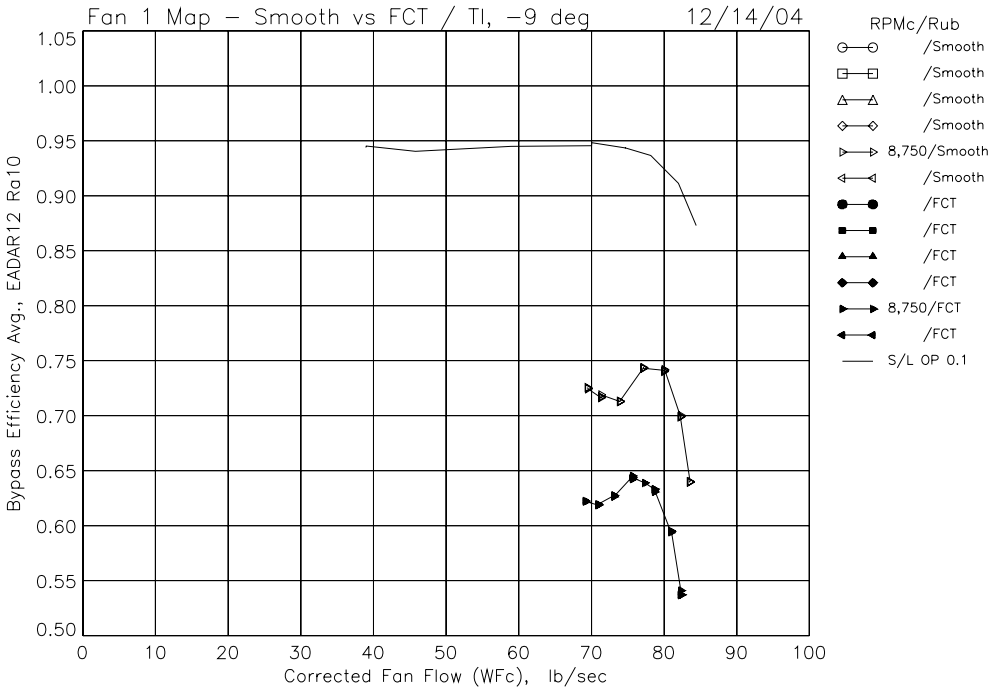

(e) Bypass 10th radius adiabatic efficiency versus total fan corrected flow, RPMc = 8,750.

Figure 43.—Smooth and FCT rubstrip single-speed, single-radius efficiency results with –9 deg blade angle, TI blades.

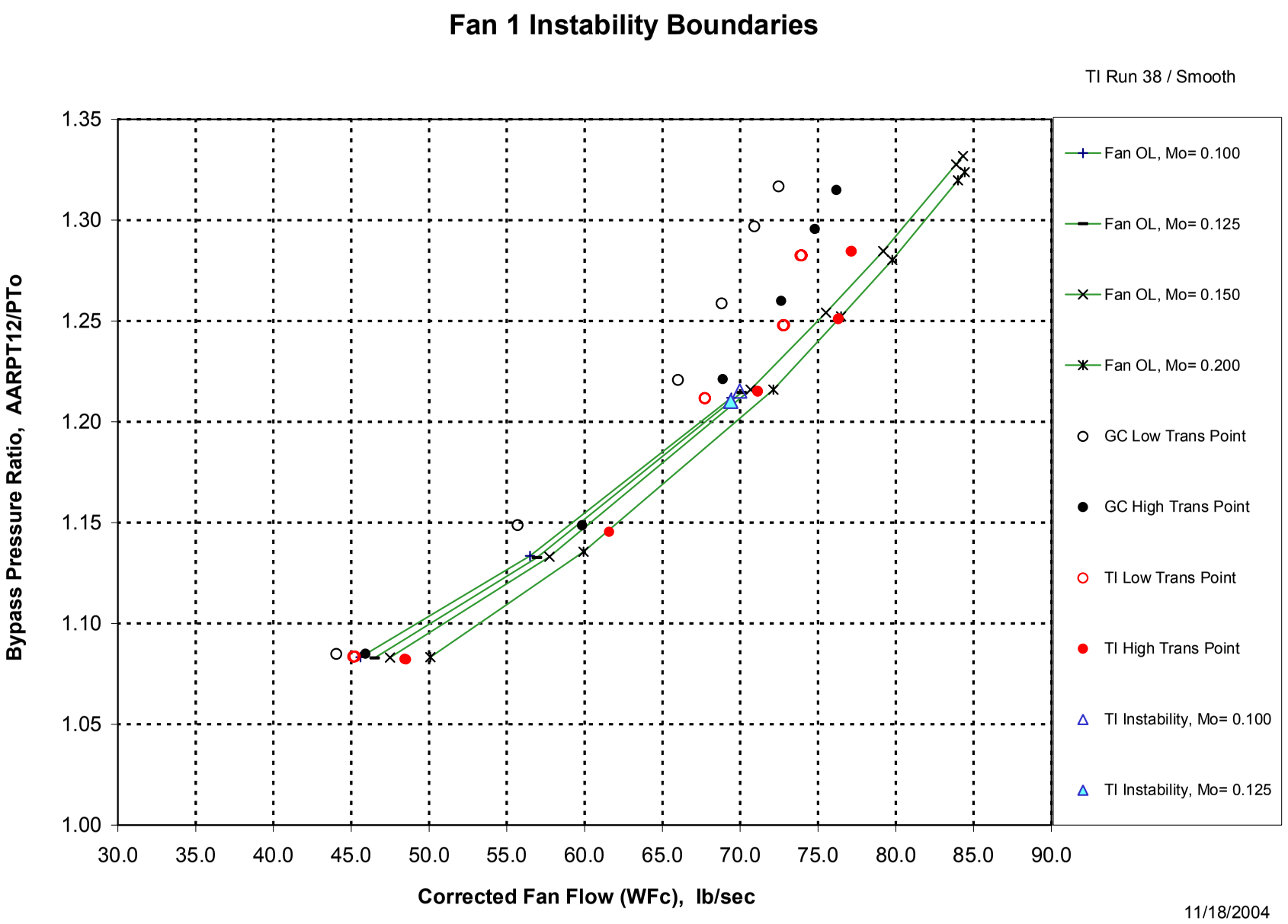

Figure 44.—TI and GC blade operating lines, transition points, and instability points with smooth rubstrip.

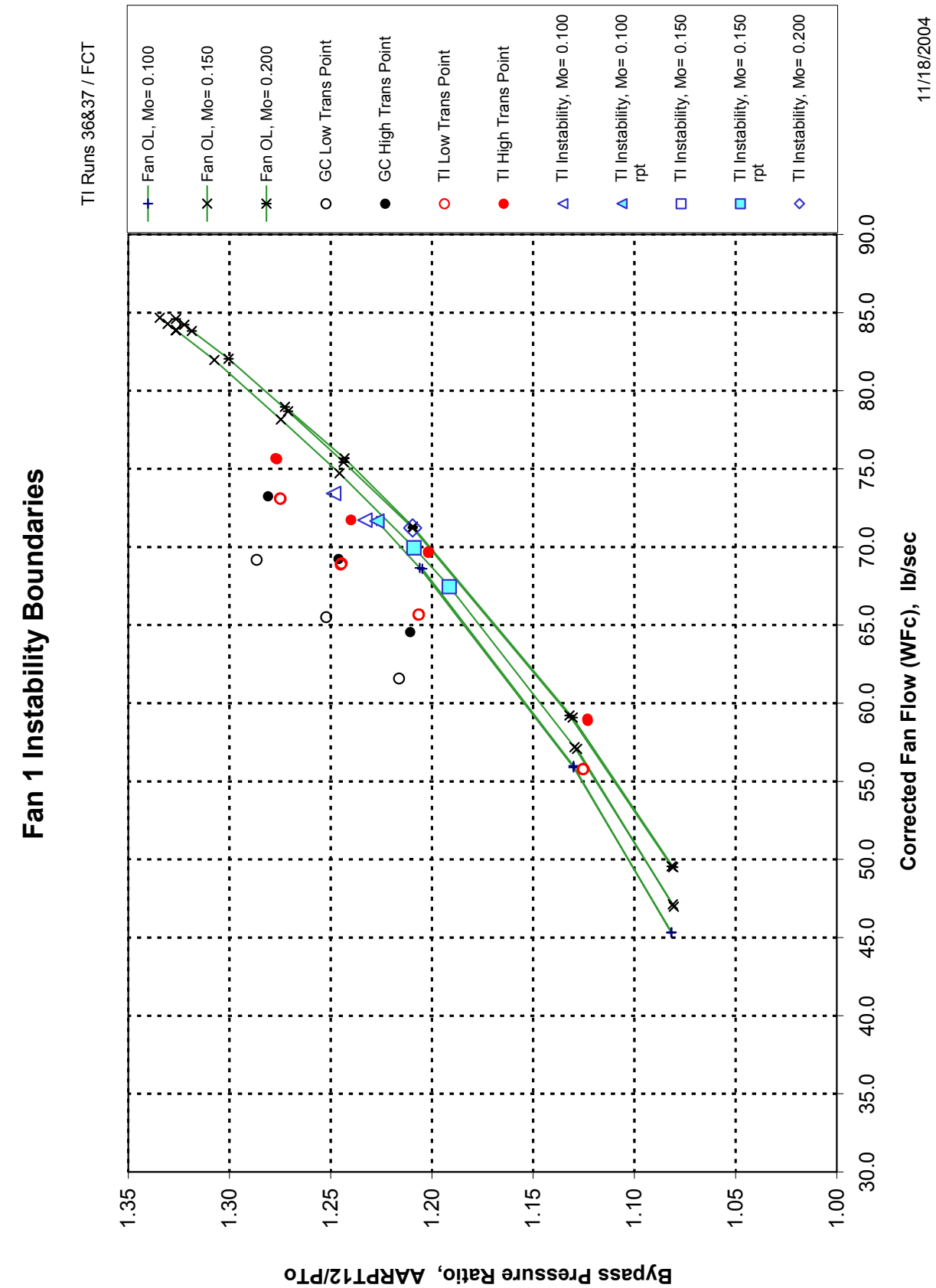

Figure 45.—TI and GC blade operating lines, transition points, and instability points with FCT rubstrip.

REPORT DOCUMENTATION PAGE

Form Approved
OMB No. 0704-0188

1. AGENCY USE ONLY (*Leave blank*)	2. REPORT DATE	3. REPORT TYPE AND DATES COVERED
	February 2006	Technical Memorandum

4. TITLE AND SUBTITLE

Comprehensive Report of Fan Performance From Duct Rake Instrumentation on 1.294 Pressure Ratio, 806 ft/sec Tip Speed Turbofan Simulator Models

5. FUNDING NUMBERS

WBS–22–781–30–50

6. AUTHOR(S)

Robert J. Jeracki

7. PERFORMING ORGANIZATION NAME(S) AND ADDRESS(ES)

National Aeronautics and Space Administration
John H. Glenn Research Center at Lewis Field
Cleveland, Ohio 44135–3191

8. PERFORMING ORGANIZATION REPORT NUMBER

E–15233

9. SPONSORING/MONITORING AGENCY NAME(S) AND ADDRESS(ES)

National Aeronautics and Space Administration
Washington, DC 20546–0001

10. SPONSORING/MONITORING AGENCY REPORT NUMBER

NASA TM—2006–213863

11. SUPPLEMENTARY NOTES

Responsible person, Robert J. Jeracki, organization code RTA, 216–433–3917.

12a. DISTRIBUTION/AVAILABILITY STATEMENT

Unclassified - Unlimited
Subject Category: 02

Available electronically at http://gltrs.grc.nasa.gov

This publication is available from the NASA Center for AeroSpace Information, 301–621–0390.

12b. DISTRIBUTION CODE

13. ABSTRACT ***(Maximum 200 words)***

A large scale model representative of an advanced ducted propulsor-type, low-noise, very high bypass ratio turbofan engine was tested for acoustics, aerodynamic performance, and off-design operability in the NASA Glenn 9- by 15-Foot Low-Speed Wind Tunnel. The test was part of NASA's Advanced Subsonic Technology Noise Reduction Program. The low tip speed fan, nacelle, and un-powered core passage were simulated. As might be expected, the effect of stall management casing treatment was a performance penalty. Reducing the recirculating flow at the fan tip reduced the penalty while still providing sufficient stall margin. Two fans were tested with the same aerodynamic design; one with graphite composite material, and the other with solid titanium. There were surprising performance differences between the two fans, though both blades showed some indication of transitional flow near the tips. Though the pressure and temperature ratios were low for this fan design, the techniques used to improve thermocouple measurement accuracy gave repeatable data with adiabatic efficiencies agreeing within 1 percent. The measured fan adiabatic efficiency at simulated takeoff conditions was 93.7 percent and matched the design intent.

14. SUBJECT TERMS

Wind tunnel; Powered model; Scale model; Turbofan; Ducted fan; Turbomachinery; Fan noise; Low noise; Low tip speed

15. NUMBER OF PAGES

147

16. PRICE CODE

17. SECURITY CLASSIFICATION OF REPORT	18. SECURITY CLASSIFICATION OF THIS PAGE	19. SECURITY CLASSIFICATION OF ABSTRACT	20. LIMITATION OF ABSTRACT
Unclassified	Unclassified	Unclassified	